To the Graduate Council:

I am submitting herewith a dissertation written by Maolian Chen entitled "Characterization of Aβ Aggregates Using Hydrogen/Deuterium Exchange Mass Spectrometry." I have examined the final electronic copy of this dissertation for form and content and recommended that it be accepted in partial fulfillment for the degree of Doctor of Philosophy, with a major in Chemistry.

Kelsey D. Cook
Major Professor

We have read this dissertation
and recommend its acceptance:

Ziling Xue

John E. Bartmess

Engin H. Serpersu

Acceptance for the Council:

Anne Mayhew
Vice Chancellor and Dean of
Graduate Studies

(Original signatures are on file with official student records.)

Characterization of Aβ Aggregates Using Hydrogen/Deuterium Exchange Mass Spectrometry

A Dissertation

Presented for the

Doctor of Philosophy Degree

The University Of Tennessee, Knoxville

Maolian Chen

December 2006

The dissertation is dedicated

to my grandparents,

Chen Chunan and Wu Shulan,

to my parents,

Chen Junyue and Li Qunying,

And

to my husband,

Thomas Pelaia II,

for their love, support and encouragement!

ACKNOWLEDGEMENTS

There are many people to whom I am so grateful for making my research experience at UTK a rewarding and successful one. Most of all, I wish to express my deepest gratitude to my advisor of this dissertation, Dr. Kelsey D. Cook. Millions of thanks for directing me in the course of my doctorate studies with great scientific knowledge and human gentleness. It never felt intimidating since I knew you would support me whenever I would encounter problems. Thank you for all of your seasoned guidance, constant help and ceaseless support and encouragement over the years! Thank you for your understanding and for getting me through difficult times! I am so fortunate to have you as a teacher in scientific thinking and writing! Your dedication and efficacy has been a source of great inspiration to me.

I am very grateful to another scientist – Dr. Indu Kheterpal. Working with you in the lab is one of the memories that will never fade. Thank you for getting me started and for giving me guidance on the Alzheimer's disease project! Thank you for helping me out with experimental and theoretical issues! Thank you for sharing your knowledge and enthusiasm for science!

My warmest thanks are due to Dr. Albert Tuiman, former director of the Center for Mass Spectrometry. Thank you for having been extremely helpful in many aspects of mass spectrometry and for providing insightful discussions concerning my research! I have learned so much from you! You opened the door to the practical world of mass spectrometry for me!

I would also like to thank Dr. John Bartmess, Dr. Engin Serpersu, Dr. Ziling Xue and Dr. Douglass Gilman for serving on my committee, for all the help and support. Special thanks go to Dr. Ron Wetzel for providing me with the opportunity to work on the Alzheimer's disease project.

My thanks extend to past and present member of the Cook group, including Dr. Benjamin Prebyl, Erik Portelius, Dr. Duane Huffer, Dr. Dave Kaleta, Elizabeth Stewart, Yu Zhu, Eloise Joyce, Teerapat Rojsajjakul, and Huifang Yao for their friendship,

scientific contributions, moral support and great company. Special thanks would be given to Dr. Kevin Bennett, former student of Dr. Kelsey D. Cook, for help with my early work on process mass spectrometry with the Questor IV instrument. I also highly appreciate the contributions that Alex Schrimpe made to the process mass spectrometry project during her summer intern here. I would like to thank her for her hard work, great company and unforgettable friendship.

Many thanks go to Dr. Ron Wetzel's group in the UT medical center for all their kind assistance and for sharing scientific knowledge. A giant thanks goes to Angie Williams, the queen of LC-MS, for always helping me out with questions. I am grateful to Dr. Jon Cooper and Dr. Chris Dealwis for the generous supply of the endothiapepsin sample. Help from Brad Benett with purifying the enzyme is highly appreciated.

Thanks to the great analytical chemists and teachers at the department for never quitting to view me as a student that has much more to learn about chemistry.

I would also greatly appreciate the generous funding from National Institutes of Health, NSF-supported measurement and Control Engineering Center. Assistantships provided by the Science Alliance and the University of Tennessee Chemistry Department are also greatly acknowledged.

My heartfelt thanks go to my parents, who are on the other side of the world, for always emphasizing the importance of hard work and education, and for always supporting and encouraging me to continue my studies as far as I wanted to go!

And last, I wish to thank the wonderful and intelligent man, my beloved husband Dr. Thomas Pelaia, II, for his deep love and for always being there for me!

ABSTRACT

The work presented in this dissertation aimed to localize the hydrogen-bonding interaction sites within Aβ aggregates associated with Alzheimer's disease using hydrogen/deuterium exchange mass spectrometry (HDX-MS) coupled with proteolysis. Toward this end, an on-line digestion system utilizing a triaxial electrospray probe as the front end to MS was developed. Using this approach, regions of Aβ(1-40) fibrils and protofibrils that are protected from HDX have been identified. The HDX data show that the C-terminal segment 35-40 and the N-terminal segment 1-19 are highly exposed to exchange in both fibrils and protofibrils, while the internal fragment 20-34 is highly protected from exchange in fibrils but much less so in protofibrils. The HDX data of fibrils match a model in which residues 11-23 and 28-36 are involved in highly protected structures, while those of protofibrils fit a model in which residues 14-20 and 31-36 are contained in highly protected structures. The N-terminal ~10 residues and the C-terminal ~ 4 residues appear to be unstructured in both fibrils and protofibrils. The 20-30 segment of Aβ(1-40) is more ordered in fibrils than in protofibrils, suggesting that, if protofibrils are a mechanistic precursor of fibrils, the transition from protofibril to fibril involves substantial ordering of this region of the Aβ peptide.

The on-line digestion system has been extended successfully with three pepsin-like enzymes (protease type XIII, protease type XVIII and endothiapepsin). Preliminary proteolysis results show that individual or combinational use of the enzymes leads to production of more fragments of Aβ(1-40) (thus potentially more detailed structural information) than using pepsin alone.

The oxidation of Aβ samples was encountered in the course of these studies. It was found that gradual corrosion of a stainless steel electrospray emitter under conditions of normal use can generate surface irregularities that sustain electrical discharge. The increased emission current can affect the electrochemical reactions associated with the spray process, including oxidation of methionine to methionine sulfoxide in Aβ(1-40) peptides. The resultant mass shift and reduced sensitivity can adversely affect HDX

experiments. These effects can be avoided by adding a redox buffer or (preferably) by re-polishing the emitter.

ABSTRACT

The elucidation of the structure of amyloid fibrils and related aggregates is an important step towards understanding the pathogenesis of diseases like Alzheimer's disease (AD), which feature protein misfolding and/or aggregation. The work presented in this dissertation aimed to localize the hydrogen-bonding interaction sites within Aβ fibrils and protofibrils associated with AD by using hydrogen/deuterium exchange mass spectrometry (HDX-MS) coupled with proteolysis. Toward this end, a novel on-line digestion system utilizing a triaxial electrospray probe as the front end to MS was developed. The triaxial probe allows introduction of rapid proteolysis and dissolution reagents before addition of the pepsin-incompatible co-solvent (typically acetonitrile in our procedures) needed to stabilize the electrospray, thereby enhancing hydrolysis without sacrificing MS sensitivity. Using this approach, regions of the Aβ(1-40) peptide containing backbone amide hydrogens that are protected from HDX when this peptide is incorporated into either amyloid fibrils or protofibrils have been identified. Study of protofibrils was facilitated by use of the protofibril-stabilizing agent calmidazolium chloride (CLC). The HDX data clearly show that both the C-terminal segment 35-40 and the N-terminal segment 1-19 are highly exposed to exchange in both fibrils and protofibrils. In contrast, the internal fragment 20-34 is highly protected from exchange in fibrils but much less so in protofibrils. The HDX data of fibrils match a model in which residues 11-23 and 28-36 are involved in highly protected structures, while those of protofibrils fit a model in which residues 14-20 and 31-36 are contained in highly protected structures. This suggests that the β-sheet elements comprising the amyloid fibril are already present in protofibrils, but that they are expanded into some adjacent residues upon the formation of mature amyloid. The N-terminal ~10 residues and the C-terminal ~ 4 residues appear to be unstructured in both fibrils and protofibrils. The 20-30 segment of Aβ(1-40) is more ordered in fibrils than in protofibrils, suggesting that, if protofibrils are a mechanistic precursor of fibrils, the transition from protofibril to fibril involves substantial ordering of this region of the Aβ peptide.

The on-line digestion system has been extended successfully with three pepsin-like enzymes (protease type XIII, protease type XVIII and endothiapepsin) with an aim to obtaining complementary structural information of Aβ fibrils. Preliminary proteolysis results show that individual or combinational use of the enzymes leads to cleavage at different peptide amide bonds of Aβ(1-40) and production of more fragments (thus potentially more detailed structural information) than using pepsin alone.

The oxidation of Aβ samples was encountered in the course of these studies. It was found that gradual corrosion of a stainless steel electrospray emitter under conditions of normal use can generate surface irregularities that sustain electrical discharge, as evidenced by an increase in the emission current. The increased current can affect the electrochemical reactions associated with the spray process, as evidenced by the oxidation of the methionine residue to methionine sulfoxide in Aβ(1-40) peptides. The resultant mass shift and reduced sensitivity can adversely affect HDX experiments. These effects can be avoided by adding a redox buffer or (preferably) by re-polishing the emitter.

TABLE OF CONTENTS

LIST OF TABLES

LIST OF FIGURES

LIST of ABBREVIATIONS AND ACRONYMS

AD	Alzheimer's disease
AFM	Atomic force microscopy
BE	Backward exchange
CE	Capillary electrophoresis
CID	Collision induced dissociation
Cr	Critical concentration
Da	Dalton(s)
ECD	Electron capture dissociation
EM	Electron microscopy
EPR	Electron paramagnetic resonance spectroscopy
ES	Electrospray
ESI	Electrospray ionization
ESI-MS	Electrospray ionization mass spectrometry
ETD	Electron transfer dissociation
FE	Forward exchange
FTICR	Fourier transform ion cyclotron resonance
HDX	Hydrogen/deuterium exchange
HDX-MS	Hydrogen/deuterium exchange mass spectrometry
HDX-ESI/MS	Hydrogen/deuterium exchange electrospray ionization mass spectrometry
HDX-MALDI/MS	Hydrogen/deuterium exchange matrix assisted desorption/ionization mass spectrometry
HDX-NMR	Hydrogen/deuterium exchange nuclear magnetic resonance
HPLC	High performance liquid chromatography
HTX	Hydrogen/tritium exchange
MALDI	Matrix assisted desorption/Ionization
MALDI-MS	Matrix assisted desorption/ionization mass spectrometry

MS	Mass spectrometry
MS/MS	Tandem mass spectrometry
m/z	Mass-to-charge ratio
NMR	Nuclear magnetic resonance
QLS	Quasielastic light scattering
S/B	Signal-to-background ratio
S/N	Signal-to-noise ratio
TFA	Trifluoroacetic acid
TOF	Time–of-flight

CHAPTER 1

INTRODUCTION

1.1 Amyloid Fibrils and Alzheimer's Disease

1.1.1 Overview

Alzheimer's disease (AD), the most common cause of senile dementia, is manifest by memory loss and cognitive impairments in the elderly [1]. The prevalence of AD is around 5% among people between 65 and 74 years of age and increases to 40–50% among persons at 85 years of age and above [2]. As human life expectancy increases, the effects of AD will continue to escalate unless methods are discovered to delay its onset or halt or reverse its progression.

It was early in the last century that Alois Alzheimer described his classic observation on the dementia of Frau Auguste D., a study that gave the first insights into the disease that now bears his name [3]. Our understanding of this and other dementing disease comes from studies in such diverse fields as genetics, cellular and molecular biology, epidemiology, and neuropathology [3]. Although remarkable progress has been made over the last few years in understanding the pathologic basis of Alzheimer's disease, the critical events leading to neuronal dysfunction, and eventually neuron death, are still not clear. Microscopic examination of Alzheimer brains reveals frequent neurofibrillary tangles, which are composed mainly of abnormally-phosphorylated *tau* protein (a neuron-specific phosphoprotein that is the major constituent of neuronal microtubules), as well as extracellular deposits called senile plaques, which consist of protein aggregates termed amyloid fibrils [4]. Although the presence of these two features is essential in confirming the diagnosis of Alzheimer's disease, their significance as factors contributing to neurodegeneration is controversial.

AD is one of several disease states termed amyloidoses in which soluble proteins aggregate into highly ordered structures termed amyloid fibrils [5-6]. Rudolf Virchow first applied the term "amyloid" (meaning "starchlike") to these diseases in 1853 based

on the staining properties of extracellular deposits in human tissue [7]. However, it is now known that amyloid deposits are actually composed of proteins [8]. Although proteins capable of forming amyloid in human diseases have no significant similarities to one another in amino acid sequence, molecular weight, or native folding patterns [5], amyloid fibrils derived from these different proteins share a number of features. For example, they all have long, unbranched, twisted fibrillar morphology in electron microscopy (EM) [8-9], and show similar binding ability to certain heteroaromatic dyes (histochemical stain Congo red and fluorescent dye thioflavin T (ThT)) and conformational antibodies [8-9]. Fibrils also share a high content of β-pleated sheet secondary structure [5]. Moreover, they are extremely stable, insoluble under physiological conditions, and are very resistant to degradation and proteolytic digestion [4, 10]. These similarities suggest related mechanisms of fibril formation among the amyloid diseases. Therefore, information derived from AD research may be applied to other amyloid diseases, such as type II diabetes, Creutzfeldt-Jakob disease, rheumatoid arthritis, prion diseases, Parkinson's disease and Huntington's disease [9].

The primary component of AD associated amyloid fibrils is the Aβ peptide [11], a hydrophobic peptide, ranging from 39 to 43 amino acids in length (Figure 1.1). The peptide is derived from amyloid precursor protein (APP), which is a 110-130 kDa glycoprotein binding covalently to membranes and expressed throughout the body [12-13]. During metabolism, APP is most often cleaved at a region near the membrane within the Aβ sequence, by another membrane-bound protease termed α-secretase [14]. Cleavage by this protease results in the release of a soluble peptide, leaving the less soluble carboxyl end of APP bound to the membrane, thereby preventing formation of the Aβ peptide. If α secretase does not cleave APP, the protein may undergo alternative processing where it is proteolytically cleaved by enzymes termed β-secretase and γ-secretase [13, 15-16]. It is likely that the Aβ peptide is generated during this processing step. β-secretase cleaves APP to form C-terminal derivatives; subsequently, the γ-secretase complex cleaves at position 39, 40, 42, and 43 to generate respectively Aβ(1-39), Aβ(1-40), Aβ(1-42) and Aβ(1-43) peptides, among which Aβ(1-40) is most abundant

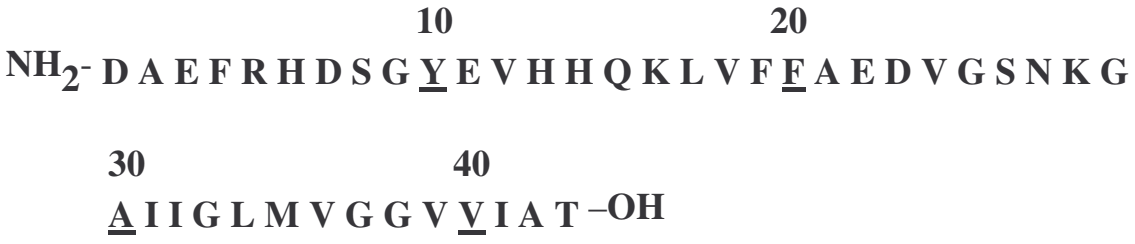

Amino Acid	3-Letter Code	1-Letter Code
Alanine	Ala	A
Cysteine	Cys	C
Aspartate	Asp	D
Glutamate	Glu	E
Phenylalanine	Phe	F
Glycine	Gly	G
Histidine	His	H
Isoleucine	Ile	I
Lysine	Lys	K
Leucine	Leu	L
Methionine	Met	M
Asparagine	Asn	N
Proline	Pro	P
Glutamine	Gln	Q
Arginine	Arg	R
Serine	Ser	S
Threonine	The	T
Valine	Val	V
Tryptophan	Trp	W
Tyrosine	Tyr	Y

Figure 1.1. The amino acid sequence of Aβ(1-43) peptide (each letter denotes an amino acid). Some variants eliminate up to 4 of the C-terminal amino acids. The table inset shows the names and abbreviations of the 20 amino acids.

and Aβ(1-42) is second-most abundant and most toxic [3]. An increase in brain Aβ levels correlates with the transition from a presymptomatic state to a symptomatic state in the progression of AD [6]. Because of this correlation, it has been hypothesized that Aβ deposition in plaques in brain tissue is the causative factor in AD, and that all other pathological symptoms (neurofibrillary tangles, cell loss, vascular damage, and dementia) follow as a result of this initial deposition [17]. Most of the strong evidence in favor of this amyloid hypothesis is genetic.

Genes responsible for early onset AD (before an average age of 60) are located on chromosomes 1 (presenilin 2 or PS2), 14 (presenilin 1 or PS1), 19 (apolipoprotein E or ApoE), and 21 (APP). Early onset forms of AD have been observed to correlate with mutations in APP [12, 17-22] and in presenilin genes [23-25]. So far, 20 pathogenic mutations in the APP gene, 124 mutations in the PS1 gene and 8 mutations in the PS2 gene have been described worldwide in families with AD [26]. The mutations have a direct effect on Aβ fibril formation. Most of these mutations have been found to map at or near cleavage sites in the primary sequence of APP that are targeted by the proteases β- and γ-secretase, and therefore generate Aβ by favoring proteolytic processing of APP, leading to a significant increase in the Aβ42/Aβ40 (concentration) ratio [17]. PSs are crucial components of the γ-secretase complex. Patients with PS1 mutations exhibit significantly higher secretion levels of Aβ(1-42) (shown to be more prone to aggregation and to be the initially deposited amyloid peptide in AD) compared to those with sporadic non-early onset AD [27]. Finally, the other genetic loci implicated in early onset AD encodes ApoE [24, 28-29]. ApoE's correlation to AD does not depend on genetic mutation but instead on genetic polymorphisms and the inheritance of one of the three variants from each parent; the ε2, ε3, and ε4 allelles (different variations of the same gene) [27]. The role played by ApoE in conferring AD susceptibility is not clear. One possibility for the involvement of ApoE in the progression of AD involves the ability to bind to neurotic plaques [24, 28]. All of the above observations are consistent with the theory that Aβ aggregation plays a causative role in AD.

All in all, the alterations within the genes responsible for early onset AD (APP, PS1, PS2, and ApoE) coincide with modifications of the generation, aggregation, or

clearance of Aβ that lead to amyloid fibril formation and deposition. Amyloid fibril formation thus appears to stand at the crossroads of many mechanisms of AD development. However, there are some concerns with the amyloid hypothesis. For example, the extent of amyloid deposits in AD brains does not always correlate with the severity of cognitive impairment, while deposition of tau protein in neurofibrillary tangles does seem to correlate with it [23]. On the other hand, recent findings have suggested that tau alterations occur after alterations in APP processing, and also that Aβ toxicity is tau dependent [23]. These observations have led to a theory that smaller soluble Aβ aggregates were at least co-responsible for the observed *in vitro* as well as *in vivo* neurotoxicity. These soluble oligomers called amyloid-derived diffusible ligands (ADDLs) [30], protofibrils [31] and amylospheroids [32], are presently considered as the relevant neurotoxic species initiating the amyloid cascade, and affecting memory processes *in vivo* [33-36]. Moreover, recent studies showed the possibility that certain amyloid morphologies may be more pathogenic than others in organs affected by amyloid diseases, which would weaken the correlation between disease symptoms and total amyloid deposition [37]. Therefore, further refinement of the amyloid hypothesis will entail the identification of specific pools of Aβ that contribute to the development of Aβ amyloid pathology and neuronal dysfunction. Moreover, besides targeting Aβ aggregation, it seems reasonable that drug design strategies that target Aβ production are also viable therapeutic approaches. The goal of the research presented here is to improve our understanding of the three-dimensional structure of Aβ fibrils and protofibrils, and of how fibrils are formed. Detailed understanding should help development of therapeutic approaches to curing AD.

1.1.2 Pathway of Aβ Peptide Fibrillization

To be able to target Aβ amyloid formation as a therapeutic approach, it is necessary to have a detailed understanding of the molecular mechanism of Aβ fibrillogenesis. Analytical ultracentrifugation, gel filtration chromatography, electron microscopy (EM), atomic force microscopy (AFM), and quasielastic light scattering

(QLS) have all shown that Aβ(1-40) and Aβ(1-42) at concentrations well above the critical concentration (*Cr*: defined as the concentration of peptide at which the rates of fibril formation and fibril dissolution are equal [38-41]) exist as both insoluble high-molecular-weight fibrillar oligomers and also soluble lower-weight oligomers [42]. The presence of the smaller oligomeric forms of Aβ suggests that the fibril assembly pathway involves discrete intermediates [42]. These intermediates involved in Aβ(1-42) fibrillization have been visualized by EM *in vitro* [42]. In this case, the earliest observed intermediates (after 0-0.5 h incubation) are globular aggregates (with a characteristic "beaded" appearance) about 4-5 nm in diameter [43]. These intermediates then gradually assemble into straight or V-shaped protofibrils (Figure 1.2a, 8.7-11.3 nm in diameter, after 0.5-2 h incubation), which undergo lateral or 'end-to-end' fusion to form short, thick fibrils with unincorporated protofibrillar branches (2-12h incubation). As the immature fibrils grow longer and thinner, the branches gradually recede and ultimately disappear, and subsequently amyloid fibrils (7-10nm in diameter, 12-24 h incubation) are formed [43]. AFM measurement of the lengths of protofibrils at various time points (2-18 days) during the fibrillization of Aβ(1-40) and Aβ(1-42) indicate that protofibril elongation involves both the incorporation of monomer and the association of immature (short) protofibrils [44]. In contrast, after dilution, protofibrils dissociate via the release of monomer only. Walsh *et al.* [31] independently reported similar findings, using light scattering and dialysis experiments to show that isolated Aβ(1-40) protofibrils are in equilibrium with low-molecular weight species and convert irreversibly to fibrils.

Since protofibrillar structures have been observed in the fibrillogenesis of both Aβ(1-40) and Aβ(1-42), they are perhaps a common intermediate in all Aβ fibrillogenesis [44, 45-48]. The presence of a protofibrillar intermediate has been interpreted as being consistent with the theory that Aβ aggregation follows a nucleation-dependent pathway [42]. Several features characterize nucleation-dependent aggregation. First, there is no aggregation at peptide concentrations below *Cr* [42]. Second, at peptide concentrations that are higher than *Cr*, there is a lag time before aggregation begins [42]. Lag time is defined as the time before amyloid formation occurs during which the peptide remains soluble [42]. Finally, during the lag time, addition of a small amount of fibril seed results

(a)

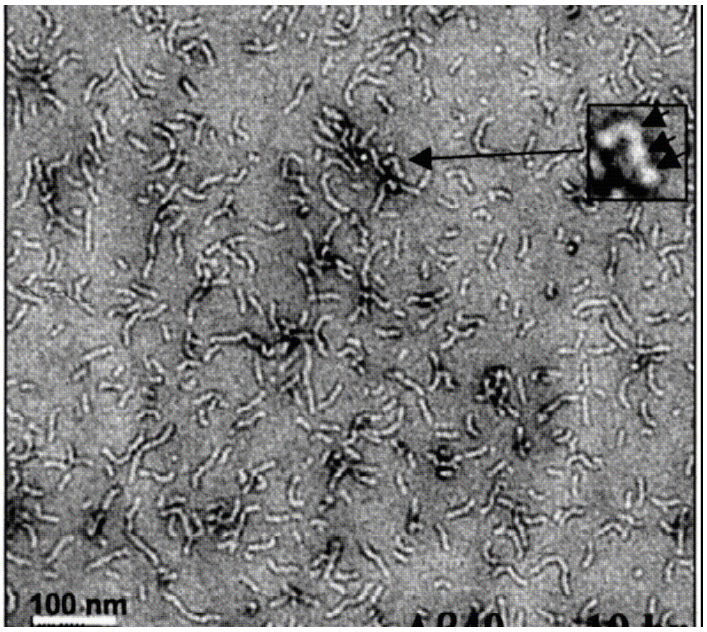

(b)

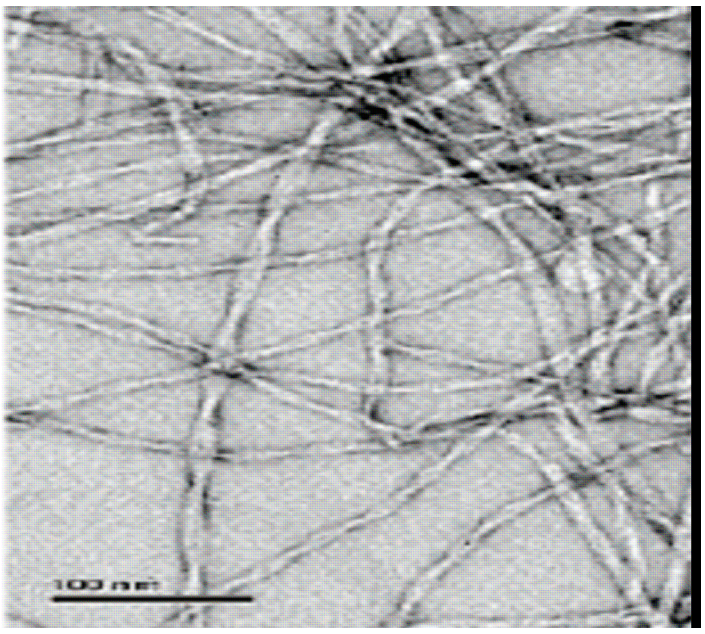

Figure 1.2. Electron micrographs of (a) Aβ protofibrils and (b) Aβ fibrils.

in faster aggregation. Nucleation-dependent aggregation is thermodynamically similar to micelle formation with respect to the critical concentration, but kinetically is much slower, possibly because the process is more complex, and there is a much greater entropic barrier to fibril organization [42].

There are thus three main steps involved in a nucleation-dependent pathway (see Figure 1.3) [42]. The first step involves conversion of the monomer peptide to a thermodynamically unstable "nucleus" that is presumed to be oligomeric. The nucleus is the least stable oligomer on the assembly pathway. Once the oligomeric nucleus contains more than the critical number of molecules, its continued growth leads to formation of more stable aggregates, featuring progressively less and less tendency to dissociate to monomer. This step is the rate-limiting step. After the formation of this "critical nucleus" comes the "elongation" step of the pathway. During this step, where addition of further monomers is thermodynamically favorable, rapid extension of aggregates occurs according to pseudo-first order kinetics (first order in both monomer and fibril growing ends, with the latter unchanging over the course of the reaction). The final phase of the pathway occurs when the peptide monomer is depleted to the point where fibril growth and dissolution are in a dynamic equilibrium.

Although fibrillization of both Aβ(1-40) and Aβ(1-42) is nucleation-dependent, the pathways are distinct, thus generating different types of oligomers. Teplow and colleagues found that at the earliest stage of monomer oligomerization, Aβ(1-40) exists as monomers, dimers, trimers, and tetramers, in rapid equilibrium, while Aβ(1-42) preferentially forms pentamer/hexamer units that assemble further into larger oligomers and protofibirils [49]. Recently it has also been found by using solid-state NMR and EM that Aβ(1-40) fibril morphology and molecular structure is sensitive to growth conditions, which suggests the existence of at least two distinct fibril nucleation mechanisms for Aβ (1-40) depending on growth conditions [37]. One mechanism, leading to quiescent fibrils (growing in vertical dialysis tubes containing an unstirred bath of buffer), may be purely homogeneous. The other mechanism, leading to agitated fibrils (growing in horizontal polypropylene tubes with gentle circular agitation using an orbital mixer), may depend on the interface between the peptide solution and the air or the walls of the sample tube.

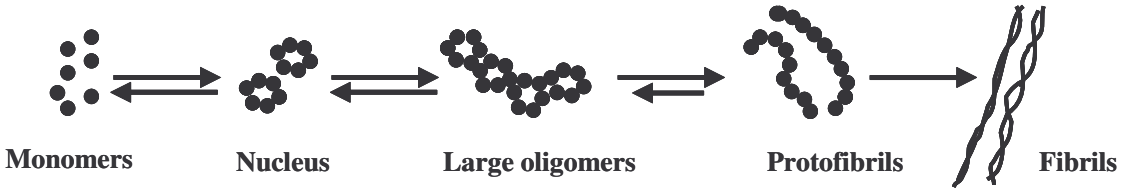

Figure 1.3. Schematic presentation of Aβ fibril formation (not to scale). Aβ fibrillogenesis is a nucleation-dependent polymerization process in which monomeric Aβ forms oligomeric nuclei, and further large oligomers from which protofibrils emanate. These protofibrils give rise to full-length fibrils.

Therefore, the molecular structure of Aβ(1-40) fibrils is not determined solely by amino acid sequence and is not purely under thermodynamic control [37].

Fibril growth is more complex *in vivo*, however. For instance, factors such as chemical damage and binding of other proteins can render fibrils resistant to dissociation [42]. For example, apolipoprotein E2 (ApoE2) is an endogenous protein that has been shown to inhibit amyloid fibril formation [42]. Also, cellular concentrations of Aβ are much lower *in vivo* (in the nanomolar range) than those typically used *in vitro* (in the micromolar range), which makes it unclear how nucleation can occur *in vivo* [42]. It may be possible that nucleation occurs in cellular organelles supersaturated with Aβ, and fibrils formed in this way can then be released from the cellular compartment and act as seeds for additional fibril formation [42]. Alternatively, it is possible that the *in vivo* critical concentration is lowered by endogenous species. For example, zinc is able to induce the aggregation of Aβ at subnanomolar Aβ concentrations *in vitro* [42].

Amyloid fibril growth *in vitro* can be monitored by Thioflavin T (ThT) fluorescence assay [50]. ThT assay is widely used because of its sensitivity, selectivity and simplicity. ThT assay can be used to monitor spontaneous aggregation of either unseeded Aβ aggregates (nucleation and elongation phases of aggregation), or seeded Aβ aggregates (elongation phase of aggregation) in solution [51]. ThT is useful in that it fluoresces upon binding to amyloid fibrils but not to precursor polypeptides, monomers, or protofibrils.

1.1.3 Structure and Assembly of Aβ Amyloid Fibrils and Protofibrils

Aβ Amyloid Fibrils

Knowledge of the three-dimensional structure of amyloid fibrils has great bearing on our understanding of how the fibrils are formed and on the rational design of therapeutics. However, progress toward high-resolution structure analysis of aggregates using X-ray crystallography or solution-state multidimensional nuclear magnetic resonance (NMR) spectroscopy has been slow and fraught with difficulties [5], due to the insolubility, heterogeneity and noncrystalline nature of the fibrils.

Our current understanding of amyloid structure is based on studies at relatively low resolution. EM and AFM show that fibrils produced by many proteins are 6-12 nm in diameter and several μm in length and are composed of a number of smaller (3-4 nm diameter) protofilaments twisted about each other along the fibril axis (Figure 1.2b) [44, 52]. Circular dichroism of nascent fibril formation reactions shows an increase in β-sheet content with Aβ incubation [53], and solid state infrared spectroscopy confirms the high β-sheet content of fibrils themselves [54]. X-ray diffraction studies also indicate that amyloid fibrils are rich in β-sheet, and further show that fibrils are organized in such a way that the β-sheets run perpendicular to the long axis of the fibrils while the hydrogen bonds between β-sheets are parallel to the axis [55] (Figure 1.4). Fibrils grown *in vitro* were indistinguishable by EM from those found in neuritic plaques [42].

Amyloid fibrils from the peptide Aβ have been a major focus of structural studies. Unfortunately, the structural roles of specific amino acid residues in the Aβ sequence remain unclear. However, a number of low-to-medium resolution methods have provided valuable insights into Aβ fibril structure, based on studies of fibrils grown *in vitro* in aqueous solutions [40, 56-71]. This information places significant constraints on the types of models that can be constructed for Aβ fibrils.

Some of these constraining insights have come from work in our group. For example, using the hydrogen/deuterium exchange mass spectrometry (HDX-MS) technique, Kheterpal et al. showed that ~ 50% of the 39 backbone amide hydrogens of Aβ(1-40) are not involved in protective hydrogen bonds associated with a β-sheet when this peptide is incorporated into the fibril structure [58-59]. Several other experiments on intact fibrils, including limited proteolysis [60], scanning proline mutagenesis analysis [40], hydrogen/deuterium exchange nuclear magnetic resonance (HDX-NMR) [61], scanning cysteine mutagenesis analysis [62] and scanning alanine mutagenesis analysis [63], confirm this, demonstrating that the N-terminal 13–16 residues of the Aβ (1–40) peptide are excluded from the packed fibril and therefore cannot be involved in the H-bonded core structure. Other groups have interpreted solid state NMR [64], electron paramagnetic resonance spectroscopy (EPR) [65], reductive alkylation [66], HDX-MS

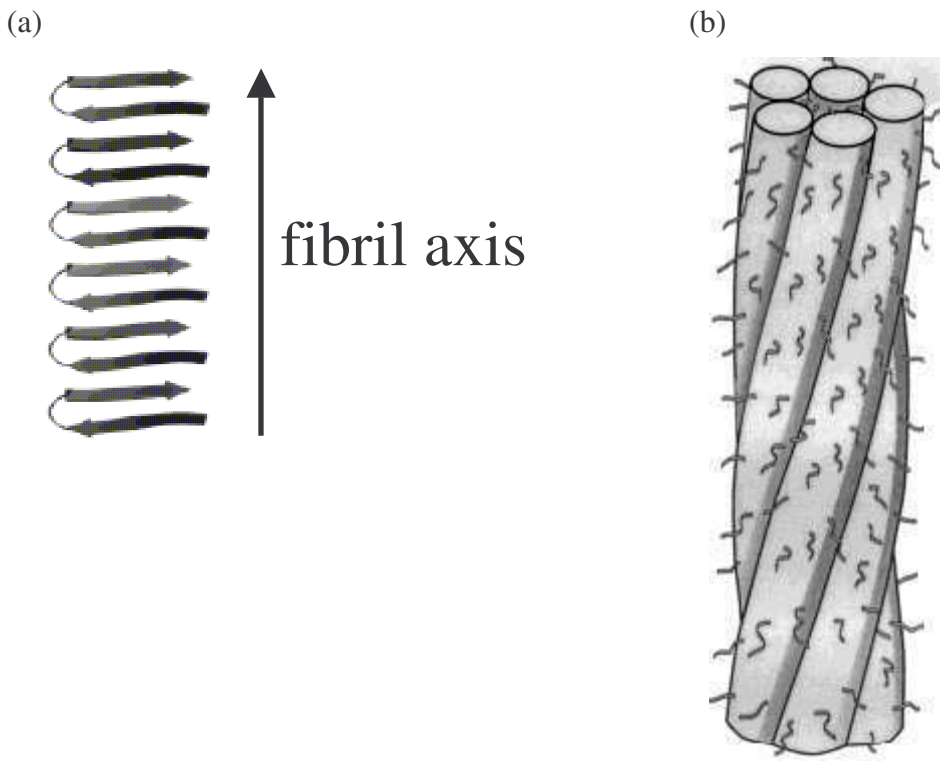

Figure 1.4. Illustrative diagrams shows (a) that the continuous, hydrogen-bonded parallel β-sheets run perpendicular to the long axis of the fibrils while the hydrogen bonds between β-sheets are parallel to the axis; (b) that bundles of protofilaments twist about each other along the fibril axis to make fibrils. The pitches emerging from the protofilaments are Aβ termini which are assumed not to be involved in the fibril structure. (Reproduced from Ref. [60])

coupled with off-line proteolysis [67] as well as other methods [68-71] to suggest a flexible N-terminal segment. Consistent with all this experimental evidence, N-terminal truncated variants of Aβ are found in amyloid plaques [5]. Consequently, the composition of the N-terminus is considered not to be critical for amyloidogenesis. On the other hand, there is disagreement on whether the C-terminus is involved in an extended β-sheet structure. Data from fluorescence quenching [72], EPR [65], scanning proline mutagenesis [40], scanning cysteine mutagenesis [62], scanning alanine mutagenesis [63], HDX-NMR [61] and HDX-MS coupled with off-line proteolysis [67] indicate that portions of the C terminus have considerable mobility. In contrast, results from reductive alkylation [66] and solid state NMR [64] suggest that portions of the C-terminus are significantly protected in the fibril.

Based on such experimental observations, many models for Aβ fibrils have been proposed [40, 63-65, 72-87]. These models are consistent with the diameter of the protofilaments and fibers and the cross-β sheet structure described above. While these models differ in many structural details (such as the structure of protofilament and in the assembly of protofilaments to form mature fibrils), they generally include antiparallel or parallel β-sheets. Antiparallel β-sheet appears to dominate amyloid fibrils made of short (less than 40 amino acids) Aβ peptides [76, 79-80]. Some models for Aβ(1-40) and Aβ(1-42) fibrils which were based on antiparallel β-sheet structures [75, 77-78, 86] are at variance with experimental intermolecular distance constraints [88-90]. Other models including a β-hairpin centered in residues 24–29, with intramolecular hydrogen bonding between β-strands on either side of a β-turn [75, 77, 85-86] are incompatible with the in-register parallel intermolecular alignment determined experimentally [88-90].

Compelling evidence from solid state NMR [64, 87], liquid suspension EPR [65], scanning proline mutagenesis [40, 74], scanning cysteine mutagenesis [62], and scanning alanine mutagenesis [63] studies on Aβ(1-40) fibrils suggests that the peptides in the fibril core are in an in-register, parallel arrangement. However, there is no consensus on a unique structural model for the fibril-folding motif, and in fact a number of models involving parallel β-sheets have been proposed [63-65, 73, 70-83]. The linear parallel

model of Aβ(16-35) [72] or Aβ(10-35) [81-83], with polar residues in the middle of the peptides, appears unfavorable based on molecular dynamics simulation experiments by Ma and Nussinov [84]. A growing body of evidence suggests the existence of turn(s) in the middle of the peptide [40, 63-65, 74-78, 91]. For example, solid state NMR reveals a possible non-β-strand region between residues 25 and 29 [64]. Kinetics analysis of fibril formation with proline replacements in Aβ(1-42) at positions 19-26 (one residue at a time) suggests a possible turn region at positions 22 and 23 [91]. Thermodynamic analysis of the stabilities of fibrils derived from proline mutants of Aβ(1-40) implicates two turn regions at residues 22-23 and 29-30 within a β-sheet-rich core region involving residues 15-36 [40, 63]. In what follows, a detailed description of the three latest models for Aβ(1-40) fibrils (parallel β-sheets) will be presented.

Torok *et al.* proposed a model based on EPR analysis of site-directed spin-labeled Aβ(1-40) fibrils (grown under agitation) [65]. The strategy involves spin-labeling specific cysteine residues, which is remarkably well tolerated in proteins. They identified three regions of Aβ(1-40) fibrils: a central region of pronounced parallelism between separate Aβ molecules from approximately residue 14 to 38, a more disordered N-terminal region with less specific parallelism, and a short C-terminal stretch where little parallelism could be detected. This data indicated that a turn may be located at residues 23-26.

Petkova *et al.* presented a structural model for Aβ(1–40) amyloid fibrils (grown under agitation) based on a set of experimental constraints from solid-state NMR spectroscopy [37, 64, 87]. According to this model, approximately the first 9 residues of Aβ (1–40) are structurally disordered in the fibrils. Residues 10–22 and 30–40 adopt β-strand conformations and form parallel β-sheets through intermolecular hydrogen bonding. Residues 23–29 contain a bend of the peptide backbone that brings the two β-sheets in contact through side chain-side chain interactions. A single cross-β unit is then a double-layered β-sheet structure with a hydrophobic core and one hydrophobic face. The only charged side chains in the core are those of Asp23 and Lys28, which form intramolecular salt bridges. Fibrils with minimum mass-per-length and diameter consist

of two cross-β units with their hydrophobic faces juxtaposed. This four-layered β-sheet structure has both "internal" (between β-sheets within a single molecular layer) and "external" (between β-sheets in different molecular layers) quaternary contacts [87]. The internal quaternary contacts are between side chains of L17 and F19 and side chains of I32, L34, and V36, while the external quaternary contacts are between the side chain of I31 and the peptide backbone at G37, and between the side chain of M35 and the peptide backbone at G33 [87].

Our group proposed a model based on scanning proline mutagenic analysis of Aβ(1-40) fibrils (grown under quiescent conditions) (Figure 1.5) [40, 74]. Scanning proline mutagenic analysis involves the introduction of a β-sheet-breaker - proline residue into amyloidogenic polypeptides and then analyzing the thermodynamic stabilities (based on ΔΔG calculated using *Cr* values of wild type (WT) and mutant fibrils; $\Delta\Delta G = -RT \times \ln[Cr^{WT}/Cr^{mutant}]$) of amyloid fibrils formed from these single proline mutants [40]. The results show that the N-terminal 10-15 residues and the C-terminal residues 37-40 of Aβ(1-40) are not involved in the H-bonded core structure of the fibril. Besides indicating that it is the 15-36 sequence of Aβ that is involved in ordered, proline-sensitive structure within the amyloid core, these data also suggest the existence of two turn regions within the 15-36 segment, one at residues 22-23 and one at residues 29-30, which are not sensitive to proline replacement. This model agrees with the results from the molecular dynamics simulations of the segment 15-36, which suggest a six-layered parallel β-helical structure for Aβ(1-40) amyloid fibrils [74]. The model was further corroborated and refined by the following data generated by our group. HDX-NMR data indicate that Aβ(1-40) fibrils have solvent-accessible N-terminal and C-terminal amino acids, and two expanses of protective structure centering around residues 15-23 and residues 28-35 [61]. Moreover, the data suggest the residues at 25 and 26 are freely exchangeable. Investigation of the orientations and spatial proximities of the amino acid side chains in the amyloid core region was achieved by using double cysteine mutagenesis analysis [93]. The results (obtained from analysis of three double cysteine mutants (Leu17/Leu34, Leu17/Met35 and Leu17/Val36)) support models of Aβ(1-40)

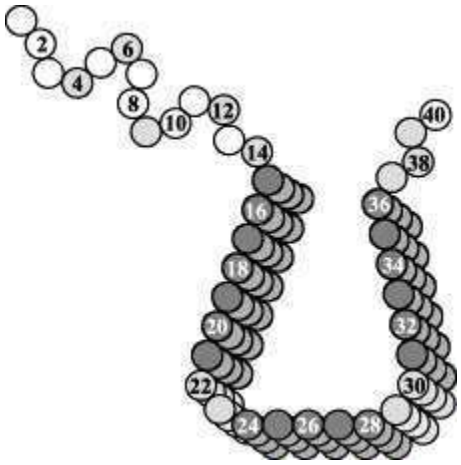

Figure 1.5. A working structural model of Aβ(1-40) fibrils. The chain of circles containing residue numbers represents one Aβ molecule, with residues 1–14 and 37–40 shown as disordered elements, sequence elements 15–21, 24–28, and 31–36 shown as highly structured elements, and residues 22, 23, 29 and 30 shown in turns. The 15–36 sequences of additional Aβ molecules are shown stacked in the H-bonding direction parallel with the fibril axis. (Reproduced from Ref. [40]).

fibrils in which the Leu17 and Leu34 side chains of the same peptide pack against each other at the β-sheet interface within the amyloid core [93]. More recent results from scanning cysteine mutagenesis analysis not only confirm the lack of structure in the N-terminus and C-terminus, but also indicate that residues 16-19 and 31-34 are likely packed into a hydrophobic amyloid core and residues 20, 30, and 35 are located in solvent exposed structure [62]. Still more recent results from alanine mutagenesis analysis suggest disordered N-terminus and C-terminus, H-bonded 16-21 segment and rigid structure (not H-bonded structure) within the 24–30 segment as well as the structural plasticity (ability of adjusting to packing changes) of Aβ amylid fibrils [63].

The models described above differ in some significant details (Table 1.1). Part of the differences may be due to limitations of experimental data and analysis; and part due to their being based on experiments conducted on different fibril conformers [37]. The recent discovery of growth condition-dependent conformational variants of Aβ(1-40) amyloid fibrils (agitated fibrils vs. quiescent fibrils) [37] complicates the goal of arriving at a consensus fibril structure derived from comparison of the literature data, since these data are based on fibrils prepared in a variety of ways. It also introduces the questions of how many other conformational variants of Aβ(1-40) might be accessible to this peptide, and which of these several form(s) might best represent the conformation of amyloid fibrils that is biologically relevant to brain neuritic plaques. So far, there is little information available concerning these uncertainties.

The goal of studying Aβ amyloid fibrils is to decipher the structure and structural energetics of amyloid fibrils similar to those located in the neuritic plaques in Alzheimer's disease brains. For every specific fibril conformer, significant insight into structure could be derived from a knowledge of the hydrogen bonding patterns within fibrils and the number of residues that make up the rigid core of the fibril structure. As described in details later in this chapter, hydrogen/deuterium exchange mass spectrometry (HDX-MS) can provide information about the number and location of residues within the Aβ peptide involved in intramolecular and intermolecular hydrogen bonding. Information on the secondary structural role of a particular sequence element along a fibril-incorporated peptide could be used to test model predictions of particular

Table 1.1. Summary of some models for Aβ amyloid fibrils.

Sequences Studied	Methods	Conformation	Core Structure	Ref.
1-43, 2-43, 4-43, 8-43, 9-43, 10-43, 12-43, 10-42, 10-23, 29-42	IR, limited proteolysis	Anti-parallel β-sheet	β- strand: residues 10-42 β-turn: residues 26-29 Disordered: residues 1-9	[85]
14-42, 14-23	Substitution studies, EM, Molecular modeling	Anti-parallel β-sheet	β-strand: residues 14-23 and 27-40 β-turn: residues 24-26	[76]
12-42	Synchrotron x-ray diffraction, molecular dynamics simulation	Anti-parallel β-sheet	β-strand: residues 12-24 and 29-40 β-turn: residues 25-28	[75]
10-35	Solid-state NMR, EM, Small angle neutron scattering	Parallel β-sheet	β-strand: residues 10-35	[81-83]
16-22, 16-35, 10-35	Solid-state NMR, Molecular Modeling, Molecular dynamics simulation	Parallel β-sheet	β-strand: residues 10-23 and 28-35 β-turn: residues 24-27	[84]
1-40, 1-42	Site-directed spin labeling EPR	Parallel β-sheet	β-strand: residues 14-22 and 27-38 β-turn: residues 23-26 Disordered region: residues 1-13 and 39-40	[65]
1-40	Solid-state NMR	Parallel β-sheet	β-strand: residues 12-24 and 30-40 β-turn: residues 25-29	[37, 64, 87]
1-40	Scanning proline mutagenesis analysis, Molecular dynamics simulation	Parallel β-helix	β-strand: residues 15-21, 24-28 and 31-36 β-turn: residues 22-23 and 29-30 Disordered region: residues 1-14 and 37-40	[40, 63, 74]

fibril conformers and to assemble improved models of specific amyloid fibril structure. In this dissertation, the studies were focused on quiescent Aβ(1-40) fibrils (and protofibrils) grown in the physiological conditions of phosphate-buffered saline buffer at 37 °C without agitation.

Protofibrils

As mentioned earlier, recent focus has been on the possible role of non-fibrillar, oligomeric states of Aβ in the disease mechanism [30-36]. Therefore, the knowledge of the three-dimensional structure of protofibrils is also critical for understanding the mechanism of how Aβ transits from soluble forms to insoluble β-sheet-rich conformers and hence for the design of possible inhibitors. In contrast to mature fibrils, however, much less is known about the molecular architecture of protofibrils and oligomers, which are particularly challenging to study due to their metastable, transient nature and their diverse morphologies [93]. They exhibit little or no response to thioflavin T [94], a poorly understood fluorescent probe for amyloid structure that is generally considered a probe of β-sheet structure. A lack or deficiency of β-sheet structure would be consistent with early models of Aβ oligomers as possessing a micelle-like structure [95] driven by the polar nature of the Aβ peptide, which possesses a hydrophobic C-terminus and a hydrophilic N-terminus. It would also be consistent with a degree of α-helical content in protofibrils, suggested by the transient appearance of α-helix in Aβ fibril formation reactions [96].

More recent studies from our group using HDX-MS capable of obtaining some data from metastable oligomeric assemblies suggest the possibility that normally isolated Aβ protofibrils might also possess some very highly stable H-bonded structure [93]: about 40% of the 39 backbone amide protons was protected from exchange. In fact, the presence of β-sheet structures was indicated by circular dichroism studies [31, 93]. Scanning proline mutagenesis analysis suggests that Aβ protofibrils (stabilized by calmidazolium chloride (CLC), Figure 1.6) contains H-bonded β-sheets, involving the same hydrophobic patches 16-21 and 30-36 as involved in fibril structure [94]. Moreover, in both fibrils and protofibrils, the N-terminal 14 residues and the C-terminal

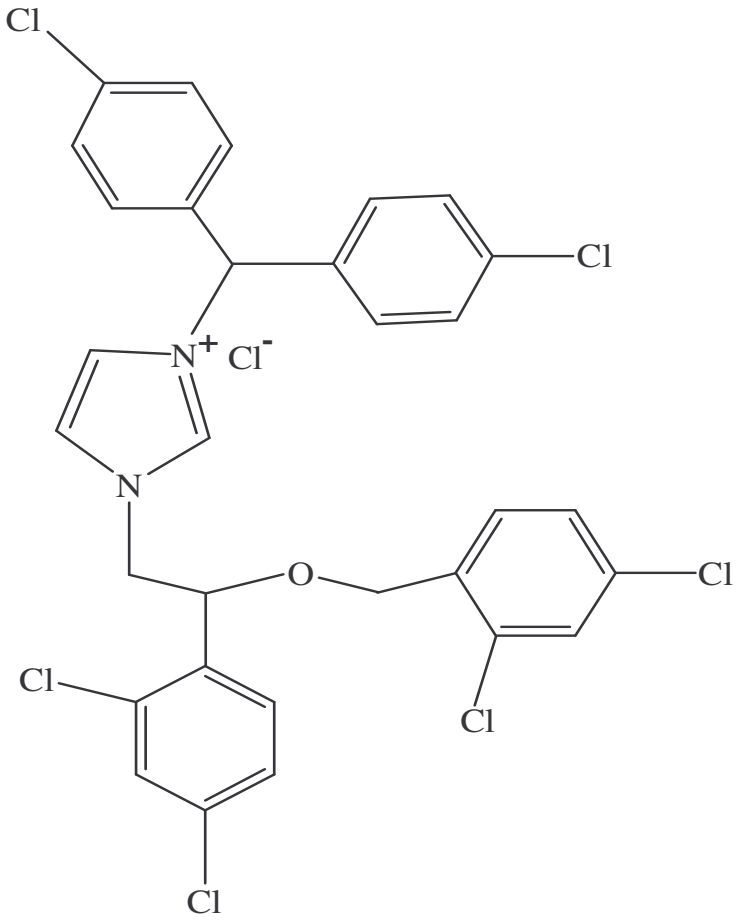

Figure 1.6. The structure of calmidazolium chloride.

3-4 residues seem uninvolved in the kind of rigid structure disrupted by proline substitution [94]. It seems that the major difference between protofibrils and fibrils lies in the 21-30 segment [94]. It is likely that protofibrils have a simple extended hairpin structure with a long, relatively flexible loop, involving residues 22-29, spanning the two β-structure segments [94].

Further progress in the analysis of Aβ protofibrils and their structural relationship to mature fibrils requires progress on two fronts: methods to stabilize protofibrils to facilitate biophysical studies, and methods to provide structural information at segmental, and ultimately, single residue, resolution. The first goal was achieved in our group through the discovery of the small organic molecule - calmidazolium chloride (CLC) (Figure 1.6), which not only accelerates the formation of Aβ protofibrils, but also stabilizes them against progress to mature fibrils [94]. The second goal can be realized through HDX-MS, in which segmental exchange information can be obtained by proteolysis before MS analysis (discussed in Chapter 4).

1.1.4 Inhibition of Amyloid Fibril Aggregation

AD is a disorder for which symptomatic treatments are available. As discussed in the previous sections, the amyloid hypothesis, which claims accumulation of Aβ in the brain is the primary influence driving AD pathogenesis, has been formally articulated and supported by a wealth of studies from many laboratories worldwide over the past 10 years [5, 97-99]. Therefore, the development of anti-Aβ therapeutics remains a rational approach to treating AD. Several therapeutic approaches have been identified which target the production, the aggregation or the clearance of Aβ (Table 1.2) [100-101]. At present, it is not known whether any approach will prove to be effective.

Inhibition of Aβ aggregation is a very appealing target for drug design [46]. Studies have shown that Aβ immunization in a murine model (model derived from mice) of AD reduces both the level of fibrillar Aβ deposition in the brain and the level of cognitive decline [124]. These findings suggest that there is a link between Aβ aggregation/deposition in the brain and congnitive decline in AD. Therefore, screening libraries of compounds for inhibitors of Aβ aggregation and/or deposition could lead to

Table 1.2. Potential anti-amyloid aggregation therapeutics.

Potentially therapeutic agent	**Molecular Target**	**Biological Consequence**	**References**
Secretase inhibitors	β-secretase, γ-secretase	Decrease Aβ production	[102-104]
Active/passive immunization	Aβ	Inhibit Aβ deposition , Enhance Aβ clearance	[104-107]
Non-steroidal anti-inflammatory agents	γ-secretase	Lower Aβ(1-42) production, Increase Aβ(1-38) production	[108-110]
Anti-aggregation compounds	Aβ	Inhibit oligomerization and fibrillogenesis	[111-115]
Secretase activator	α-secretase	Lowering Aβ production by enhance α-cleavage	[116-118]
Activators of Aβ-degrading enzymes	Aβ-degrading enzymes	Increase Aβ degradation and clearance	[119-121]
Metal chelators	Aβ	Solubilization of Aβ deposits and prevention of aggregation by metalchelation	[122-123]

the discovery of novel drug candidates for treating AD. Interpretation of the results of such screening is complicated, however, due to uncertainty about what the toxic aggregate is (i.e the possibility that an intermediate on the fibril assembly pathway may be the toxic species, while mature amyloid fibrils may actually be protective) [17]. Thus, it seems reasonable that drug design strategies that target Aβ production may also be a viable therapeutic approach [51]. Since Aβ generation depends on the proteolytic cleavage of APP by β- and γ-secretase (as mentioned previously), these enzymes are targets for the development of novel protease inhibitors for AD. However, it has been reported that β- or γ-secretase inhibitors induced death in rodent and human neuronal cell lines [125]. This highlights the challenge to identify non-toxic drug candidates for clinical trials, in particular with a view to target prevention. Moreover, it should be realized that Aβ has a widespread distribution through the brain and body, even in cognitively normal individuals, and soluble Aβ serves a variety of physiological functions, including modulation of synaptic function, facilitation of neuronal growth and survival, protection against oxidative stress, and surveillance against neuroactive compounds, toxins and pathogens [126]. Caution needs to be exercised when developing therapeutic strategies to remove Aβ from the brain. Ideally, such strategies should target forms of Aβ that are not bioavailable, such as fibrillar Aβ, or forms that are thought to be over-expressed in Alzheimer's disease (such as oligomers) while leaving normal soluble Aβ(1–40) and Aβ(1–42) intact. Finally, AD is an extremely complicated neuronal degeneration disease. Our knowledge of the causes of the disease, of the mechanisms of disease onset and progression is still not mature. Therefore, many issues remain to be resolved in order to discover more promising therapies.

1.2 Mass Spectrometry

Mass spectrometry (MS) is emerging as an extremely important tool in biochemical research capable of analyzing small and large molecules. Analytical

chemists have added fresh impetus to bioresearch with two revolutionizing mass spectrometry soft ionization tools, electrospray ionization (ESI) and matrix-assisted laser desorption/ionization (MALDI). Commercial availability of these technologies has made routine the analysis of compounds including proteins, peptides, carbohydrates, oligonuleotides, natural products, and drug metabolites, offering picomole to femtomole sensitivity and enabling the direct analysis of biological fluids with a minimum amount of sample preparation. MS allows for the analysis of small and large biomolecules through "mild" desorption and ionization methods. Their utility now extends beyond simple molecular weight characterization. Nonconvalent interactions, protein and peptide sequencing, DNA sequencing, protein folding, in vitro drug analysis, and drug discovery are among the areas to which mass spectrometry is being applied. Rapid technical developments in the areas of front-end sampling devices, ionization techniques, mass analyzers, and data analysis software will ensure that MS will play an even greater role for biophysical studies of proteins in the near future.

1.2.1 ESI-MS

ESI-MS Overview

Electropspray ionization (ESI) is an atmospheric-pressure ionization method that produces small charged droplets from a liquid medium under the influence of an electric field [127-134]. The first attempt to use electrospray (ES) as an ionization source for generating gas-phase ions can be traced to the analysis of the molecular weights of synthetic polymers (e.g. polystryrene) with electrospray/drift-tube experiments, and achieved some limited success [135-136]. On a parallel track, the work by Evans and Hendricks [137] and the Cook group [138] led to establishment of electrohydrodynamic ionization MS in which the field prompts ion desorption directly from the meniscus into vacuum. The greatest success of ESI is attributed to the creative work by Fenn and co-workers [139-141] and Alexandrov and co-workers [142] since 1984. ES MS has since become one of the most powerful techniques for the anlaysis of biomolecules [139].

Figure 1.7 is a schematic diagram of a typical ESI-MS system in which the electrospray ion source at atmospheric pressure is interfaced with a mass analyzer

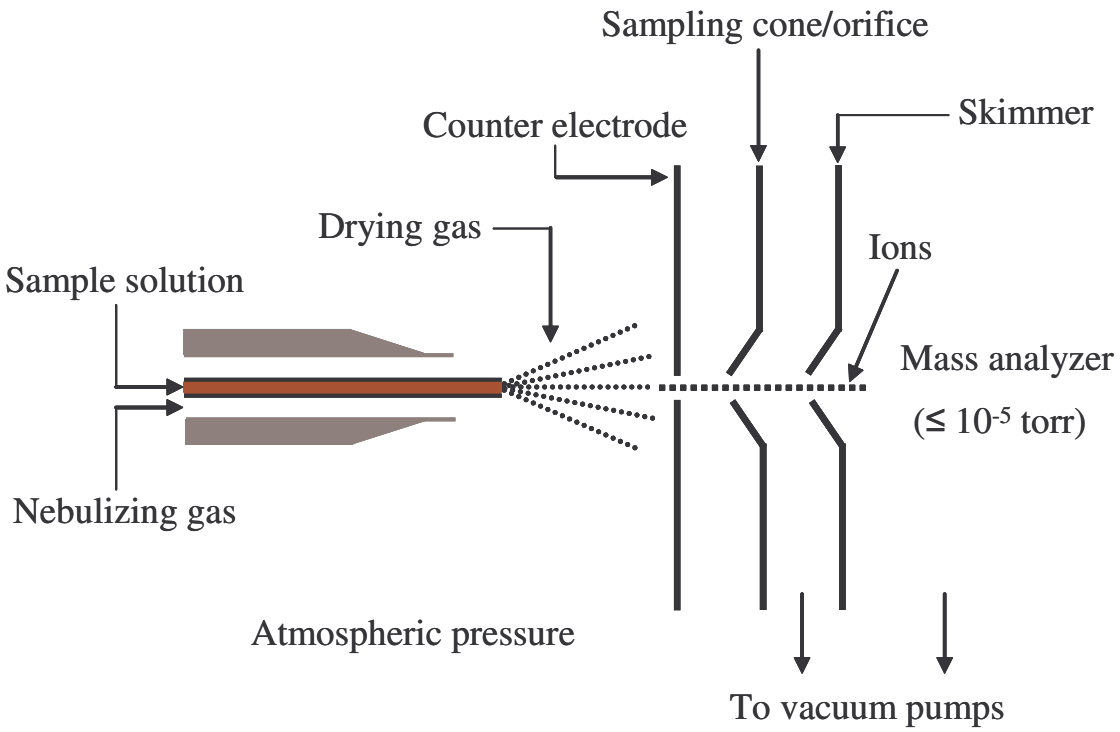

Figure 1.7. Schematic diagram of a typical ESI-MS system.

through a gently heated sampling optical system (usually an orifice and skimmer) which is maintained at reduced pressure (typically ~10^{-3} torr). The use of a drying gas and/or counter-current gas in the ESI-MS interface is a key leading to production of dry ions by eliminating ion re-solvation and ion cluster formation [141]. Sampling is accomplished by applying high voltage (e.g. 3 - 6 kV) to the ES emitter (typically a metal tip). Sample solution at a low flow rate (typically 1-10 µl/min) is introduced through a silica capillary into the emitter. When the electric field is applied, the emerging liquid containing sample ions is dispersed as a fine spray of charged droplets. The charged droplets further subdivide into smaller "offspring" droplets as a result of solvent evaporation and coulombic repulsion [143]. At some stage, ions are desorbed from small droplets into the gas phase. The ions are directed into an orifice through electrostatic lenses leading to the MS analyzer. Since ESI is usually operated under mild conditions (e.g. moderate electrostatic field, gentle heating and atmospheric pressure at the ion source), deposition of energy to the molecular ions is usually low. Therefore, intact molecular ions with little or no fragmentation can be readily detected.

The formation of gaseous analyte ions by ESI involves three main steps: formation of charged droplets, shrinkage of the droplets due to solvent evaporation, transfer of ions to the gas phase. Two models have been developed to describe the ESI process: the ion evaporation model [135] and the charge-residue model [144]. The *charged-residue model* predicts successive cycles of solvent evaporation and droplet fission at the Rayleigh limit, until an isolated ion is eventually produced. The *ion-evaporation model*, based on the transition-state theory, predicts direct ejection of ions to the gas phase from nm-size droplets before they reach the Rayleigh instability limit. To gain experimental evidence allowing a clear-cut discrimination between these two alternative mechanisms has represented a major challenge for researchers in this field [145-146]. However, recent reports suggest that small ions follow the behavior predicted by the ion-evaporation model, whereas desolvated macroions (e.g. charged proteins) are most probably formed according to the charge-residue mechanism [147].

Common Features of ESI-MS

Sampling ions from solution phase

Unlike MALDI which employs laser beams to desorb ions from a solid (crystal) matrix [148-149], ESI generates gas-phase ions from the liquid phase at atomospheric pressure, which is more like the natural state of most biological samples. This feature also makes ESI-MS particularly well suited for coupling with liquid phase separation techniques such as high performance liquid chromatography (HPLC) [150] and capillary electrophoresis (CE) [151] for analysis of complex biological samples.

Production of multiply charged ions

A distinctive and enabling feature of ESI-MS is the production of multiply charged ions from bio-polymer molecules [141]. Ion series corresponding to different charge states are usually distributed as a bell-shaped envelope. This feature can impact MS analysis in several ways. First of all, it lowers the m/z values of ions, allowing measurement of high mass with virtually any type of mass spectrometer such as quadrupole instruments. It also provides independent estimates of molecular weight from ions carrying different charges, thereby improving the precision with which molecular weight can be determined [152-153]. In addition, fragmentation of large molecular ions through collision-induced dissociation (CID) can be facilitated at high charge states due to high kinetic energy [154-156], which is essential for determination of biopolymer structures**.** Multiple-charged ions are also preferred for other newly-emerged fragmentation techniques such as electron capture dissociation (ECD) [157-158] and electron transfer dissociation (ETD) [159] because electron capture cross section is proportional to the square of the ion charge.

Tandem MS - CID

The fragment ions produced from intact biomolecular ions can be used to deduce the sequence of large biomolecules. A commonly employed technique in tandem MS (MS/MS) for ion fragmentation is CID. In a CID experiment, a precursor ion is mass-selected by mass analyzer 1 (MS1) and focused into a collision region preceding a second

mass analyzer (MS2). Inert gas such as N_2 or Ar is generally introduced into the collision region and collisions occur between the precursor ion and inert gas atoms (molecules). The major fragmentation channel of electrospray-generated multiply-charged polypeptide cations is the heterolytic cleavage of the peptide bond, yielding "*b*", "*y*" type fragments, as defined in Figure 1.8 [160].

Mass analyzers

In ESI-MS, different ion analyzers can be used. Most common ones are quadrupole [161], ion-trap [162], time-of-flight (TOF) [163], or Fourier-transform ion cyclotron resonance (FTICR) [164]. The newly emerged hybrid quadrupole-TOF (Q-TOF) instruments [165] are widespread because of their full scan sensitivity, good mass spectral resolution (> 8K) and mass accuracy (1-10 ppm), and the MS/MS ability to select and fragment analytes using CID.

Solvent Characteristics

In conventional ESI-MS, the flow rate, applied voltage, conductivity, and liquid surface tension must be properly balanced in order to accomplish the formation of a stable ES spray. As for the solvent, besides its volatility, its surface tension should be within the range that facilitates the generation of a stable spray. It is generally easy to create a stable spray in the positive ion mode with conductive solutions that have at least 50% of a moderately polar organic solvent such as methanol or acetonitrile, and with the rest of the solvent being water [166-171]. As the solution becomes more aqueous, its surface tension increases, and it becomes increasingly more difficult to adjust the ES parameters such that a stable spray can be achieved. In some cases, however, organic content above about 80% can actually result in a decreased ES response [172]. This decrease in response is likely due to the liquid surface tension being decreased below the ideal for maximum spray stability. On the other hand, it is also difficult to achieve stable ES operation with nonpolar liquids [173] such as hexane or trichloromethane, due to their very low surface tension, high volatility, and low dielectric constant. Because spray dynamics are highly dependent on instrumental parameters, the percentage of organic

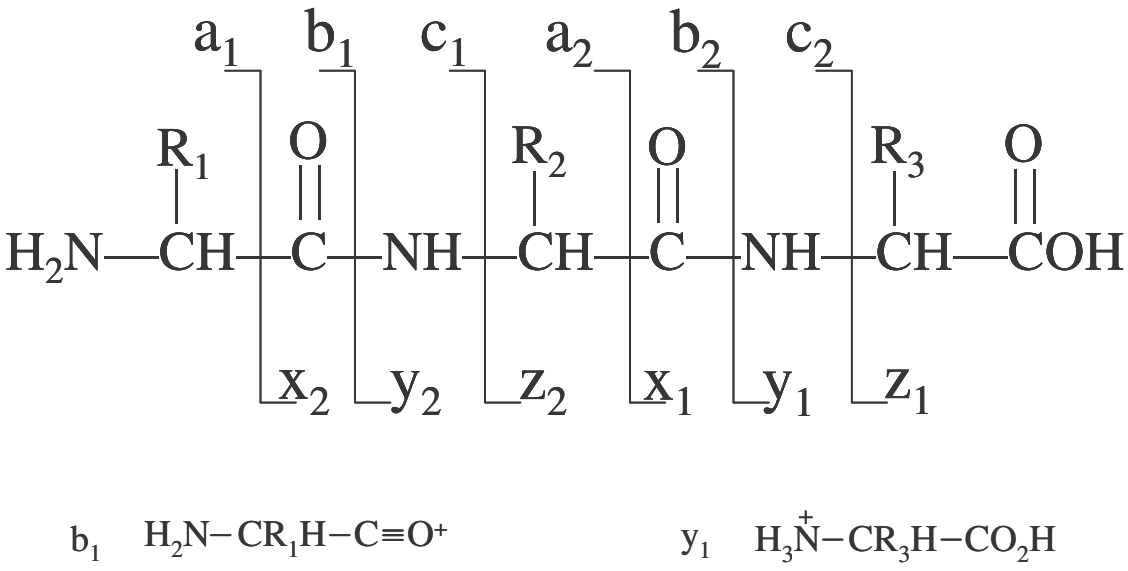

Figure 1.8. Nomenclature of polypeptide chain fragmentation.

content that maximizes ES response will vary, depending on the parameters chosen. Worth noting is that non-covalent interactions and protein conformations may be affected by the incorporation of organic solvents. It is also worth noticing that nanospray can be used to spray pure aqueous solutions from an emitter with an i.d. of ~1-3 μm (as compared with the 100 um i.d. capillary used in conventional ES) at as low as 0.2 nl/min [174-176]. This technique not only reduces the consumption of samples, but also enhances the concentration sensitivity due to higher ionization and/or sampling efficiency [177].

ES ion source as a constant-current electrolytic cell

As mentioned previously, generated gas-phase ions in the ESI source are guided to the counter electrode by the electric field. This flow of ions is collected as a current i_{ES} (equivalent to the rate at which charge leaves the capillary in the form of charged droplets) [130], as shown in Eqn. 1.1:

$$i_{ES} = [(4\pi/\varepsilon)^3 (9\gamma)^2 \varepsilon_0^5](\kappa E)^{3/7} v_f^{4/7} \qquad \text{Eqn. 1.1}$$

where ε and ε_0 are respectively the permittivity of the solvent and the permittivity of the vacuum, γ is the surface tension of the solvent, κ is the conductivity of the solution, v_f is the flow rate, and E is the imposed electric field at the metallic tip [143, 178-179]. The above equation is based on the experimental results of Pfeiffer and Hendricks [134] on electrohydrodynamic spray, and later supported by semi-empirical derivations [131, 180-182]. If the counterelectrode is large and planar, the electric field E is expressed as in Eqn. 1.2:

$$E = \frac{2V}{r \ln(4d/r)} \qquad \text{Eqn. 1.2}$$

where r is the capillary outer radius, V is the applied electric potential and d is the distance from the capillary tip to the counter-electrode [130, 183-184]. The electric field strength is typically ~10^6-10^7 V m^{-1} [130, 184]. From Eqn. 1.1 and 1.2, one can concluded that that the ES current will increase with increasing applied potential which was shown by Kebarle and Tang [143]. However, de la Mora et al derived and experimentally verified an equation [185], where ES current was independent of the

applied voltage as shown in Eqn. 1.3:

$$i_{ES} = f(\varepsilon)(\gamma \kappa v_f \varepsilon_r)^{1/2} \quad \text{Eqn. 1.3}$$

where $f(\varepsilon)$ is a function of the solvent dielectric constant (it is roughly equal to 18 for $\varepsilon \geq$ 40, such as water and methanol) [185-186]. In Eqn. 1.3, it is seen that the charge production is proportional to the square root of the volumetric flow rate. Therefore, the excess charge available for a solute will increase as the flow rate increases. For sufficiently conducting solutions, the effect of the electric field can be neglected [182]. The magnitude of the ES current is typically not higher than a few hundred nA.

A phenomenon that has to be considered in order to fully understand ESI is its electrochemical nature. This ionization source can indeed be seen as a special kind of electrolysis cell, where the anode is the emitter and the counter electrode (usually the atmospheric sampling aperture plate or inlet capillary and the various lens elements and detector of the mass spectrometer) is the cathode (reversed polarity in negative ion mode) [178, 187-188] (Figure 1.9). The conduction through this cell is supported by the motion of the ions in the solution and then in the gas phase before reaching the counter electrode. In this electrochemical flow cell, the limiting step is the droplet ejection that determines the ES current (i_{ES}). From an electrochemical standpoint, the ES source can be considered as a controlled-voltage electrochemical cell, but since the resistance of the gas phase is very large (on the order of GΩ) and the charge separation process controls the current in the circuit, ES ion source is often called a controlled-current electrolytic (CCE) cell [187]. To sustain the production of charged droplets from the ES source, electrochemical reactions must occur at the conductive contact to the solution. Oxidation reactions in positive ion mode and reduction reactions in negative ion mode dominate at the emitter electrode, whereas reduction reactions in positive ion mode and oxidation reactions in negative ion mode dominate at the counter electrode. A brief list of the electrochemical reactions on the ES electrode is shown below.

In the oxidative mode

- Oxidation of metals like Cr and Fe present in the electrode. For example:

  $Cr \rightarrow Cr^{3+} + 3e^-$ (E^o = -0.74V vs. SHE [189]) Eqn. 1.4

  $Fe \rightarrow Fe^{2+} + 2\ e^-$ (E^o = -0.443V vs. SHE [189]) Eqn. 1.5

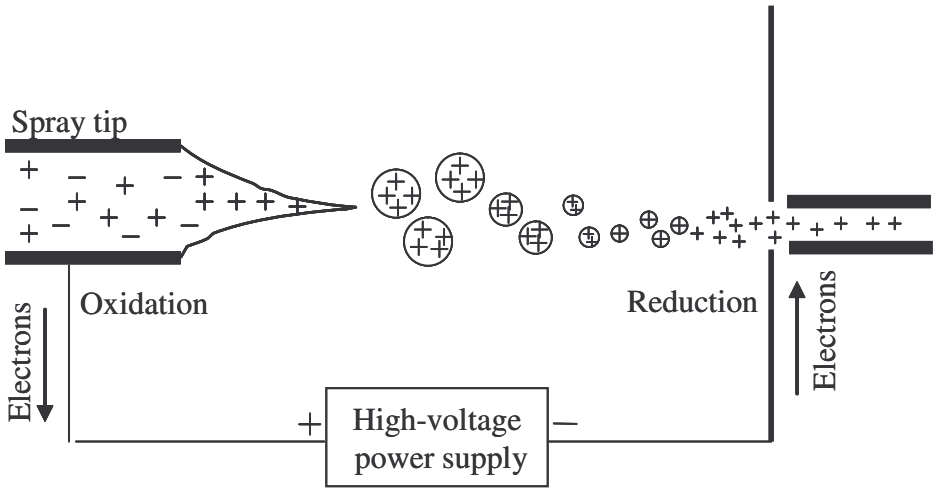

Figure 1.9. Schematic presentations of electrochemical processes in positive-mode ESI.

$Fe \rightarrow Fe^{3+} + 3\ e^-$ (E^o = -0.036V vs. SHE [189]) Eqn. 1.6

- Oxidation of solvents like water and methanol. For example:

$2H_2O \rightarrow O_2 + 4H^+ + 4e^-$ (E^o = 1.229V *vs.* SHE [189]) Eqn. 1.7

$2H_2O \rightarrow H_2O_2 + 2H^+ + 2e^-$ (E^o = 1.776V *vs.* SHE [189]) Eqn. 1.8

$H_2O \rightarrow O(g) + 2H^+ + 2e^-$ (E^o = 2.42 V *vs.* SHE [189]) Eqn. 1.9

- Oxidation of analytes and other solutes

In the reductive mode

- Reduction of solvent. For example:

$2H_2O + 2\ e^- \rightarrow H_2 + 2OH^-$ (E^o = -0.828V vs. SHE [189]) Eqn. 1.10

- Reduction of analytes and other solutes

The law of continuity of the current implies that the Faradaic current i_F associated with the oxidation of species from the electrolyte solution at the anode is always equal to the spray current i_{ES}. Those species with the lowest oxidation potential will be first oxidized, then if the current level is sufficient, compounds with a higher oxidation potential will then undergo oxidation, in order to keep the current flowing [178]. The Faradaic current is usually controlled by the diffusion of the reactants to the electrode, and is given by the following equation [169]:

$$i_{ES} = i_F = F\sum_i n_i C_i v \qquad \text{Eqn. 1.11}$$

where n_i is the number of electrons involved in the electrochemical reaction of one molecule of species i, C_i is the concentration of species i, v is the solution flow rate through the ES capillary, and F is the Faraday constant (96,485 C mol^{-1}).

Electrochemical events associated with ES ionization have been investigated by Van Berkel's group [178, 190-193]. The controlled-current electrochemical behavior, as well as the relation between the spray current and the applied electric field, proposed by Pfeifer and Hendricks (Eqn. 1.1) [130], were later confirmed experimentally by Van Berkel *et al.* [194], and Bateman [195].

The electrochemical reactions that take place in the ES emitter can alter the composition of the solution being electrosprayed [196-197]. These changes include modification in the mass or charge of the original analyte present in solution, changes in

solution pH through electrolytic H^+ or OH^- production/elimination, and/or the introduction/elimination of specific species to/from solution (e.g., introduction of Fe^{2+}, ions from corrosion of a stainless steel emitter) [198-199]. These reactions also include electrochemical ionization that can be exploited to ionize neutral and non-polar electroactive analytes that would otherwise go undetected in ESI-MS [200-202]. Reactions of the latter types might be troublesome for analyses involving unknown analytes or quantification. The ability to control the extent of any or all of these analyte electrochemical reactions would be an analytical advantage [178, 200, 202-204]. As far as the induction of pH change due to the electrochemical behavior of ES, the relevant concentrations of protons can be estimated from Eqn. 1.12 [197]:

$$[H^+]_e \, or \, [OH^-]_e = i_{ES} / n_i F \nu \qquad \text{Eqn. 1.12}$$

Where $[H^+]_e$ or $[OH^-]_e$ represent the eletrolytically generated excess concentrations and others are defined above. It was demonstrated that this shift could attain 4 pH units decrease in a non-buffered system [197]. As seen from Eqn. 1.12, this trend is highly dependent on flow rate and i_{ES}.

Regardless of the interface used, the electrochemical reactions need to be considered by the scientist in order to understand the properties of the ES source. Also, any mass spectrometrist should keep in mind that electrochemical processes involved in electrospray ionization are likely to induce changes in the analyte solution composition.

Corona Discharge

As mentioned previously, ES process is the dispersion of a liquid into electrically charged droplets and, as such, combines two processes: droplet formation and droplet charging. The formation of small, micrometer-sized drop does not present a problem if the liquid's flow rate, surface tension and electrolyte concentration are low. An increase in one or more of these variables makes it more difficult for the electric field to produce the desired charged aerosol for MS. The electric field strength at the sprayer tip can be increased to try to overcome the adverse effects of the aforementioned three variables, but too high an electric field will give rise to a corona discharge (electric discharge) accompanying the ES process.

Corona discharge in ES is a phenomenon that has been described by Yamashita and Fenn [139-141]. A corona discharge is a process by which a current develops between two high-potential electrodes in a neutral fluid, usually air, by ionizing that fluid so as to create a plasma around one electrode, and by using the ions generated in plasma processes as charge carriers to the other electrode. Corona discharge usually involves two asymmetric electrodes, one highly curved (such as the tip of a needle, or a narrow wire) and one of low curvature (such as a plate). The high curvature ensures a high potential gradient around one, for the generation of a plasma. Corona discharge depends on the applied voltage, and the size, shape and spacing of the two electrodes. In ES, when a high voltage is applied to the sharp tip of the electrode, a corona discharge is set up if the voltage gradient exceeds the dielectric breakdown threshold of the medium in the gap. Spray current is normally below 1 μA, while the discharge current quickly rises to 1 μA or more.

Corona discharge is particularly troublesome in the formation of negatively charged droplets. In the negative-ion mode, the sprayer tip is at a high negative potential with respect to other parts of the source, and field emission of electrons from the sharp spray needle or from the solution cone (the Taylor cone, [130, 205]) is a facile process. Electrons are accelerated by the electric field between the sprayer and the surrounding source walls and ionize the mixture of gases and solvent vapors in the source. The corona discharge can be quenched by the capture of electrons by means of an electron-scavenging gas, such as oxygen [140], N_2 doped with Freon [206], SF_6 [207], or the vapor of a chlorinated solvent [208].

1.2.2 MALDI-MS

MALDI was introduced in the late 1980s by the group of Hillenkamp [209-210]. A related concept was developed independently by Tanaka and co-workers at the Shimadzu Corporation in Kyoto, Japan [211]. Since MALDI is also a soft ionization method like ESI, it can be used to obtain molecular weights of biomolecules with little or no fragmentation [209-210]. In MALDI, the analytes are mixed with a solution of matrix, and the mixture is then co-crystallized on a target plate. A pulsed laser beam

irradiates the co-crystal on the target causing desorption and ionization of the matrix containing the sample molecules. The matrix absorbs the energy from the laser. Energy is subsequently transferred to the analyte that becomes desorbed into the gas phase. The ionization mechanism is not fully understood and several suggestions are still debated [212]. A diagram of the MALDI process is shown in Figure 1.10.

MALDI produces mainly singly charged ions, and this feature means it is excellently suited for analysis of complex biological mixtures such as protein digests [213]. The MALDI ionization process is less sensitive to salts than is electrospray ionization [214-215]. Nevertheless, salts and other impurities will cause peak broadening with the formation of adducts. This will lower mass accuracy and limit sensitivity [214-215]. Due to its pulsed nature, the MALDI source has traditionally been coupled to TOF mass analyzers, which have no theoretical upper limit to the m/z ratio. For example, biopolymers with a mass of >300 kDa can be analyzed by this technique [216]. The introduction of delayed extraction [217-219] and the mass reflectron [220] has helped increase the resolution and sensitivity of MALDI-TOF-MS dramatically. High-mass capability and high detection sensitivity are hallmarks of the MALDI-TOF-MS combination. In summary, simplicity, high mass accuracy (typically ± 0.1%, and ± 0.01% for polypeptides below 10 kDa), theoretically unlimited mass range and extreme sensitivity (pmol to subpmol range) have made MALDI-TOF-MS an excellent method for routine mass analysis of biomolecules [221-224].

1.3 HDX-MS for Characterization of Proteins

1.3.1 History of HDX

In the mid-1950s, Linderstrøm-Lang and colleagues first introduced HDX and described the relationship between the rate of HDX and protein dynamics mathematically [225-227]. During the 1960s, the advent of liquid scintillation technology spurred the use of hydrogen/tritium exchange (HTX) to study native protein exchange rates and the amount of isotopic exchange within a sample could be determined [228]. In the 1980s,

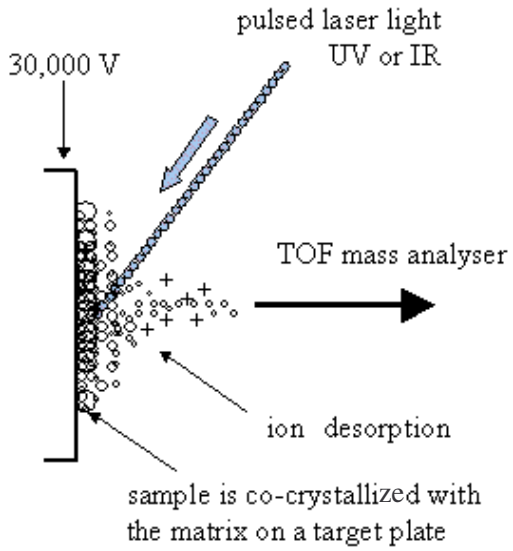

Figure 1.10. Schematic description of the MALDI process.

labeled proteins were enzymatically digested and separated by HPLC prior to analysis with liquid scintillation analysis. This improved the spatial information obtained with HTX [229].

Because of the increase in the mass of a protein (one Da increase for each hydrogen exchanged by a deuterium), mass spectrometry is an ideal technique to study HDX [230-247]. Zhang and Smith [233] were the first to combine HDX with fast atom bombardment mass spectrometry (FAB-MS), while Katta and Chait were the first investigators to use the HDX-ESI/MS combination to probe the conformational changes in proteins [232]. Johnson and Walsh [234] first reported the coupling of LC with ESI for HDX studies. Although ESI is now the most commonly used mass spectrometry approach to monitor HD isotopic exchange rates, MALDI can also be combined with HDX to probe conformational exchanges in peptides and proteins [238-241]. HDX-MS has become an essential tool to examine protein structure, protein dynamics, protein stability, protein modification and aggregation, protein-ligand interactions, protein–protein interactions and protein–DNA/RNA interactions [242-247].

Besides the combination with MS, the HDX and NMR combination has been a great asset in determining the conformational dynamics and intermediates [248-253]. NMR has the advantage of providing structural and dynamic information at the site-resolved level. Its disadvantages, however, include molecular weight limitations (< 30K), problems with analyzing complexes containing paramagnetic ligands, difficulties with correlating site-specific dynamics with distinct conformers, and the need for relatively high protein concentrations (typically 0.5 – 3 mM) and high purity [254-255]. By contrast, mass spectrometry methods require relatively little protein (micrograms at most), mass measurements can be exact and up to 10^6 Da, and information is obtained almost instantaneously [256]. Moreover, mass spectrometry is unique in that it measures differences in individual populations within the bulk solution, whereas NMR is a sample average technique. HDX-MS is capable of detecting and characterizing individual conformational states that may co-exist in solution at equilibrium. HDX-MS in conjunction with fragmentation procedures either in solution or in the gas phase has made it possible to obtain residue-specific information, potentially competing with NMR as a

high-resolution structural probe [242-247].

1.3.2 Theory of HDX

Exchange of protons between a protein and the surrounding aqueous solvent occurs as a spontaneous chemical process. With respect to HDX, there are basically three categories of hydrogen atoms in proteins [230, 257]. The first category is hydrogen atoms covalently bonded to carbon, which essentially don't exchange. The second category is hydrogen atoms in the side chains bound to N, O, or S, which exchange so rapidly that their exchange rates can not be measured by isotope exchange methods. The third category of hydrogen atoms is those attached to the amide positions in the protein backbone, and it is these hydrogen atoms that are monitored with HDX. Each amino acid, except proline, contains one amide hydrogen atom, which means that amide hydrogen exchange rates can be investigated more or less along the entire protein backbone. The intrinsic exchange time can range from milliseconds to many years and the opening of the secondary and tertiary structures of a protein may increase the amide hydrogen exchange rate by as much as 10^8 [258]. The variation in exchange change rates reflects the diversity of local environments for individual amide hydrogens. Solvent-exposed amide hydrogens will readily exchange protons with water, while the slower exchange rates are obtained for amide hydrogens located in hydrogen-bond-participating α-helixes and β-sheets, and the hydrophobic core of a protein (where access to solvent is limited) [259]. Besides a protein's structure, the intrinsic rate of exchange for a particular proton also depends on the experimental variables such as temperature and pH, and local inductive or steric effects caused by adjacent amino acid side chains [260]. Implicit in many HDX studies is the assumption that isotopic labeling does not affect the overall properties of the protein. However, such an assumption may not always be correct [261-263]. For example, Connelly *et al.* showed that the presence of different isotopes in hydrogen-bonded positions may affect hydrogen bond strength; the effect on local stability and HDX rates may be minimal, but the effect on global stability may be significant [261]. Cioni *et al.* claimed that D_2O significantly increases the rigidity of most protein structures; the structure tightening effect is generally amplified by the

increase of temperature as well as by the de-stabilization of the folded state (the folded state is more stable in D_2O than in H_2O) [262]. Scheiner *et al.* reported that stability of H bonds and D bonds are different in the gas phase (raising the temperature tends to stabilize H bonds over D bonds); the difference may persist in solution [263].

Hydrogen exchange in proteins is catalyzed by H^+ and OH^- ions. The intrinsic chemical exchange rate constant (k_{in}) is the sum of the rate constants for acid (k_H) and base-catalyzed (k_{OH}) reactions, as indicated in the following equation [260]:

$$k_{in} = k_H [H^+] + k_{OH} [OH^-] \qquad \text{Eqn. 1.13}$$

Detailed studies of amide hydrogen exchange in polyalanine model compounds indicate that $k_{H \text{ and } } k_{OH}$ have values of 41.7 and 1.12×10^{10} M^{-1} min^{-1}, respectively, at 20 ºC and low concentrations of salt [260]. As a typical example, Figure 1.11 shows the effect of pH on the exchange rate for the unprotected amide hydrogen in polyalanine [260]. The resulting V-shaped plot has a minimum around pH 2.7. For values greater than ca. pH 5, k_{in} increases by a factor of ten with each unit of pH. The high pH sensitivity of isotopic exchange rates indictates a need for careful control of pH in all hydrogen exchange experiments. Furthermore, this sensitivity is the basis for quenching isotopic exchange, thereby facilitating determination of exchange rates by mass spectrometry. The exchange rate also decreases as the temperature decreases; it changes threefold for each 10 ºC change [260].

Currently accepted mechanisms for protein amide HDX involve two types of reactions [230]: (i) reversible protein unfolding that disrupts the H-bonding network or burial of amides, thus exposing them to bulk solvent, and (ii) isotope exchange at individual unprotected amides.

$$\text{Folded (H)} \underset{k_{-1}}{\overset{k_1}{\rightleftharpoons}} \text{Unfolded (H)} \xrightarrow[D_2O]{k_{in}} \text{Unfolded (D)} \underset{k_1}{\overset{k_{-1}}{\rightleftharpoons}} \text{Folded (D)}$$

$$k_{ex} = \frac{k_1 k_{in}}{(k_{-1} + k_{in})} \qquad \text{Eqn. 1.14}$$

In the general case, the overall HDX kinetics is determined by both reactions. The rate constant (k_{ex}) of the overall process is given by Eqn. 1.14, where k_1, k_{-1} and k_{in} are the rates of the protein unfolding, folding and the intrinsic exchange rate constants. Usually

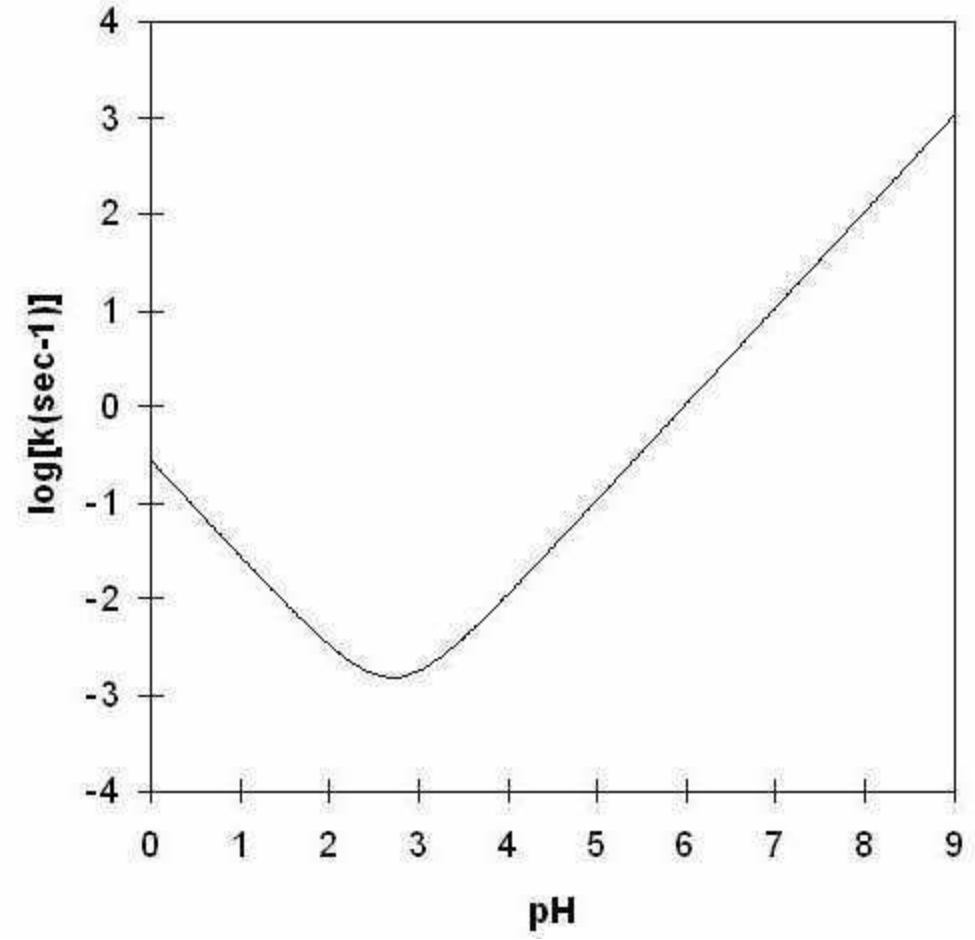

Figure 1.11. Plot of the rate constant for isotopic exchange of hydrogen located on peptide amide linkage in polyalanine as a function of pH, based on Eqn. 1.13. (Reproduced from Ref. [260]).

two ideal limiting cases are considered [230, 243]: if the protein refolding rate constant k_{-1} is small compared to intrinsic exchange rate k_{in} (i.e. $k_{-1} << k_{in}$), all of the amide hydrogens undergo isotopic exchange during one folding event. This exchange is commonly referred to as EX1 (correlated exchange) and is described in Eqn.1.15:

$$k_{ex} = k_1 \qquad \text{Eqn. 1.15}$$

Hydrogen/deuterium exchange via EX1 kinetics leads to a mixture of peptide molecules with regions that either have no deuterium or fully deuterated. Consequently, peptides that are deuterated under EX1 conditions have bimodal isotope patterns in MS that can be described by two binomial distributions (Figure 1.12) [264-267]. Under conditions that obey EX1 kinetics [268], the exchange rate constants for unfolding proteins, k_1 ($=k_{ex}$), can be determined by fitting the expression in Eqn. 1.16 to the experimental MS data. The unfolding equilibrium constant, K ($= k_1 / k_{-1}$), can be determined from the steady-state populations of folded and unfolded forms (assessed using relative intensities of the corresponding peaks). The concentrations of folded ([F]) and unfolded ([U]) forms under non-equilibrium conditions are again determined by the relative intensities of the corresponding peaks in the mass spectra at time t [269]:

$$[U] = [K/(K+1)][1-\exp(-k_1(K+1)/K)t] \qquad \text{Eqn. 1.16}$$

If protein refolding is much faster compared to the intrinsic exchange (i.e. $k_{-1} >> k_{in}$), the opening and refolding of a protein will occur many times before any isotopic exchange takes place and the overall exchange will follow more complex kinetics governed by both the unfolding equilibrium and the intrinsic rate (Eqn. 1.17), or the so-called EX2 mechanism or uncorrelated exchange.

$$k_{ex} = (k_1 k_{in}) / k_{-1} = K k_{in} \qquad \text{Eqn. 1.17}$$

Hydrogen exchange via EX2 leads to a random distribution of deuteriums among the peptide molecules or binomial isotope patterns in MS (Figure 1.12).

Protein amide HDX under native conditions occurs almost exclusively via the EX2 mechanism [242]. On the other hand, if the native state becomes destabilized by altering solvent conditions either with extremes of pH or the presence of detergents, then the EX1 mechanism becomes more favorable. However, it is likely that both

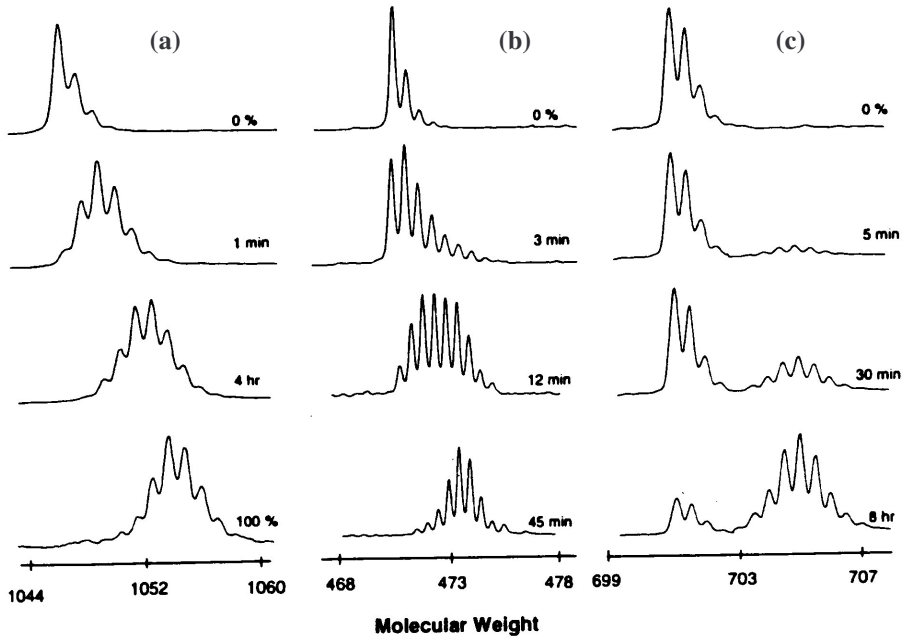

Figure 1.12. Distinctive isotope patterns characteristic of EX2 and EX1 kinetics. (a) A protein exhibiting EX2 kinetics. A single envelope is obvious. (b) A protein exhibiting EX1 kinetics; the overlap between the two envelopes is severe. (c) A protein exhibiting EX1 kinetics and clear separation of the two envelopes. 0% and 100% refer to respectively fully protonated and fully deuterated control samples.

mechanisms operate simultaneously in a protein having regions that are in the native state and others undergoing slow local unfolding and refolding [269]. A more extensive review of hydrogen exchange kinetics is provided by Clarke and Itzhaki [269].

The use of hydrogen isotopes in proteins and solvent may impose a variety of effects on measured HDX behavior. *Kinetic isotope effects* (a variation in the rate of a chemical reaction when an atom in one of the reactants is replaced by one of its isotopes) modify exchange *rates,* and therefore can affect measurements of protein stability. An *equilibrium isotope effect* occurs when the hydrogen isotopes used partition unequally between protein and solvent so that the isotopic ratio in the protein (i.e., protein-D/protein-H) is unequal to solvent-D /solvent-H at exchange equilibrium), and therefore may affect the number of protein sites measured when isotopic species compete in a labeling experiment. *Solvent isotope effect* is the difference between catalysis by OH^- and OD^- and it depends on the relative basicities of these species, and may lead to exchange rates in H_2O different from those in D_2O. These isotope effects in the peptide group HDX reaction were investigated by Connelly *et al.* using poly-DL-alanine as the test analyte [261]. It was found that *kinetic isotope effects* in amide hydrogen exchange are small because exchange pathways are not limited by bond-breaking steps, but depend on the concentration of the solvent species (H^+ or D^+ and OH^- or OD^-) and their diffusion coefficients which are very similar for similar species. This is because formation of the hydrogen-bonded encounter complex is diffusion-limited. Only small *equilibrium isotope effects*, which can lead to an excess equilibrium accumulation of the heavier isotopes by the peptide group, were observed. Since HDX experiments are normally done in solvents that are close to 100% of either H_2O or D_2O, equilibrium isotope effects are not easily detected. For the solvent isotope effects, results show nearly identical rate constants for acid catalysis of NH and ND in H_2O. However, the exchange of NH is faster by 2-fold in D_2O than in H_2O because D_3O^+ is a stronger acid than H_3O^+. For base-catalyzed exchange of NH and ND by OH^-; rate constants decrease slightly in the order NH > ND.

1.3.3 HDX-ESI/MS

Method Overview

Although continuous FAB-MS was used for the earliest HDX-MS measurements [233], electrospray ionization (ESI) is the preferred and most commonly used method to produce ions from deuterated samples for subsequent mass spectrometric analysis because of its high sensitivity and facile coupling to HPLC. Several mass analyzers, including magnetic sector, quadrupole, ion cyclotron resonance, and ion trap, have been used successfully for HDX-MS.

Several different approaches are used to determine the amide hydrogen exchange rates. Continuous labeling and pulsed labeling are two common approaches [272-275]. In continuous labeling experiments, a fully protiated protein is incubated in D_2O (or a fully deuterated protein is incubated in H_2O), and at various times the reaction is quenched by moving an aliquot of sample to a quench buffer. Thus, the protein is exposed to D_2O while the populations of folded and unfolded states are changing. Molecules or regions that are or become unfolded during the labeling time may be completely deuterated depending on their kinetics and molecules that did not unfold during this time have less deuterium. Deuterium levels in proteins labeled continuously effectively integrate the number of molecules that unfold during the labeling time, which may be as short as milliseconds or as long as days. In continuous labeling, a cumulative summary of the populations of the molecules is evident in the spectra. Continuous labeling is useful for looking at populations of protein molecules under conditions where the folded state is favored since the minor contribution of the unfolded states is integrated over time. Experiments of this kind can provide information on the conformational dynamics of a protein under equilibrium conditions [270-273].

In pulsed-labeling experiments, the protein is put under specific conditions for a period of time (i.e. in denaturant for 30 minutes). Then a short pulse of deuterium (typically 10 ms) is introduced and the reaction is quenched. In pulsed-labeling experiments, the exposure of the protein to D_2O is short relative to the time scale of the folding/unfolding dynamics and the time required for isotope exchange in the folded form of the protein. Failure to meet the latter requirement may lead to poorly resolved

envelopes of isotope peaks. Since little unfolding or folding occurs during the labeling step, the deuterium levels resulting from pulsed labeling indicate the instantaneous populations of folded and unfolded molecules. In pulsed-labeling, an instantaneous snapshot of the protein populations is evident. Pulsed labeling is useful for measuring the unfolding (starting with folded proteins) and refolding (starting with unfolded proteins) rate constants in conditions where the population of the unfolded state has been artificially increased by addition of denaturant, heat or pH changes [274-275].

Both continuous labeling and pulsed labeling can be used to study global as well as localized structural changes. The technical details of these two strategies will be described next.

(a) HDX for detection of global changes in proteins

Continuous labeling & indirect MS analysis (with HPLC separation prior to MS analysis)

Using the continuous labeling technique, the unfolding (k_1) and folding (k_{-1}) kinetics of an intact protein can both be studied. In a typical ESIMS procedure for the measurement of the rate constant for the folding process, the protein is dissolved in D_2O buffered to the desired pD [276]. The solution is heated (>=75 ºC) to ensure that the protein is completely unfolded. For proteins that can't withstand the extreme of higher temperatures, the unfolding is achieved alternatively by adding a suitable denaturing agent. Because of the unfolding of the protein, all amide hydrogens can be deuterated. The fully deuterated protein is lyophilized, and redissolved in D_2O. The exchange is initiated by diluting (100-fold) the concentrated D_2O solution of the protein with H_2O that has been adjusted to the desired pH. The samples are withdrawn at several time points, and analyzed by ESIMS.

To study the kinetics of the unfolding process, lyophilized folded protiated protein is dissolved in D_2O at a pH where folded and unfolded states coexist [276]. Samples are withdrawn at different time intervals, and are analyzed by ESIMS. The unfolding process can be measured with a different approach. In this case, the protiated protein is first dissolved in a H_2O solution that was adjusted to an appropriate pH where the protein

is not denatured, and the labeling is achieved by diluting the protein with an excess of D_2O solution of the same pH.

For the aforementioned experiments, a sample cleanup, typically done by HPLC, is essential prior to ESI-MS analysis to remove excess buffer, salts and high concentrations of denaturants required to destablize the protein. This strategy poses a problem because long chromatographic runs can result in higher levels of artifactual exchange (loss or gain of deuteriums, discussed in more details later) because the eluting solvents in HPLC contain water and organic acid (typically formic acid or TFA) [233, 236, 247].

Continuous labeling & Direct MS analysis (without HPLC separation prior to MS analysis)

HPLC separation can be eliminated in some experimental strategies. For example, ESI-MS-based online HDX experiments are used for continuous labeling experiments on the millisecond time scale [277-279]. This approach provides a powerful tool for monitoring protein structural dynamics under mildly denaturing equilibrium conditions by correlating three complementary structural probes: the ESI charge state distribution, ligand binding state, and isotope exchange kinetics. In this technique, the ESI mass spectrum of the protein is recorded at different time intervals after initiation of HDX in a continuous-flow apparatus involving rapid online mixing. Labeling of the protein is initiated by exposing the protein solution to a D_2O buffer solution at a basic pH where the protein is partially denatured, and where the chemical exchange step is fast, thus favoring EX1 exchange. Specifically, the protein solution and the D_2O buffer solution are driven separately through two separated narrow fused silica capillary tubes by two syringe pumps and mixed in a low dead volume mixing Tee. Varying the length and/or the i.d of the reaction capillary that is connected between the mixing tee and the ESI source controls the labeling time. The experimental setup for the study of conformational dynamics of partially denatured myoglobin is shown in Figure 1.13 [279].

Kheterpal and Cook developed a similar technique which has been successfully

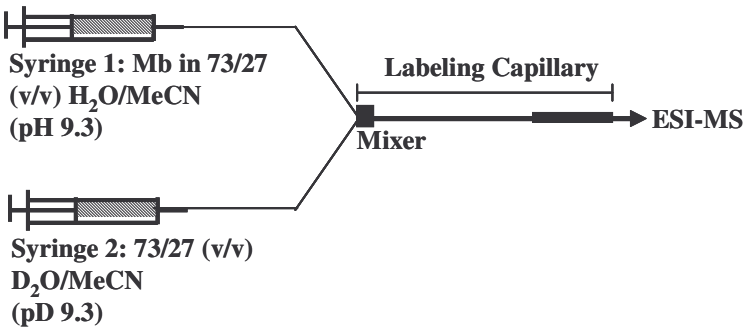

Figure 1.13. Schematic diagram of continuous-flow setup used for time-resolved ESI-MS with online HDX study of partially denatured myoglobin (Mb). The pH was adjusted to 9.3 using NH_4OH in syringe 1 and ND_4OD in syringe 2. (Adapted from Ref. [279]).

used to study insoluble amyloid fibrils without resorting to HPLC [58-59]. The general methodology is illustrated in Figure 1.14. The experimental setup involves a tee connected to a standard coaxial electrospray probe. They have monitored the kinetics of deuterium exchange into fibrils by a process involving on-line mixing of a fibril suspension undergoing slow deuteration with a quenching/disaggregating/dissolving solvent (50:50:0.2 (v/v/v) water/acetonitrile/formic acid) followed by immediate infusion into an ES source, within 10 s. The elimination of salts and buffer is achieved prior to MS analysis by spinning down the insoluble fibrils in a centrifuge and decanting the salt, then re-suspending the fibrils in the 2.0 mM Tris buffer, which appears to be compatible with MS. Experimental details will be presented in Chapter 2.

Pulsed labeling in a quench-flow setup with off-line MS analysis

HDX in the pulsed-labeling technique is traditionally studied in a quenched-flow apparatus [276, 280]. This approach is well suited to determination of the isotopic exchange rates of rapidly exchanging amide hydrogens. The mass spectrometry-based pulsed-labeling approach has been modeled on NMR studies of a similar nature [281-282]. With the pulsed-labeling procedure, the protein is first dissolved in D_2O in which a strong denaturant is present. The unfolded and deuterated protein in a D_2O buffer is injected into a quench-flow system similar to that shown in Figure 1.15, and the refolding is initiated by mixing (at the mixing tee marked T1) the injected protein solution with a large excess of a denaturant-free H_2O solution that is typically buffered to pH 5-6. The length of the folding time (millisecond to seconds) in the quench-flow appraratus can be controlled by varying the size of the folding tube. After this folding period, an exchange pulse is applied by mixing (at T2) the protein solution with a basic pH (>7.0) H_2O solution. The labeling time is typically 10 ms and the labeling is achieved typically by 10- or 20 –fold dilution of the protein solution with the labeling reagent (such as H_2O). Because the rate of hydrogen exchange is very fast above pH 7, the exposed deuteriums will now be exchanged essentially instantaneously. The sites where deuteriums are retained represent the folded structure. The next step is to quench the labeling by acidification of the solution (at T3). The spatial H/D distribution of each protein reflects

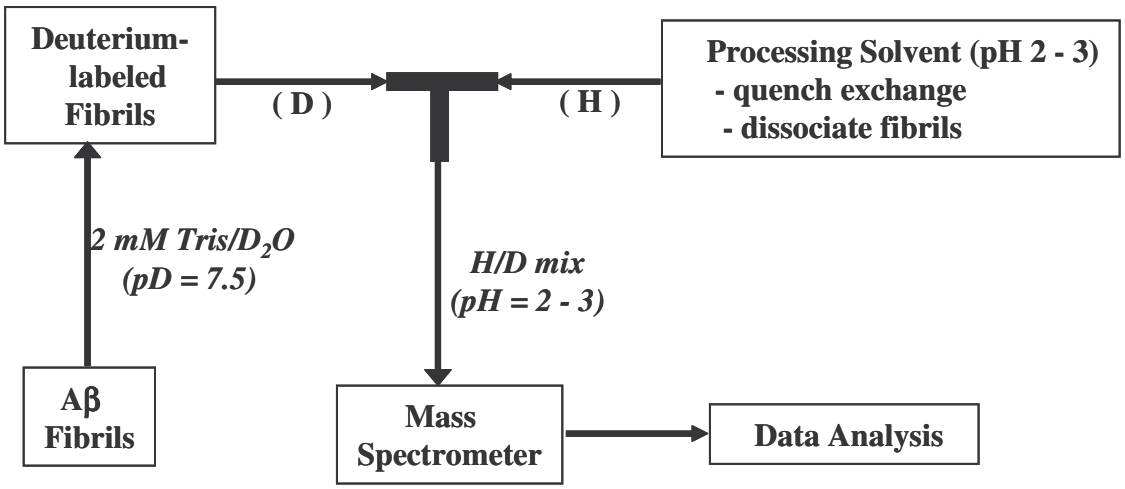

Figure 1.14. Flow chart depicting HDX methodology developed by Kheterpal *et al*. [58].

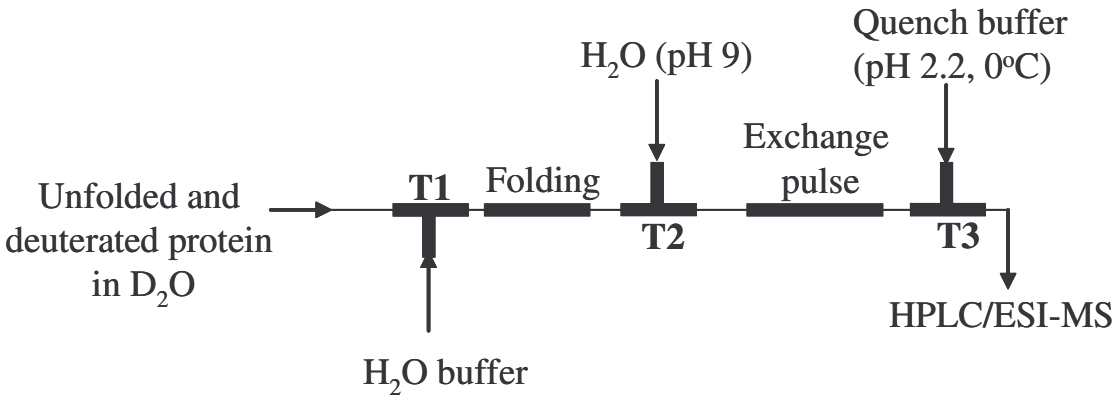

Figure 1.15. Schematic diagram of quench-flow apparatus that can be used in the pulsed labeling technique.

its conformation at the time of the labeling pulse. The isotope-exchange patterns are subsequently studied off-line by MS. It is noted that the quenching step is necessary because exchange would quickly start to occur in protected regions of the protein because the exchange is fast at pH > 7, as can be seen from Figure 1.11. Moreover, a HPLC cleanup step (involving protic solvents) prior to MS analysis is usually performed. Worth noting is that the reverse experiment in which a protiated protein is dissolved in H_2O solution of a denaturant, and subjected to a short exchange pulse with an excess of D_2O solution, can also be performed in a similar manner.

Pulse labeling in continuous-flow setup with on-line MS analysis

In traditional pulse-labeling experiments, quenching, desalting and MS analysis are performed off-line, making sample handling more labor intensive and limiting reproducibility. Recently, Simmons & Konermann have shown that time-resolved ESI-MS can be used to analyze pulse-labeled proteins on-line, "quasi-instantaneously" after labeling [283]. Instead of terminating isotope exchange through a rapid mixing step in traditional pulse-labeling experiments, the protein solution was injected directly into the ESI source of the mass spectrometer. Here, HDX is quenched by analyte desolvation on a time-scale of 1 msec [284-285]. With this approach, the different charge- and ligand-binding states in the ESI mass spectrum are directly correlated with the HDX levels observed for each peak. This technique, therefore, allows the exchange behavior of different protein conformations and different ligand-binding states to be monitored with an extremely high selectivity. The experimental setup is shown in Figure 1.16. It should be noted that the use of urea, guanidinium salts, or other nonvolatile solvent additives can be incompatible with ESI-MS. The use of other refolding triggers such as a pH jump or a temperature jump may be alternatives. The combination of a continuous-flow setup with on-line dialysis techniques for rapid de-salting may increase the versatility of the on-line approach [286].

(b) Determination of hydrogen exchange in short segments of proteins

Although substantial information can be obtained by examining the exchange

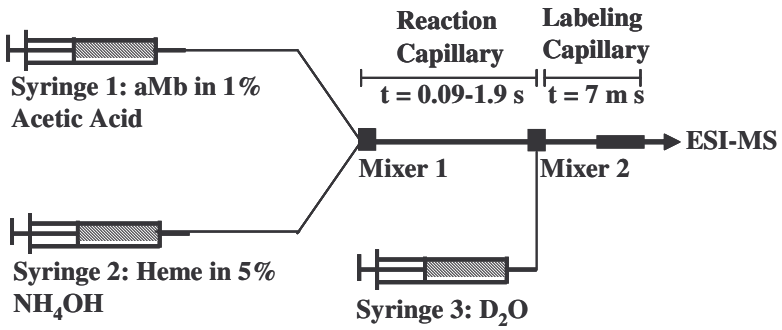

Figure 1.16. Schematic diagram of continuous-flow setup used for time-resolved ESI-MS with online pulse-labeling HDX study of myoglobin (Mb) reconstitution (formation of native holomyoglobin from free heme and unfolded apomyoglobin (aMb)). (Reproduced from Ref. [283]).

pattern of the intact protein, it is possible to increase the structural resolution of the experiment by examining exchange into localized segments. Smith and his associates introduced a proteolytic step under quench conditions (i.e. rapid proteolytic digestion at 0 ºC and pH 2.5, where k_{in} is minimal in Eqn. 1.15) prior to mass analysis [233, 268, 287]. A HPLC separation step is usually employed before mass analysis not only to remove buffers and denaturant, but also to reduce peptide overlapping. The larger the protein, the greater the likelihood that overlapping peaks of fragments will be produced, a problem that is exacerbated as their isotopic envelopes broaden and perhaps even cross one another during exchange.

A typical continuous-labeling procedure used in the protein fragmentation-mass spectrometry approach is illustrated in Figure 1.17. In this protocol, the folded protein is incubated in a D_2O solution at an appropriate pD for a defined time interval. At the end of the defined time interval, the exchange process is quenched by adjusting the pD to ~ 2.5 and the temperature to 0 ºC. Next, the protein is digested with proteases (enzyme solution or immobilized enzyme column) at an acidic pH. Peptide fragments in the digest are measured with HPLC on-line with continuous-flow FAB [233, 288-289] or ESI-MS [234-235, 290-291].

The pulsed-labeling approach can also be used to study the isotope exchange reaction in short segments of a protein [234-235, 292-293]. A quench-flow apparatus is used for these experiments. Also, an immobilized enzyme column is added to perform an on-line peptide digestion. The proteolytic fragments are separated and analyzed by the HPLC-ESIMS combination. A schematic diagram of this method apparatus is shown in Figure 1.18.

Data Analysis

(a) Interpretation of mass spectra (EXI vs. EX2)

The type of exchange kinetics occurring for a protein or a region of the protein (obtained from proteolysis) determine how the data are processed [230]. HDX via EX2 kinetics gives a binomial distribution of isotope peaks (a single envelope) (Figure 1.12), from which the centroid or average mass can be determined. HDX via EX1 kinetics

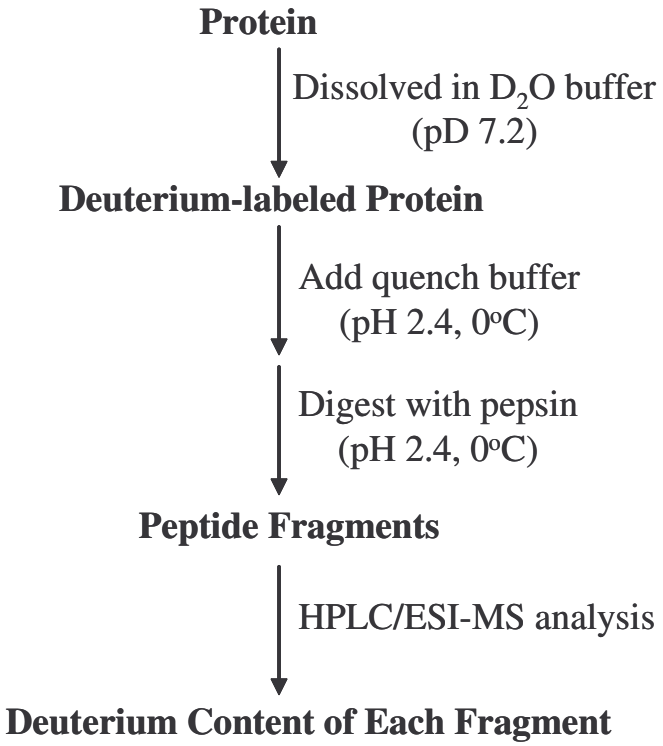

Figure 1.17. Flow chart of a typical procedure used to determine deuterium levels at peptide amide linkages in short segments of intact proteins following HDX.

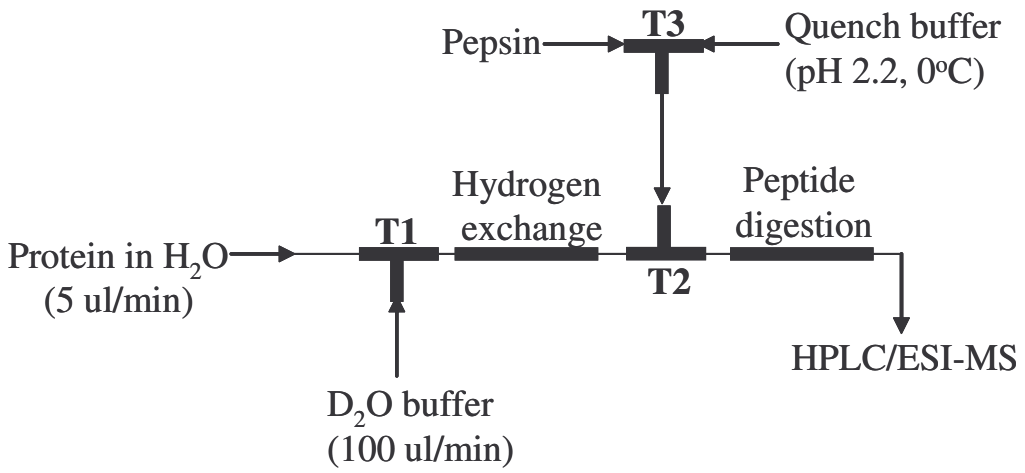

Figure 1.18. Schematic diagram of quench-flow apparatus used in the pulsed-labeling technique for the determination of HDX in proteolytic segments of proteins.

gives a bimodal isotope pattern, with two envelopes of mass appearance: (1) a low-mass envelope, which indicates the non-exchanged population; and (2) a high-mass envelope, which represents the exchanged population (Figure 1.12). The distance between the two envelopes indicates the number of amide hydrogens involved in cooperative unfolding; the relative intensity (area) of the two envelopes is directly related to the relative folding and unfolding rate constant for the cooperative transition (as illustrated in Eqn. 1.16). When the envelopes are completely separated, the average mass of each envelope can be determined separately. If the two envelopes overlap, various computer programs (such as Peakfit, SPSS software) can be used to estimate the relative intensities of incompletely resolved envelopes.

(b) Correction for artifactual exchange

Even though experimental parameters are chosen to minimize isotopic exchange at peptide amide linkages during sample workup for HDX studies, some artifactual exchange (loss and gain of amide deuteriums) after quenching is unavoidable. In most HDX experiments coupled with MS analyses, the exchange reaction is quenched with acid, and then proteolytic digestion and HPLC/ESI-MS analyses are performed immediately in undeuterated acidic solution to localize the deuterated region [235]. Since HPLC step is performed with protiated solvents, deuteriums from side chains and amino/carboxy termini that exchange much faster than amide linkages are essentially removed. Therefore, data obtained by this method should be interpreted cautiously. Basically, two important sources of error during the LC-MS analysis of hydrogen exchange must be corrected during data reduction. First, after quenching and during digestion, deuterium in the reaction mixture continues to exchange with peptide hydrogens, leading to forward exchange (gain of amide deuteriums, called artifactual in-exchange). A second source of error is back-exchange, where deuteriums incorporated into peptides exchange-out with hydrogen from water. Deuterons may also back exchange with water vapor during mass spectral analysis by ESI-MS [233] or with matrix protons by MALDI-MS [238]. Simple adjustments can be made to correct these artifactual exchanges, as described next.

The method of Zhang and Smith [233] has been used widely for correcting back exchange and further forward exchange of amide protons during HDX studies on globular proteins and proteolytic fragments [234, 294-298]. In this approach, nondeuterated and fully deuterated protein samples are analyzed using the same work-up (exchange-in initiation, quenching exchange, HPLC separation and then MS analysis) as the incubated (partially exchanged) sample, and the corrected deuterium content (D_{corr}) in the backbone amides of the target sample is then given by

$$D_{corr} = \frac{m - m_{0\%}}{m_{100\%} - m_{0\%}} \times N \qquad \text{Eqn. 1.18}$$

where m, $m_{0\%}$, and $m_{100\%}$ are the observed average molecular weights of the same peptide in the partially deuterated sample, in the zero time control and in the fully deuterated control, respectively. N is the number of backbone amide hydrogens. The denatured state of a globular protein is typically used to obtain a fully deuterated control. The zero time control ($m_{0\%}$) is performed to measure the extent of artifactual forward exchange occurring after quenching and during digestion, in which quenching buffer (pH 2.4) was added to protein before D_2O, with the same final ratio of D_2O to acidic buffer as used in experimental samples (partially deuterated peptides), followed by proteolysis and LC-MS analysis. The 100% control ($m_{100\%}$) is conducted to measure the amount of backward exchange, where the fully deuterated peptide is subjected to the same analysis as the partially deuterated sample and the subsequent loss of deuteriums during the analysis is measured.

Another method of correcting artifactual exchange was developed by Resing *et al.* [299]. The forward-exchange-corrected peptide mass $M_{\text{corr (FE)}}$ is derived from the following equations [299]:

$$M_{corr(FE)} = (m - L_{FE} M_D)/(1 - L_{FE}) \qquad \text{Eqn. 1.19}$$

$$L_{FE} = (m_{0\%} - MW)/(M_D - MW) \qquad \text{Eqn. 1.20}$$

where L_{FE} is the fractional artifactual forward exchange, M_D is the theoretical average molecular weight of the fully deuterated peptide and MW is the theoretical average molecular weight of the protonated peptide . ($M_D - MW$) is equal to the total number of backbone amides in a peptide excluding proline residues (having no amide proton). m

and $m_{0\%}$ are the same as previously defined. The fractional backward exchange L_{BE} is shown in Eqn. 1.21:

$$L_{BE} = (M_D - m_{100\%})/(M_D - MW) \quad \text{Eqn. 1.21}$$

Following an estimation of the forward exchange and backward exchange, the artifactual-exchange-corrected mass of the protein M_{corr} and D_{corr} are given by the following equations:

$$M_{corr} = MW + \frac{(M_{corr(FE)} - MW)}{1 - L_{BE}} \quad \text{Eqn. 1.22}$$

$$D_{corr} = M_{corr} - MW = \frac{M_{corr(FE)} - MW}{1 - L_{BE}} \quad \text{Eqn. 1.23}$$

The two correction methods mentioned above are used for HDX experiments on soluble or relatively soluble proteins involving HPLC separation prior to MS analysis. There are used for correction of artifactual exchange occurring during quenching, digestion (~30 s - 5 min) and HPLC separation. The whole process generally takes at least 20 min [243]. These correction equations for data from soluble proteins are considered to be accurate to approximately 5% (although deviations of >25% are noted in some instances) [233, 299]. Resing *et al.* tries to account for the fact that FE and BE exchange rates may not be equal to one another [299]. Both methods try to compensate partially for the fact that these rates depend on the specific amino acids' presence and overall protein structure [233, 299].

There is one method which was developed in Cook's group to correct for artifactual amide exchange associated with direct on-line MS analysis of deuterated insoluble amyloid fibrils without HPLC separation [58-59, 40]. The entire on-line process (quenching, dissolution, and sampling) can be accomplished in < 10 s (Figure 1.14) [58]. The method is developed for treatment of data from experiments involving solubilization before analysis. This method has been proved more proper for the 10-s online analysis of insoluble intact amyloid fibrils than other correction methods reported elsewhere [59]. This method involves two steps. First, artifactual exchange into rapidly exchanging side-chains, terminal and ionization protons are corrected. These protons exchange so rapidly that the final measured deuterium content should include an

equilibrium distribution into these sites [58]. Therefore, the deuterium incorporation into these sites reflects the percentage of water that is D_2O in the final solvent composition. For Aβ(1-40) fibrils, there are totally 27 labile side-chain and terminal sites. Consequently, the molecular masses which are corrected for side chains, terminal and ionization protons will be calculated as $\{m/z \times z - z - (z \times \%D_2O) - (27 \times \%D_2O)\}$(m/z: mass-to-charge ratio; z: charge state, equal to the number of ionizing protons for Aβ). For example, when the fraction of water that is D_2O in the T is 10%, a total of 2.7 (10% of 27) deuteriums should be subtracted from the measured masses to correct for artifactual exchange into side-chain and terminal protons, and a total of $0.1z$ (10% of z) deuteriums needs to be subtracted from the measured masses to correct for artifactual exchange into ionization protons. (Comment: If an HPLC step is used prior to MS analysis, then the bulk solvent is generally 100% protonated. In that case, protons gained during ionization and fast exchanging side-chain and terminal protons are not deuterated and no extra correction for these protons is required.) Second, artifactual exchange into backbone protons are corrected. This involves measuring forward exchange (*FE,* H exchanged for D) and backward exchange (*BE,* D replaced by H) for fully protonated and deuterated samples, respectively, using the same work-up conditions as the partially exchanged sample of interest, and calculating the corrected deuterium content (D_{corr}) in the backbone amides of the target sample according to

$$D_{corr} = m - MW + BE - FE \qquad \text{Eqn. 1.24}$$

where m is the measured average molecular weight (after correcting for fast exchanging protons as described above) obtained by mixing sample of interest in D_2O with protiated processing solvent, and *BE* and *FE* are as described next. Forward exchange is measured by infusing the protonated form of the appropriate sample (fibrils, protofibrils or monomer depending on the sample of interest) in protonated buffer into one arm of the T in Figure 1.14 and mixing it with a "quenching" solvent containing sufficient D_2O to give a final solvent composition identical to that obtained in the analysis of the sample of interest (Figure 1.9). Since the solvent mixture during sample processing is the sole source of deuterium, this amount of exchange is the forward exchange taking place during sample work-up, or

$$FE = m_{0\%} - MW \quad \text{Eqn. 1.25}$$

where $m_{0\%}$ is the measured average molecular weight (after correcting for fast exchanging protons as described above) of the forward exchange sample described above, and *MW* is the measured average molecular weight of the monomer in protonated fibrils. Note that the D_2O percentage in the water component is determined by the relative flow rates of the sample and processing solvent streams. For example, when partially deuterated fibrils (the sample of interest) in D_2O (0.5 µL/min) are mixed with quenching solvent (9 µL/min of 50/50/0.5 [v/v/v] H_2O/MeCN/HCOOH), then a final sample mixture in which 10% of the water comes from D_2O is produced. To obtain the $m_{0\%}$ value, protonated fibrils (0.5 µL/min) is mixed with quenching solvent (9 µL/min of 5.6/44.4/50/0.5 [v/v/v] D_2O/H_2O/MeCN/HCOOH) to generate a final solution after mixing in the T in which 10% of the water content is D_2O. (For convenience, we will subsequently refer to this composition as 10% D_2O, overlooking the acetonitrile. So we can say 16.7% D_2O in the protocols described in Chapter 2). The backward exchange value is obtained by measuring the exchange of a fully deuterated sample treated with protonated processing solvent. Fully deuterated fibrils and protofibrils are grown in deuterated buffers as described in Chapter 2. If there were no back exchange taking place during sample processing, 39 deuteriums would be measured for these samples. Any deviation from 39 represents the amount of back exchange taking place during sample processing, or

$$BE = MW + N - m_{100\%} \quad \text{Eqn. 1.26}$$

where $m_{100\%}$ is the measured average molecular weight (after correcting for fast exchanging protons as described above) of the fully deuterated sample and N is the total number of backbone amide protons (39 for Aβ (1-40)).

All the correction methods mentioned above are based on the assumption that the amount of backward and forward amide exchange in the partially deuterated peptide is identical to that observed in the fully deuterated and protonated same peptide [**59**]. Moreover, to some extent, they overlook the site specificity of the forward and backward exchange rates [59]. All the above correction methods will be evaluated in terms of performance for the analysis of HDX data of Aβ fibrils obtained in this study; details

will be presented in section 3.3.

(c) Calculation of rate constants

Following data correction for artifactual forward exchange and back-exchange using one of the methods mentioned above, the number of incorporated deuteriums can be plotted as a function of exchange time, from which one can estimate rate constants describing isotope exchange. When the deuterium concentration in the solution is large and the pH and temperature are constant, isotopic exchange of each amide hydrogen follows first-order kinetics, i.e., the number of unexchanged hydrogens decreases exponentially with time during the exchange period [299]. Although single amino acid resolution is not generally possible, exchange rates describing groups of hydrogens with similar exchange rates can be calculated. Rate constants can be fit to the experimental data by using the equation 1.27 [230, 293, 300]:

$$D_{corr} = N - \sum_{i=1}^{N} \exp(-k_i t) \qquad \text{Eqn. 1.27}$$

where D_{corr} is the corrected deuterium content of a peptide, N is the number of peptide amide linkages in a segment, k_i is the exchange rate constant for each amide hydrogen, and t is the time allowed for isotopic exchange. Practically, the data is binned as fast-, medium- and slow-exchanging populations. Rates and amplitudes are obtained for each population. The analysis can be executed using the computer program LAPLACE, written and provided by Dr. Zhongqi Zhang [301-302].

High Resolution HDX-ESI/MS

HDX-MS coupled with proteolysis provides only medium resolution (10-20 amino acids) of localizing exchange sites, limited by the number and size of peptic fragments. The resolution can be further increased by using tandem MS (MS/MS) (generally with CID or ECD) to fragment the proteolytic peptides in the gas phase into daughter ions leading to deuteration kinetics of individual amides [157-158]. Viability of this approach has been demonstrated by several groups [235, 303-304]. Direct analysis of the protein using MS/MS is an alternative approach [305-308]. Fourier transform ion

cyclotron resonance mass spectrometry (FTICR-MS) will facilitate tandem MS analysis, due to its high polypeptide ion fragmentation and detection efficiency, and the high resolution and mass accuracy [305-308]. It is important to note that the gas-phase fragmentation process, however, may be complicated by deuterium scrambling [235, 304, 309-313]. The extent of scrambling observed depends on the fragmentation technique employed and the type of ion examined. For example, the *b* ions produced in a typical CID MS/MS experiment appear relatively robust to scrambling, whereas the *y* ions appear unreliable [304].

Non-specific proteolysis results in many peptides whose sequences may overlap. Manual subtraction of the number of deuteriums incorporated into the overlapping peptides can lead to increased spatial resolution for deuterium localization (within 2 to 3 amino acids) [299]. For example, overlapping peptic fragments 1-19 and 4-19 from Aβ(1-40) can provide deuterium incorporation information for the peptide 2-4. Therefore, another way to improve spatial resolution is to generate more proteolytic fragments to improve the likelihood of peptide overlapping. One approach is to perform enzyme digestion under slightly denaturing conditions [314]. Alternatively, peptide overlap can be increased using multiple acid-stable proteases with differing specificities [314]. Furthermore, if extensive disulfide bonding is a problem (preventing digestion and/or resulting in liberation of large disulfide cross-linked peptides), inclusion of a reducing agent can assist digestion [315]. Worth noting is that the more proteolytic fragments are produced, the more likely their mass spectral peaks will overlap. The utility of LC preparation can help reduce the problem. However, high level of back exchange can be troubling with LC/MS.

1.3.4 HDX-MALDI/MS

Although ESI is the most commonly used mass spectrometry approach to monitor HDX rates, MALDI has emerged as an alternative in this field [238-241]. The general scheme for deuterium introduction prior to MS analysis is the same as that employed in HDX-ESI/MS studies. Only minor modifications of established MALDI sample preparation protocols are required to carry out HDX experiments. To be specific,

exchange-in (incorporation of deuteriums) reactions involve dissolving lyophilized protein or diluting concentrated protein solutions into D_2O. The exchange process is allowed to procceed for a certain period of time and is then quenched by addition of acidified matrix solution at low temperature, and then followed by rapid drying of samples on the MALDI target to insure minimal loss of deuterons from peptide amide groups. Although the sample remains completely dry and is kept under high vacuum during the analysis, the deuterium content of the peptides decreases gradually over time [238-241]. A correction for the deuterium loss prior to mass analysis has been described by Mandell *et al.* [238]. In this work, several replicate HDX samples were simultaneously placed on a MALDI target and dried. Subsequent analysis of each sample took 3–5 min. The measured number of deuteriums (D_{meas}) decreased for successive samples, tangentially approaching a value B_1 at long sample analysis time (t). An effective rate constant (k) for this decay process was determined by fitting D_{meas} to a single-exponential curve:

$$D_{meas} = B_1 + B_2 e^{-kt} \qquad \text{Eqn. 1.28}$$

where $B_1 + B_2$ is the initial total number of amide deuteriums in the peptide prior to sample work-up. Using values of B_2 and k from the fit, the number of deuterons that would have been present on the peptide (D_{corr}) at any earlier analysis time (especially at $t = 0$) can be estimated from D_{meas} at a given analysis time as

$$D_{corr} = D_{meas} + B_2(1 - e^{-kt}) \qquad \text{Eqn. 1.29}$$

This correction method will be evaluated in terms of performance for correcting HDX data of Aβ aggregates (see section 3.3).

HDX-MALDI/MS has become a standard tool for folding experiments carried out under equilibrium conditions [238-241, 316-318]. HDX measurements of intact proteins measured by MALDI-MS have provided insight into a variety of biological processes [318-321]. A variation of the experiment employing varying concentrations of denaturant has led to a methodology (termed SUPREX: stability of unpurified proteins from rate of H/D exchange) capable of measuring stability against unfolding for both purified and even crude proteins in cell extracts in a high throughput manner [316-318].

HDX-MALDI/MS has drawbacks of high back-exchange (30% - 40%) due to

back-exchange with protons from the matrix, solvent or the water vapor in the atmosphere, and lower coverage than ESI-MS due to less efficient ionization and overlap of peaks in complex spectra [238, 240]. Efforts have been made to reduce back exchange [323-325], such as using deuterated matrix solution, preparing samples and carrying out exchange reactions under N_2 flow [325], adjusting pH to the HDX minimum (pH 2.4), cooling the sample target to -20 ºC before sample preparation, and using thin-layer preparation to reduce sample preparation time. Another potential complication with using MALDI concerns the identification of the peptide fragments. In favorable cases, this can be done by exact mass matching or post-source decay (PSD), but more generally it is necessary to do a separate tandem MS/MS experiment. The advent of MALDI-MS/MS instruments will make online tandem MS available [326-327].

On the other hand, compared to standard ESI techniques, MALDI-MS clearly affords the advantage of straightforward sample preparation (standard protocols available), the tolerance to chemical denaturants and modifiers, the simple appearance of the spectra (often dominated by singly charged ions), elimination of the HPLC separation of proteolytic fragments before mass analysis, better sensitivity (at sub-picomolar level), faster analysis times, and the potential for high-throughput assay [238-241, 316-318]. With the possible enhancement of spatial resolution through further fragmentation [328], together with new developments in MALDI instruments and improvement in MALDI experimental procedures, MALDI-MS will also become a standard tool for HDX kinetic studies.

HDX/MALDI-MS has been utilized to study the aggregation kinetics of Aβ (1-42), and C-terminally truncated peptides Aβ (1-40) and Aβ (1-36) [329]. However, for the purpose of the study presented in this dissertation, only HDX-ESIMS is employed.

1.4 Enzymes for HDX-MS

As discussed in section 1.3.3, a key aspect of HDX-MS is the quenching of isotope back exchange because digestion, as well as subsequent HPLC separation (if

needed) and mass spectrometric analyses is realized in hydrogenated solvents and in denaturating conditions (if employed) [233, 260, 300]. The quenching step is accomplished at pH 2-3 and at (typically) 0 °C. Since the proteolytic step for localizing deuterium distribution is introduced under quenching conditions, proteases working at low pH and low temperature must be used. Pepsin-like proteinases (also classified as aspartic proteinases), which typically have molecular weights in the range of 33,000-35,000 Daltons and whose catalytic activity is due to the presence of two invariant aspartic acid residues at the catalytic center, have optimum pH range of 1.5-5 [331-332]. Therefore, they could be used in HDX studies, given that they are readily available, cost-effective, of good activity and produce characteristic fragmentation patterns. Detailed information about various acid proteases can be found in the review by Dunn [333] and on the website http://srdata.nist.gov/HIVdb.

Pepsin is most commonly used aspartic proteinase for HDX studies because of its maximum activity at a pH of 2 – 4, good activity at low temperature, and easy availability [233]. Moreover, this enzyme has no detectable effect on HDX rates [229]. Other enzymes which have been employed for HDX studies include carboxypeptidases [314, 334], protease type XIII [237, 298, 314, 334], and protease type XVIII [237, 314, 334], which all belong to peptidase family A1, the pepsin-like enzymes [363]. Using pepsin or the other A1 proteases, sequence coverage is not always complete, and the spatial resolution of the exchange rate is limited by the sizes of the resulting peptides (typically 10-20 amino acids). On the other hand, aforementioned alternative pepsin-like enzymes can generate cleavage patterns very different from pepsin and from each other under slowed exchange conditions [237, 314, 334]. It has been demonstrated that the fragmentation patterns resulting from simultaneous and/or sequential proteolysis by combinations of these enzymes are additive in their effect on fragmentation [237, 314, 334]. Therefore, pepsin-like enzymes may be used individually as complementary experiments or together in a protease ‘‘cocktail’’. In this manner, rapid (30 seconds) high-resolution localization of deuterium labels to 1-5 amino acid long peptides, and highly efficient and varied fragmentation has been achieved [237, 334].

The enzymes can be used in solution or immobilized on a solid support and

packed in a column [229, 236, 298, 314, 334]. Solution enzymes are convenient and requires less equipment, but they may have the disadvantages of incomplete digestion, longer digestion time (typically ~ 4-5 min, leading to high deuterium back exchange), interference of pepsin and its autolysis products (confusing data analysis), as well as plugging the HPLC columns [236]. In contrast, it has been claimed that immobilized enzymes can offer the following possible advantages, including higher enzymatic activity, higher extent of digestion, less digestion time (typically ~ 30 s, less deuterium back exchange), lower protein concentrations, less contamination from the enzyme itself or fragments of the enzyme, multiple use of the enzyme resulting in reduced cost and enabling full automation such that proteins can be exchanged, quenched, and digested, and then the resulting proteolytic peptides analyzed for deuterium content by HPLC/ESI-MS [236, 314, 334-336]. When needed, sequential proteolysis by rapidly flowing a sample over a series of different enzyme columns can be done, and it is also possible to further proteolyze such product peptides on-line as they emerge (partially separated) from the reversed phase HPLC column [314, 334]. Although the intensities of individual peptides may be different for soluble and immobilized pepsin due to different degrees of interference from the enzyme and different extent of digestion, the cleavage sites were rather similar and highly reproducible [236].

Pepsin, protease type XIII, protease type XVIII, and endothiapepsin are 4 nonspecific proteases that cleave preferentially at hydrophobic residues, and have some degree of secondary and tertiary structural specificity [299]. Since their cleavage specificity is not well defined, peptide identities must be confirmed by collision-induced dissociation MS/MS in combination with accurate peptide mass measurements [233, 236, 243]. Analysis of these digests by HPLC/ESI-MS facilitates identification the peptic fragments. With current instruments and analysis software, it is possible to identify the constituent peptides of large proteins in a few hours. Varying the concentration, time and temperature often alters the sites of preferred cleavage; LC/MS/MS therefore must be performed under conditions identical to those used in the deuterium exchange experiment [243].

In what follows, a brief description of the four enzymes (pepsin, protease type

XIII, protease type XVIII, and endothiapepsin) will be addressed.

Pepsin. Pepsin used in the studies presented in this dissertation is porcine pepsin, which was crystallized in 1930 [337] and consists of a single polypeptide chain and arises from its precursor, pepsinogen, by removal of a 41-amino acid segment from the amino end [331]. Porcine pepsin consists of 326 amino acids, with a molecular weight of 34628.2 Da and pI value of 3.36. The pH range of peptide hydrolysis is from 1 to about 6 [338]. An assay of pepsin activity is most commonly carried out at pH near 2 using cattle hemoglobin as substrate [339]. Pepsin has a broad specificity and it prefentially cleaves large hydrophobic residues, such as Phe, Leu, Glu, Tyr and Trp [340-341]. Other residues may be cleaved, with very variable rates. Important structural features of pepsin are shared by other aspartic proteases, such as fungal enzymes.

Type XIII protease. Type XIII protease is isolated from Aspergillus saitoi fungus [342]. The optimal pH of the enzyme for milk casein digestion is in the range of pH 2.5-3.0 and the protease is fairly stable over the range of pH 2.5-6 [343]. The activity assay is typically conducted at pH 2.8 using cattle hemoglobin as the substrate [331]. Type XIII protease has been observed to hydrolyzes the following bonds in the oxidized B chain of insulin: Leu-Tyr, Phe-Phe, His-Leu, Ala-Leu and Tyr-Leu [344], which contains at least one hydrophobic residue. Type XIII protease consists of 325 amino acids, with a molecular weight of 34302 [345].

Type XVIII protease. Type XVIII protease is isolated from Rhizhopus fugus [346]. The activity maximum of this enzyme varies from pH 2.9 to 4.5, depending on the substrate under investigation. The activity assay is typically conducted at pH 3 using cattle hemoglobin as the substrate [331]. Type XVIII protease exhibits a very broad specificity and cleavages occur most readily between aromatic or bulky hydrophobic residues [346]. For example, it can cleave the following bonds in the oxidized B chain of insulin: Phe-Val, His-Leu, Leu-Val, Val-Glu, Glu-Ala, Ala-Leu, Leu-Leu, Leu-Tyr, Tyr-Leu, Gly-Glu, Glu-Phe, Phe-Phe, Phe-Tyr. Based on the digestion of insulin, one can conclude

that type XVIII protease seems to have a wider specificity than type XIII protease. The amino acid sequence of this enzyme still remains unknown, but its molecular weight is on the order of 33000 [347].

Endothiapepsin. The aspartic proteinase from the chestnut blight fungus (Cryphonectria or Endothia parasitica) is referred to as endothiapepsin. The proteinase is secreted by the fungus and has a digestive role in the growth medium. Endothiapepsin is a single chain proteinase of 330 amino acids and has a molecular weight of 33.8 kDa [348-350]. It cleaves protein substrates with a specificity similar to that of porcine pepsin, preferring hydrophobic residues [351-352]. Williams et al. analyzed the cleavage sites in the oxidized B-chain of insulin and found the rates of cleavage to be as follows: Phe-Phe > Tyr-Leu > Gln-His >>> Leu-Val > Asn-Gln [382]. Its catalytic activity may be assayed by the use of chromogenic substrates containing para-nitrophenylalanine [353-354].

1.5 Objectives

The motivation for the research efforts in this dissertation is the importance of understanding of the roles of Aβ amyloid fibrils and protofibrils in Alzheimer's disease (AD) and of finding ways to intervene in these roles. A critical issue is to find out the details of how the polypeptide chains fold together to form the protofilament sub-structures of fibrils. The research aims to develop a detailed understanding of the three-dimensional structure of the Aβ amyloid fibrils and protofibrils, and of how Aβ monomer aggregates into insoluble fibrils, which could facilitate the design of fibril-targeted anti-AD therapeutics. First, a novel on-line proteolysis (using pepsin) system involving a triaxial electrospray probe was developed to facilitate the study of the secondary structures of Aβ aggregates using HDX-MS. In the second part of this work, the secondary structures of Aβ(1-40) amyloid fibrils and CLC-stablized Aβ(1-40) protofibrils have been studied using HDX-MS coupled with proteolysis. The novel on-line proteolysis system has also been tested with 3 pepsin-like enzymes to obtain

complementary structural information of Aβ fibrils. In the course of these studies, a peculiar electrochemical phenomenon interference (oxidized form of Aβ. samples) was noted, identified and characterized. This work provides a proteolysis system that could be used for the studies of other protein aggregates, and provides potent structural information of Aβ amyloid fibrils and protofibrils.

CHAPTER 2

EXPERIMENTAL

2.1 Chemicals and Sample Preparation

2.1.1 Chemicals

Chemical used, their sources and purities are listed in Table 2.1. Unless otherwise mentioned, the chemicals and biochemicals were used as received from the indicated vendor.

2.1.2 Sample Preparation

Deuterated and protonated Tris buffers

100 mM stock solution of deuterated Tris.DCl (D-Tris-DCl) buffer was prepared by dissolving tris(hydroxymethyl)aminomethane in D_2O (99.9% D) under nitrogen (to exclude atmospheric moisture) and DCl was used to adjust pD to 8. 2 mM D-Tris-DCl buffer (pD 7.5) was obtained by addition of 10 µL of 100 mM D-Tris-DCl buffer to a 500 µL ampule of D_2O (100% D) under nitrogen. (pD values were read directly from either pH paper or a pH meter and have not been corrected for any isotope effects [355]). 100 mM stock solution of protonated Tris.HCl (H-Tris-HCl) buffer was prepared by dissolving tris(hydroxymethyl)aminomethane in HPLC water, and then adding 10 M HCl to adjust pH to 8. 2 mM H-Tris-HCl buffer (pH 7.5) was obtained by diluting the stock solution by a factor of 50 using HPLC water.

Aβ samples

Monomers. Dry Aβ monomer was pretreated to remove any aggregates as described by Zagorski and colleagues [356]. Specifically, Aβ peptide was first dissolved with TFA at 1µg/µl and sonicated for 15 min. The TFA was then evaporated off under a stream of

Table 2.1. List of chemicals and biochemicals used in this work.

Reagent	Supplier	Purity
Aβ(1-40) peptide	Keck Biotechnology Center	Reagent grade
Acetonitrile	Fisher Scientific	HPLC grade
Ammonium hydroxide	Acros	Reagent grade
Argon	National Welders	>99.999%
Bovine serum albumin	Sigma	≥ 98%
CLC[1]	Sigma	Reagent grade
Concentrated HCl	Sigma	Reagent grade (12.1M)
Deuterated oxide	Acros	Reagent grade (100%D)
Deuterated oxide	Cambridge Isotope Laboratories	Reagent grade (99.9%D)
DMSO[2]	Sigma	≥ 99.9%
HFIP[3]	Acros	Reagent grade
Methanol	Fisher	HPLC grade
Neurotensin	Sigma	Reagent grade
Nitrogen	National Welders	Prepurified grade
Porcine pepsin	Sigma	Reagent grade
Potassium chloride	Sigma	Reagent grade
Protease type XIII	Sigma	Reagent grade
Protease type XVIII	Sigma	Reagent grade

(Table 2.1 Continued)

Reagent	Supplier	Purity
Sodium azide	Sigma	Reagent grade
Sodium chloride	Sigma	Reagent grade
TCEP[4]	Sigma	Reagent grade
TFA[5]	Pierce	Reagent grade
Thioflavin T	Sigma	Reagent grade
Triethylamine	Acros	Reagent grade (99.7%)
Tris[6]	Sigma	Reagent grade
water	Fisher Scientific	HPLC grade

CLC[1]: Calmidazolium chloride; DMSO[2]: Dimethyl sulfoxide; HFIP[3]: 1,1,1,3,3,3-hexafluroisopropanol; TCEP[4] : Tris(2 - carboxyethyl) phosphine; TEA[5]: Tetraethyl ammonium; Tris[6]: Tris(hydroxymethyl)aminomethane.

argon in a fume hood. The monomer was then dissolved in HFIP to a final concentration of 1μg/μl and incubated at 37°C for 1 hour before being dried using a stream of argon in a fume hood. The monomer was again dissolved in HFIP at 1μg/μl. After the removal of HFIP using argon, this processed monomer was then used to prepare protonated and deuterated monomer samples for HDX studies, and to synthesize (ptotonated and deuterated) fibril and protofibrils as described below.

For monomer samples used in HDX studies, dried peptide after organic solvent treatment was dissolved in 2.0 mM protonated Tris.HCl or deuterated Tris·DCl. Vigorous mixing at this step can result in precipitation and must therefore be avoided. To ensure that no higher-order structures are present that can seed aggregation reactions, solutions of monomeric peptide were subjected to high speed ultracentrifugation (Beckman Optima TL 100 Ultracentrifuge, Fullerton, CA) overnight at 85,000g at 4°C to remove any remaining aggregates. The supernatant was carefully collected, and the concentration of Aβ was determined by reversed-phase HPLC (Hewlett-Packard, Palo Alto, CA) (see details below). These Aβ peptide solutions were then snap-frozen and stored at –80 ºC prior to use. The protonated and deuterated monomer samples were prepared at a concentration of 5 – 42 μM in 2.0 mM protonated Tris.HCl and 2.0 mM deuterated Tris·DCl, respectively.

Fibrils. After the organic solvent was evaporated off under argon, the monomer was dissolved in 2 mM NaOH in H_2O to 1 μg/μl. An equal volume of phosphate buffered saline (PBS) buffer (20.4 mM Na_2HPO_4, 3.6 mM KH_2PO_4, 274 mM NaCl, 5.4 mM KCl, pH 7.4) containing 0.05% sodium azide was added to the monomer solution to a final concentration of 0.5 μg/μl. The resultant solution was then ultracentrifuged overnight at 85,000g at 4°C to remove any remaining aggregates. The monomer was then "seeded" by adding fibrils from a previous stock at 1:750 (w/w) to ensure historical consistency. Aliquots were incubated *without agitation* at 37°C for 4-6 days. Fibril growth was monitored by thioflavin T (ThT) fluorescence (see details below) [50] until complete (~5-7 days). The quality of fibrils was assessed by electron microscopy. Fully deuterated fibrils were prepared according to the same procedure described above for growing

protonated fibrils, except that 2 mM NaOD in D_2O (instead of NaOH in H_2O), deuterated phosphate-buffered saline and deuterated fibrils (seed) were employed. The monomer equivalent concentration of the fibrils was determined by measuring the amount of Aβ in an aliquot of the fibrils dissolved in 1/99 (v/v) TFA/H_2O using reversed-phase HPLC (see details below). All fibrils were snap-frozen in liquid nitrogen, and stored at – 80 ºC.

Protofibrils. To generate Aβ(1–40) protofibrils, ~ 30 μM monomer rigorously disaggregated as described above was incubated with 100 μM calmidazolium chloride (CLC) in 10/90 [v/v] DMSO/PBS buffer undisturbed at 37°C for 2 days. The resultant CLC-stablized aggregates were then centrifuged at 315, 000g for 30 minutes, the supernatant was removed, and the pellet was resuspended in PBS. This whole process was repeated three times to remove any remaining unbound CLC from the reaction mixture. Fully deuterated protofibrils were prepared according to the same procedure for growing protonated protofibrils, except that deuterated phosphate-buffered saline were employed. The concentration of the protofibrils was determined by measuring the amount of Aβ in an aliquot of the protofibrils dissolved in 1/99 TFA/MeOH using reversed-phase HPLC (see details below). All the aggregates were snap-frozen, and stored at –80 ºC until used.

Pepsin solutions

Stock solutions of pepsin were prepared daily at a concentration of 1 μg/μl in 0.01M HCl. Working solutions were prepared by dilution of the stock solution with appropriate amounts of water, MeCN, and/or formic acid to generate solutions with final composition consistent with the desired MS processing solvent. For the digestion of monomer, fibrils and protofibrils, the concentration of pepsin was 0.03 – 0.7 μg/μl.

2.2 Methods

Thionflavin T Assay

Thioflavin T (ThT) assay for monitoring fibril growth was performed on a Perkin-Elmer LS50B luminescence spectrometer (Norwalk, CT) by transferring an aliquot of samples into a 1-cm quartz cuvette containing 15 μM ThT in PBS. ThT fluorescence was then monitored by excitation at 450 nm and fluorescence emission at 482 nm. Because the ThT signal varies linearly with fibril mass for any given amyloid fibril, the signal (normalized for constant monomer weight) can be used as a measure of the completeness of the fibril formation reaction [357].

Isolation and buffer exchange of fibrils and protofibrils

Since high ionic strength PBS buffers compromise the sensitivity of ESI-MS detection, exchange reactions have to be carried out in low ionic strength deuterated buffer [358]. Mature fibrils or CLC-stablized protofibrils were isolated by centrifugation at ~14,000 rpm for 30 minutes in a benchtop Eppendorf centrifuge. This long centrifugation time is required because fibrils or CLC-stablized protofibrils do not pellet well in low ionic strength buffer; centrifugation at very high g-forces is not a viable option because ultracentrifuged pellets are difficult to quickly resuspend for the HDX measurement. After decanting and discarding the supernatant buffer, the resulting fibril or CLC-stablized protofibrils pellet was washed with 2 mM Tris-HCl (the washing volume was the same as the starting sample volume) followed by centrifugation for 30 mins. At this stage it is critical to remove as much of the protonated buffer as possible from the pellet. Gel loading tips (Fisher Scientific) are ideal for removing final traces of the protonated solvent without disturbing the pellet. Deuterated 2 mM Tris-DCl buffer was then added, under nitrogen, to the fibril pellet. This marks the start of the exchange reaction and the formation of partially deuterated samples. The solution was vortexed vigorously to resuspend the fibrils or CLC-stablized protofibrils from the pellet, after which aliquots from the exchanging suspension were sampled for HDX-MS analysis as described below. To prepare fully protonated control samples, the buffer exchange

described above was performed with protonated Tris buffer. For preparing fully deuterated control samples, 2 mM deuterated Tris buffer was the solvent for washing and resuspending. The monomer equivalent concentrations of fibril or CLC-stablized protofibril samples used in the HDX experiments were determined using HPLC (see below) and were between 8 and 60 μM.

Assessment of the effect of acetonitrile on pepsin

To assess the effect of acetonitrile on pepsin activity (discussed in Chapter 3), Aβ monomer solution in 2 mM tris was digested with freshly-made pepsin solutions in the presence of water, 0.5% formic acid, and varying amounts of MeCN (0%, 15%, 30%, 50%). Solutions also contained 0 or 0.06 mg/ml (~14 μM) Aβ monomer and 0 or 1.2 mg/ml pepsin (providing a 20:1 w/w pepsin:Aβ ratio, or roughly a 2.5:1 mole ratio, when both are present). Solutions containing pepsin were generally mixed in an Eppendorf vial using a vortex mixer. The digestions were quenched by adding sufficient 0.2 M ammonium hydroxide to bring the final solution pH to around 8. Following quenching, 100-μL aliquots were analyzed by HPLC and HPLC/MS (details below). The retention time of Aβ was around 15.0 min. Hydrolysis products eluted in the range of 8 to 16 min.

Purification of pepsin-like enzymes

Dialysis of protease type XIII, protease type XVIII and endothiapepsin. 1 mL of aqueous solution of proteases type XVIII (0.28 μg/μL), 1 mL of aqueous solution of type XIII (0.38 μg/μL), and 200 μl of 1 μg/μL endothiapepsin saturated in ammonium sulfate solution were dialyzed at 4°C against H_2O with four change of the H_2O buffer after 4, 8, 12 and 20 hours. The dialysis was allowed to continue overnight, totaling 26 h. The membrane used was Fisherbrand regenerated cellulose dialysis tubing (Fisher Scientific, Pittsburgh, PA), with a molecular weight cut-off of 12000-14000.

Concentration determination using BCA assay. The final concentrations of the three dialyzed proteins were determined by "BCA Assay" using the BCA™ Protein Assay Kit (Pierce Biotechnology Inc., Rockford, IL). In this assay, bovine serum albumin (BSA)

was used to as the standard to construct the standard curve. The assay procedure is as follows. First, 25 mL of working reagent mixture was prepared by mixing BCA™ reagent A and BCA™ reagent B at a ratio of 50 to 1. Second, BSA solutions for constructing the calibration curve were prepared by mixing 1mL of working reagent mixture with 0 (blank), 10, 20, 30, 40, 50 µL of 0.5 µg/µL BSA. Third, sample solutions were prepared by mixing 15, 30, 50 µL of dialyzed protease type XIII, protease type XVIII and endothiapepsin with 1 mL working reagent mixture. Fourth, all the samples were incubated at 60°C for 30min. The samples were then cooled to room temperature before the absorbance measurement. The absorbance of these solutions was measured at the wavelength of 562nm using a SpectraMax Plus microplate spectrophotometer (Molecular Devices, Sunnyville, CA). The calibration curve was constructed using the blank-corrected absorbance of BSA solutions as a function of BSA concentrations. The concentrations of the enzyme samples in H_2O were then determined based on the calibration curve and their absorbance as well as their sampling volumes. Totally 1 mL ~ 0.8 µg/µL protease XVIII, 1 mL ~ 0.2 µg/µL protease XIII and 200 µl of 0.75 µg/µL endothiapepsin were obtained after the dialysis.

Preparation of pepsin-like enzyme solutions for on-line proteolysis. The aqueous solutions of the three enzymes after dialysis were added with formic acid to such an extent that the final solutions contained 0.5/100 (v/v) HCOOH/H_2O. The stock solutions of *unpurified* protease type XIII and protease type XVIII were prepared at 1 µg/µl in 0.5/100 (v/v) HCOOH/H_2O. Working solutions were prepared by diluting the above stock solutions with the solvent containing 0.5/100 (v/v) HCOOH/H_2O. The final concentrations of the enzymes employed in the on-line digestion experiments presented in Chapter 4 were ~ 0.05 µg/µl - 0.2 µg/µl.

Procedure for polishing eroded electrospray emitter tips

A Dremel model 395 Moto-Tool (Montreal, Canada) equipped with a ¾ inch diameter medium sander disc was used to polish the emitter tips described in Chapter 5. Polishing compound (#421, Dremel) was applied to the tip to help obtain a smooth

rounded surface. After polishing, the tube was flushed with 500 µL chloroform to remove any residual polishing compound using a syringe connected to the unsmoothed end through a 1/16 in. Valco metal union with Teflon ferrules. The capillary was then rinsed with 500 µL of HPLC water**,** and then blown dry with nitrogen gas.

2.3 Instrumentation

Mass Spectrometry

Q-Star XL mass spectrometer

A Q-Star XL quadrupole time-of-flight hybrid instrument (Applied Biosystems, Foster City, CA) equipped with an Ionspray source was used to acquire ESI-MS mass spectra presented in Chapter 3 (unless otherwise mentioned) and in Chapter 5, and all ESI-MS/MS mass spectra presented in this dissertation. All experiments were performed in the positive ion mode. Source parameters including the sprayer position were optimized for high sensitivity and stability. The IonSpray voltage and declustering potential were 4500 V and 60 V, respectively. Except as noted, the sprayer tip was positioned about 12 mm away from the curtain plate with a lateral displacement about 5 mm off-axis at an angle of 45 degrees to the ion sampling axis. A microammeter (Model 27, Simpson Electric Co., Chicago, IL) was connected between the high voltage power supply and the ion source connector to enable monitoring of the emission current. Nitrogen from liquid boil-off was used as nebulizer, curtain, and collision gas. The pressure of nebulizer and curtain gases were respectively 40 psi and 25 psi, while the gas pressure in the collision cell was set at 3 for the MS mode and 5 for the MS/MS mode. All MS spectra were acquired in the multichannel accumulation mode from m/z 650 to 1200 for intact peptide and from m/z 300 to 1200 Da for proteolytic fragments for 1 min (60 scans). MS/MS spectra were acquired using a 3 Da window for MS1 and collecting data from MS2 over the range 100-2000 m/z for 5 - 10 min. To minimize artifactual deuterium exchange, the hole from the source leading to the venturi pump was blocked so that moist laboratory air was prevented from being sucked into the source housing. Also,

extra nitrogen gas (500 mL/min) was introduced into the source through the "make-up" hole on the ionspray source housing.

The Q-Star IonSpray™ probe includes two stainless steel microvolume tees (Figure 2.1). The tee nearer the spray tip (T3) is used to introduce nebulizing gas via stainless steel Tube 3, while the other tee (T2) can be used to provide a continuous stream of sample via Tube 2. A third tee (T1; 0.25-mm diameter PEEK; Valco Instruments, Houston, TX) was added to enable on-line addition of processing solvent. Sample and processing solvent were infused into T1 via separate 100-µm i.d. fused silica capillaries (Polymicro Technologies, Phoenix, AZ) using the built-in and Harvard Apparatus (South Natick, MA) model 11 syringe pumps, respectively. The resulting mixture flowed through the fused silica Tube 1 (75 µm ID × 190 µm OD) to the spray tip.

The probe was operated in two modes. In the standard ("coaxial") mode, the spray end of Tube 1 was flush with the end of the stainless steel (316 grade) Tube 2 (220 µm ID × 410 µm OD) and the third arm of T2 was unused (so that Tube 2 was left open to air). In the "triaxial mode", Tube 1 was retracted slightly (~ 5 mm) from the spray end of Tube 2, thus providing a small volume (~ 0.19 µL) for mixing with a secondary solvent that was delivered from T2 via Tube 2 using a Harvard Model 22 syringe pump. For both modes, Tube 3 was ~ 0.5 mm back relative to Tube 2. For simplicity and convenience, "coaxial probe" and "triaxial probe" are the terms used for describing the two configurations in the following discussion.

When the Q-Star Ionspray™ probe was used as a coaxial probe, flow rates for Aβ sample solution and processing solvent (generally 46/54/0.5 (v/v/v) H_2O/MeCN/HCOOH) were 0.85 µl/min and 9.25 µl/min, respectively. For analysis using the triaxial probe, sample (0.85 µL/min) was mixed with the initial processing solvent (generally 0.5% formic acid in water, 4.25 µl/min) in T1 and then mixed with MeCN (containing 0.5% formic acid, 5 µl/min) at the probe tip. The total flow through Tube 1 was twice as high in the coaxial probe, so the length of Tube 1 was doubled (46 cm vs. 23 cm) in the coaxial probe, to match the total time from mixing to the end of Tube 1 (~12 seconds). With the triaxial probe, there was an additional 1.1 second transit time for the 0.19-µL volume after Tube 1. Electrical contact was made at T2, making

(a)

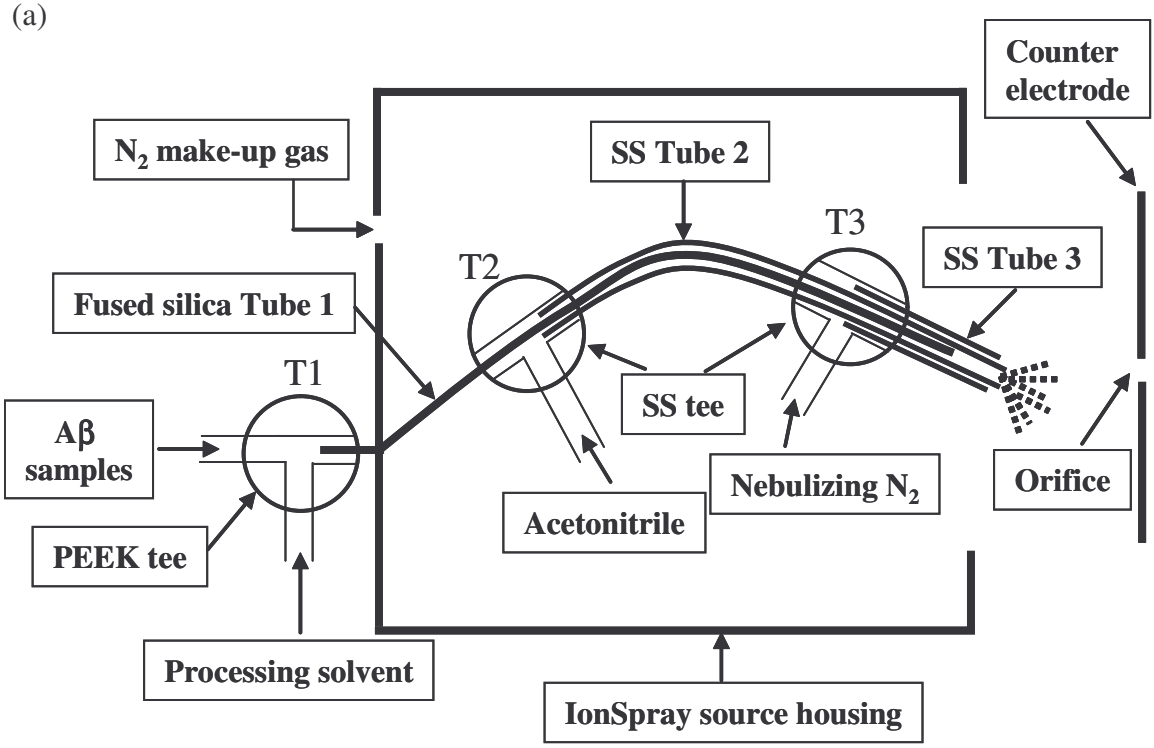

(b)

Triaxial probe:

Tube 1: 190um (OD) × 75um (ID) × 23 cm (length) (fused silica)

Tube 2: 420 um (OD) × 220um (ID) (stainless steel)

Coaxial probe:

Tube 1: 190um (OD) × 75um (ID) × 46 cm (length) (fused silica)

Tube 2: 420 um (OD) × 220um (ID) (stainless steel)

Figure 2.1. (a) Diagram of the modified electrospray probe (not to scale) on the Q-Star XL instrument, shown in the triaxial configuration (Tube 1 ~ 5 mm back relative to Tube 2). For coaxial operation, Tube 1 is extended flush with the end of stainless steel (ss) Tube 2; (b) tube diameters associated with both probes.

Tube 2 the anodic emitter for both geometries.

ProteinProspector 4.0.5 software (University of California, San Francisco, CA) was used to identify possible matches for proteolytic fragments from the Aβ primary sequence, which were then confirmed using MS/MS analysis of protonated Aβ monomer with collision energies between 30 and 45 eV (as needed for adequate dissociation of a given fragment).

Quattro II mass spectrometer

All HDX kinetics studies presented in Chapter 4 were carried out with a Micromass (Manchester, U.K.) Quattro II triple quadrupole electrospray ionization mass spectrometer equipped with a Z-spray source. Experiments were performed in the positive ion mode with a capillary voltage of 3.5 kV (unless otherwise noted) and a cone voltage of 20 V. Source temperature and desolvation temperature were maintained at 100°C and 110°C, respectively. The spectrometer was modified to allow monitoring of the ES emitter current by connecting a Keithley 600A electrometer (Keithley Instruments, Cleveland, OH) in series with the high voltage emitter power supply line. All MS spectra were acquired in the multichannel accumulation mode from 650 to 1200 m/z for the intact peptide and from 300 to 1200 Da for the proteolytic fragments. Triplicate spectra were collected for each sample.

For on-line proteolysis experiments, a home-made triaxial probe was used as a front end to the Z-spray source (Figure 2.2). Aβ samples (0.85 μL/min) and the solvent (pepsin in 0.5% formic acid, 4.25 μL/min) were infused into a 0.25-mm inner diameter Valco T union (mixing T in Figure 2.2) using two 50-μm i.d. fused silica capillaries (Polymicro) connected to Harvard Bioscience Model 22 and Model 11 syringe pumps. Fibrils were dissolved and proteolyzed as this mixture was delivered through the innermost silica tube (Tube 1) of the triaxial probe (50 μm i.d. and 360 μm o.d.). Acetonitrile with 0.5% formic acid was infused using a third Harvard Bioscience Model 11 syringe pump (10 μL/min, unless otherwise specified) into the middle stainless steel tube (Tube 2) (410 μm i.d. and 720 μm o.d.) and mixed with the dissolved and proteolyzed samples only near the tip of the electrospray emitter. Tube 1 was ~ 3 mm

(a)

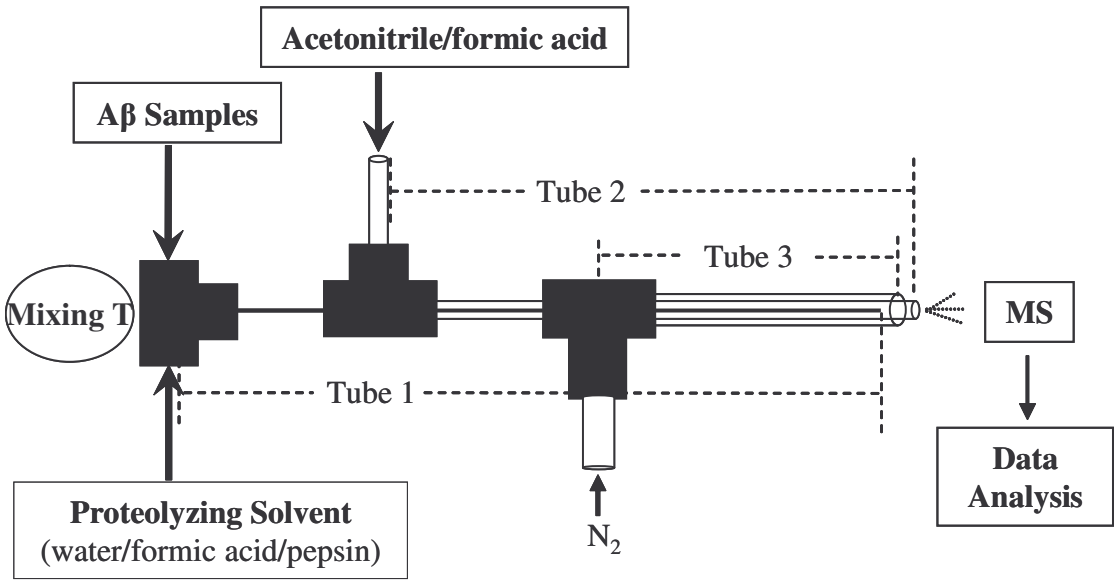

(b)

Tube 1: 360um (OD) × 50um (ID) × 52cm (length) (fused silica)

Tube 2: 720 um (OD) × 410um (ID) (stainless steel)

Tube 3: 1100um (OD) × 860um (ID) (stainless steel)

Figure 2.2. Schematic of the triaxial probe (not to scale) on the Quattro II instrument designed for HDX-MS experiments in conjunction with on-line proteolysis. Tube 1 is ~ 3 mm back relative to Tube 2, while Tube 3 is ~ 0.5 mm back relative to Tube 2. Processing solvent is optimized to quench exchange, disaggregate and dissolve fibrils, and generate defined peptide fragments; the acetonitrile-formic acid stream prepares the same for the mass spectrometer; (b) tube diameters associated with the probe.

(unless otherwise mentioned) back with respect to Tube 2, creating a dead volume of ~ 0.4 µl (corresponding to ~ 1.6 s mixing time when the total liquid flow rate is ~ 15 µl/min). Nebulizing gas (nitrogen) was delivered to the outermost stainless steel tube (Tube 3) (860 µm i.d. and 1100 µm o.d), which was ~ 0.5 mm back relative to Tube 2. The flow rates of N_2 nebulizing gas and N_2 drying gas were set at 50 liter/h and 300 liter/h, respectively. The length and diameter of Tube 1, and the flow rates, control the time from mixing to the end of Tube 1 (i.e. the time for digestion: ~ 12 s). This approach provides effective and rapid (~ 12 s) on-line proteolysis, while minimizing artifactual exchange (discussed in Chapter 3 and Chapter 4)).

The standard coaxial probe on the Quattro II is made up of two stainless steel tubes. Aβ samples were infused to one arm of a 0.25 mm internal diameter Valco T union (Mixing T, Figure 2.3) using a Harvard Biosciences model 22 syringe pump and a 75 µm i.d. fused silica capillary. Solvent was pumped through a second fused silica capillary to another arm of the Mixing T using a Harvard Biosciences model 11 syringe pump. The third arm of the mixing T is connected to an ESI probe via a ~23 cm long and ~110 µm i.d. stainless steel capillary (Tube 1, Figure 2.3). Tube 2 passes through a larger tube, accommodating nitrogen nebulizing gas (to assist the spray process). Tube 2 is ~ 0.5 mm back relative to Tube 1. During the use of this probe, the flow rates of nebulizing gas and drying gas were set at 20 liter/h and 300 liter/h, respectively.

Tips for HDX data collection

To obtain reproducible mixing time between sample and solvent, and hence reproducible data, the syringe pumps delivering sample and solvent into the mixing T should be turned on and off simultaneously. Aggregates tend to settle in the syringe during long-term kinetics experiments resulting in a loss of MS signal; it is therefore important to make sure that the sample in the syringe is either changed frequently (30-60 min in our hands), or is remixed periodically. It is also very important to clean the mixing T and the capillaries used for sample and solvent delivery, by flushing with water and solvent respectively, between each run. Adequate cleanliness is validated by collecting data for a blank run between each new sample. Any clogs in the mixing T can

(a)

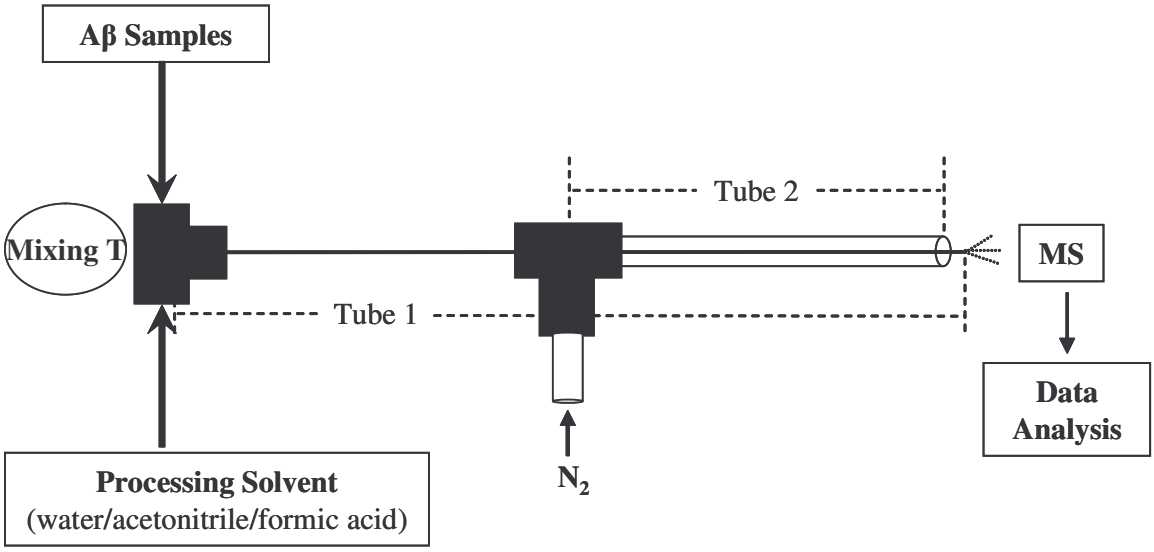

(b)

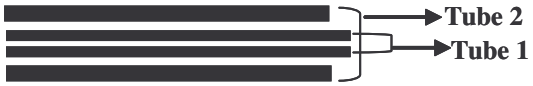

Tube 1: 240um (OD) × 110um (ID) × 23 cm (length) (stainless steel)

Figure 2.3. Schematic of the coaxial probe (not to scale) on the Quattro II instrument. Tube 2 is ~ 0.5 mm back relative to Tube 1. Processing solvent is optimized to quench exchange, disaggregate and dissolve fibrils, and prepare sample for mass spectrometry; (b) tube diameters associated with the probe.

be removed by dismantling the T and sonicating it in the processing solvent.

During HDX-MS experiments, since the processing solvent is generally protonated and the sample exchange buffer is deuterated, there is always a percentage of D_2O present in the final solvent mixture. The expected percentage can be easily calculated from the ratio of the solvent and the sample flow rates, and can be confirmed by comparing the ratio of the acetonitrile dimer peak at mass-to-charge (m/z) 83 $[(CH_3CN)_2 + H]^+$] and at m/z 84 $[(CH_3CN)_2 + D]^+$. The ratio of this pair of peaks should be monitored during data collection to ensure consistency in flow rates. Any blockage in the experimental set-up will affect the mixing rate and this change is reflected in the ratio of the acetonitrile peaks at m/z 83 and 84. MS data on control samples (fully protonated and fully deuterated fibrils) should be collected at least once a day, to ensure that the instrument has worked fine and to provide data for correcting artifactual exchange of the partially deuterated samples.

High performance liquid chromatography (HPLC) and HPLC-MS

Revered-phase HPLC instrument used for determination of the concentrations of monomer, fibril and protofibril samples was an Agilent 1100 LC system with a ZORBAX SB-C3 column (3×150mm), an autosampler, and a UV detector. The solvent flow rate was 1 mL/min, and the temperature was controlled at 25 °C. The solvents used were 0.1% TFA in water (solvent A), and 0.1% TFA in MeCN (solvent B). The column equilibrated to 1% solvent B prior to injection, and then the sample was eluted with a linear gradient of 1%-51% solvent B over a 40 min period. The separation was monitored by absorbance at 215 nm.

HPLC-MS experiments were conducted with an Agilent 1100 Series LC/MSD system with a ZORBAX SB-C3 column (3×150mm), an autosampler, serial UV and electrospray MS detectors, and a splitter (splitting ratio: 100:1). The solvent flow rate was 1 mL/min, and the temperature was controlled at 25 °C. Solvent A was 0.1% formic acid in water, and solvent B was 0.1% formic acid in MeCN. The column equilibrated to 1% solvent B prior to injection, and then the sample was eluted with a linear gradient of 1%-51% solvent B over a 40 min period. The separation was monitored by absorbance at

215 nm and by MS scans from m/z 300 to 2000.

The LC-MS experiments employed a single quadrupole instrument equipped with a standard Agilent electrospray source operating in the positive ion mode. The drying gas flow (N_2), nebulizer pressure (N_2), drying temperature, and capillary voltage were set at 3 L/min, 35 psig, 300 ºC and 3000 V, respectively.

Scanning electron microscopy (SEM)

Electron micrographs were taken on a Hitachi S-3500N Scanning Electron Microscope (Hitachi High Technologies America, Inc., Schaumburg, IL). X-ray fluoresence mapping was conducted using a Leo 1525 Scanning Electron Microscope (Carl Zeiss SMT inc., Thronwood, New York). The magnification was 200, unless otherwise noted. The voltage was 20 kV for both microscopes. The samples (stainless steel tubes) were attached to the sample stage via scotch tape for SEM analysis.

2.4 Data Analysis

Calculation of average masses

MS data obtained from the Q-Star instrument were isotopically resolved due to the high resolution (up to 11000), so calculation of average molecular weights was done using the equation

$$MW_{avg} = \frac{\sum_n (I_n \times M_n)}{\sum_n I_n} \qquad \text{Eqn. 2.1}$$

where I_n is the intensity (height) of n_{th} isotopic peak and M_n is the centroid mass of that peak (corrected for ionizing protons). For ions detected with multiple charge states, neutral molecular masses obtained from those charge states were averaged to obtain the molecular masses.

To obtain molecular masses of MS data acquired using the Quattro II instrument, peaks were first smoothed by using the Savitzky Golay method incorporated in the

Micromass Masslynx software package. For cases where isotopic clusters were resolved and only a single peak cluster was identified, the molecular masses were determined using Eqn. 2.1. For cases where isotopic clusters were not resolved and only a single peak envelope was identified, centroids of the unresolved peak envelopes were used to obtain the average molecular weights. For cases where overlapping peaks were identified, data were first deconvoluted using the Pearson VII equation in the PeakFit (Systat) program (see details in Chapter 4), and then the centroids of the deconvoluted peaks were used to obtain the average molecular weights. For ions detected with multiple charge states, neutral molecular masses obtained from those charge states by subtracting the mass of ionizing groups (protons) were averaged to obtain the molecular masses.

Determination of the amount of water oxidation participating in oxidation of Aβ

The ^{18}O incorporated into Aβ in experiments involving $H_2{}^{18}O$ (described in Chapter 5) was estimated by treating each isotopic cluster in the experimental spectrum as a linear combination of the spectrum obtained with unlabeled water, and a hypothetical spectrum for fully labeled Aβ. The latter spectrum was modeled simply by shifting each peak in the unlabeled cluster upward by 2 Da (shifting m/z upwards by 2/z). This avoided the need for an expensive, fully deuterated standard, and will be accurate as long as the sensitivities to the labeled and unlabeled Aβ are the same - a very reasonable assumption. All peaks in a given isotopic cluster were considered. (Note that not even the Q-star resolution (up to 11000) was adequate to distinguish isobars in the Aβ isotopic clusters, given its molecular weight of 4329.9 Da.).

CHAPTER 3

A TRIAXIAL PROBE FOR ON-LINE PROTEOLYSIS COUPLED WITH HDX-MS

HDX-MS analysis of intact proteins provides insight into the overall exchange protection of the entire protein molecule. Determination of specific exposed and protected sites by HDX-MS requires coupling with proteolysis and/or MS/MS (typically CID or ECD). There is some risk of intramolecular scrambling of deuterium labels during CID or ECD [235, 304, 309-313], as discussed in section 1.3.3. Peptide digestion can offer an alternative or supplement to direct CID or ECD for localizing incorporated deuterium with HDX-MS. Pepsin has proven to be particularly useful for this purpose because of its good activity at the low pH values used to minimize artifactual hydrogen exchange (spurious incorporation or loss of deuterium) during sample work-up after exchange (section 1.4). A typical protocol involves incubation of deuterium-labeled proteins with pepsin at about pH 2 for ~5 min at 0 ºC (low temperature also reduces artifactual exchange). The digest is then subjected to liquid chromatography (LC), with on-line MS or MS/MS analysis to assess the deuterium content of individual digestion products (section 1.3.3) [230, 235]. Relatively high quantities of pepsin are used to minimize digestion time and the corresponding opportunity for scrambling; this can complicate direct analysis of the hydrolysate without LC separation (due to increased background) [236]. Use of an immobilized enzyme in a continuous-flow column can mitigate these problems (section 1.4) [236, 314, 334-335].

ESI-HDX/MS methodologies have been adapted by our group for analysis of the Aβ amyloid fibrils [58-59]. To dissolve fibrils after deuteration and prior to MS analysis while limiting artifactual exchange, we have used continuous flow mixing of the deuterated fibril suspension with a low-pH quenching and dissolving solvent that contains acetonitrile (MeCN) to facilitate electrospray and to reduce artifactual exchange

(by reducing the protic solvent concentration in the final mix) (Figure 1.14). Using this approach we have determined that roughly half of the 39 Aβ (1-40) amide protons are protected from HDX in fibrils grown from the peptide [58-59]. In anticipation of efforts to further localize the protected sites, we needed a way to achieve rapid proteolysis with minimal scrambling. Use of an immobilized enzyme would require fibril dissolution prior to passing through an enzyme column; a faster sample treatment protocol would be desirable. This Chapter will demonstrate the utility of a triaxial electrospray probe (Figure 2.1) to facilitate effective and rapid on-line dissolution and proteolysis of fibrils at room temperature. The performance is compared with that of the coaxial probe used previously [58-59]. Validation of a method for correcting HDX data obtained from the triaxial probe for artifactual exchange is also presented.

3.1 Why Use a Triaxial Electrospray Probe?

3.1.1 Conditions for On-line Proteolysis Using a Coaxial Probe: The Effect of Acetonitrile on Pepsin Activity

Given the compatibility of pepsin with low pH and the occasional enhancement of enzyme activity by organic solvents [359-360], the simplest approach to on-line proteolysis of fibril-derived Aβ would be to add pepsin to the processing solvent used to arrest H/D exchange, dissolve the fibrils, and facilitate ESI. Figure 3.1a illustrates the results obtained using this simple approach with Aβ monomer. There is no evidence of pepsin digestion of Aβ even at an enzyme:monomer weight ratio as high as 40:1, using the 50/50/0.5 (v/v/v) H_2O/MeCN/HCOOH processing solvent used previously for fibril analysis without proteolysis [58-59]. Only intact Aβ is detected (labeled peaks); all other peaks above noise were attributable to solvent and/or pepsin background. Similar results (not shown) were obtained with the digestion of Aβ fibrils at the same weight ratio. There are two possible explanations for these observations: either the enzyme is inactive under these conditions, or the signals due to proteolysis products are suppressed (e.g., by more hydrophobic intact material) [361].

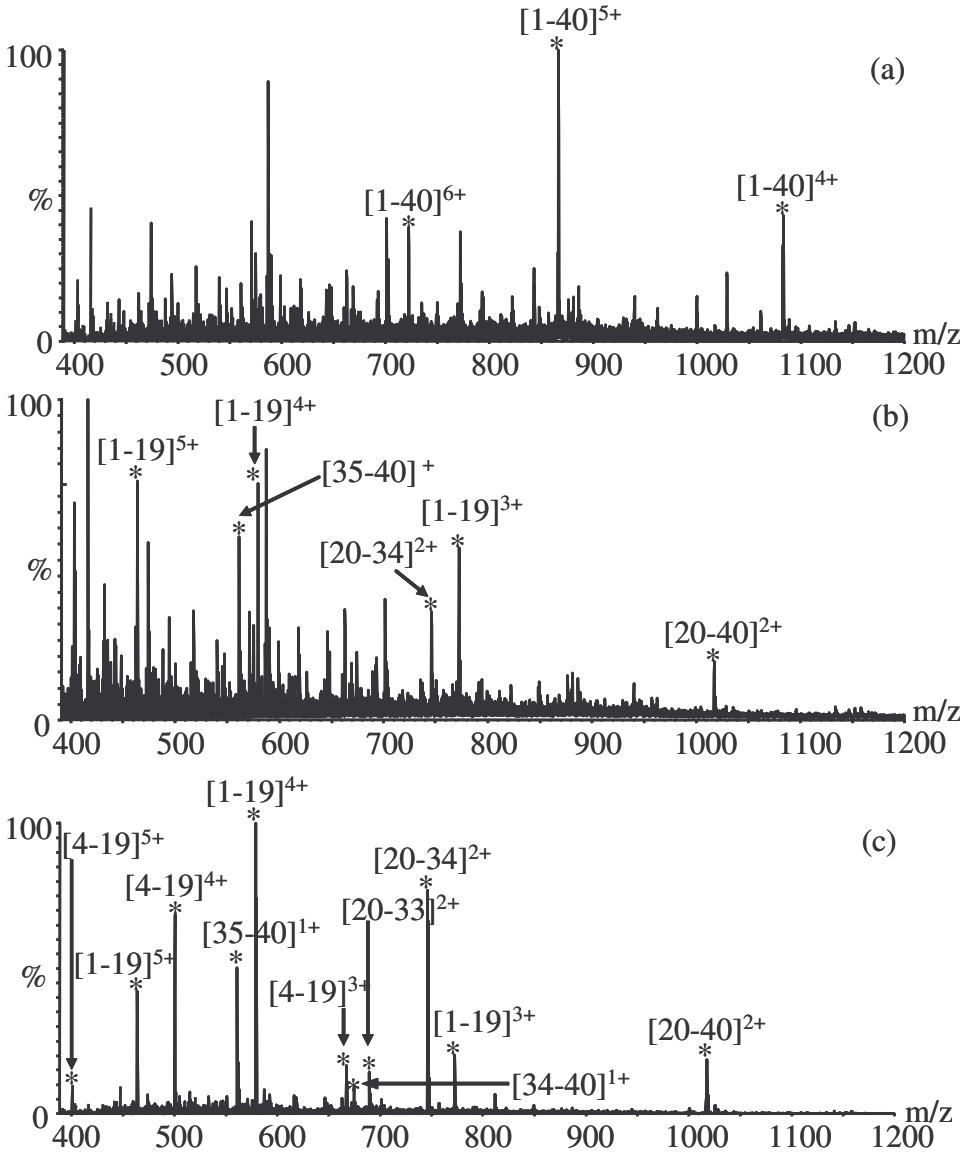

Figure 3.1. ESI mass spectra obtained from on-line digestion of Aβ(1-40) monomers with pepsin (a) in 50/50/0.5 (v/v/v) H_2O/MeCN/HCOOH using a coaxial probe (enzyme/peptide = 40/1 [w/w]); (b) in 85/15/0.5 (v/v/v) H_2O/MeCN/HCOOH using a coaxial probe (enzyme/peptide = 43/1 [w/w]); (c) in 100/0.5 (v/v) H_2O/HCOOH using a triaxial probe (enzyme/peptide = 0.9/1 [w/w]). Intact peptide and digestion products are labeled and marked with asterisks; unlabeled peaks are from pepsin and solvent background.

To distinguish between these possibilities, digests with varying MeCN concentrations were analyzed by HPLC using UV and MS detection (described in section 2.2). In the first control experiments, pepsin was omitted, allowing determination of the chromatographic retention time of the intact Aβ monomer. In the absence of pepsin, the monomer peak was detectable with roughly constant sensitivity and retention time (15.0 min) for all digestion solvents tested. Upon addition of pepsin (20:1 w/w pepsin:Aβ), incubation for 20 sec (approximating the time available for on-line digestion using the coaxial probe) and quenching with NH_4OH, the monomer peak disappeared if the solvent contained 0 to 30% MeCN, indicating effective hydrolysis. At 50% MeCN, pepsin attenuated the monomer peak to about 31% of the peak area observed when pepsin was absent, indicating significant inhibition of enzyme activity (Table 3.1). When the amount of enzyme was reduced to 2:1 (w/w) with 50% MeCN, the intensity of the monomer was not attenuated measurably unless the mixing time was increased substantially; after 1 min of digestion, the signal for intact peptide was attenuated by 6%, and 5 min digestion resulted in 23% attenuation.

In addition to the attenuation of the peak for the intact peptide, enzyme activity was evidenced by the appearance of new peaks in the HPLC experiments. With the MS detector it was possible to confirm that these arose from proteolytic Aβ fragments (Table 3.1). The prominence of fragment 1-19 (resulting from cleavage between Phe_{19} and Phe_{20}) is consistent with the known preference of pepsin for cleavage of Phe-Phe bonds [362]. The complementary 20-40 fragment grows with increasing MeCN concentration, at the expense of smaller fragments which result from cleavage between Leu_{34} and Met_{35}, and between Gly_{33} and Leu_{34}, presumably subsequent to the Phe_{19}/Phe_{20} cleavage. This and the overall inhibition of enzyme activity in the presence of MeCN are consistent with the reported effect of organic solvents, including MeCN [334, 363-365], on pepsin activity. As evident from Figure 3.2, the seven fragments observed are consistent with the preferences of the relatively non-specific proteolysis of pepsin (cleavages on the N- and/or C-terminal side of Phe (F), Leu (L), Glu (E), Trp (W), and Tyr (Y) [362, 366]).

Based on the LC results, a preliminary on-line experiment was attempted using 30% MeCN and an enzyme:Aβ ratio of 20:1 [w/w]. Relatively little hydrolysis, plus a

Table 3.1. Fragments observed by LC following digestion of Aβ(1-40) monomer with pepsin (20 sec digestion time, enzyme:substrate = 20:1 w/w, except where noted) in the solvents indicated. Also listed are the observed LC retention times and peak areas. Fragment assignments were confirmed by MS/MS.

		Solvent composition (H_2O : MeCN : HCOOH) (v/v/v)			
		100 : 0 : 0.5	85 : 15 : 0.5	70 : 30 : 0.5	50 : 50 : 0.5
Fragment	**Retention time (min)**	**UV Area (arbitrary unit)**			
[4-19]	8.2	128 ± 6	0	0	0
[35-40]	8.5	62 ± 2	93 ± 4	76 ± 15	9 ± 2
[1-19]	9.0	638 ± 13	994 ± 19	970 ± 47	257 ± 54
[20-33]	9.5	110 ± 7	48 ± 3	28 ± 4	0
[34-40]	11.4	20.0 ± 0.4	46 ± 2	14 ± 2	0
[20-34]	12.1	387 ± 3	359 ± 4	266 ± 23	14 ± 6
[20-40]	15.5	12 ± 3	27 ± 5	138 ± 23	145 ± 24
[1-40]	15.0	0	0	0	468 ± 12
[1-40][1]	15.0	-	-	-	1531 ± 26

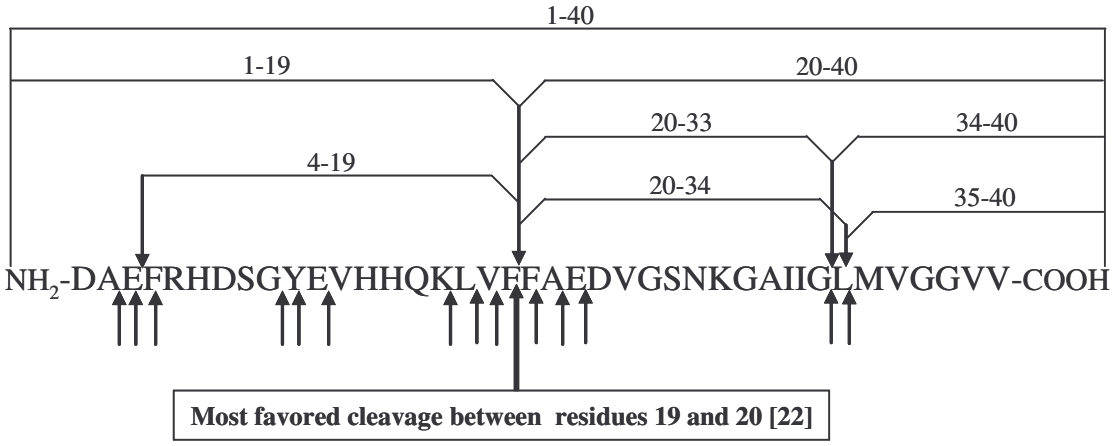

Figure 3.2. Comparison of the favored and observed pepsin cleavage sites on the Aβ(1-40) peptide. The down arrows represent the experimentally observed cleavage sites during 12 seconds digestion using a triaxial probe, while the up arrows indicate the cleavage sites expected to be preferred by pepsin. Phe (F)-Phe (F) cleavage is especially favorable.

strong background similar to that shown in Figure 3.1a were detected, possibly due to the shorter (12 sec vs 20 sec for the LC experiments) reaction time and suppression of signal by autolysis products (data not shown). Given the necessity for some MeCN to assure stable spray [171, 361, 367], 15% MeCN was selected as a reasonable compromise between acceptable signal and retention of enzyme activity. Even under these conditions (85/15/0.5 H_2O/MeCN/HCOOH), a high enzyme concentration (roughly 43:1 w/w enzyme:Aβ) was needed to fully attenuate the signal from intact peptide during on-line digestion of 15-μM monomer samples, and roughly 110:1 was needed for 16-μM (equivalent monomer concentration) fibrils. The higher pepsin requirement for fibrils likely reflects the shorter time available for hydrolysis due to the finite time needed to dissolve the fibrils and to expose cleavable sites. Under these extreme conditions, hydrolysis products were detectable (Figure 3.1b). However, at such high enzyme concentrations, autolysis of pepsin can become a significant competing reaction, leading to a strong background (Figure 3.1b). Furthermore, in the absence of pepsin, the signal-to-background ratio (S/B) (background assessed as the average intensity between m/z 1100 and m/z 1200) for the 5+ charge state base peak for the intact Aβ monomer using 15% MeCN was around half that obtained using 50% MeCN. Thus, such an on-line digestion system is far from being ideal.

3.1.2 On-line Proteolysis Using a Triaxial Probe

The triaxial probe pictured in Figure 2.1 was used to allow separate optimization of proteolysis and electrospray conditions by delaying introduction of MeCN until just before spraying. For this setup, the processing solvent 0.5/100 HCOOH/H_2O serves to dissolve fibrils, quench H/D exchange and accommodate pepsin, while the sheath liquid 0.5/100 HCOOH/MeCN serves to facilitate ESI operation. With the triaxial probe, only a 0.9:1 (w/w) pepsin:Aβ was required to reduce the monomer signal from 15 μM Aβ to baseline, *vs* 43:1 with the coaxial probe; the final solvent composition was 50.5/49.5/0.46 H_2O/MeCN/HCOOH for the triaxial probe (vs 86.3/13.7/0.46 H_2O/MeCN/HCOOH for hydrolysis with the coaxial probe). Moreover, the same 7 major Aβ fragments were observed (S/N > 70; Figure 3.1c) as from the bench-top digestion (Table 3.1), *vs* only 4

fragments (among strong interfering background peaks) using the coaxial probe (Figure 3.1b). The performance for digestion of fibrils (18 μM) was also enhanced; the 10.6:1 weight ratio pepsin:Aβ needed to eliminate the signal from intact fibrillar Aβ was roughly 1/10 the amount needed using the coaxial probe (final solvent composition: 86.3/13.7/0.56 H_2O/MeCN/HCOOH). Under these conditions the fibrils gave the same fragments as those observed for monomer in Figure 3.1c.

Although some expected cleavages were "missed" in the 12-second digestion time (evident in Figure 3.2), the fragments produced have the potential to provide structural information about the N-terminus (1-19), C-terminus (35-40), and part of the protected core (20-34) [40, 63, 74]. The observed cleavage between positions 19 and 20 for the fibrils is particularly significant, since this site is believed to be involved in the β-sheet network [40, 63, 74]; dissolution of fibrils evidently precedes hydrolysis, exposing sites involved in the secondary structures. HDX studies of these peptic fragments should contribute to the testing and refinement of structural models [40, 63, 74]. Although detailed discussion is presented in Chapter 4, feasibility of such HDX experiments is considered next.

3.2 Triaxial Probe vs. Coaxial Probe for HDX-MS Studies

In order to be useful for HDX-MS studies of amyloid fibrils, the triaxial probe must not only provide effective proteolysis, but it must do so without compromising sensitivity, impairing the dissolution of fibrils, or introducing additional artifactual exchange. These figures of merit were assessed in the series of experiments described next.

Sensitivity and signal stability. Similar sensitivity was achieved for both probes, as evidenced by nearly identical base peak ($[1\text{-}40]^{5+}$ at m/z 867) absolute intensities ($(1.8 \pm 0.06) \times 10^4$ for the triaxial probe, vs $(1.9 \pm 0.04) \times 10^4$ for the coaxial probe) and signal-to-background ratios (750 for the triaxial probe, vs 850 for the coaxial probe) for Aβ

monomers run on the two probes under conditions where the final solution composition is identical (50.5/49.5/0.46 H_2O/MeCN/HCOOH) (Figure 3.3). The relative standard deviation (RSD) of the absolute intensity of the base peak from 600 scans averaged over a 10-minute period is also nearly identical for the two probes (3% RSD for the triaxial probe, vs 2% for the coaxial probe), suggesting good signal stability for both probes.

It is interesting to note that while the base peaks and overall charge-state distributions in Figures 3.3a and 3.3b are similar, the relative abundance of the +6 charge state is somewhat higher with the triaxial probe (29% ± 2%, *vs* 21% ± 3% with the coax probe), despite the fact that the emission current was lower (0.25 μA, *vs* 0.5 μA for the coaxial probe) so that the pH would be expected to be higher [197, 368-370]. This difference was reproducible from scan-to-scan, but sensitive to tuning parameters, as observed elsewhere [371]. One contributing factor could be the difference in spray tip and "electrode" geometries. For the triaxial probe, electrical contact is made at least ~ 5 mm from the sprayer tip, whereas for the coaxial probe the contact is made only when the liquid from the silica tube 1 wets the steel tube 2 near the emitter tip. Other possible contributors include space charging and mixing efficiency, which are considered next.

Space charge effect. Space charge effects are a consequence of the mutual repulsion between particles of like charge [372]. To test for contributions from space charge effects to the enhancement of the 6+ peak in Figure 3.3 [373-374], the relative intensities of the +6 and +5 charge state monoisotopic peaks of Aβ monomer were monitored while moving the emitter horizontally across the entrance aperture. Results are shown in Figure 3.4. The profile for the coaxial probe was obtained while running 0.5-μM Aβ monomer in 50/50/0.5 (v/v/v) H_2O/MeCN /HCOOH at 10 μL/min in tube 1. The results for the triaxial probe were generated by running 1-μM Aβ monomer in 0.5/100 (v/v) HCOOH/H_2O at 5 μL/min in tube 1 and 0.5/100 (v/v) HCOOH/MeCN at 5 μL/min in tube 2, giving the same final composition and total flow. The two curves show similar trends. The fact that the biggest ratios were obtained when the probe tip was farthest away from the orifice is consistent with space charge, which would preferentially repel more highly charged ions to the periphery of the electrospray. Also plotted in Figure 3.4

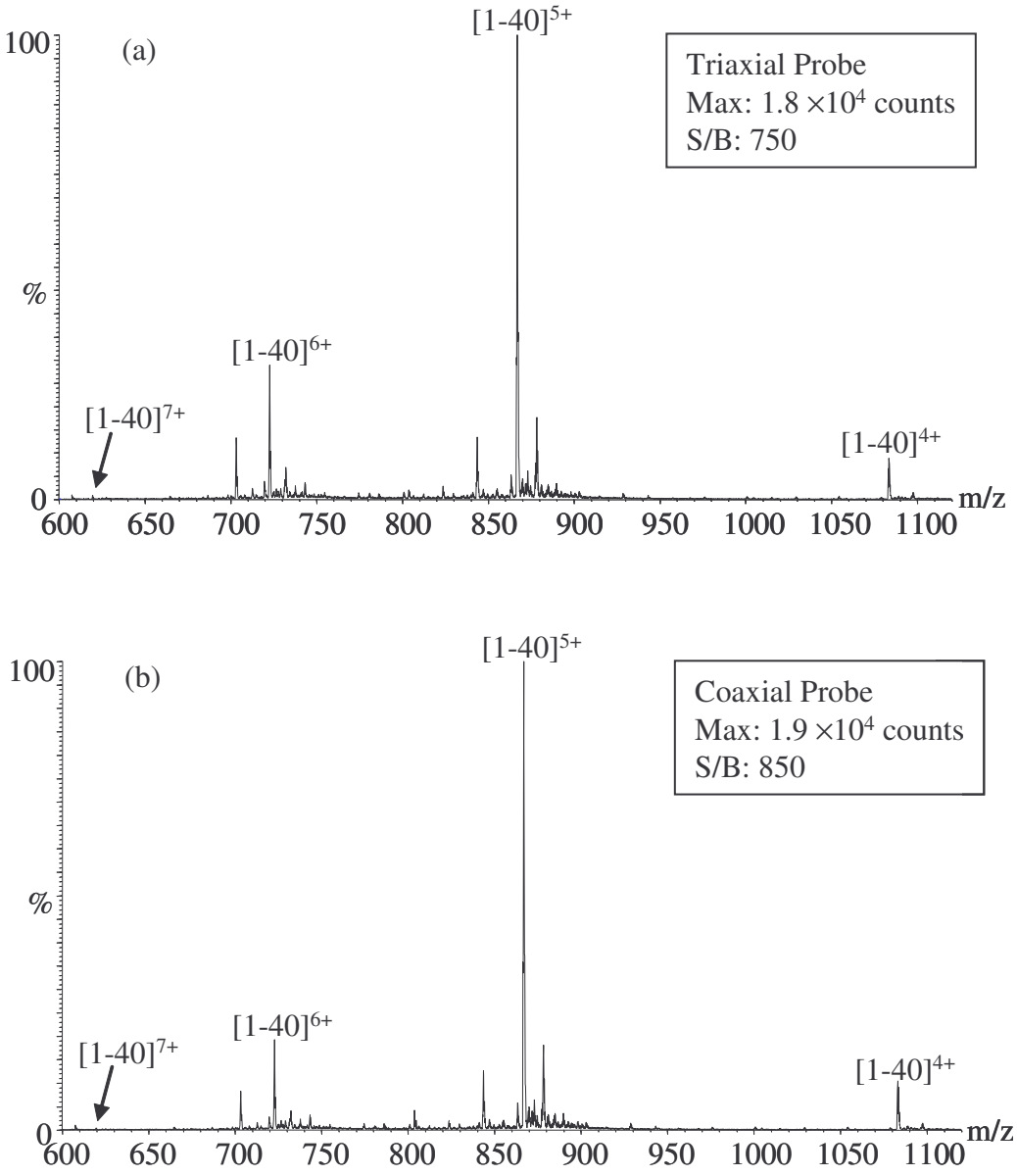

Figure 3.3. Mass spectra of Aβ(1-40) obtained using (a) the triaxial probe and (b) the coaxial probe. The inset shows the absolute intensity (counts) and signal-to-background ratio (S/B) of the highest monoisotopic peak (m/z 867) accumulated over a one-minute period. Background was assessed as the average intensity between m/z 1100 and m/z 1200.

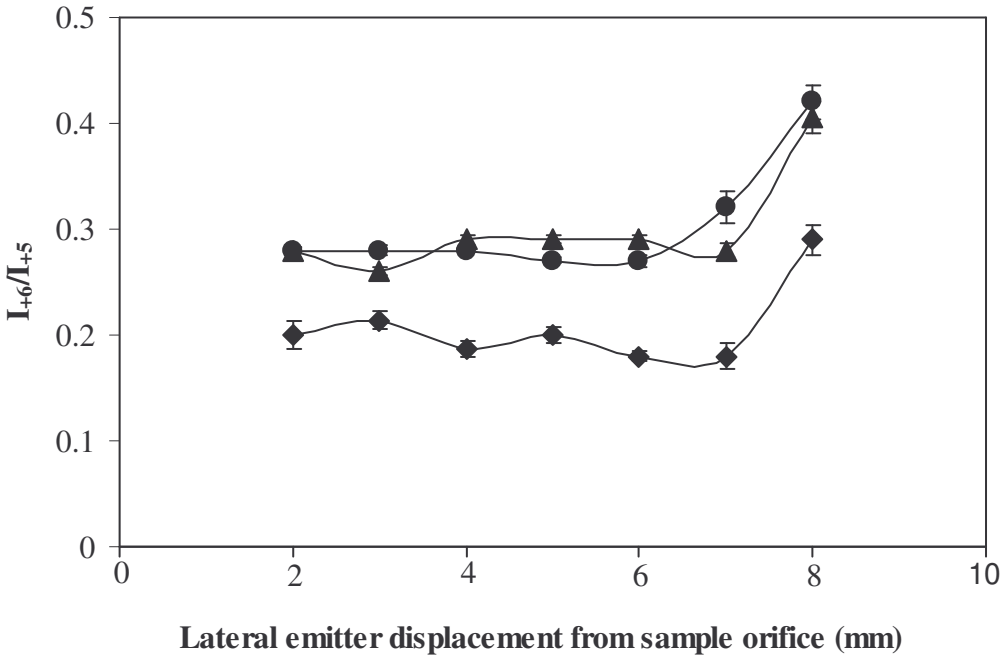

Figure 3.4. The intensity ratio of the +6 charge state peak to the +5 charge state peak versus the position of the probe tip relative to the sample orifice. Data were obtained from solutions containing Aβ(1-40) monomer in 50/50/0.5 (v/v/v) H_2O/ MeCN /HCOOH in tube 1 on the coaxial probe (◆); Aβ monomer in 100/0.5 (v/v) H_2O/HCOOH in tube 1 mixed on-line with 100/0.5 (v/v) MeCN/HCOOH through tube 2 using the triaxial probe (▲); or pre-mixed Aβ (1-40) monomer with 50/50/0.5 (v/v/v) H_2O/ MeCN /HCOOH in both tube 1 and tube 2 on the triaxial probe (●). The axial displacement was fixed at 12 mm. At 0 mm, the probe tip is on-axis with the sample orifice. Error bars represent the standard deviation of ratios from triplicate mass spectra.

are the ratios obtained when the premixed solution was run through both tube 1 and tube 2 of the triaxial probe (5 μL/min in each tube). The curve is indistinguishable from that obtained using the separated solvents, suggesting little (if any) effect of imperfect mixing which could have affected the solvent dielectric and therefore the charge–state distribution [375]. We conclude that space charge and resulting ion sampling effects are the primary contributors to the small differences evident in Figure 3.3. The higher currents for the coaxial probe may result in higher space charge, and therefore more scattering and less efficient sampling of more highly charged ions [373].

Mixing. Because of the rapid kinetics of proton exchange of reasonably strong acids and bases, the protonation/deuteration of triethylamine (TEA) was used as a probe of mixing efficiency. To mimic the flow conditions used above, 10/90 (v/v) D_2O/ MeCN was pumped at 5.1 μL/min through tube 2, while 0.1μM TEA in 0.5/100 HCOOH/H_2O was delivered to both arms of T1 in Figure 2.1 (flow rates of 0.85 μL/min and 4.25 μL/min), and then to tube 1 (total H_2O flow rate 5.1 μL/min). If the mixing at the sprayer tip is 100% efficient, the $[TEA+D]^+$:$[TEA+H]^+$ ratio would be 1:10, so that the signal intensity at m/z 103 would be ~ 16.8% of that at m/z 102 (including contributions from D, ^{13}C and ^{14}N). If there is no mixing at all at the sprayer tip, there would be no excess $[TEA+D]^+$ and the signal at m/z 103 would be just 6.8% of that at m/z 102, reflecting the normal isotopic abundance. Experimentally, the measured ratio was 14.8% ± 0.3%, suggesting a mixing efficiency of roughly 80% ± 3% ((14.8-6.8)/(16.8-6.8); the ^{13}C and ^{14}N contributions are subtracted). This in turn would provide 36% ± 1% MeCN in the "final" mix, instead of the expected 45%. By contrast, when the solutions were premixed 1:1 and run through all tubes at the indicated flow rates, the experimental ratio was 17.1 % ± 0.2%, very close to the theoretical prediction. The mixing efficiency at T1 in Figure 2.1 was tested separately using the coaxial probe. In this case, 0.1μM TEA in D_2O (0.85 μL/min) was mixed with 46/54/0.5 (v/v/v) H_2O/ MeCN /HCOOH (9.25 μL/min) in T1, and then the whole mixture was delivered and sprayed through tube 1. The measured i_{103}/i_{102} ratio was 26.8% ± 1.0%, matching the expected value of ~ 26.8% for perfect mixing, indicating that the mixing efficiency in T1 is ~ 100% within the experimental

error. For comparison, a value of 27.5% ± 0.7% was obtained from a 0.85:9.25 premixed solution, also within the experimental error of the expected value. These mixing efficiencies should be interpreted as maximum values, since they are based on the mixing of water, protons and the small TEA molecule; slower diffusion or increased viscosity in solutions of a larger molecule like Aβ might result in less homogeneity. Nevertheless, it is clear that mixing at the emitter tip for the triaxial probe is reasonable, though not perfect.

Fibril dissolution. Rapid disaggregation/dissolution of fibrils into monomers is essential for HDX-MS studies of fibrillar structure. Earlier studies found that more than half of the fibrils present in suspensions with ~11 μM equivalent monomer concentration could be dissolved in < 10 sec using the coaxial probe [58]. Studies of the kinetics of deuteration and parallel work with HDX-NMR suggest that the dissolved fraction represents full dissolution of a representative fraction of all fibrils, rather than sampling a readily dissolved fraction of each fibril or a subset of fibrils [58-59, 61]. To compare the dissolution efficiency achieved with the coaxial and triaxial probes, the intensities from on-line dissolution of fibril suspensions of varying effective monomer concentrations were compared with those obtained from monomer calibration curves (5 to 42 μM monomer flowing into one arm of T1 in Figure 2.1 at 0.85 μL/min for both probes). To improve precision, neurotensin was incorporated as an internal standard in the processing solvent (0.23 μM in 46/54/0.5 (v/v/v) H_2O/MeCN/HCOOH flowing at 9.25 μL/min for the coaxial probe and 0.5 μM in 100/0.5 (v/v) H_2O/HCOOH flowing at 4.25 μL/min for the triaxial probe). For the triaxial probe, 100/0.5 (v/v) MeCN/HCOOH at 5 μL/min was introduced through T2 as usual. Quantitation was based on the ratio of the summed intensities of monoisotopic peaks from the observed charge states of Aβ (+4 to +7) and neurotensin (+2 and +3).

Table 3.2 summarizes the results of this study. The measured monomer concentration increases monotonically with increasing fibril load, suggesting that saturation (equilibration) is not achieved. At monomer equivalent concentrations of ~8 μM or ~14 μM, the dissolution of the fibrils with either probe is efficient, but the coaxial

Table 3.2. Comparison of on-line solubility of Aβ(1-40) fibrils in the mixing tee (T1 in Figure 2.1) using the triaxial probe and the coaxial probe. Indicated concentration is the monomer concentration equivalent to the quantity of fibrils in 2 mM tris buffer flowing into one arm of T1 (Figure 2.1). The indicated uncertainties are standard deviations based on triplicate acquisitions of mass spectra.

Initial fibril concentration in 2mM tris buffer	Measured concentration (% dissolved)	
	Triaxial probe	Coaxial probe
8.0 μM	7.3 ± 0.9 (91 ± 11)	7.9 ± 0.7 (99 ± 8)
14.0 μM	11 ± 1 (81 ± 9)	12 ± 1 (89 ± 9)
29.6 μM	12.6 ± 0.5 (43 ± 2)	16.0 ± 1.5 (54 ± 5)

probe is slightly more efficient than the triaxial probe. At ~30 μM, neither probe is efficient, and the difference is somewhat bigger. The decrease in dissolution *efficiency* (reflected as % dissolution) with increasing fibril concentration confirms kinetics control, with slower dissolution and faster redeposition at higher fibril loads. Even though different loadings of Aβ fibrils demonstrate different solubility on the two probes, preliminary results from HDX-MS studies of Aβ fibrils at different equivalent concentrations (13 μM, 18 μM and 28 μM) using the triaxial probe gave rise to similar deuteration levels in the same time frame, indicating the preservation of the core structure at the concentrations studied (details to be reported in Chapter 4).

To ascertain whether the evident poorer dissolution efficiency of the triaxial probe is related to the incomplete mixing described above and/or to the shorter exposure to MeCN, a series of experiments was undertaken to assess the dependence of fibril dissolution on the concentration of MeCN. For these experiments, fibrillar suspensions were prepared with equivalent monomer concentration of 2.0 μM, 0.5% formic acid, 0.2 mM tris, and MeCN concentrations of 0%, 15%, 30%, 45%, 60% or 90% (v/v). A suspension was centrifuged and decanted 2 hr after mixing, and the monomer concentration in 100-μL aliquots of the supernatants was determined using HPLC/UV (as described above). The fibrils were then resuspended by shaking in a vortex mixer for 1 min. Centrifugation and LC measurements were then repeated 22 hour later. As evident in Figure 3.5, fibril solubility in 90% MeCN was negligible. Otherwise, dissolution was enhanced whenever both MeCN and water were present, with essentially complete dissolution after 24 hr in 30% MeCN. In contrast, the solution with no MeCN achieved only about 47% dissolution after 2 hr, and solubility did not increase after an additional 22 hr; this sample apparently reached its equilibration concentration within the first 2 hr (although it is possible that further dissolution may have occurred after a longer incubation time). Comparison of data from Figure 3.5 and Table 3.2 suggests that fibrils may equilibrate in the aqueous solution with no MeCN even within the short mixing time in the triaxial probe. Table 3.2 shows 43% dissolution of 29.6 μM (initial equivalent) fibrils in the triaxial probe. Under the conditions of Table 3.2, these fibrils will have been diluted to ~6 μM with 100/0.5 (v/v) H_2O/HCOOH for about 12 sec, followed by

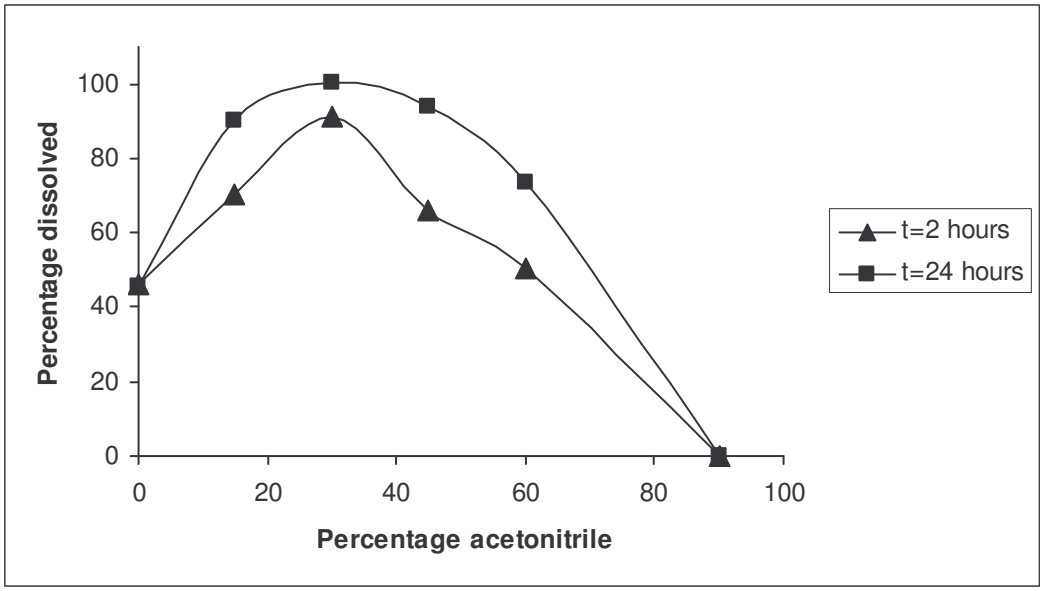

Figure 3.5. Effects of acetonitrile on the solubility of 2-μM (monomer equivalent concentration) Aβ(1-40) fibrils (2 hours and 24 hours incubation). The solvent mixture contains 0.5% formic acid, 0.2 mM tris and the indicated percentage of acetonitrile (balance water). The concentration of acetontrile-water-formic acid mixtures is reported as percentage volume-volume (v/v).

further dilution to ~ 3 μM with MeCN for the last 1.1 sec at the probe tip. Although the final MeCN concentration was 41%, the 43% dissolution more closely resembles that for the pure aqueous solution in Figure 3.5 (47%, *vs* > 60% at 45% MeCN). The imperfect mixing described above is unlikely to cause such a large effect, given the relatively weak dependence of solubility on MeCN concentration around 41% in Figure 3.5; the triaxial probe evidently does not allow adequate mixing time to realize the full enhancement of dissolution afforded by MeCN. More complete fibril dissolution might be obtained by using slower flow rates (longer time), but this would lead to increased exposure to back-exchange and therefore to loss of structural information. Use of relatively low fibril concentrations to assure good dissolution appears to be a reasonable compromise.

Artifactual exchange. As noted in section 1.3.3, post-incubation sample processing steps involving protic solvents can introduce artifactual exchange in HDX-MS, adding to (forward exchange – FE) or removing (back-exchange – BE) the deuterium incorporated during incubation in D_2O. While methods exist to correct for these artifacts when calculating total deuterium incorporation (see section 1.3.3 and 1.3.4) [233, 361], assessment of the extent of exchange and especially localization of exchange (e.g., by MS/MS) will be more reliable if artifactual exchange can be minimized [233, 59]. Such minimization contributed to the choice of MeCN as a non-protic co-solvent in earlier studies [58-59], reducing the effective concentrations of H_2O and D_2O while facilitating electrospray. This proved to be effective with the coaxial probe [58-59]; artifactual exchange was within the range reported elsewhere using other methods [59]. However, effectiveness might be compromised by delayed introduction of MeCN and incomplete mixing. Thus, as a final measure of the utility of the triaxial probe for HDX-MS studies, the extent of artifactual exchange was assessed and compared with that using the coaxial probe.

Aβ monomers were chosen as probes for these tests because they represent a "worst-case scenario"; their exposure to artifactual exchange is not mitigated by slow dissolution, as is the case for fibrils. FE was assessed by mixing a 25 μM aqueous solution of monomer in 2mM tris (0.85 μL/min) with processing solvent (80/20/0.5

(v/v/v) H_2O/D_2O/HCOOH at 4.25 µL/min in T1 (Figure 2.1) followed by addition of MeCN at 5 µL/min via tube 2 for the triaxial probe; 36.8/9.2/54/0.5 (v/v/v/v) H_2O/D_2O /MeCN/HCOOH at 9.25 µL/min in T1 for the coaxial probe) chosen to generate a final solution in which 16.7% of the water was D_2O. For assessment of BE, 25 µM fully deuterated monomer in 2 mM fully deuterated tris (0.85 µL/min) was mixed in T1 with an H_2O-based processing solvent (100/0.5 (v/v) H_2O/HCOOH at 4.25 µL/min followed by 100/0.5 (v/v) MeCN/HCOOH in T2 for the triaxial probe; 46/54/0.5 (v/v/v) H_2O/MeCN/HCOOH at 9.25 µL/min for the coaxial probe), which again gave a final solution in which 16.7% of the water was D_2O. Such analyses represent standard steps in obtaining data for correction of artifactual exchange (discussed in section 1.3.3) [59]. As in previous studies, labile side chain, terminal and ionizing protons are assumed to be statistically labeled; their contribution was subtracted to allow assessment of BE and FE relevant to backbone amides [59]. BE and FE were then calculated using Eqn. 1.26 and Eqn. 1.25 (presented in section 1.3.3), respectively.

Results show that BE was 6.5 ± 0.05 (D replaced by H) and FE was 1.5 ± 0.03 (H exchanged for D) using the coaxial probe, while the numbers are slightly higher with the triaxial probe (BE: 6.8 ± 0.1; FE: 2.0 ± 0.03), probably reflecting the slightly longer mixing time (13.1 *vs* 12 sec for the coaxial probe) and the higher effective water concentration due to imperfect mixing. In both cases, the difference is less than 1 exchanged proton/deuterium, well within the uncertainty with which total exchange is usually determined. BE exceeds FE, reflecting the fact that H_2O (rather than D_2O) is the primary water component (83.3%) after mixing.

3.3 Validating a Method for Correcting Artifactual Exchange on the Triaxial Probe

As discussed above, BE and FE are evident on both probes. This artifactual exchange (occurring during quenching and further sample processing prior to injection into the mass spectrometer) compromises the accurate and precise assessment of the

extent of exchange [59, 233]. Therefore, correcting data for artifactual exchange is necessary. As addressed in Chapter 1, several approaches are available to determine the extent of amide exchange prior to quenching [59]. The correction method (Eqn. 1.24-1.26 in section 1.3.3) developed by our group demonstrated its robustness when it was applied to correcting HDX data of Aβ(1-40) intact fibrils obtained from the coaxial probe [59]. The validation of the method was based on a study of the flow rate dependence of the corrected deuterium content [59]. The sum of the sample and processing solvent flow rates determines the time available for artifactual exchange, whereas the relative flow rates of the sample and processing solvent determine the final solvent composition. Because neither of these should affect the pre-processing deuteration, the constancy of corrected values obtained at various flow rates should provide a sensitive test for the robustness of a correction method. To validate a method for correcting artifactual exchange of Aβ fibrils on the triaixial probe, we took a similar approach. In this approach, the flow rates of the sample (partially deuterated Aβ(1-40) fibrils incubated in D_2O for 100 h) and the processing solvent stream (0.5/100 HCOOH/H_2O) were proportionally varied, resulting in times of 25.8, 12.0, 9.1 and 7.3 seconds for the mixing between the sample and the processing solvent (Table 3.3). At the same time, the flow rate of the sheath liquid (0.5/100 HCOOH/MeCN) was varied accordingly to attain final total flow rates of 10, 15, 20 and 25 μL/min (Table 3.3). The percentage of water that is D_2O in the final solvent mixture was maintained at 16.7%. For all the studies presented in this section, the experiments were conducted on the Quattro II mass spectrometer, and the molecular masses are corrected before substitution into various equations by subtracting artifactual exchange into ionization, side-chain and terminal protons as described in section 1.3.3.

Figure 3.6 presents the flow-rate dependence of the measured (uncorrected) deuterium content (= *m-MW*, *m* and *MW* are defined in section 1.3.3) in partially deuterated Aβ(1-40) fibrils (d-fibrils). Cursory inspection of Figure 3.6 shows that, as expected, longer mixing times before MS analysis (slower flow rates) led to increased undesired exchange. For example, the amount of deuterium measured in backbone amides of d-fibril samples varied from ~ 11.0 to 13.0 as the flow rate changed from 10 to

Table 3.3. Summary of the flow rates used in the experiments to provide HDX data for testing correction methods.

Flow Rate (µl/min)			**Total Flow Rate (µl/min)**	**Mixing Time (second)**
Sample (Aβ(1-40) d-fibrils)	Solvent (0.5/100 HCOOH/H_2O)	Sheath liquid (0.5/100 HCOOH/MeCN)		
0.56	2.82	6.62	10	25.8
0.85*	4.25*	10.0*	15*	12.0
1.13	5.63	13.24	20	9.1
1.41	7.04	16.55	25	7.3

* Flow rates optimized for the triaxial probe setup on the Quattro II mass spectrometer (see section 2.3).

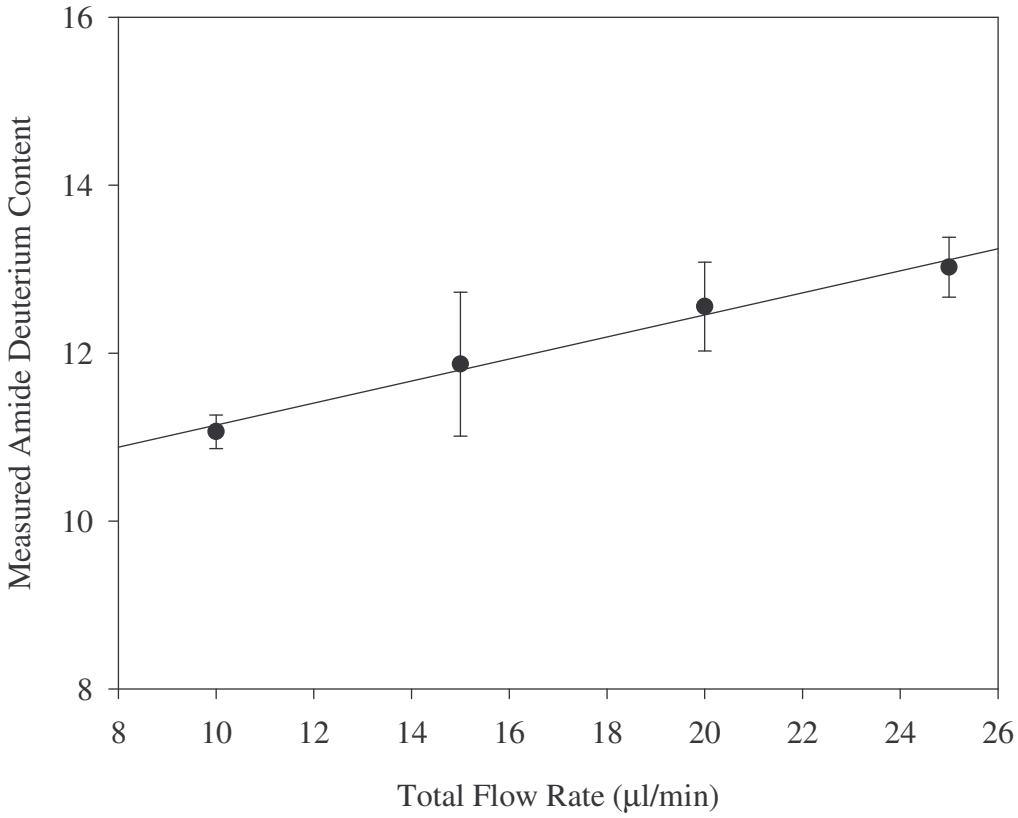

Figure 3.6. Measured amide deuterium content for partially deuterated Aβ(1-40) fibrils versus total flow rate. The error bars were calculated using propagation of errors [376].

25 µl/min.

Ideally, plots of corrected deuterium content versus flow rates should be horizontal lines if a correction method is perfect. That is, the slope of the least squares line should be zero and the Y-intercept should be equal to the average corrected deuterium value. These values should provide a quantitative means for evaluating the performance of a correction method. Figure 3.7 and Table 3.4 show the applications of various correction methods (discussed in section 1.3.3 and section 1.3.4), using fibril-based $m_{100\%}$ and $m_{0\%}$ values to calculate the corrected deuterium content. The data (corrected using Method E: Eqn. 1.24-1.26) obtained in the previous study using the coaxial probe are used as the benchmark for comparison and are included in Table 3.4. As evident from Figure 3.7 and Table 3.4, none of the methods gave perfect results (Figure 3.7 and Table 3.4). For Method A (Eqn. 1.18, by Zhang and Smith [233]) and Method B (Eqn. 1.19-1.23, by Resing *et al.* [299]), the D_{corr} values vary significantly as the flow rate is changed (Figure 3.7a and 3.7b, and Table 3.4). Indeed, the slopes are much higher (0.66 ± 0.02 for method A; 0.14 ± 0.03 for method B), the intercepts much lower (10.8 ± 0.4 for method A; 9.7 ± 0.5 for method B) and the corrected number of deuteriums much lower (12.5 ± 0.4 for method A; 12.2 ± 0.5 for method B) than the corresponding data obtained in the previous study using the coaxial probe [59] (Table 3.4).

Method C (Eqn. 1.28-1.29, by Mandell *et al.* [238]) was developed to correct for artifactual exchange occurring during HDX-MALDI-MS. The decay in deuterium content is analogous to the changes in D_{meas} (= *m-MW*) observed with increasingly long mixing times (lower flow rates). By replotting these data as a function of mixing time (calculated using the flow rate and the length of the capillary from the mixing T to the ES source) and fitting a single-exponential decay curve, it was possible to calculate k, B_1, and B_2 as in equation 1.28; resulting parameters are listed in the legend to Figure 3.7c. The corrected amide deuterium content (D_{corr}) was then calculated at each mixing time using equation 1.29. For comparison with the other correction schemes, the resulting data are plotted as a function of flow rate in Figure 3.7c. It can be seen that this method provides both flow rate independence (slope for the linear fit = 0.04; Table 3.4) and a good match

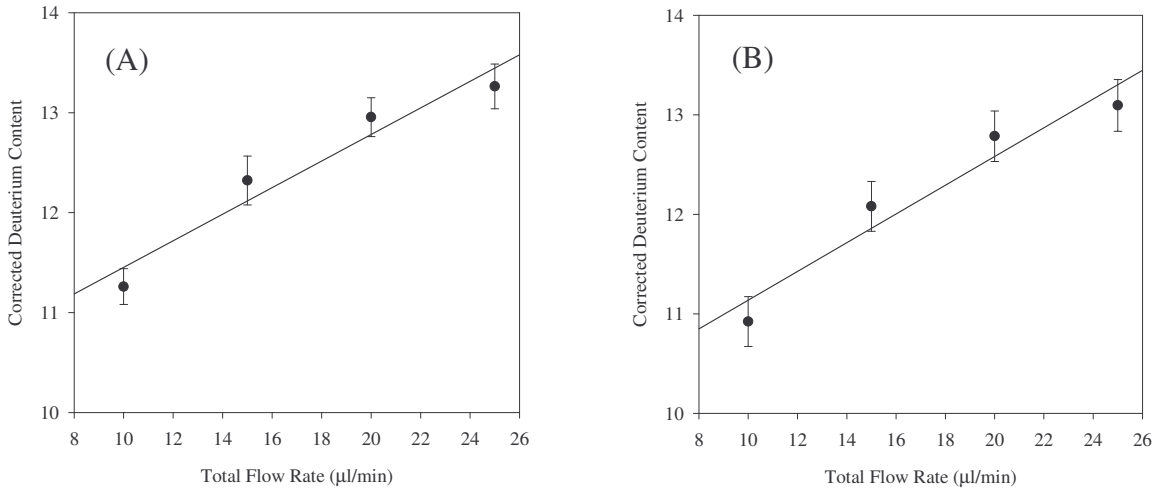

Figure 3.7. Amide deuterium content (corrected using various methods) versus total flow rate. (A) Method A, as described in Eqn. 1.18 (Zhang and Smith 1993). (B) Method B, as described in Eqn. 1.19-1.23 (Resing *et al.* 1999). (C) Method C, as described in Eqn. 1.28-1.29 (Mandell *et al.* 1999). The parameters needed for use of Eqn. 1.28 were determined by plotting D_{meas} (= *m-MW*) as a function of mixing time (calculated from flow rate), and then fitting to a single exponential function (Eqn. 1.28) as described in the text. The best-fit equation was $D_{meas} = 11.0 + 7.0\ (e^{-0.168t})$. (D) Method D, a modification of Method C using Eqn. 3.1 instead of Eqn. 1.28 to determine the parameters needed for use of Eqn. 1.29. The best-fit equation was $D_{meas} = 6.5 + 7.2\ (e^{-0.0186t})$. (E) Method E, as described in Eqn. 1.24-1.26 (Kheterpal *et al.* 2001). The error bars were calculated using propagation of errors [376].

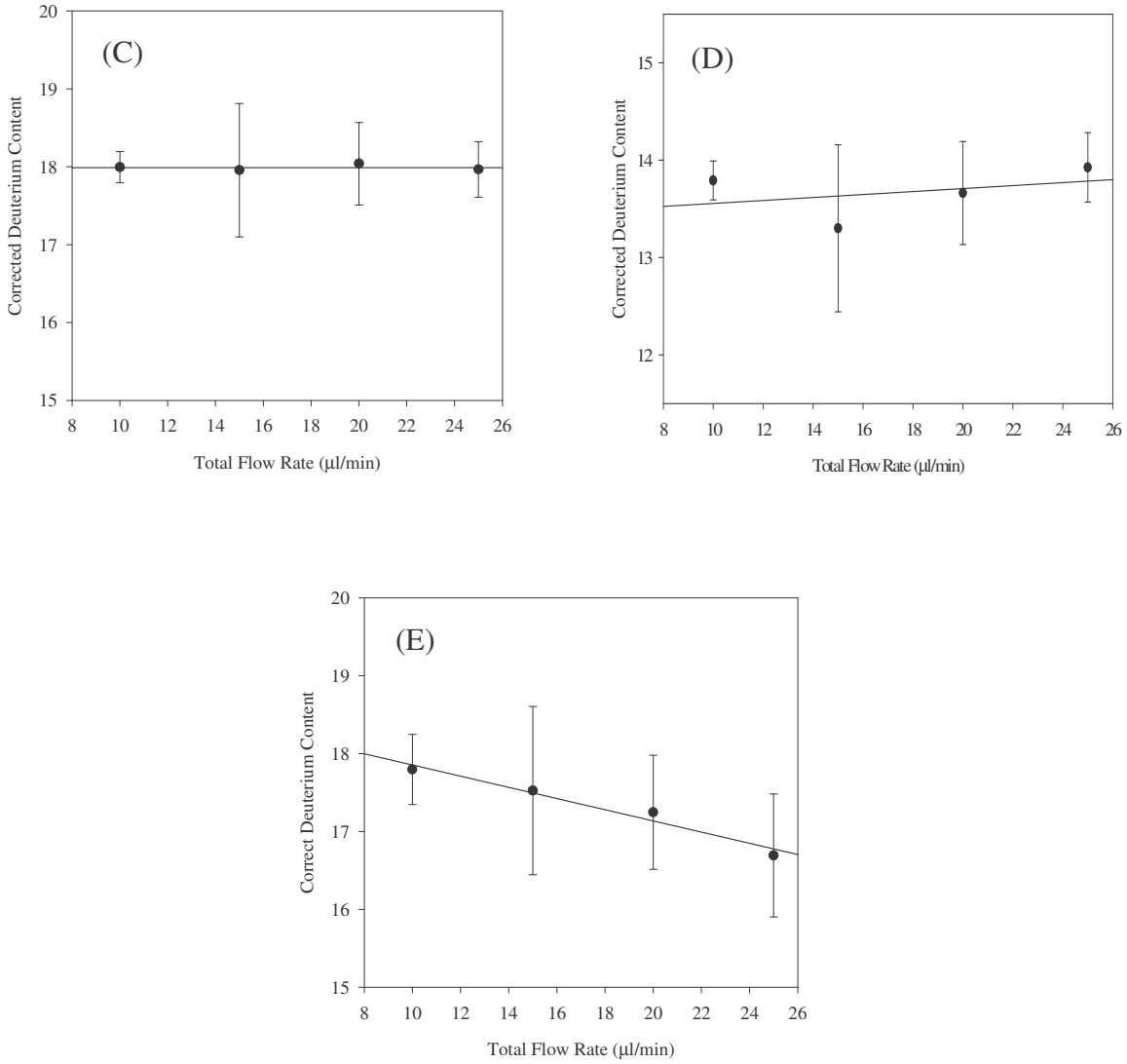

(Figure 3.7 continued)

Table 3.4. Quantitative analysis of the performance of correction methods based on HDX data obtained from analysis of Aβ(1-40) fibrils incubated for 100 h using the triaxial probe on the Quattro II mass spectrometer.

Correction method (16.7% D2O in the final solvent mixture)	***Average corrected deuterium content[1]***	***Intercept[2]***	Slope[2]
Method A (Eqn. 1.18; Zhang and Smith 1993)	12.5 ± 0.4	10.8 ± 0.4	0.66 ± 0.02
Method B (Eqn. 1.19-1.23; Resing et al. 1999)	12.2 ± 0.5	9.7 ± 0.5	0.14 ± 0.03
Method C (Eqn. 1.28-1.29; Mandell et al. 1998)	18.0 ± 0.04	18.0 ± 0.08	1×10^{-5} ± 0.004
Method D (Eqn. 3.1 and Eqn. 1.29)	13.7 ± 0.3	13.4 ± 0.5	0.02 ± 0.03
Method E (Eqn. 1.24-1.26; Kheterpal et al. 2001)	17.3 ± 1.6	18.6 ± 0.2	-0.07 ± 0.01
Data from the coaxial probe [3] (using Method E)	**18.9 ± 0.5**	**19.6 ± 0.4**	**-0.06 ± 0.03**

[1] The average of the corrected deuterium content at all measured flow rates.

[2]Intercept and slope for linear fit to plots of corrected deuterium content vs. flow rate.

[3] The data is from analysis of Aβ(1-40) fibrils incubated for 100 h using the coaxial probe on the Quattro II mass spectrometer [59]. The percentage of D_2O in the final solvent mixture was 18.18%.

to the expected average corrected deuterium content ($\overline{D_{corr}}$ = 18.0 ± 0.04, consistent with the expected value of 18.0 ± 0.08 and close to the value of 18.9 ± 0.5 obtained from the coaxial probe; Table 3.4). One limitation to Method C is that it requires routine collection of data at several flow rates in order to obtain k and B_2 from Eqn. 1.28.

Method D (Eqn. 3.1 and Eqn. 1.29) is a modified form of the method C. The ultimate equilibrium value of D_{meas} (B_1) in Eqn. 1.28 of Method C can be predicted independently of the fitting routine since the final solution conditions in the ES experiments described here are relatively well-defined. For example, 16.7% of the water in the final solvent mixture was D_2O, so that at equilibrium (t = ∞), 6.5 amide protons (16.7% of the 39 amides) will be deuterated (i.e., B_1 = 6.5). Equation 1.28 can be modified slightly to reflect this added information:

$$D_{meas} = 6.5 + B_2 e^{-kt} \qquad \text{Eqn. 3.1}$$

Fitting the d-fibril data presented in Figure 3.6 to the exponential decay function described in Eqn. 3.1 resulted in k and B_2 values (reported in the legend of Figure 3.7d). These k and B_2 values were again used with Eqn. 1.29 to determine a corrected amide deuterium content for data at each flow rate; results are presented in Figure 3.7d. Method D provides results with little flow-rate-dependence, as evident from the slope of 0.02 for the linear fit (Table 3.4). However, the average D_{corr} value is too low: 13.7 ± 0.3 compared with the benchmark of 18.9 ± 0.5 obtained from the coaxial probe [59]. Thus, the performance of Method D was deemed to be inadequate for fibril HDX.

For Method E (Eqn. 1.24-1.26; Kheterpal *et al.* [59]), the results show a slight flow-rate dependence, as evidence by the small slope of the linear fit of these data (-0.07 ± 0.01) (Figure 3.7e and Table 3.4). Moreover, the average D_{corr} value from Figure 3.7e is 17.3 ± 1.6 deuteriums, equivalent to the intercept (18.6 ± 0.2) and to that (18.9 ± 0.5) obtained using the coaxial probe [59] within the experimental error (Table 3.4). Among all the methods evaluated above, Method E shows a good compromise in terms of practicability and performance. Unlike Method C, it offers a practical compromise that requires determination of m, $m_{100\%}$, and $m_{0\%}$ at only *one* flow rate. Method E is the method which has been used to correct for all the HDX data presented in this dissertation.

Note that Method E uses fully protonated fibrils and fully deuterated fibrils (rather than corresponding monomers) as the control samples to correct HDX data for BE and FE (discussed in Chapter 1). The basis for these choices is evident in Figure 3.8. FE of protonated Aβ(1-40) fibrils (H-fibrils) has a less extent than protonated monomer (H-monomer), as indicated by the lower m/z of the H-fibril peak than that of the H-monomer peak in the M_0 solvent (Figure 3.8a). There is also less BE in fully deuterated Aβ(1-40) fibrils (D-fibril) compared to fully deuterated monomer (D-monomer) (Figure 3.8b), so that the D-fibril peak falls at a higher m/z than the D-monomer peak. All this is attributable to the finite time required for fibril dissolution, which reduces the time available for forward exchange and back exchange, explaining why fully protonated and deuterated fibrils are grown for our forward exchange and back exchange control samples. Also worth noting is that the molecular weight measured for the protonated Aβ(1-40) sample (*MW* in Eqn. 1.24-1.26), instead of the theoretical molecular mass (4329.9 Da), was used to correct for the day-do-day variability in mass calibration of the Quattro II instrument, although the latter two numbers generally agree to within 0.5 Da.

Also worth noting is that isotopic effects on BE and FE are negligible when using Method E to correct HDX data obtained from fibrils incubated in D_2O buffer for 24 hours or longer. The exchange essentially reached a plateau after 24 hours incubation (discussed in Chapter 4), so the exchange was under equilibrium control. Since *kinetic isotope effects* and *equilibrium isotope effect* in HDX are small (see section 1.3.2), the rates for BE and FE were mainly determined by the concentration of D_2O and H_2O in the processing solvent. Since 16.7% D_2O and 83.3% H_2O were used in our experiments, BE was bigger than FE (see section 3.2).

3.4 Conclusions

The triaxial probe represents a classic compromise in trying to optimize independent processes. While its performance in terms of signal stability, artifactual exchange, and fibril dissolution, does not match that of the standard coaxial probe, the

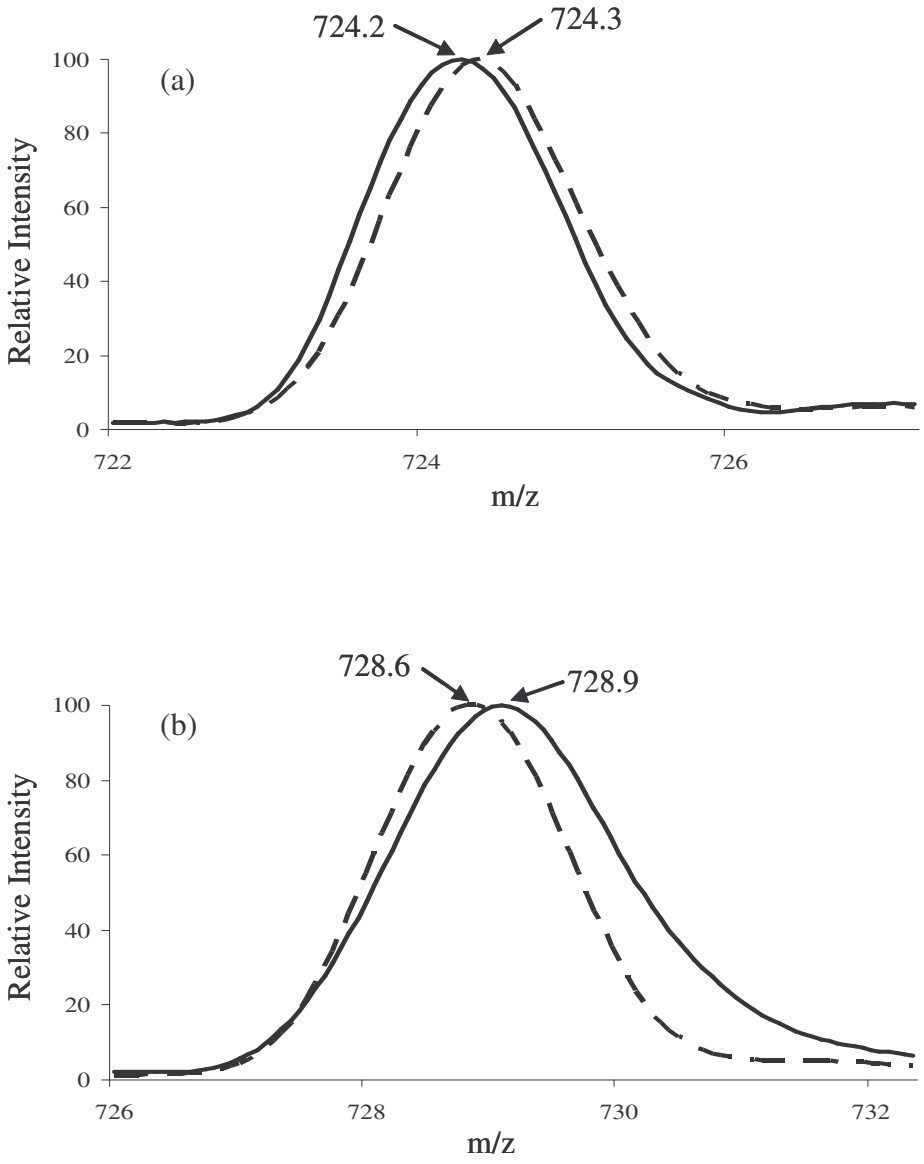

Figure 3.8. ESI-MS of the +6 charge state peak of Aβ(1-40) peptide obtained using (a) fully protonated fibrils (solid line) and fully protonated monomer (dashed line) as $m_{0\%}$ sample; (b) fully deuterated fibrils (solid line) and fully deuterated monomer (dashed line) as $m_{100\%}$ sample. Each peak is labeled with centroid m/z values. The data shown here have been smoothed using Savitzky Golay method implemented in the MassLynx program from the Quattro II mass spectrometer.

differences are relatively small, especially when compared with the major enhancement in the effectiveness of on-line proteolysis. By decoupling reaction and spray optimization, the probe may enable a wide range of on-line reactions to facilitate system characterization in HDX-MS and other applications. Performance with respect to the other figures of merit in other applications may be improved by re-optimizing flow rates and tube diameters.

CHAPTER 4

CHARACTERIZATION OF Aβ(1-40) AMYLOID FIBRILS AND PROTOFIBRILS USING HDX-MS COUPLED WITH ON-LINE PROTEOLYSIS

As discussed in Chapter 1, high-resolution structural information about fibrils and protofibrils is lacking because of the insoluble, heterogeneous and non-crystaline nature of fibrils, and because of the metastable, transient nature of protofibrils. Therefore, structural information of Aβ fibrils and protofibrils at lower resolution has become increasingly important. HDX-MS studies have shown that both fibrils and protofibrils have a core resistant to HDX; about 60% (for fibrils) and 40% (for protofibrils) of the 39 backbone amide protons in the Aβ(1-40) are protected from exchange after two days of incubation in aqueous deuterated buffer [58-59]. This suggests that a significant portion of this relatively short sequence is in fact not involved in the presumably protective H-bonded structure. Such data immediately introduce the questions of which regions of the peptide are exposed to exchange and which portions are involved in β-sheet structure. One method to obtain such information is to proteolyze deuterated fibrils and protofibrils, inject the samples into the MS system, and measure the amount of deuterium exchanged in the smaller peptides. The triaxial probe discussed in Chapter 3 enables on-line digestion to gain insights into regional exchange protection of Aβ(1-40) fibrils and protofibrils, thus to elucidate the extent and pattern of individual residues involved in β-sheet formation within the fibril and protofibril structure. This chapter will discuss the structural information obtained from the HDX-MS data of peptic fragments derived from fibrils and protofibrils, and the potential of obtaining complementary structural information using 3 pepsin-like enzymes.

4.1 Hydrogen/Deuterium Exchange and Proteolysis (Using Pepsin) of Aβ(1-40) Amyloid Fibrils and Protofibrils

4.1.1 Hydrogen/Deuterium Exchange and Proteolysis of Aβ(1-40) Amyloid Fibrils

With the on-line proteolysis approach using the triaxial probe on the Quattro II mass spectrometer, Aβ(1-40) fibrils (grown in PBS under quiescent conditions described in section 2.2) were disaggregated and digested using pepsin. Fragments 1-19, 4-19, 20-34, 35-40, 20-33, 34-40, and 20-40 were observed for protonated fibrils and confirmed using MS/MS as described in Chapter 2. However, for fragments 20-33, 34-40, and 20-40 derived from partially and fully deuterated fibrils, they were of insufficient intensities (or poor S/N) for accurate mass measurement. As a result, only HDX data of fragments 1-19, 4-19, 20-34, 35-40 were discussed here. Representative spectra of the intact fibrils and four non-overlapping fragments after 24 h of exchange are presented in Figure 4.1. The blue and red lines in each panel of the Figure 4.1 correspond to the spectra obtained from fully protonated and fully deuterated Aβ(1-40) monomers (H-monomer and D-monomer, respectively). In all cases, broadening of mass spectral peaks was observed due to the natural isotope distribution as well as deuterium exchange. All the HDX data discussed below were corrected for fast exchanging side chain, terminal, and ionization protons, as well as artifactual exchange into backbone amide protons, as described in section 1.3.3 [59]. Note that while the proteolysis strategy gives information on the segmental spread of protection within the Aβ peptide, it also inevitably leads to some loss of information. Pepsin cleavage generates a rapidly exchanging amino group from a slow-exchanging amino group, so that the HDX information housed in the amino proton is completely lost by the time the fragment is analyzed in the MS. This loss of exchange protection information has to be kept in mind, for example, when comparing fragments to full length peptide or to fibril structure models.

The spectrum of partially deuterated intact fibrils (d-fibrils, solid black lines in Figure 4.1a), obtained by exposure of Aβ fibrils to D_2O exchange conditions, shows two Aβ populations represented by two peaks (peak A and peak B). The centroid of peak A varies with exchange time, while the higher mass peak B is superimposable with that of

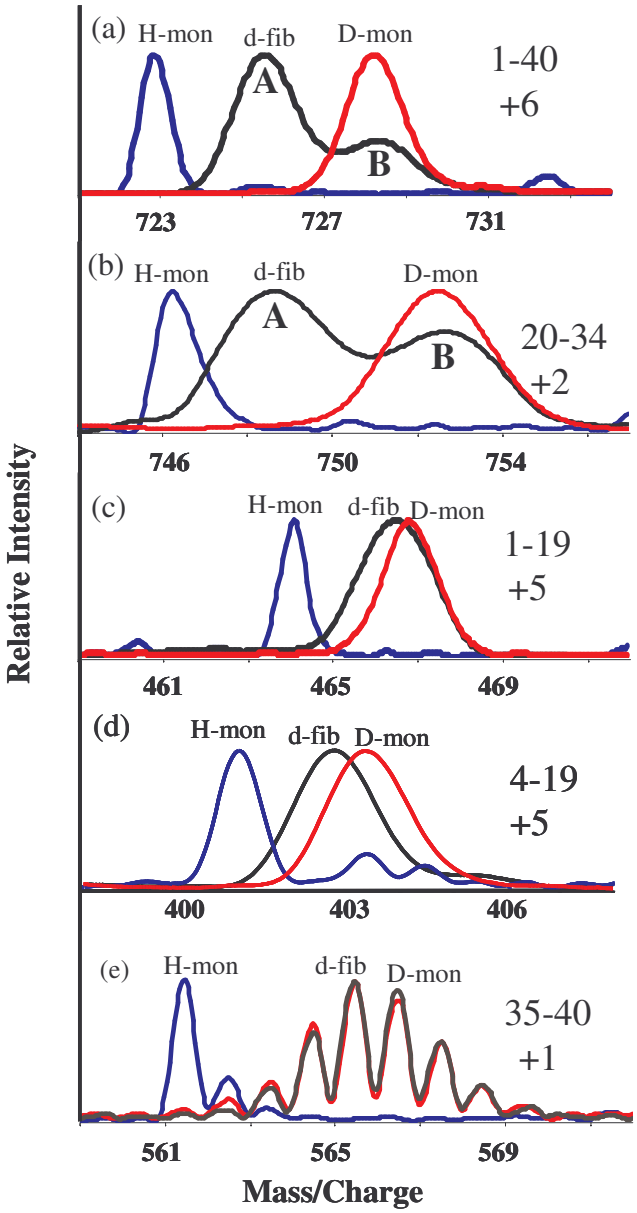

Figure 4.1. ESI-MS of (a) intact Aβ(1-40) fibrils and proteolytic fragments (b) 1-19, (c) 20-34, and (d) 35-40. The blue and red lines in each spectrum represent fully protonated monomer (H-mon) and fully deuterated monomer (D-mon), while the black solid line represent partially deuterated fibrils (d-fib). The charge states shown for each fragment are marked in each panel.

fully exchanged D-monomer. The number of deuteriums exchanged into intact Aβ fibrils was calculated using the molecular mass obtained from the centroid of peak A. Since charge states +5 and +6 were consistently observed with good signal-to-noise ratio for intact Aβ fibrils, molecular masses obtained from these charge states were averaged for all calculations. The corrected number of deuteriums after 24 h of exchange for intact Aβ(1-40) fibrils (peak A) was determined to be 17.1 ± 1.3 (Table 4.1), in good agreement with our previously published data for a similar exchange time obtained using the coaxial probe (17.0 ± 1.1) [58-59, 61]. The corrected number of deuteriums in peak B is equivalent to the number of deuteriums exchanged into the unprotected monomeric Aβ peptide. The existence of a fully deuterated component (peak B) in the analysis of Aβ(1-40) fibrils and its growth with time was reported previously [58]. The origin of peak B requires further investigation, but it does not interfere with the analysis of exchange protection in peak A. A number of possible sources of the fully exchanged component will be discussed later in this chapter.

Figure 4.1b-d illustrates the differences in the extent of exchange in four non-overlapping fragments (20-34, 1-19, 4-19 and 35-40) after 24 h of exchange time. The mass spectrum of the peptide spanning residues 20-34 (Figure 4.1b), from the digestion of partially deuterated Aβ(1-40) fibrils, contains two peaks, with peak B corresponding to the fully deuterated species, in analogy to that observed for the intact Aβ peptide as discussed above. The lower m/z peak A clearly contains a population of Aβ significantly protected from HDX compared to the fully exchangeable species in peak B. The deuterium exchanged into this fragment was determined from the m/z of peak A in Figure 4.1b. The charge state obtained for this peptide is +2, based on its mass and confirmation by MS/MS as described in Chapter 2. The total number of amide protons is 14, and the total number of side-chain and terminal protons is 10. (Note that even if residues 20 and 34 are protected in the fibril, they become terminal sites in the proteolytic fragment and will therefore be statistically deuterated.) The resulting corrected number of deuteriums exchanged into the amide sites of this peptide after 24 h was only 4.3 ± 0.3, indicating that most of the 14 amino acids in this segment of the peptide were protected from exchange.

Table 4.1. Summary of segmental protection data for Aβ(1-40) aggregates after 24 hours of exchange.

Fragment	Amyloid Fibrils		CLC-stablized protofibrils	
	Amide protons exchanged	**Protected amide protons (Total amide protons)**	**Amide protons exchanged**	**Protected amide protons (Total amide protons)**
1-40	17.1 ± 1.3	21.9 ± 1.3 (39)	26.2 ± 1	12.8 ± 1 (39)
1-19	10.2 ± 0.5	7.8 ± 0.5 (18)	12.4 ± 0.6	5.6 ± 0.6 (18)
4-19	6.5 ± 0.5	8.5 ± 0.5 (15)	9.9 ± 0.6	5.1 ± 0.6 (15)
20-34	4.3 ± 0.3	9.7 ± 0.3 (14)	9.5 ± 0.4	4.5 ± 0.4 (14)
35-40	3.9 ± 0.1	1.1 ± 0.1 (5)	4.1 ± 0.1	0.9 ± 0.1 (5)

Mass spectra of the N-terminal peptide 1-19 obtained from partially deuterated fibrils and fully deuterated monomer showed considerable overlap (Figure 4.1c), consistent with the low level of protection expected for this region [37, 40]. If the B peak in Figure 4.1a derives from fully-exchanged monomers as described above, proteolysis of these monomers would be expected to give analogous B peaks for all product peptides. However, there is only 1 peak evident in the spectrum of the 1-19 (and 4-19) fragment derived from partially deuterated fibrils (Figure 4.1c and Figure 4.1d; charge state 5+ is shown), and that peak is at an m/z slightly lower than expected for the corresponding B peak. This can be explained by the relatively low resolution, which would cause coalescence of the A and B peaks to a single peak representing the weighted average, if the degree of protection and the resulting mass difference were small.

Assuming then that there are two unresolved peaks in Figure 4.1c (as for the 1-40 and 20-34 spectra), the m/z of the partially exchanged component (peak A) was obtained by deconvolution of this composite peak, as follows. First, the m/z of the peak derived from fully deuterated Aβ monomer was determined (466.8). The envelope for this peak was fit using a Pearson VII function in the PeakFit (Systat) software, as this function gave a better fit than the other available functions (e.g., Gaussian). The mass spectrum of the fragment 1-19 obtained from partially deuterated fibrils was then deconvoluted into A and B peaks using the Pearson VII equation with the number of peaks fixed at 2, the position of peak B fixed at the value determined from the monomer, and the relative abundance of peaks A and B fixed at the value measured for the 20-34 fragment (A:B ~ 1.5:1; Figure 4.1b). This ratio was selected in preference to the (clearly larger) ratio for the intact monomer (Figure 4.1a), since proteolysis was observed to preferentially attenuate the B peak of the intact 1-40 (data shown later). Data from all fragments are part of a single spectrum and should reflect the same relative contributions from materials derived from A and B peaks of the intact 1-40. Non-linear regression analysis was run iteratively until convergence of the single variable constituting the position of the fragment 1-19 A peak, giving a value of 466.2 for the data shown in Figure 4.1c. The corrected number of backbone amide protons exchanging into the fragment 1-19 after 24 h of incubation in deuterated buffer was thus 10.2 ± 0.5 (averaged over the +4 and +5

charge states), based on the centroid of the calculated peak A; roughly 8 (of a possible 18) amide protons are protected in this portion of the molecule. The mass spectra of the 4-19 proteolytic fragment of d-fibrils (Figure 4.1 d) were deconvoluted into A and B peaks in a similar way. After the deconvolution, the number of backbone amide protons exchanged into this fragment after 24 h of incubation in deuterated buffer was determined to be 6.5 ± 0.5 (averaged over the +4 and +5 charge states), again based on the centroid of the calculated peak A. The difference in deuterium content between 1-19 and 4-19 is 3.7 ± 0.7, suggesting the first 3 amino acids are completely exchanged. This is consistent with a fully exposed N-terminus [37, 40].

The C-terminal peptide 35-40 showed the least amount of protection as illustrated by the almost complete overlap of mass spectra derived from partially deuterated fibrils and fully deuterated monomer (Figure 4.1e). As discussed above, one would still expect there to be distinct contributions from A and B peaks of the intact 1-40. However, the mass spectra of the singly charged 35-40 fragment are isotopically resolved, which makes fitting using Peakfit (as described above) difficult. Instead, molecular masses were calculated assuming that the centroid of the isotopic distribution is a simple linear combination of the centroids of A and B distributions, with the latter estimated from the data for the deuterated monomer:

$$\text{Centroid}_{\text{d-fibril}} = 0.6 \times \text{Centroid}_{\text{X}} + 0.4 \times \text{Centroid}_{\text{d-monomer}} \qquad \text{Eqn. 4.1}$$

Here, $\text{Centroid}_{\text{d-fibril}}$ and $\text{Centroid}_{\text{d-monomer}}$ are the experimental values from the partially deuterated fibril and the fully deuterated monomer (564.2 and 564.4, respectively, from Figure 4.1e), and $\text{Centroid}_{\text{X}}$ is the desired value for the unresolved A peak. The weighting factors (0.6 and 0.4) are those derived from Figure 4.1b, as described above for the [20-34] fragment. Solving for $\text{Centroid}_{\text{X}}$ in the above equation yields the deconvoluted m/z of 564.2, which indicates a neutral mass within experimental error (~ ± 0.2 Da) of the value for the B peak. The corrected number of deuteriums exchanged into this fragment after 24 h of H/D exchange time was 3.9 ± 0.1 (of a possible 5).

The course of isotopic exchange can be visualized through plots of the content of deuterium per peptide molecule versus incubation time. Time-dependent HDX results for the Aβ(1-40) intact peptide and the peptic fragments are presented in Figure 4.2a. As

(a)

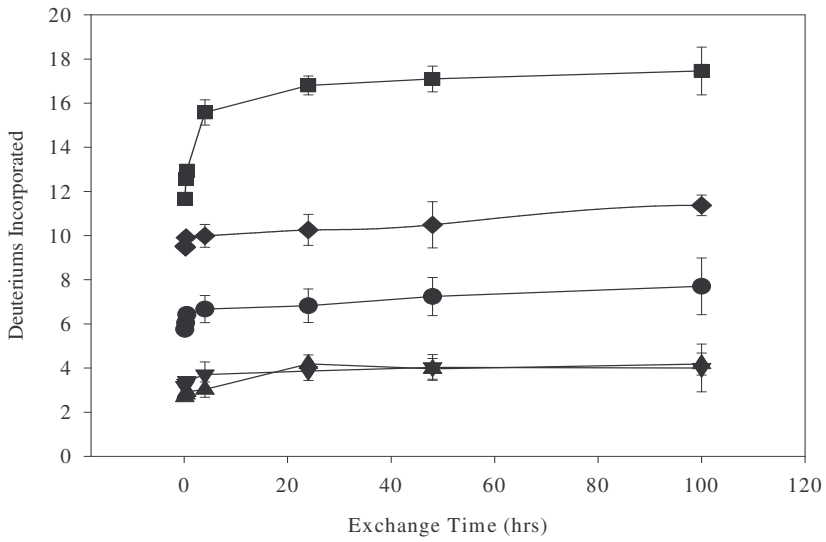

(b)

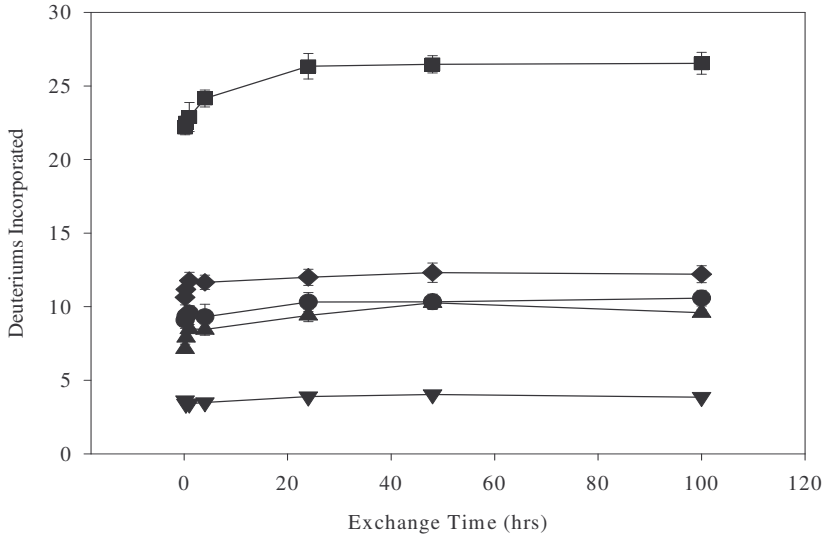

Figure 4.2. Number of deuteriums incorporated as a function of time for (a) Aβ(1-40) fibrils (■) and peptic fragments 1-19 (♦), 4-19 (●), 20-34 (▲), 35-40(▼) obtained from digestion of Aβ(1-40) fibrils; (b) Aβ(1-40) protofibrils (■) and peptic fragments 1-19 (♦), 4-19 (●), 20-34 (▲), 35-40(▼) obtained from digestion of Aβ(1-40) protofibrils (stabilized by CLC).

evident from Figure 4.2a, exchange was essentially complete in 24 hours, justifying the selection of this time point as the example to illustrate exchange kinetics as described in this section. Table 4.1 summarizes the number of backbone amide protons exchanged (exposed) and protected (buried or involved in secondary structure) in both intact monomer and proteolytic fragments from Aβ(1-40) fibrils exposed to 24 h of incubation in deuterated Tris buffer. The proteolytic fragmentation results reveal significant variations in protection from exchange within different regions of the Aβ(1-40) peptide. The order of protection, as a percentage of available backbone amide protons, was found to be 20-34 > 4-19 > 1-19 > 35-40. These data exhibit a gratifying degree of internal consistency. The sum of the number of amide protons exchanging in fragments 1-19, 20-34 and 35-40 is 18.4 ± 0.6, which, within error, is equivalent to the 17.1 ± 1.3 exchanging backbone amide protons obtained for the intact peptide under similar conditions. As discussed earlier, two amide protons are lost in proteolytic cleavage at 19-20 and 34-35 and therefore cannot be directly accounted for in the fragment analysis. If these were unprotected (and therefore exchanged) in the fibril, the revised total for exchanging amide protons in the fragments would be 20.4, significantly higher than the full length value of 17.1. This suggests that the "invisible" amide protons from residues 20 and 35 are also protected in the fibril, consistent with most other available data on PBS/quiescent Aβ(1-40) amyloid fibrils [63] (see below). Assuming that protection is an all-or-none phenomenon, these data suggest that 8, 10, and 1 backbone amide protons are protected in fragments 1-19, 20-34 and 35-40, respectively.

Figure 4.3 shows an interpretation of the fibril data, in the context of literature data on this particular Aβ(1-40) amyloid conformation. Line B shows the consensus secondary structure prediction from a combination of proline and alanine scanning mutagenesis, coupled with HDX experiments monitored by NMR (summarized in section 1.1.3) [63], with "x" signifying residues in loose structure expected to be open to exchange, and "β" indicating residues expected to be in protected, β-sheet structure. Part C shows a model for β-structure in these fibrils generated by incorporating the exchange protection data on fibrils summarized in Table 4.1 into the consensus model from line B. Each dash in the sequence represents an amide proton; thin dashes represent exchanging

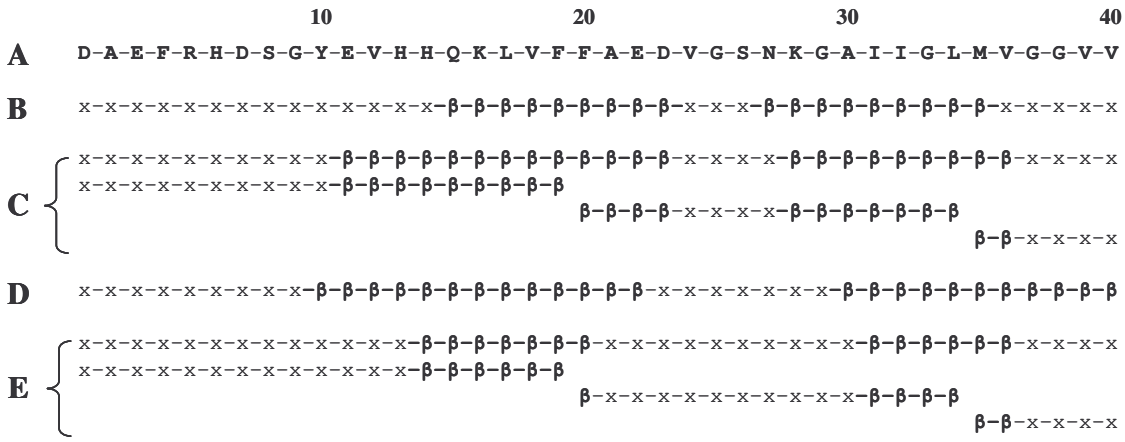

Figure 4.3. Models of secondary structure in Aβ(1-40) aggregates. A. Amino acid sequence of Aβ(1-40). B. Consensus model of β-extended chain regions in mature fibrils grown in PBS at 37 °C without stirring, derived from Pro and Ala scanning mutagenesis and HDX-NMR experiments (presented in section 1.1.3) [63]. C. Model for β-extended chain segments in mature fibrils grown in PBS at 37 °C without stirring, derived from HDX-MS / pepsin analysis (this work). D. Model for β-extended chain segments in mature fibrils grown in low salt with agitation, as analyzed by solid state NMR (presented in section 1.1.3) [87]. E. Model for β-extended chain segments in CLC-protofibrils derived from HDX-MS / pepsin analysis (this work). In C and E, the top line shows the model for the entire Aβ(1-40) peptide and the three lines below top show the models for how β-extended chain might be distributed within each pepsin fragment.

protons and thick dashes represent protected protons. Below the full length sequence in Part C are the three proteolytic fragments showing how the amount of protection within each fragment is consistent with the model for the exposed/protected amide hydrogens in the full-length peptide. Since the pepsin cleavage sites at residues 19-20 and 34-35 are both modeled to be in β-structure, the sum of the protected residues of the fragments is expected to be about two less than the number of protected residues in the intact peptide, consistent with the reasoning above. The model assumes that strongly protected N-H groups will not be isolated in the linear sequence, but rather will be collected in a limited number of contiguous stretches of β-structure. While the H-bond status of most of the N-terminus cannot be directly addressed by our data, the difference in protection levels between the 1-19 and 4-19 fragments (3.7 ± 0.7, Table 4.1) suggest that the very N-terminus of Aβ(1-40) is not involved in H-bonded structure in the PBS/quiescent fibril.

The results presented here are in agreement with HDX-NMR [61], and scanning proline [40] and scanning alanine [63] analysis of PBS-quiescent amyloid fibrils of Aβ(1-40). The data for a free C-terminus are in contrast with solid state NMR results showing that the entire C-terminal segment of Aβ(1-40) is involved in H-bonded β-sheet structure in amyloid fibrils [37, 87]. The distribution of secondary structure in Aβ(1-40) incorporated into amyloid fibrils grown with agitation under low salt conditions, as deduced from solid state NMR experiments [19], is shown in Part D of Figure 4.3. These differences are consistent with the unusual plasticity (the capability of adjusting to packing changes) of the amyloid fibril structure [40, 63], as well as with the observation that at least two stable, self-propagating conformations of fibrils can be formed from the Aβ(1-40) peptide depending on growth conditions [Petkova 2005]. There is little information about the nature of the structural differences between the reported conformations. The work presented here suggests that one difference may be in the nature of the H-bonding network that defines the β-sheets within the amyloid fibril. As evident in Figure 4.3, the major secondary structural differences between low salt, agitated fibrils (Figure 4.3D) and PBS, quiescent fibrils (Figure 4.3C) are the number of residues in the 30-40 and 35-40 segments that are in protective, H-bonded structure.

Note that interpretation of the HDX data assumes that sites which are protected

from exchange in fibrils and protofibrils (discussed later) are involved in H-bonded β-sheet structure because previous studies suggested fibrils and protofibrils are rich in β-sheets [33, 53-55, 58-65, 93-94] (see section 1.1.3). This does not rule out other possible mechanisms for exchange protection. For example, some amide hydrogens may be positioned within or near the fibril core so that they have limited access to deuteriums in the solvent and are protected from exchange. Alternatively, D_2O may be inaccessible to some amide hydrogens in the protein because of hydrophobic interactions.

4.1.2 Hydrogen/Deuterium Exchange and Proteolysis of CLC-stabilized Aβ(1-40) Protofibrils

The on-line triaxial probe proteolysis methodology was also used to determine the hydrogen exchange protection pattern in a form of Aβ(1-40) protofibrils. These aggregates of Aβ(1-40), promoted and stabilized by the small organic molecule CLC (Figure 1.6), resemble transient authentic Aβ protofibrils in a number of features, including their EM image and overall HDX protection [94]. Figure 4.4 displays representative spectra of intact CLC protofibrils and three non-overlapping fragments after 24 h of exchange, with the blue and red lines in each panel corresponding to spectra obtained from fully protonated and fully deuterated Aβ(1-40) monomers. In contrast to the corresponding spectra for the Aβ amyloid fibril analysis shown in Figure 4.1, CLC protofibrils exhibit only a single peak, one that reflects intermediate exchange (i.e., peak A), and no fully exchanged peak (B). This is true for both full length (undigested) Aβ(1-40) peptide as well as for all the pepsin fragments. The results show that these CLC protofibrils consist of a very homogeneous structural population. The numbers of deuteriums exchanged into intact Aβ(1-40) and proteolytic fragments of these CLC protofibrils were calculated using the centroids of the unresolved isotopic envelopes, and these data were corrected for fast exchanging side chain and terminal protons and artifactual exchange into backbone amide protons as described previously [59]. The corrected numbers of deuteriums exchanged into Aβ peptides in CLC protofibrils after 24 h are summarized in Table 4.1. The time-dependent HDX exchange results for intact peptide of CLC protofibrils and its peptic fragments are presented in Figure 4.2b.

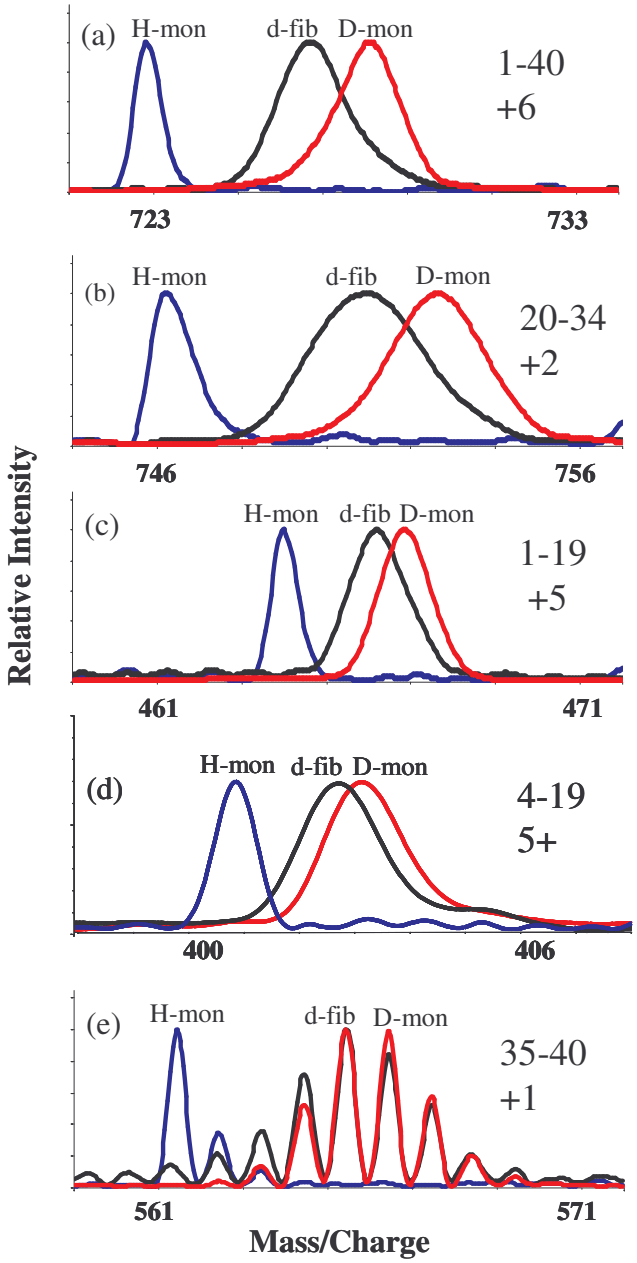

Figure 4.4. ESI-MS of (a) intact Aβ(1-40) calmidazolium stabilized protofibrils and proteolytic fragments (b) 1-19, (c) 20-34, and (d) 35-40. The blue and red lines in each spectrum represent fully protonated monomer (H-mon) and fully deuterated monomer (D-mon), while the balck solid line represent partially deuterated fibrils (d-fib). The charge states shown for each fragment are marked in each panel.

Using the triaxial probe procedure, the number of backbone amide protons found to exchange in intact Aβ peptide in CLC protofibrils after 24 h of exchange time is 26.2 ± 1. These data are in good agreement with our previously reported value for these CLC protofibrils, 27.6 ± 1.3, using the coaxial probe methodology [94]. An almost exact match between the sum of exchange into the three non-overlapping fragments (12.4 + 9.5 + 4.1 = 26.0) and the value for intact CLC protofibrils (26.2) is another remarkable feature of these data. That this agreement between the exchange observed in fragments and intact CLC protofibrils is better than that observed in fibrils (Table 4.1) is possibly due to the more homogenous nature of these CLC protofibrils, and because deconvolution of A and B peaks was not required in the analysis of the CLC protofibril data. If the "silent" amide protons at the 19-20 and 34-35 pepsin cleavage sites also significantly exchange in the CLC protofibril, the fragment total would be 28.0, significantly higher than 26.2. This implies that these two protons are probably largely protected from exchange in the protofibril as in the fibril.

Our interpretation of this data is shown in Part E of Figure 4.3, which places the highly protected, presumably β-sheet residues in two contiguous elements of β-extended chain analogous to the two segments of β-extended chain elements in fibrils. This is supported by previous proline scanning analysis of CLC protofibrils, which found highly proline-sensitive residues concentrated in the 16-21 and 30-36 segments of Aβ(1-40) [94]. Figure 4.3E shows that the segmental HDX data fit best to a model in which residues 14-20 and 31-36 are contained in highly protected structure. The model shows that the C-terminal segment of Aβ(1-40) is not involved in highly protected structure in the protofibril. As with the similar conclusion for quiescent amyloid fibrils above, this assignment appears to be unequivocal, given the almost complete lack of protection in the short 35-40 pepsin fragment that encompasses these residues. The model also suggests that the main difference in secondary structure between quiescent Aβ(1-40) amyloid fibrils and CLC protofibrils is that the 21-30 segment of Aβ is completely lacking in highly protected structure in the latter. A second difference is that residues 11-13, which are in protected, H-bonded structure in the fibril, appear to be open to facile exchange in the CLC protofibril and hence not in strong H-bonded structure. It is significant that this

distribution of presumed β-extended chain residues in the CLC protofibril generates two β-sheets of similar widths of seven and six residues. This is easily accommodated into a duplex β-sheet such as that recently observed in the X-ray crystal structure of a small, amyloidogenic peptide fragment of the yeast prion protein sup35 [377].

4.1.3 Implications of Peak B in Fibrils, Authentic Protofibrils and CLC-stablized Protofibrils

As mentioned above, a striking difference in the data from CLC-stablized protofibrils, compared to that from mature fibrils as well as from normally isolated authentic protofibrils (chromatographically isolated from amyloid assembly reaction of Aβ(1-40)) [59], is the absence of a significant fully exchanged peak B in either the full-length peptide or fragments. Since the fully exchanged peak B may limit the ability of HDX-MS to provide interpretable data in other systems, some discussion of this technical issue is warranted. In our experiments, since fibrils are isolated by centrifugation immediately prior to subjecting them to the deuterium exchange, this completely deuterated Aβ component is not a result of any monomer present in the original fibril suspension. In principle, the presence of peak B in the HDX-MS of an aggregate could come from a second class of peptide molecules that are part of the aggregate structure but not held in place by strong H-bonds. Alternatively, it could derive from the dissociation of Aβ from the aggregate during the exchange period, generating a relatively unstructured, and unprotected, monomer. A third mechanism is one involving dissociation, full exchange, and reassociation. The latter two possibilities would be consistent with the demonstrated ability of Aβ(1-40) fibrils and protofibrils to dissociate [41, 44, 378].

The fully exchanged peak B we observe in analysis of mature amyloid fibrils is probably due to a dissociation-exchange-reassociation mechanism, since we typically observe a larger proportion of material in peak B than can be accounted for by the known C_r of the peptide under these buffer conditions. A similar dissociation-exchange-reassociation mechanism has been invoked to explain the appearance of fully exchanged material in the HDX-MS of other amyloid fibrils [379]. According to this mechanism,

there may be a dynamic system - an equilibrium existing between the insoluble fibril and the soluble monomer. In a mass spectrometric analysis of the solubilized fibrils, two peaks would then be observed since MS can detect and characterize populations of molecules with different degrees of exchange [265]: peak A, which represents the population of molecules that has not yet dissociated from the fibrils and that is still exposed to the deuterated solvent, and peak B, which represents the population that has dissociated from the fibrils, exchanged and then been reincorporated.

The fully exchanged peak B observed in the analysis of authentic Aβ(1-40) protofibrils not stabilized by CLC [59] probably derives from dissociation to a monomer pool during the exchange reaction, contributed by (a) the relative ease with which these aggregates dissociate [44] coupled with (b) their poor ability to act as a template for (re)addition of monomeric Aβ(1-40) molecules [94]. In contrast, the lack of a fully exchanged peak in the CLC protofibril data reported here is most consistent with a barrier to dissociation due to the stabilizing influence of the CLC [94]. Even after 14 days of incubation at 37 °C, the CLC protofibrils contain a single homogeneous structural population exhibiting similar amount of deuterium exchange as the CLC protofibrils isolated after day 2 shown in Figure 4.4a.

It is noted that as the incubation time increased, the intensity of peak B increases relative to that of peak A for both full-length peptide (Figure 4.5a) and fragment 20-34 (Figure 4.5c) obtained from mature fibrils. However, the relative intensity ratio of peak B to peak A is much bigger for fragment 20-34 than for full-length 1-40 peptide at the same time point. For example, at the 100-h time point, the ratio was 1.1 for fragment 20-34, while the ratio was only 0.5 for intact peptide. It was found that after the on-line proteolysis of Aβ(1-40) fibrils, some of the peak A of intact Aβ still exists (Figure 4.5b), suggesting that proteolysis of this class of Aβ molecules is not complete. Also, the ratio of peak B to peak A is lower in the MS spectra of "leftover" intact 1-40 peptide obtained after digestion (Figure 4.5b) than in the MS spectra of intact 1-40 peptide obtained in the absence of pepsin (Figure 4.5a) for the same time point. For example, at the 100 h time point, the ratio was 0.23 for the leftover intact 1-40 peptide, while the ratio was 0.53 for the intact 1-40 peptide obtained in the absence of pepsin. The fact that the ratio of peak

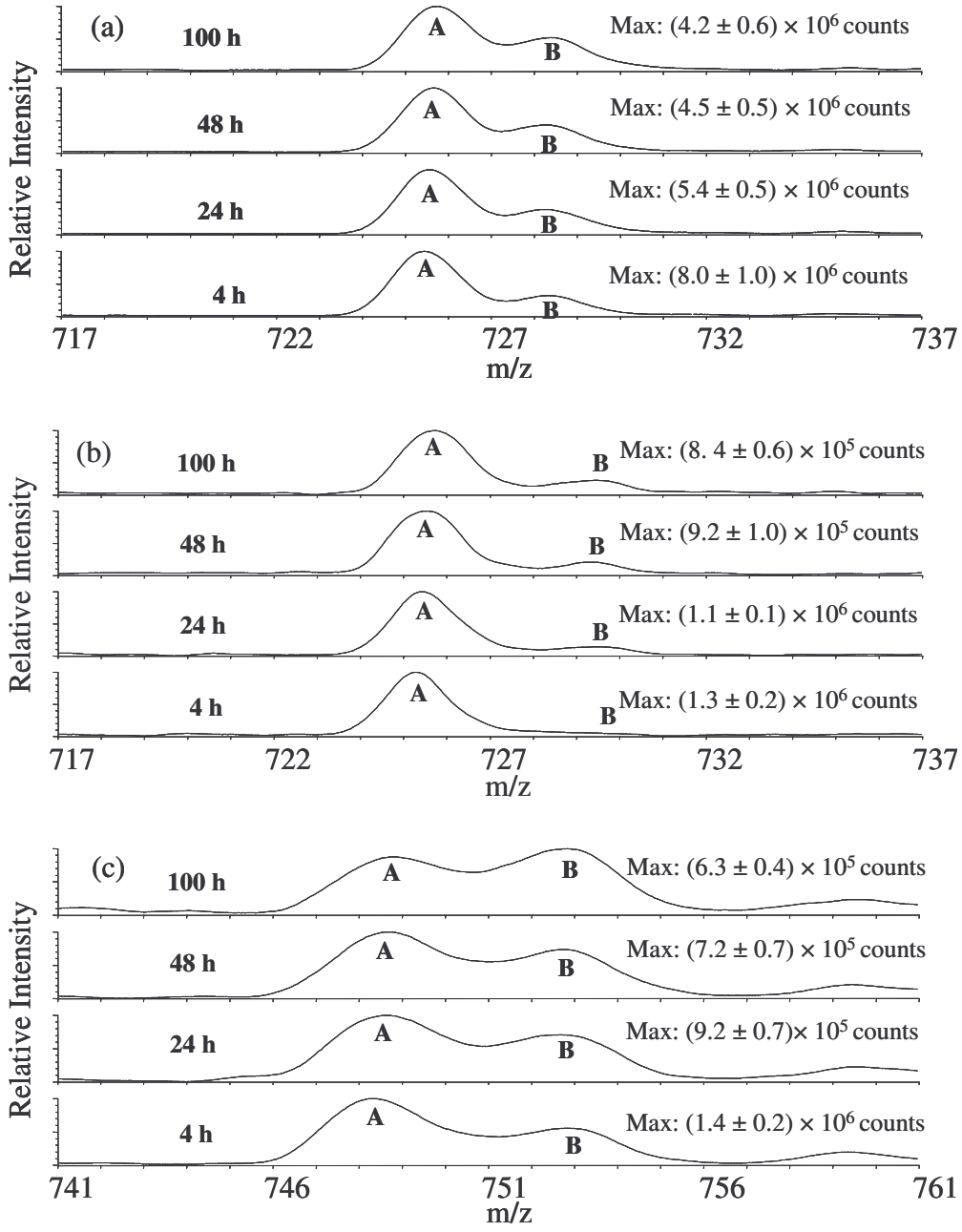

Figure 4.5. Mass spectra illustrated of (a) intact Aβ(1-40) (+6 charge state) in the absence of pepsin; (b) leftover intact Aβ(1-40) (+6 charge state) after the digestion; (c) 20-34 segment (+2 charge state) following incubation of 4 h, 24,h, 48 h and 100 h. The intensity insets are for the base peaks in the spectra.

B to peak A is smaller for the intact Aβ(1-40) than for the fragment 20-34 is consistent with longer exposure to pepsin, possibly due to more rapid detachment of fully exchanged molecules comprising peak B than partially exchanged molecules (comprising peak A) present in the core structure of Aβ(1-40). The fact that peak B of the intact Aβ(1-40) was attenuated more relative to peak A can be attributable to easier digestion of monomers by pepsin than fibrils (discussed in Chapter 3). The observation here further validates the use of the peak B to peak A ratio obtained from the fragment 20-34 (instead of intact Aβ(1-40)) to deconvolute the peaks of the fragments 1-19 and 4-19, as described above.

4.1.4 Possible Correlation of Protofibrils with Fibrils

Although the efforts of a large number of research groups using technological approaches have led to much insight into the structures of organized Aβ aggregates associated with Alzheimer's disease (see section 1.1), there remain a number of critical issues left to be resolved. Which aggregates are toxic and what is the mechanism of their toxicity? What are the structural differences between protofibrils and fibrils, and between different conformational states of mature fibrils? What is the role of protofibrils in the assembly mechanism of mature fibrils? The HDX-MS analysis reported here helps to address some of the latter questions on structure and assembly.

Studies on spontaneous fibril assembly by Aβ(1-40) as well as by the NM fragment of the *psi* yeast prion protein sup35 have led to the suggestion that protofibrils are on-pathway intermediates that are capable of (a) undergoing a key conformational rearrangement to generate the nucleus for fibril growth and (b) adding intact to the growing end of fibrils as a mechanism for elongation [42, 380]. Other studies show that all aspects of this mechanism are not absolutely essential for fibril growth. Thus, solutions of monomeric Aβ(1-40), even at very low concentrations where protofibril formation is slow, can support fibril elongation [381-382]. Likewise, solutions of monomeric Sup35 NM are able to elongate mature fibrils through monomer addition [383]. In addition, monomeric Sup35 NM preparations are able to support spontaneous fibril formation through a nucleation mechanism involving a critical nucleus containing

very few monomers, rather than a transformation within a protofibril [383]. While the latter studies suggest that protofibril formation is not an absolute requirement for fibril growth, it nonetheless remains of great interest how fibril nucleation and growth is mediated by protofibrils under those conditions in which they are involved.

Even if protofibrils are on-pathway intermediates in fibril formation, they may not bear a structural resemblance to fibrils at the molecular level. That is, the transition from protofibril to fibril could involve a massive structural reorganization. Likewise, the fact that protofibrils share a number of structural features with fibrils (as shown above) is not an absolute proof of an on-pathway role in fibril assembly, although the structural relationship between these two forms is certainly *consistent* with an on-pathway role. Previous studies of protofibrils isolated from an on-going fibril assembly reaction revealed a structural relationship, in showing that (a) protofibrils, like fibrils, possess a complement of very highly protected backbone amide protons, consistent with H-bonded β-sheet, and (b) protofibrils, like fibrils, selectively incorporate an Aβ point mutant Glu22Gly (the residue glutamic acid at position 22 replaced with glycine) into the aggregate from a 1:1 mix of wild type and mutant Aβ monomers [59]. The results described in this chapter provide further support for a structural relationship, by showing that the distribution of HDX-sensitive and resistant amide hydrogens within protofibrils is similar to that within quiescent fibrils: the N-terminus and C-terminus of Aβ are open to exchange in both, as are some residues in the center of the hydrophobic C-terminal half of the molecule. The fact that protofibrils contain very stably protected backbone amide protons most consistent with H-bonded β-structure does not rule out the possibility that these or other temporal intermediates in Aβ fibril assembly might not also contain some α-helical structure, as suggested by others [96].

The results presented here suggest that the 21-30 segment becomes progressively more ordered as assembly proceeds toward mature fibrils. Thus, quiescent fibrils exhibit more backbone amide hydrogens protected from HDX in this segment compared to protofibrils (Figure 4.3). In addition, previous studies reveal no sensitivity of aggregate stability to Pro insertions in this segment in protofibrils [94], while in mature fibrils Pro insertion at several residue positions in the segment lead to fibril destabilization [40]. If

protofibrils prove to be on-line assembly intermediates in amyloid fibril formation, the structural comparison of these two aggregate forms suggests that early formation of packed, central β-sheet elements are likely to be the critical first steps in the formation of organized aggregates, with acquisition of order in other sequence elements occurring subsequently.

4.2 Proteolysis of Aβ (1-40) Fibrils Using Pepsin-like Enzymes

As evident from previous discussion, the digestion of Aβ fibrils on-line using pepsin in a relatively short time period (12 seconds) gives rise to limited fragmentation, thus providing limited structural information. Although increasing the digestion time could increase the extent of digestion, shorter digestion time is preferred because of the reduction of artifactual exchange in HDX-MS studies. One way to obtain more structural information is to use other enzymes that could produce more and/or different fragments. As addressed in section 1.3, type XIII protease, type XVIII protease and endothiapepsin are HDX-compatible pepsin-like enzymes (working at low pH and low temperature to limit artifactual exchange during proteolysis). In this section, results are presented for the digestion of Aβ samples using each enzyme as well as using combinations of enzymes simultaneously. The triaxial probe was used to allow separate optimization of proteolysis and MS solvents.

4.2.1 Comparison of Digestion Efficiency: Before Cleanup vs. After Cleanup

As presented in Figure 4.6b, the on-line digestion of Aβ(1-40) monomer using protease type XVIII (used as received from Sigma) produced 8 fragments at a 45/1 [w/w] enzyme/monomer ratio, which reduced the signal for intact monomer to the baseline. Unfortunately, the spectrum contains a strong background from the enzyme solution, as evident in Figure 4.6a. Those interfering peaks could be due to autolysis of the enzyme or from contaminants present in the enzyme sample. As a test for autolysis, a type XVIII water blank (formic acid omitted) was measured. The same interfering peaks as those in

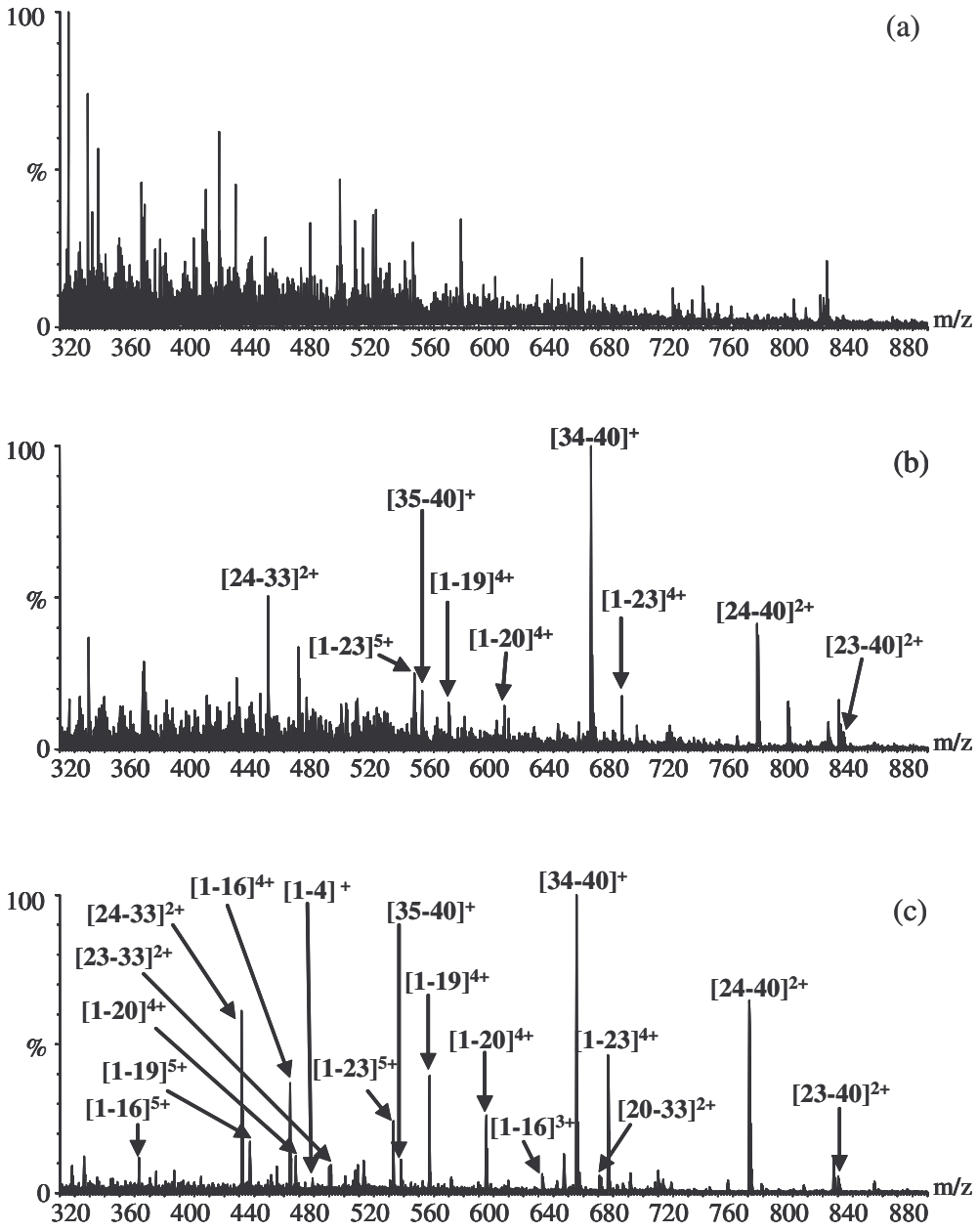

Figure 4.6. Mass spectra obtained from (a) 0.1 μg/μl type XVIII protease in 0.5/100 HCOOH/H_2O; (b) digestion of Aβ(1-40) monomer with unpurified type XVIII protease at an enzyme-to-monomer ratio of 45-to-1; (c) digestion of Aβ(1-40) monomer with purified type XVIII protease at an enzyme-to-monomer ratio of 18-to-1 (Only peaks of fragments with S/B ≥ 5 are labeled).

Figure 4.6a were present in this blank, despite the fact that the enzyme is completely inactivated above pH 6 [331]. Therefore, purification of the enzyme is apparently necessary to achieve higher digestion efficiency and cleaner mass spectra.

Since the interfering peaks are of MW <3000 and the enzymes type XVIII have a MW of ~33,000, dialysis using a membrane with a MW cutoff at 12000~15000 was undertaken (see section 2.2). Dialysis substantially improved Aβ spectra obtained with this enzyme, as shown in Figure 4.6c. Totally 18 fragments were identified for the monomer digestion, vs 8 obtained using unpurified enzyme. Also, the lower background gives better sensitivity for the fragments. For example, the signal-to-background ratio (S/B, background assessed as the average intensity between m/z 1100 and m/z 1200) of the base peak at m/z 674 ($[34\text{-}40]^+$ ion) increased by a factor of 5 after dialysis. The complete digestion (defined as reducing the signal for intact Aβ to the baseline) of Aβ monomer with purified type XVIII protease was achieved at an enzyme-to-monomer ratio of 18:1 (w/w), a factor of two and a half decrease as compared to using unpurified protease type XVIII. However, the mass recovery of this enzyme after dialysis was only ~ 30%, indicating a small net loss of activity per microgram. This may be attributable to the loss of some enzyme, while removing contaminants.

Protease type XIII is another enzyme employed in this study. Before purification of the protease type XIII, the complete digestion of Aβ(1-40) monomer with this enzyme produced totally 9 fragments at a 25/1 [w/w] enzyme/monomer (Figure 4.7b). However, the spectrum is dominant with intense peaks from the enzyme solution. The peaks from the fragments are of relatively low intensities (Figure 4.7b). For example, the intensity of the peak of the most abundant enzymatic fragment ion (i.e. $[24\text{-}40]^{2+}$ ion at m/z 786 in Figure 4.7b) was only around 20% of the base peak at m/z 354. Purification though dialysis improved Aβ spectra obtained with this enzyme dramatically, as shown in Figure 4.7c. Totally 18 fragments were observed in a very clean and nice mass spectrum with a S/B of 180 for the base peak at m/z 378 (Figure 4.7c), 9 more fragments than using the unpurified type XIII enzyme (Figure 4.7b). The amount of enzyme needed for complete monomer digestion decreased by a factor of 5 (from 25:1 to 5:1). However, the mass recovery of this enzyme was only ~ 5%, suggesting substantial contamination and/or

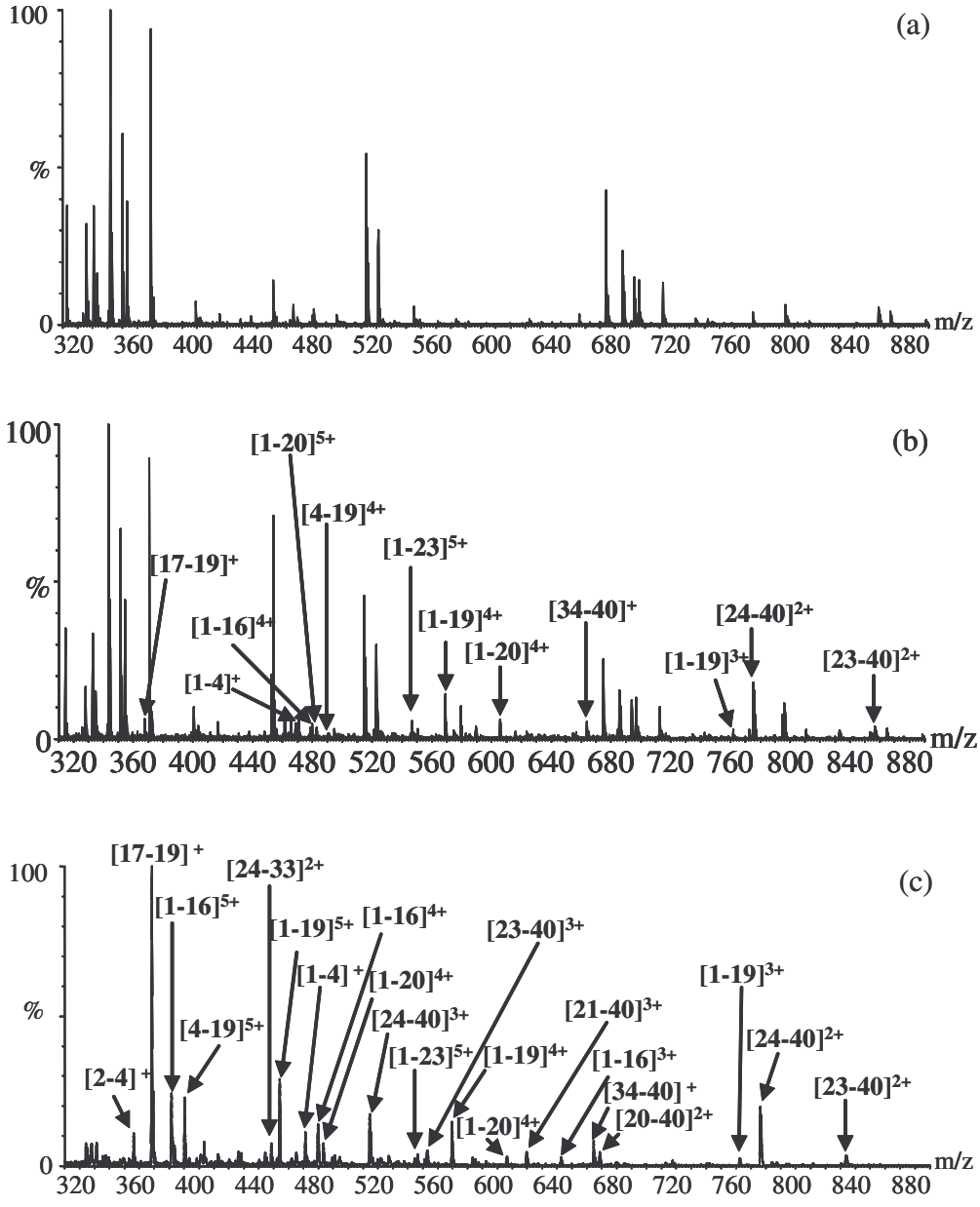

Figure 4.7. Mass spectra obtained from (a) 0.1 μg/μl type XIII protease in 0.5/100 HCOOH/H_2O; (b) digestion of Aβ(1-40) monomer with unpurified purified type XIII protease at an enzyme-to-monomer ratio of 25-to-1; (c) digestion of Aβ(1-40) monomer with purified type XIII protease at an enzyme-to-monomer ratio of 5-to-1 (Only peaks of fragments with S/B ≥ 5 are labeled).

possible loss of some enzyme, as well as some loss of activity per microgram. Although digestion of monomer using the enzyme type XIII shares the same 18 fragments as the digestion using the enzyme type XVIII, the intensities of the fragments are different, as evident in Figure 4.7c and Figure 4.6c.

The enzyme endothiapepsin was also used in this work. It was a generous gift from Dr. Chris Dealwis at the University of Tennessee-Knoxville. This enzyme was of crystallographic purity and was stored in saturating ammonium sulfate salt. Except for desalting by dialysis (described in section 2.2), no other purification was conducted prior to digestion experiments. The complete digestion of Aβ(1-40) monomer using this enzyme needed an enzyme-to-monomer ratio of 6:1 and 12 fragments were identified (Figure 4.8).

The results from the digestion of monomer using all four enzymes (protease type XVIII, protease type XIII, endothiapepsin and pepsin) are summarized in Table 4.2 and the sequences of the peptides obtained with each protease are shown in Figure 4.9. Compared to pepsin, which requires an enzyme-to-monomer weight ratio of 0.9:1 to attenuate the monomer peaks to background level (discussed in Chapter 3), all three pepsin-like enzymes are much less active; protease type XVIII is the least active one. Like pepsin, none of these pepsin-like proteases is really specific, but the digestion pattern was of good reproducibility. These pepsin-like enzymes prefer the cleavage of hydrophobic residues on the N- and/or C-terminal sides, such as Phe (F), Leu (L), Met (M) and Val (V), as evident from the results summarized in Table 4.3. Pre-purified protease type XVIII and protease type XIII were used in the fibril experiments discussed below. (Due to the limited availability of endothiapepsin, no digestion of fibrils with this enzyme was undertaken.).

4.2.2 Proteolysis of Aβ(1-40) Fibrils with Individual Enzymes

Figure 4.10 shows results for the digestion of Aβ fibrils using proteases type XVIII and type XIII. At a 5-to-1 enzyme-to-fibril weight ratio, the digestion of fibrils was not complete using either enzyme. For the digestion using protease type XVIII, the same number of fragments (18 fragments) were identified as for the digestion of

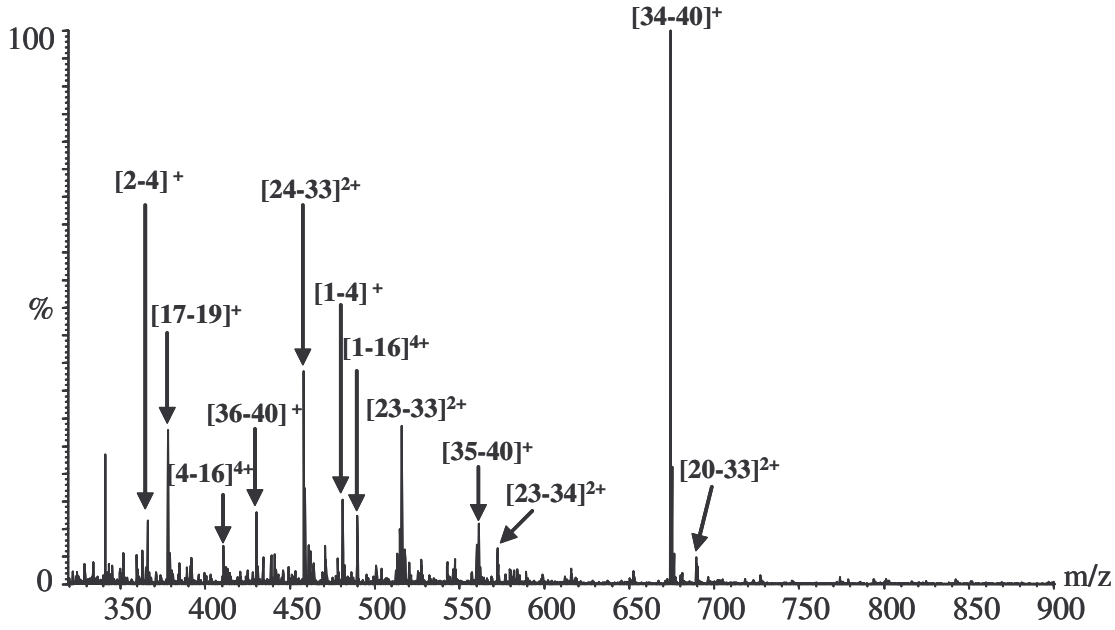

Figure 4.8. Digestion of Aβ(1-40) monomer with endothiapepsin at an enzyme-to-monomer ratio of 6-to-1.

Table 4.2. Summary of results from digestion of Aβ(1-40) monomer using protease type XVIII, protease type XIII, endothiapepsin and pepsin.

	$W_{enzyme}:W_{mon}$		**Total # fragments (before *vs* after dialysis**	**Weight Recovery**
Enzymes	**Before cleanup**	**After cleanup**		
Type XVIII	45:1	18:1	8 *vs* 18	30%
Type XIII	25:1	5:1	9 *vs* 18	5%
Endothiapepsin	6:1		12	N/A
Pepsin	0.9:1		7	N/A

Figure 4.9. Peptide mappings. The sequences of the peptides obtained with digestion of Aβ(1-40) monomer using pepsin, desalted endothiapepsin, pre-purified protease type XVIII and pre-purified type XIII are shown as underlining bars under the Aβ(1-40) sequence.

Table 4.3. A summary of peptide fragments identified.

Fragment	M/Z	Charge State	Mass	Peptide Sequence	Cleavage Site
1-4	481.19	1+	480.19	DAEF	F-R
1-16	489.48	3+	1953.87	DAEFRHDSGYEVHHQK	K-L
	652.30	4+			
	391.78	5+			
	517.75	4+			
1-19	772.04	3+	2313.09	VGSNKGAIIGLMVGGVV	F-F
	579.28	4+			
	463.63	5+			
1-20	616.05	4+	2460.16	DAEFRHDSGYEVHHQKLV FF	F-A
	493.04	5+			
	411.03	6+			
1-23	926.10	3+	2775.27	DAEFRHDSGYEVHHQKLV FFAED	D-V
	694.82	4+			
	556.06	5+			
	463.55	6+			
	397.47	7+			
2-4	366.17	1+	365.16	AEF	D-A F-R
4-16	410.70	4+	1638.77	FRHDSGYEVHHQK	E-F K-L
4-19	667.00	3+	1997.99	DAEFRHDSGYEVHHQK LVF	E-F F-F
	500.50	4+			
	400.61	5+			
	334.01	6+			
17-19	378.35	1+	377.35	LVF	K-L L-V
20-33	689.35	2+	1376.69	FAEDVGSNKGAIIG	G-L
	459.91	3+			
20-34	745.90	2+	1489.78	FAEDVGSNKGAIIGL	F-F L-M
	497.60	3+			
20-40	1017.04	2+	2032.07	FAEDVGSNKGAIIGLMVGG VV	F-F
	678.36	3+			
21-40	943.51	2+	1885.00	AEDVGSNKGAIIGLMVGG VV	F-A
	629.34	3+			
	472.26	4+			
	378.01	5+			

(Table 4.3 Continued)

Fragment	M/Z	Charge state	Mass	Peptide sequence	Cleavage sites
23-33	515.78	2+	1029.55	DVGSNKGAIIG	E-D G-L
23-34	572.32	2+	1142.63	DVGSNKGAIIGL	E-D L-M
23-40	843.37	2+	1684.74	DVGSNKGAIIGLMVGGVV	E-D
	562.65	3+			
	422.24	4+			
24-33	915.53	1+	914.52	VGSNKGAIIG	D-V G-L
	458.27	2+			
24-40	785.95	2+	1569.89	VGSNKGAIIGLMVGGVV	D-V
	524.30	3+			
	393.48	4+			
	314.99	5+			
34-40	674.39	1+	673.38	LMVGGVV	G-L
	337.70	2+			
35-40	561.31	1+	560.30	MVGGVV	L-M
36-40	430.27	1+	429.26	VGGVV	M-V

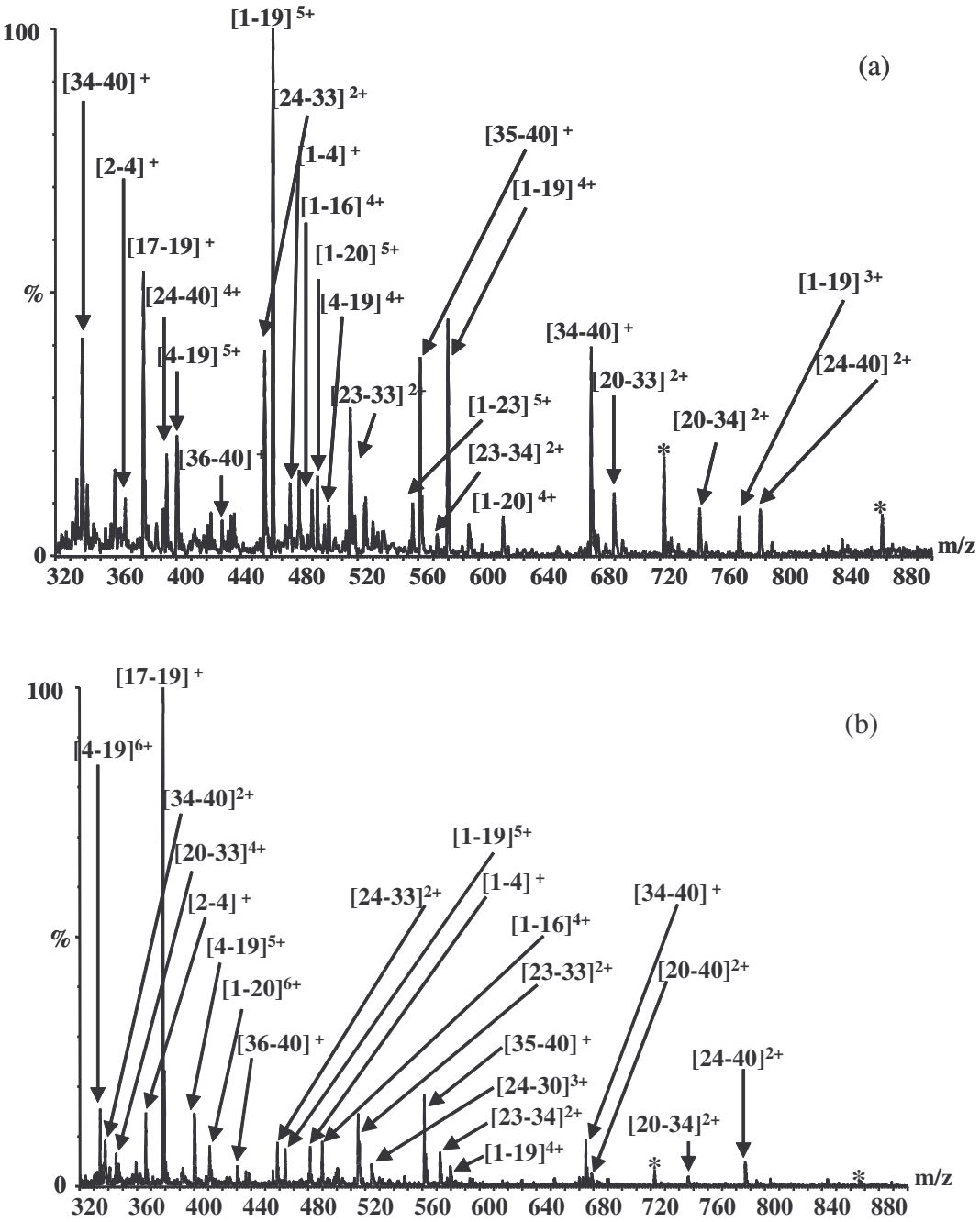

Figure 4.10. Digestion of Aβ(1-40) fibrils with (a) pre-purified type XVIII protease at an enzyme-to-monomer ratio of 5-to-1; (b) pre-purified type XIII protease at an enzyme-to-monomer ratio of 5-to-1. Only peaks of fragments with S/B ≥ 5 are labeled. +5 and +6 charge state peaks from intact Aβ peptide leftover are labeled with "*".

monomer, with the peak of intact Aβ peptide comprising around 20% of the base peak (m/z 464; $[1\text{-}19]^{5+}$) (Figure 4.10). Fragments 20-34 and 36-40 were observed only with the digestion of fibrils, while fragments 23-40 and 21-40 were observed only with the digestion of monomer. It is interesting to note that for the digestion of fibrils the base peak was from the fragment ion $[1\text{-}19]^{5+}$ at m/z 464, while the peak from the fragment ion $[34\text{-}40]^{+}$ at m/z 674 was around 42% of the base peak (Figure 4.10a). In contrast, for the digestion of monomer, the base peak was from the fragment ion $[34\text{-}40]^{+}$ at m/z 674, while the peak from the fragment ion $[1\text{-}19]^{5+}$ at m/z 464 was around 50% of the base peak (Figure 4.6c). The above observed digestion differences may be due to the fact that digestion of insoluble fibrils is controlled not only by kinetics of cleavage but also by kinetics of dissolution to expose cleavable peptide bonds, while the digestion of soluble monomer is controlled only by kinetics of cleavage. As a result, there is presumably more digestion time available for monomer than for fibrils, thus leading to different digestion product profiles. Of course, the comparison would be more meaningful if complete digestion was also achieved for fibrils.

For the digestion of fibrils with protease type XIII, totally 19 fragments were observed in a very clean spectrum, with the peak of intact Aβ peptide detected with only around 5% of the base peak intensity (Figure 4.10b). The digestion of fibrils shared 17 fragments with the digestion of monomer. Fragment 1-23 was observed only with the digestion of monomer, while fragments 20-34 and 36-40 were observed only with the digestion of fibrils. It is interesting to note that the base peak in Figure 4.10b is from the $[17\text{-}19]^{+}$ fragment ion. The sequence of the peptide corresponding to that ion is LVF (leucine, valine, phenylalanine), which is a highly hydrophobic peptide and is therefore favored in ESI mass spectra [384]. As always, electrospray intensities may not directly reflect relative abundances. Calibration (preferably with an internal standard) would be needed for quantitation. Nevertheless, comparison of qualitative and even semi-quantitative information among similar samples should be valid.

4.2.3 Proteolysis of Aβ(1-40) Fibrils with Enzyme Mixtures

Since sample may be limited, it would be useful if the enzymes could be

combined to gain broad structural information in a single experiment. This would require that they don't inhibit or digest one another on the timescale of the experiments. As a test, digestion of fibrils using all binary and tertiary combinations of protease type XVIII, protease type XIII, and pepsin was conducted. Results are shown in Figure 4.11 – Figure 4.14 and summarized in Table 4.4. The binary mixture of protease type XIII and pepsin was additive in their effects on fragmentation under the conditions used. However, the other binary mixtures and the tertiary mixture were not additive in their effects on fragmentation. For the mixture of protease type XVIII and pepsin, the 1-23 fragment was missing, while for the mixture of protease type XVIII and protease type XIII, 20-34 and 23-34 fragments were missing. For the tertiary mixture, the missing fragment was 1-23. The fact that some specific ions evident in the single-enzyme spectra may be missing or not be detected in the mixtures can be attributed to the following two reasons. First, less than the optimum amount of each enzyme was used in the enzyme mixtures (avoiding problems associated with using high total enzyme concentrations), thus leading to non-strict addition. Second, in the presence of multiple enzymes, possible further fragmentation of previously-generated fragments by enzymes (suggesting the importance of experimental optimization) can lead to their relative intensity attenuation or even their vanishing. For example, the fragment 20-40 can be further cleaved to produce fragments 20-33 and 34-40 or 20-34 and 35-40, thus leading to possible attenuation of its intensity or possible disappearance. The use of enzyme mixtures can facilitate the cleavage of the peptide. For example, pepsin favors the cleavage between residue 19 and 20 to produce the fragments 1-19 and 20-40 [360]. Protease type XIII can cleave the fragment 1-19 further to produce the fragment 17-19 and 1-16. Another advantage of using enzyme mixtures is that the amount of each enzyme needed can be significantly reduced. For example, the use of the mixture of protease type XIII and pepsin required less than one-third of the amount of either enzyme used alone to attenuate the intact peptide peak to the same degree, as evident in Table 4.4. This would justify the preferred use of the mixture of protease type XIII and pepsin over using protease type XIII alone, although they produced the same fragments.

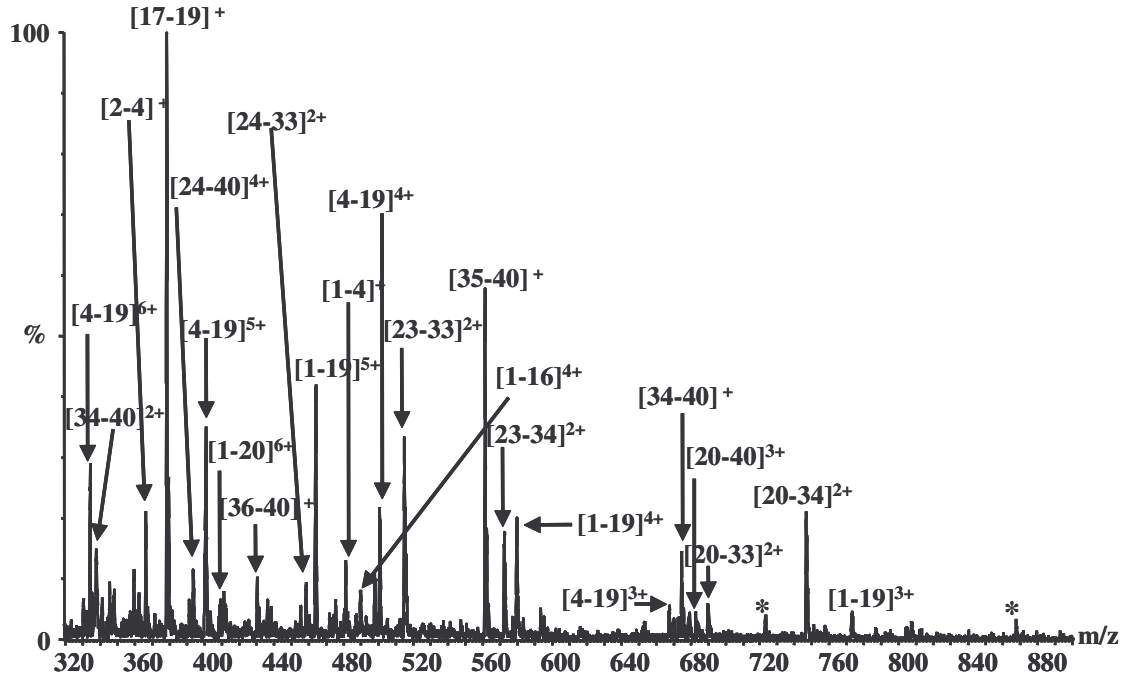

Figure 4.11. Digestion of Aβ(1-40) fibrils with the enzyme mixture composed of pre-purified protease type XIII and pepsin. Only peaks of fragments with S/B ≥ 5 are labeled. +5 and +6 charge state peaks from intact Aβ peptide leftover are labeled with "*".

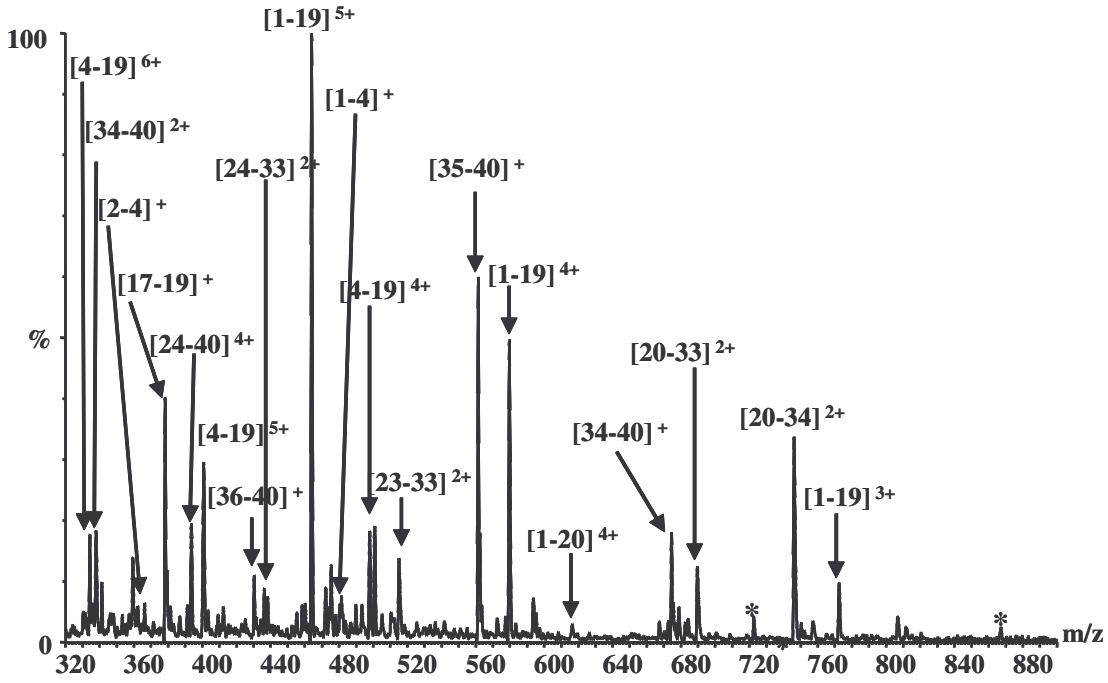

Figure 4.12. Digestion of Aβ(1-40) fibrils with the enzyme mixture composed of pre-purified protease type XVIII and pepsin. Only peaks of fragments with S/B ≥ 5 are labeled. +5 and +6 charge state peaks from intact Aβ peptide leftover are labeled with "*".

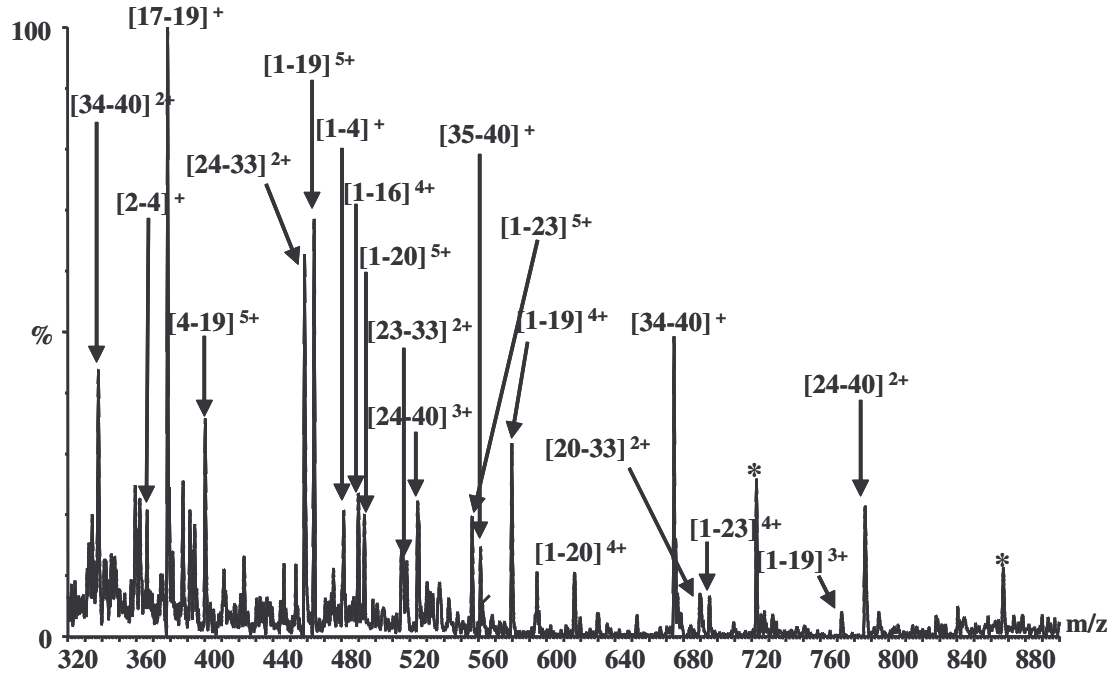

Figure 4.13. Digestion of Aβ(1-40) fibrils with the enzyme mixture composed of pre-purified protease type XVIII and type XIII. Only peaks of fragments with S/B ≥ 5 are labeled. +5 and +6 charge state peaks from intact Aβ peptide leftover are labeled with "*".

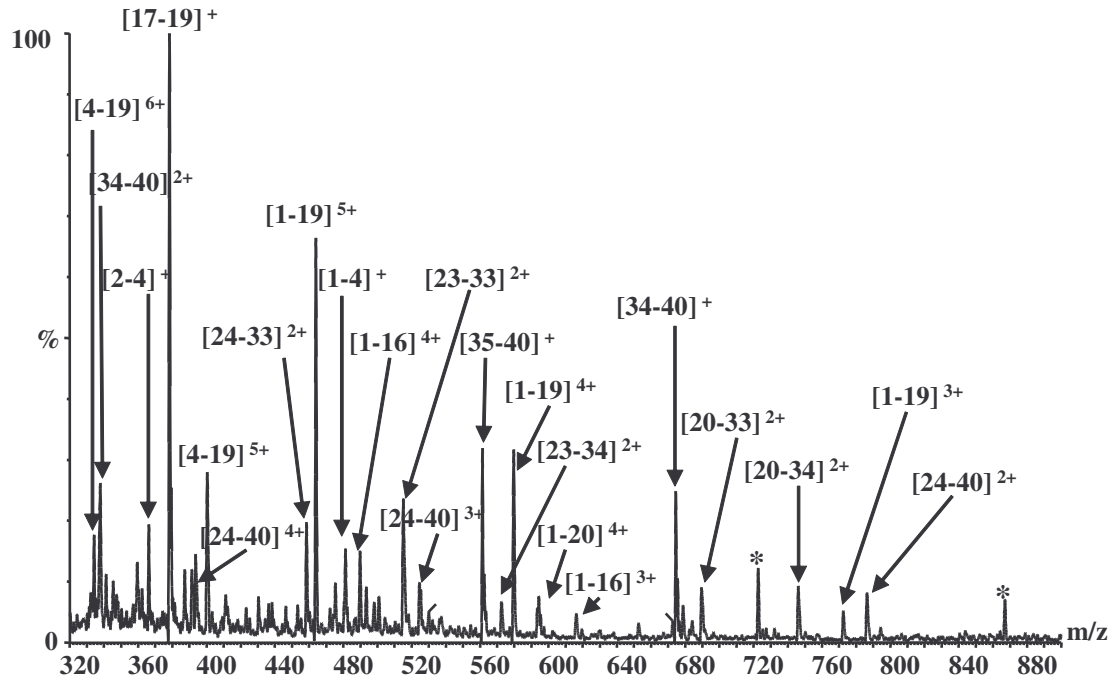

Figure 4.14. Digestion of Aβ(1-40) fibrils with the enzyme mixture composed of pepsin, pre-purified protease type XVIII and type XIII. Only peaks of fragments with S/B ≥ 5 are labeled. +5 and +6 charge state peaks from intact Aβ peptide leftover are labeled with "*".

Table 4.4. Summary of results from digestion of Aβ(1-40) fibrils using individual enzymes and enzyme mixtures. Signal-to-background ratio (S/B) is based on the base peak. Background was assessed as the average intensity between m/z 1100 and m/z 1200. The master list includes the combined fragments obtained from the digestion using all the following enzymes either individually or in combination.

Enzyme	Weight Ratio	Observed Fragment (#)	Relative intensity of intact peptide peak (+6) to the base peak (S/B)
Pepsin	$W_{pep}:W_{fib} = 8 : 1$	**1-19, 4-19, 20-33, 20-34, 34-40,35-40, 20-40 (7)**	**8% (45)**
XIII	$W_{XIII}:W_{fib} = 5 : 1$	**1-4, 1-16, 1-19, 1-20, 2-4, 4-19, 17-19, 20-33, 20-34, 20-40, 21-40, 23-33, 23-34, 23-40, 24-33, 24-40, 34-40, 35-40, 36-40 (19)**	**5% (139)**
XVIII	$W_{XVIII}:W_{fib} = 5 : 1$	**1-4, 1-16, 1-19, 1-20, 1-23, 2-4, 4-19, 17-19, 20-33, 20-34, 20-40, 23-33, 23-34, 24-33, 24-40, 34-40, 35-40, 36-40 (18)**	**20% (30)**
XIII+Pepsin	$W_{XIII}:W_{fib} = 1.25 : 1$ $W_{pep}:W_{fib} = 2.5 : 1$	**1-4, 1-16, 1-19, 1-20, 2-4, 4-19, 17-19, 20-33, 20-34, 20-40, 21-40, 23-33, 23-34, 23-40, 24-33, 24-40, 34-40, 35-40, 36-40 (19)**	**5% (53)**
XVIII+Pepsin	$W_{XVIII}:W_{fib} = 2.5 : 1$ $W_{pep}:W_{fib} = 1.25 : 1$	**1-4, 1-16, 1-19, 1-20, 2-4, 4-19, 17-19, 20-33, 20-34, 20-40, 23-33, 23-34, 24-33, 24-40, 34-40, 35-40, 36-40 (17)**	**5% (42)**
XIII + XVIII	$W_{XVIII}:W_{fib} = 5 : 1$ $W_{XIII}:W_{fib} = 0.425 : 1$	**1-4, 1-16, 1-19, 1-20, 1-23, 2-4, 4-19, 17-19, 20-33, 20-40, 21-40, 23-33, 23-40, 24-33, 24-40, 34-40, 35-40, 36-40 (18)**	**33% (15)**
XIII + XVIII + Pepsin	$W_{XVIII}:W_{fib} = 2.5 : 1$ $W_{XIII}:W_{fib} = 0.625 : 1$ $W_{pep}:W_{fib} = 0.3 : 1$	**1-4, 1-16, 1-19, 1-20, 2-4, 4-19, 17-19, 20-33, 20-34, 20-40, 21-40, 23-33, 23-34, 23-40, 24-33, 24-40, 34-40, 35-40, 36-40 (19)**	**13% (36)**

Master list: 1-4, 1-16, 1-19, 1-20, 1-23, 2-4, 4-19, 17-19, 20-33, 20-34, 20-40, 21-40, 23-33, 23-34, 23-40, 24-33, 24-40, 34-40, 35-40, 36-40

4.2.4 Structural Information Implicit in the Enzymatic Fragments

As evident from the above discussion, the use of any of the three pepsin-like enzymes or the enzyme mixtures produced more fragments, thus increasing sequence coverage and potentially providing more structural information than using pepsin alone in HDX studies. Among the individual enzymes and enzyme mixtures studied here, the mixture of protease type XIII and pepsin seems to be the best choice for the digestion of fibrils under the conditions used, in terms of the number of fragments, intensities of fragments and S/B of the base peaks. Digestion using this combination could provide important insights into the secondary structures of Aβ fibrils. Specifically, deuteration information from enzymatic fragments such as peptides 1-4 and 2-4 could allow for determination of solvent accessibility about the very N-terminus. Deuterium incorporation in fragments such as 17-19, 20-33, 20-34, 23-33, 23-34 and 24-33 could provide detailed information about the core structure (involving residues 15-36 [40, 63, 74]) of Aβ(1-40). The number of deuteriums incorporated into fragments 34-40, 35-40 and 36-40 should provide consistent structural information about the C-terminus, thus helping resolve the controversy concerning whether the C-terminus is exposed or protected [40, 63, 74]. The difference in deuterium content between the overlapping fragments could provide further information of the N-terminus, C-terminus and the core structure, permit verification of deuterium incorporation into certain fragments and enable the localization of deuteriums to smaller peptides or even single residues, as evident in Table 4.5.

4.3 Conclusions

HDX-MS methods were developed and applied to map the hydrogen bonding pattern and extent of the β-sheet network in amyloid fibrils and protofibrils. These methods can be used to obtain information on particular aggregates, as well as to compare structures of different aggregates. To localize the hydrogen-bonding interaction sites within the peptide, we have coupled HDX-MS with on-line proteolysis using pepsin.

Table 4.5. A summary of non-overlapping peptide amides derived from differences of overlapping fragments produced by digestion of Aβ(1-40) fibrils using the mixture of protease type XIII and pepsin.

Overlapping Peptide Fragments	**Non-overlapping backbone peptide amides**
1-4 and 1-16	5-16
1-4 and 1-19	5-19
1-4 and 1-20	5-20
1-4 and 2-4	2
1-16 and 1-19	17-19
1-16 and 1-20	17-20
1-19 and 1-20	20
1-19 and 4-19	2-4
1-19 and 17-19	2-17
4-19 and 17-19	5-17
20-33 and 20-34	34
20-33 and 20-40	34-40
20-33 and 23-33	21-23
20-33 and 24-33	21-24
20-34 and 20-40	35-40
20-34 and 23-34	21-23
20-40 and 23-40	21-23
20-40 and 24-40	21-24
20-40 and 34-40	21-34
20-34 and 35-40	21-35

(Table 4.5 Continued)

Overlapping Peptide Fragments	Non-overlapping backbone peptide amides
20-34 and 36-40	21-36
23-33 and 23-34	34
23-33 and 23-40	34-40
23-33 and 24-33	24
23-34 and 23-40	35-40
24-33 and 24-40	34-40
23-40 and 24-40	24
23-40 and 34-40	24-34
23-40 and 35-40	24-35
23-40 and 36-40	24-36
24-40 and 34-40	25-34
24-40 and 35-40	25-35
24-40 and 36-40	25-36
34-40 and 35-40	35
34-40 and 36-40	35-36

The methods have been validated in that the results obtained with wild type Aβ(1-40) quiescent amyloid fibrils agree very well with other structural approaches applied to identical fibrils [40, 61, 63]. The on-line HDX-MS method of analysis of aggregate structure is rapid and reproducible. Future development and applications of these methods will include use of pepsin-like enzymes tolerant of low pH, and/or the use of multi-enzyme digestion (simultaneously or sequentially), which should allow better sequence coverage and increase resolution of exchanged deuterium localization by generating abundant overlapping fragments.

CHAPTER 5

ELIMINATING OXIDATION ARTIFACTS IN ESI-MS ANALYSIS OF Aβ

As discussed in Chapter 1, the electrospray ion source behaves like a controlled-current electrolytic cell, and electrochemical processes must occur within the ES capillary to maintain charge balance during the ES process [171, 178, 194,]. Under normal electrospray conditions, currents < 1 μA are sustained. For protein and peptide analysis, the ES capillary is usually raised to a high positive potential, and oxidation of solvent, emitter, or/and analyte can occur at the capillary wall. Individual species are generally oxidized in order of their increasing redox potential until the required current is supplied [178]. If the electric field strength is too high, an electric discharge will occur, and higher and unstable currents > 1 μA will be produced [139-140]. Oxidation of solvent or/and analyte, and corona discharge can lead to the production of reactive radicals, which can initiate a cascade of oxidation reactions in both the solution and gas phases [385-386].

Methionine is one of the most readily oxidized amino acid constituents of proteins [387-392]. Oxidation of methionine residues by reactive oxygen species can result in significant conformational and/or functional changes in peptides and proteins [393]. It plays a crucial role in protein aging [394] and is known to decrease the biological activity of proteins [395]. For example, the oxidation of methionine in Aβ peptides further increases the insolubility of Aβ fibrils [396-397]. This modification may occur under conditions of oxidative stress, aging, or/and during the pathogenesis of Alzheimer's disease [398]. Thus, identifying the presence and quantifying the percentage of oxidized species in methionine-containing peptides and proteins are significant. Although ES-MS has proved to be a powerful technique for identifying and quantifying components in

protein mixtures, the electrospray-induced oxidation of methionine-containing peptides and proteins can complicate interpretation by introducing oxidized artifacts [386, 399-400]. In this chapter, we identify the cause and the means to control oxidation of the methionine-containing Aβ(1-40) peptide, as well as the dependence of oxidation on instrumental configurations.

5.1 Aβ Peptide Oxidation: Source and Cause

5.1.1 Identification of Aβ Peptide Oxidation

Figure 5.1b shows a portion of a mass spectrum of Aβ(1-40) obtained with the Q-Star using an emitter (emitter A) that had been in service for around 200 hours of spray time. An unusual aspect of this spectrum is that, in addition to the typical $[M+5H]^{5+}$ ion (base peak), another species with a similar isotopic pattern and with maximum intensity ~ 77% ± 3% (compared to the $[M+5H]^{5+}$ ion) is seen at a mass 16 Da higher than expected. This "heavy" peak was also observed for other charge states (+4: 78% ± 6%; +6: 82% ± 4%) (Figure 5.1a). In the light of the fact that Aβ(1-40) peptides contain a methionine residue at position 35, it may be suspected that the "heavy" ions are due to oxidative degradation prior to and/or during analysis by ESI-MS. This hypothesis was verified by MS analysis of the peptic fragments of Aβ(1-40). Among the 7 fragments (1-19, 4-19, 20-33, 20-34, 34-40, 35-40 and 20-40), only the isotopic peaks of fragments 34-40, 35-40 and 20-40 had peaks shifted by 16 Da, consistent with oxidation of the methionine residue at position 35. MS/MS analysis of the 16Da-higher cluster from the peptide (35-40) produced a series of b_n ions shifted by 16 Da (Figure 5.2), thus confirming that the methionine residue was indeed modified.

Although the peak of the $[M+16+5H]^{5+}$ ion was ~ 77% of the peak of the $[M+5H]^{5+}$ ion using the triaxial probe on the Q-Star, analysis of the same sample by HPLC indicated only 4% of the oxidized species present. One possible explanation is that MS is much more sensitive to $[M+16+5H]^{5+}$ ions than to $[M+5H]^{5+}$ ions. However,

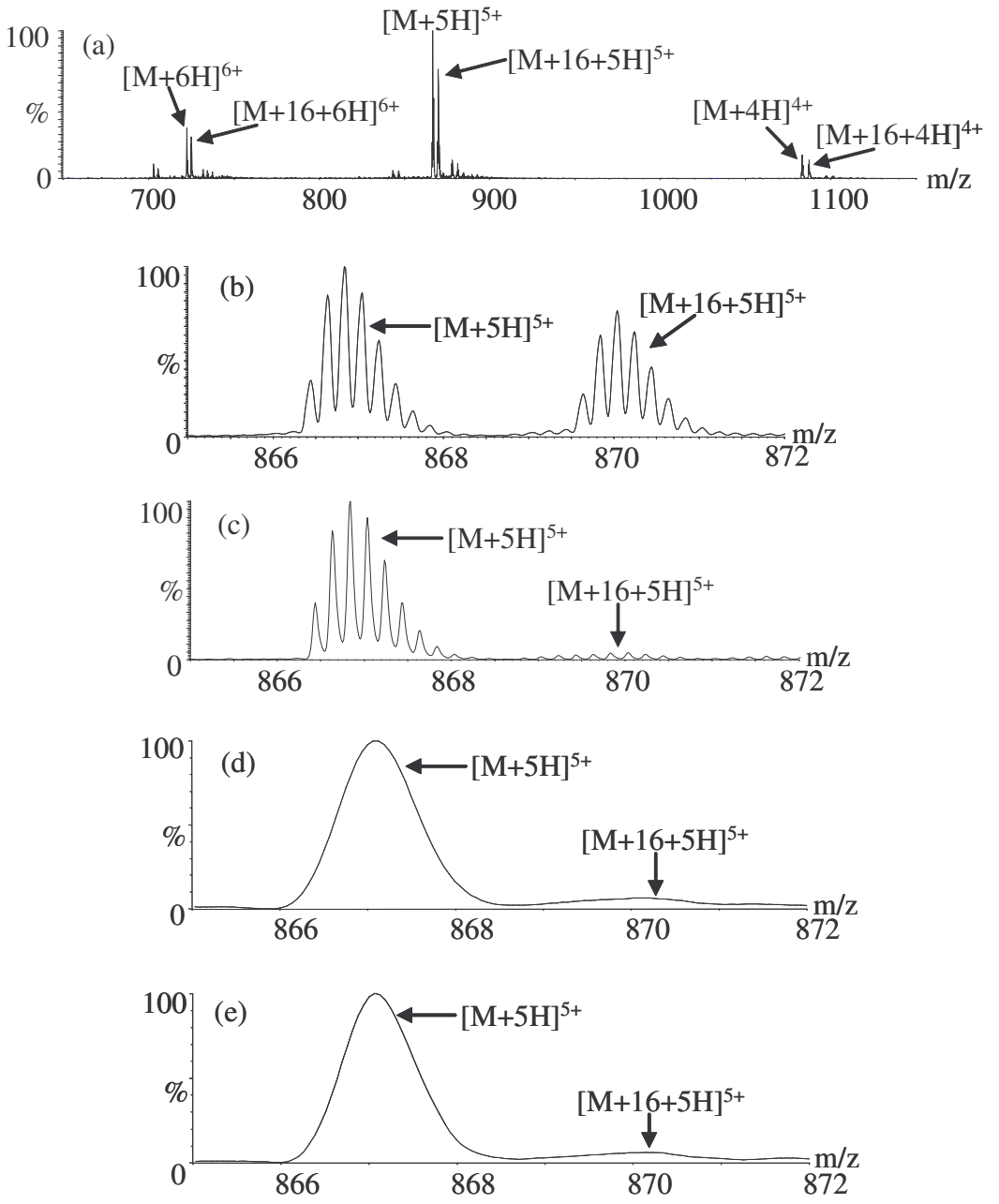

Figure 5.1. ESI mass spectra of Aβ(1-40) peptide obtained using different instrumental configurations (at 4.5kV): (a) Q-Star + triaxial probe (showing +4, +5, +6 charge states); (b) Q-Star + triaxial probe (showing +5 charge state); (c) Q-Star + coaxial probe (showing +5 charge state); (d) Quattro II + coaxial probe (showing +5 charge state); (e) Quattro II + triaxial probe (showing +5 charge state). M is the molecular mass of the Aβ peptide.

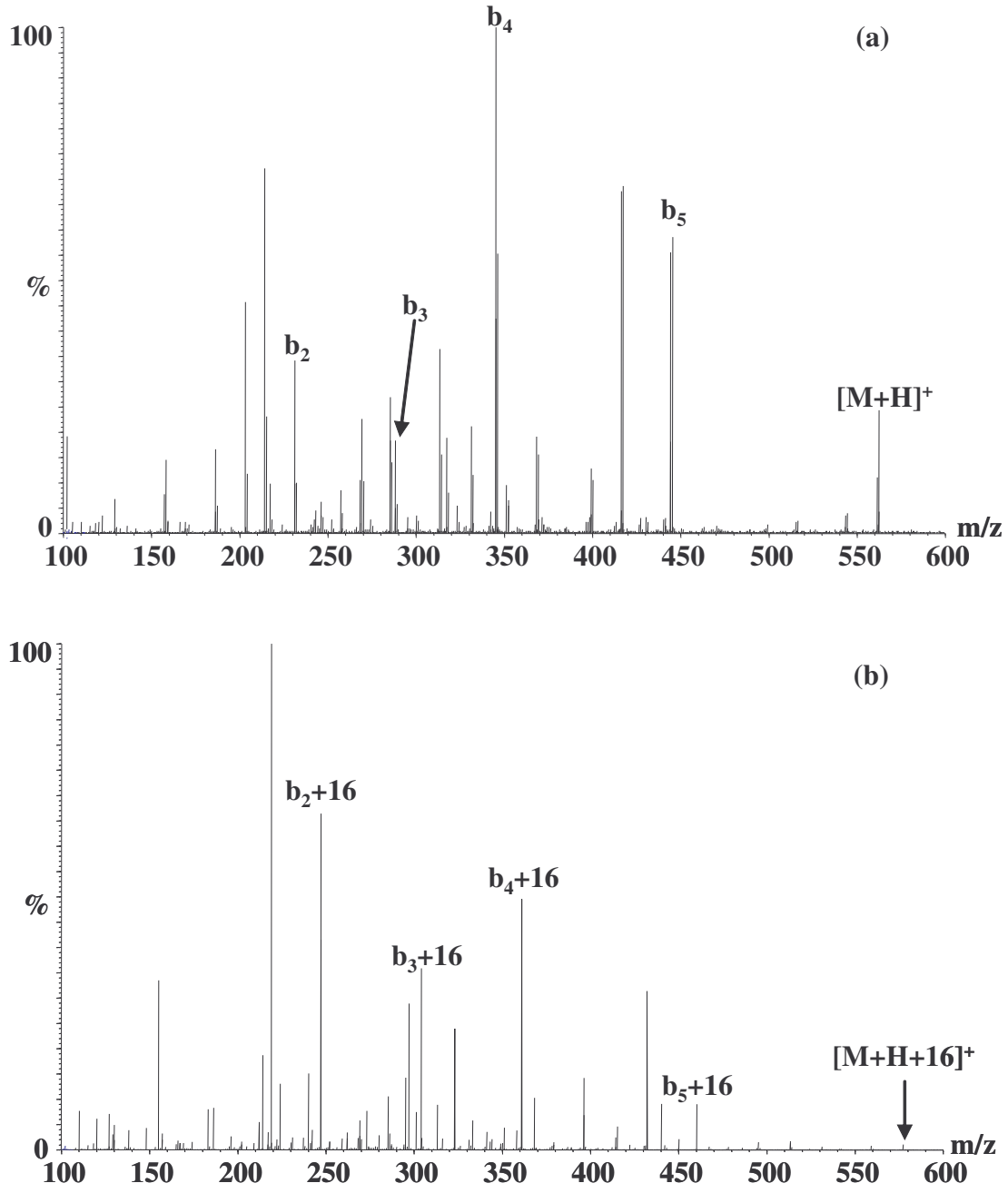

Figure 5.2. MS/MS spectra of (a) the unoxidized species ($[M+H]^+$ ions) and (b) the oxidized species ($[M+H+16]^+$ ions) derived from the peptic fragment (35-40) (M = the molecular weight of the 35-40 peptide). Signal corresponding to *b*-type ion series have been annotated to show the difference between the two spectra.

running the same sample under the same mass spectrometric conditions using the coaxial probe on the Q-Star instrument, resulted in the $[M+16+5H]^{5+}$ species being significantly eliminated from the spectrum (i.e., its intensity dropped to ~ 4% of the base peak) (Figure 5.1c). Comparable large extra peaks were not only about ~ 6% relative abundance (Figure 5.1d) using the coaxial probe on Quattro II, but were not observed with that probe in previous studies [58-59]. Furthermore, experiments with the same sample and same voltage using the triaxial probe on Quattro II produced the $[M+16+5H]^{5+}$ peak only ~ 6% of $[M+5H]^{5+}$ peak (Figure 5.1e). All this suggests that MS response difference between $[M+5H]^{5+}$ ions and $[M+16+5H]^{5+}$ ions, if there is any, is not likely the cause of the occurrence of the strong peak of the $[M+16+5H]^{5+}$ ion. Alternatively, chemical modification of the peptide in the ES ion source using the triaxial probe on the Q-Star resulted in excessive $[M+16+5H]^{5+}$ ions.

5.1.2 Cause of Oxidation

An ES current readout on a mass spectrometer provides a means of detecting a successful electrospray and the onset of an unwanted corona discharge. In our studies, installation of a current meter between the power supply and the ion source enables the monitoring of the ES current. Under the conditions of Figure 5.1a or Figure 5.1b, the measured ES current drifted between ~ 6 μA and ~ 12.6 μA over a period of 3 min. This is much higher than typical for ESI and the drift is inconsistent with operation as a constant-current device [178]. Furthermore, as the emitter voltage was varied, both the current and the oxidation extent varied in direct proportion (Figure 5.3), again suggesting that the operation apparently did not take place in the constant current section of the ES gap's current. All this could indicate the presence of corona discharge, which is characterized by high and unstable currents (> 1 μA) [139-140].

Corona discharge depends on the applied voltage, the size, shape and spacing of the two electrodes, and the dielectric of the medium in the gap. When a high voltage is applied to the sharp tip of the electrode, a corona discharge will occur if the voltage gradient exceeds the dielectric breakdown threshold of the medium in the gap. During the onset of discharge, electrons are accelerated towards the electrode tip (in

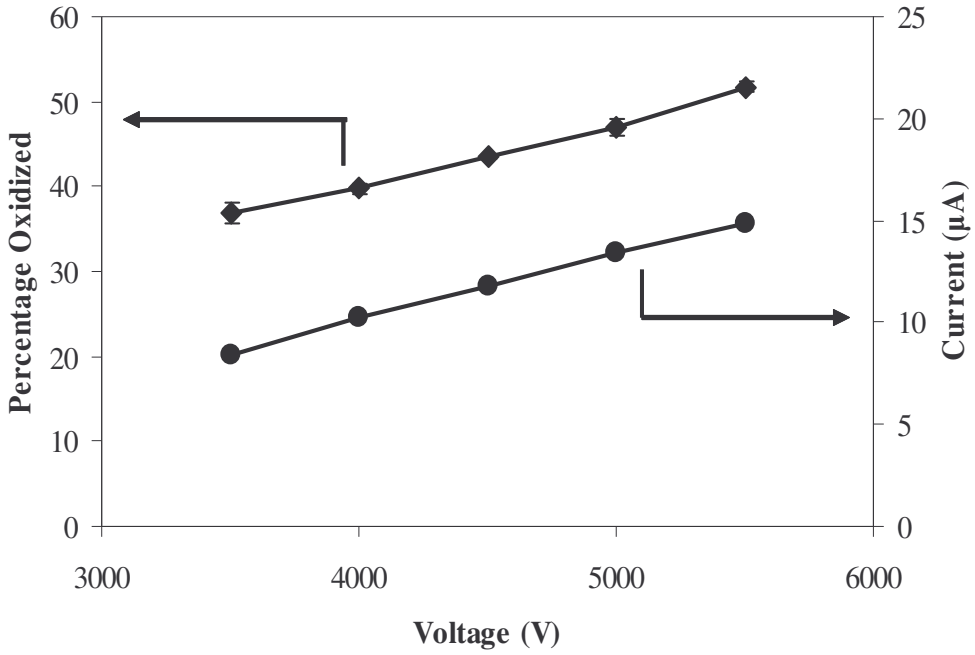

Figure 5.3. The plot of electrospray current vs emitter voltage (●) and the oxidation extent vs emitter voltage (♦). The value of the electrospray current is the maximum value observed at each voltage. The oxidation extent is expressed as the ratio of the intensity of the oxidized product to the sum of the intensity of the oxidized and unoxidized species, based on the +5 charge state peak (base peak). Error bars represent the standard deviation of ratios from triplicate mass spectra.

the positive mode), exciting molecules present in the medium around the tip [139-140]. As a consequence, a reactive plasma is produced. The flux of electrons and positive ions in the plasma is responsible for the high current. Since oxygen molecules have positive electron affinity and readily capture free electrons, the reactive plasma could contain radical oxygen species, which can attack at the methionine residue to result in the oxidized species [284]

5.1.3 Origin of the Oxygen Atom

Since samples were degassed using dry N_2 and extra N_2 flow was supplied to the ion source during and for 4 hours before sample injection, the oxygen atom inserted into the Aβ peptide was not likely to be from oxygen dissolved in the sample solution and/or present in the ion source chamber. Alternatively, the reactive oxygen species could be from the oxygen molecules generated by oxidation of water and it was further ionized in the process of discharge. A consequence of the high applied voltage and corresponding high spray current using the triaxial probe on the Q-Star mass spectrometer, is that the electrolysis of water occurs readily at the metal/solution interface. For the positive ion ES process, the electrolytic oxidation reaction of water in Eqn 1.7 is a relatively facile process, thereby generating oxygen molecules which can be turned into reactive oxygen species by corona discharge at the sprayer tip. When the current is high, the reactions shown in Eqn. 1.8 and 1.9 may also take place, creating reactive molecular species like H_2O_2 and O (g) [399]. This can lead to the chemical oxidation of analytes.

Previous studies using ^{18}O water and/or using nonaqueous MeCN as the solvent to investigate ES-induced oxidation of peptides have established that electrolysis of water can participate in the oxidation of peptides [386, 399-400]. In order to find out if the electrolysis of water led to the oxidation of Aβ samples, experiments using ^{18}O water were carried out. ($H_2{}^{18}O$ was a generous gift from Dr. Albert A. Tuinman at the University of Tennessee.) Specifically, 4 μM Aβ monomer in 56/44/0.5 (v/v/v) $H_2O/H_2{}^{18}O$/HCOOH was run at 5 μl/min in tube 1 on the triaxial probe, while 100/0.5 (v/v) MeCN/HCOOH was run at 5 μl/min in tube 2, leading to a final solution containing

44.1% ^{18}O (excluding the ^{16}O from HCOOH). In the control, $H_2{}^{18}O$ was substituted by $H_2{}^{16}O$. Representative spectra acquired in these two experiments were shown in Figure 5.4. If the oxidation of Aβ monomer results from oxygen produced during water oxidation, then the oxidized peak should be 44.1% ^{18}O. The experimental result (averaged over +4, +5, +6 charge states) shows 42.6% ± 2.1% ^{18}O or ~ 96.6 % ± 4.8% of the expected value. Although this is within experimental error, the fact that the value is low is consistent with the HPLC evidence for ~ 4% contaminant present in the original sample.

Besides reducing sensitivity to analyte (by distributing ion intensity among different ion signals), solvent oxidation can result in a dramatic change in the solution pH since the oxidation of water induces the generation of protons (shown in Eqn. 1.7-1.9). This pH change has been well described by Van Berkel *et al.* and Cook *et al.* [197, 366-368]. The efffect is highly dependent on flow rate and the electrospray current and as well as on buffering. These electrochemically induced pH changes can cause protein unfolding if time allows [366]. For HDX studies of proteins, the decrease in pH may result in more artifactual exchange [230] if the final pH deviates from the optimum value [260]. Also, possible overlay of the partially deuterated peak with the oxidized peak will lead to imprecise determination of the number of incorporated deuterium labels. Besides possible oxidation of analytes, the produced oxygen can form bubbles and cause an unstable electrospray [401]. Minimization of the effect is desirable for all of these reasons.

5.2 Effects of Instrumental Configurations on the Extent of Oxidation

As discussed above, discharge is the cause of oxidation and water oxidation is responsible for supplying the oxygen atom. Either discharge or water oxidation occurs only with certain instrumental configurations and under certain operating conditions. Two design parameters that affect the oxidation extent are the electrical field and current density. The equation (Eqn. 1.2) for calculating the electric field strength is

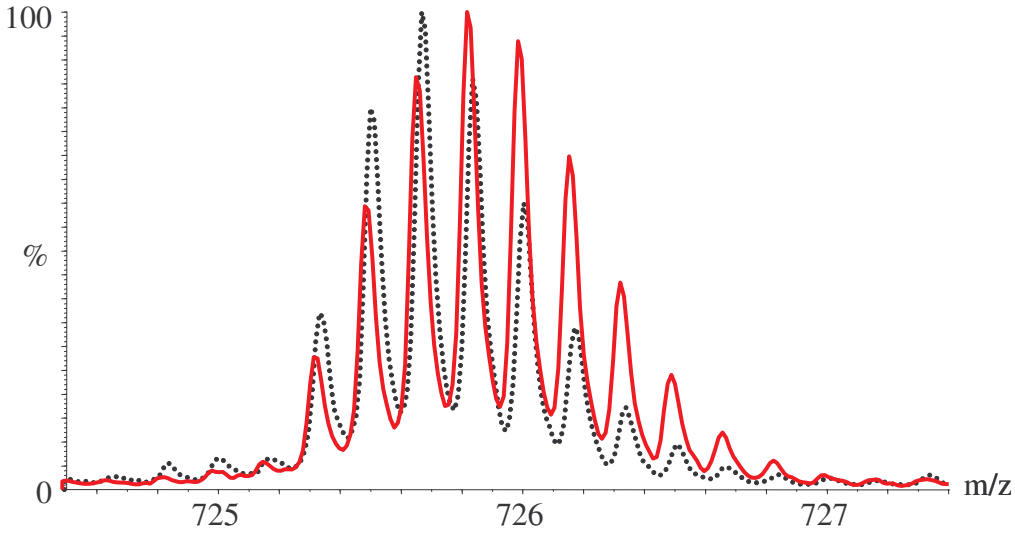

Figure 5.4. The peak clusters of the +6 charge state of Aβ obtained from running Aβ in 56/44/0.5 (v/v/v) $H_2O/H_2{}^{16}O$/HCOOH (black dotted line) and in 56/44/0.5 (v/v/v) $H_2O/H_2{}^{18}O$/HCOOH (red solid line).

described in section 1.2.1. The current density is a function of the electrode area for a fixed current. Effective electrode area is defined as the internal surface area of the ES emitter capillary, from the spray-tip upstream into the capillary, over which redox reactions actually occur [402]. This area will be the same or less than the physical area of ES emitter capillary. The effective electrode area might be less than the physical area because of limited electric field penetration into the liquid at the spray tip and because of other limits to ionic transport in the solvent [402]. In an ES ion source providing a given current, i_{ES}, in which the emitter is a conductive tubular capillary of radius r, an average current density j, for an effective electrode length l, can be calculated using Eqn. 6.1 [402]:

$$j = \frac{i_{ES}}{2\pi r l} \qquad \text{Eqn. 6.1}$$

Note that the current is considered to be distributed evenly along the length of electrode for the following discussion.

5.2.1 Oxidation extent on the Q-Star: triaxial probe vs. coaxial probe

Several factors can contribute to high oxidation extent on the Q-Star triaxial probe. First, because of the low conductivity of MeCN (as indicated by negligible current when running pure acetonitrile in Tube 2 in Figure 2.1), good electrical contact is made ~ 5 mm (where the solvents mix) before the triaxial tip end. For the coaxial probe, electrical contact is made in a smaller area only when the spraying liquid from the inner silica Tube 1 wets the outer metal Tube 2. Also, for the coaxial probe, the presence of silica Tube 1 at the tip affects the electric field gradient (silica is less conductive than air). As a result of these differences, the total emitter current was only ~ 2.2 μA (stable) on the coaxial probe, compared to a maximum of ~ 12.6 μA on the triaxial probe. Worth noting is that the current density at the metal/solution contact is different for the two probes. For the coaxial probe, it is reasonable to assume that electrical contact is limited to the annular area at the tip of Tube 2, which has an area of ~ 3.6×10^{-8} m^2 (see information about diameters in Figure 2.1), so that the current density was ~ 60 A/m^2. In the case of the triaxial probe, the electrical contact area likely includes the 5 mm inner surface of

Tube 2 as well as the annular area of the tip surface, which totals ~ 3.5×10^{-6} m^2, so the current density was ~ 3.6 A/m^2. Therefore, the current density on the coaxial probe is ~ 17 times that on the triaxial probe, while the oxidation is contradictorily lower on the coaxial probe. Although it is not easy to define the effective electrical contact area for the coaxial probe, this difference is large compared with the uncertainty; another factor must affect the oxidation extent. One possibility is the composition of the spraying solution. As detailed in Chapter 3, the mixing between the acetonitrile stream in Tube 2 and the Aβ sample solution in Tube 1 on the triaxial probe on the Q-Star instrument is imperfect. This suggests the resultant solution adjacent to the electrode had a higher content of water than that using the coaxial probe. Therefore, the spraying solution on the triaxial probe had higher conductivity and surface tension, which suggests higher susceptibility to discharge because high electrical field is necessary for droplet formation at the ES sprayer tip. Moreover, if the electrochemical reaction occurs only in the aqueous portion, the concentration of Aβ sample in the aqueous droplets would be higher with the triaxial probe due to imperfect mixing, resulting in more effective /more rapid methionine oxidation.

To test whether the imperfect mixing on the triaxial probe contributes to the different oxidation extent between the coaxial probe and the triaxial probe, we ran Aβ sample in premixed solution (with the same final composition as that used on the coaxial probe: 50.5/49.5/0.46 water/MeCN/formic acid) in both Tube 1 and Tube 2 (emitter A in service for 200 h) in Figure 2.1 or only in Tube 2. The results show that the current was ~ 2.2 μA and the oxidation extent was similar to that using the coaxial probe (~ 4%). This clearly indicates that the imperfect mixing contributed to the high oxidation extent on the triaxial probe. Worth noting is that the droplet size is bigger on the triaxial probe (bigger outer diameter for the emitter) than on the coaxial probe. However, it is not clear that this will affect oxidation.

5.2.2 Oxidation extent on the triaxial probe: Q-Star vs. Quattro II

The following factors contribute to the difference in promoting analyte oxidation on the Q-Star and the Quattro II. First, the electrical field strength is different. At

a voltage of 4.5kV, the electric filed strength at the sprayer tip of the triaxial probe sprayer on the Q-Star (gap distance: ~ 1.2 cm; outer diameter of the emitter: ~ 420 μm) is 7.9×10^6 $V.m^{-1}$, which is ~ 1.8 times that on Quattro II (4.4×10^6 $V.m^{-1}$; corresponding to a gap distance of ~ 2.5 cm and an outer diameter of the emitter of ~ 720 μm). Therefore, the triaxial probe on the Q-Star is more prone to discharge. Second, the compositions of the spraying solutions on the two triaxial probes on the two instruments may be different. As can be seen in Table 5.1, the velocity of the analyte is 15.4 times that of MeCN on Quattro II, while on the Q-Star the difference is only a factor of two. Although not investigated in this study, the much bigger difference in the velocity between the analyte and MeCN may cause worse mixing on the Quattro II than on the Q-Star. According to the earlier discussion, imperfect mixing favors oxidation. This suggests oxidation could be more serious for the triaxial probe on the Quattro II, which is contradictory to the observation. Another contributing factor could be current density. For the triaxial probe on the Quattro II instrument, the metal/solution area (effective electrode area) was 6.4×10^{-6} m^2 (refer to Figure 2.2 for diameters) and the current was ~ 3.7 μA, thus leading to a current density of 0.6 A/m^2, significantly lower than that for the Q-Star (~ 3.6 A/m^2, see section 5.2.1). From the above discussion, it is clear that a combination of the discussed factors (and yet-to–be discovered factors) that had caused the oxidation difference on the triaxial probe on the two instruments.

Worth noting is that for the standard coaxial probe on the Quattro II instrument, unlike the coaxial probe on the Q-Star, the sample transfer line is a ~ 23 cm long stainless steel tube (Tube 1 in Figure 2.3). Due to the fact that the current (~ 2.2 μA) was diluted over the whole surface of the electrode (i.e. low current density, 0.03 A/m^2), only ~ 6% relative abundance for the oxidized Aβ was observed (Figure 5.1d).

5.3 Progression of Oxidation

The oxidation problem on the triaxial probe of the Q-Star instrument became more pronounced as emitter A aged. By 300 hours of use, the measured maximum

Table 5.1. The flow velocities of the MeCN stream and the sample mixture stream calculated for the triaxial probes on the Quattro II and the Q-Star instruments. Tube 1 and Tube 2 are indicated in Figure 2.1 and Figure 2.2.

Triaxial probe	**Quattro II**	**Q-Star**
ID (Tube 1)	50 μm	75 μm
OD (Tube 1)	360 μm	190 μm
ID (Tube 2)	410 μm	220 μm
Annulus area (for MeCN stream)	1.2×10^5 μm^2	3.9×10^4 μm^2
Tube 1 inner cross-section area (for sample mixture stream)	7.9×10^3 μm^2	1.8×10^4 μm^2
Flow rate of MeCN (= flow rate of sample)	5.1 μl/min	5.1 μl/min
Flow velocity of MeCN (flow rate/annulus area)	0.7 mm/s	2.2 mm/s
Flow velocity of sample (flow rate/Tube 1 inner cross-section area)	10.8 mm/s	4.8 mm/s
Velocity ratio (sample/ MeCN)	15.4	2.2

current increased to 13.5 μA (vs. ~12.6 μA at 200 h) at a voltage of 4.5 kV, and the oxidized peak became the base peak (relative abundance of the unoxidized peak was ~ 90% ± 3%) (Figure 5.5a). Installing a new emitter (emitter B; Figure 5.6a) reduced the oxidized peak to ~ 5.2% ± 0.1% relative abundance with an emission current of ~ 0.2 μA (stable). After ~ 50 h use, the current increased to a maximum value of ~ 5 μA (drifting between ~ 1 and ~ 5 μA) and the oxidized peak grew to ~ 11% ± 1% of the unoxidized peak. After ~ 100 h, the current increased to a maximum value of ~ 11 μA (drifting between ~ 5 and ~ 11 μA) and the oxidized peak was ~ 51% ± 4% relative abundance (Figure 5.6b). After ~ 150 h, the current increased to a maximum value of ~ 20 μA (drifting between ~ 7 and ~ 20 μA) and the $[M+5H+16]^{5+}$ ion became the base peak, while the $[M+5H]^{5+}$ ion was only 39% ± 3% of the base peak.

5.4 Control of Oxidation

Use of redox buffers

One way to reduce analyte oxidation could be to use a redox buffer to hold the potential at the metal/solution interface below that necessary to oxidize water and thereby eliminate oxidation [403]. Tris(2 - carboxyethyl) phosphine (TCEP) was chosen as the reducing agent in the studies here. The Eº of TCEP is not available, but it is known that this is a stronger reducing agent than dithiothreitol, whose redox potential is -0.110V (vs. SHE at pH 7)) [31, 48]. Using emitter A after ~ 200h use, addition of 100 μM TCEP to the 0.5% formic acid processing solvent effectively reduced the $[M + 5H+16]^{5+}$ ion from 77% ± 3% to only ~ (6.2% ± 0.3%) of the $[M + 5H]^{5+}$ base peak, suggesting that TCEP served as an effective scavenger for the oxidizing species. Since the oxidation extent increased with increased usage time of the emitter, a corresponding increase in TCEP concentration was required to suppress oxidation effectively. For emitter A after ~ 300h use, ~ 150 μM TCEP was required to decrease the oxidized peak to around ~ 6% of the unoxidized peak. It is conceivable that such a high concentration of TCEP can

(a) Before polishing

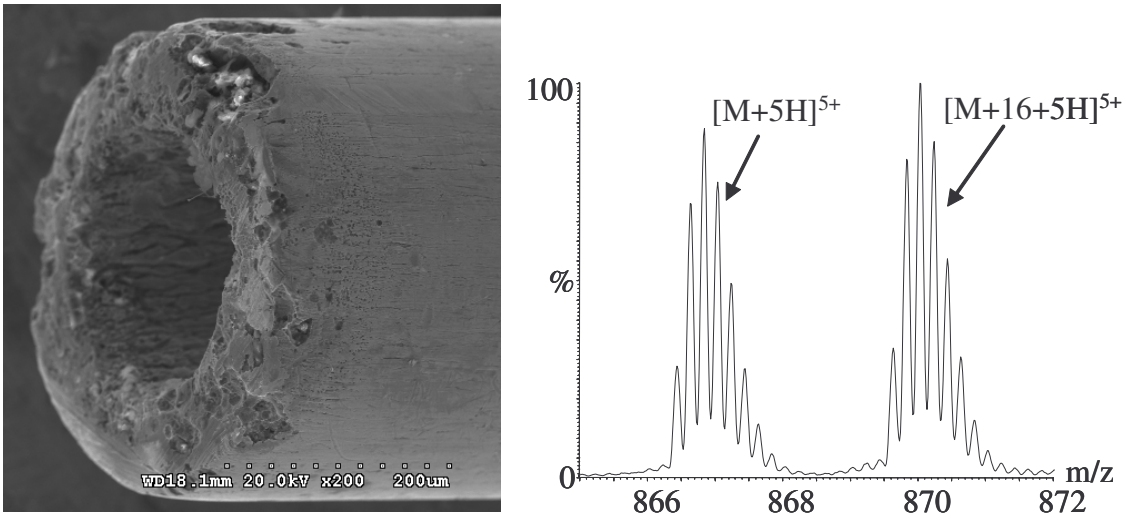

(b) after polishing

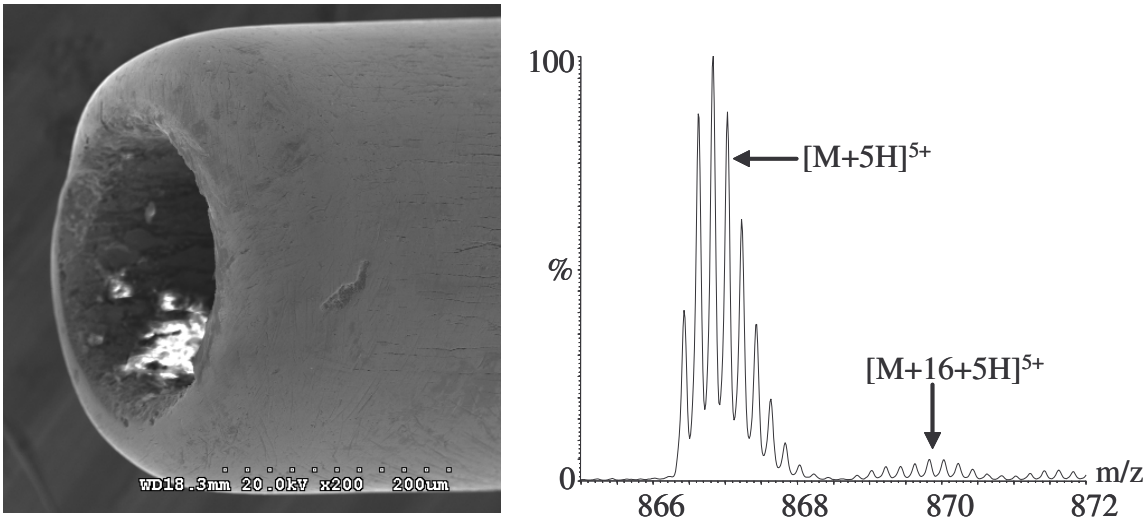

Figure 5.5. Electron micrographs and mass spectra acquired using emitter A (after ~ 300 h use) in the triaxial mode on the Q-Star instrument (at 4.5 kV): (a) before polishing; (b) after polishing.

(a) < 1 h in service

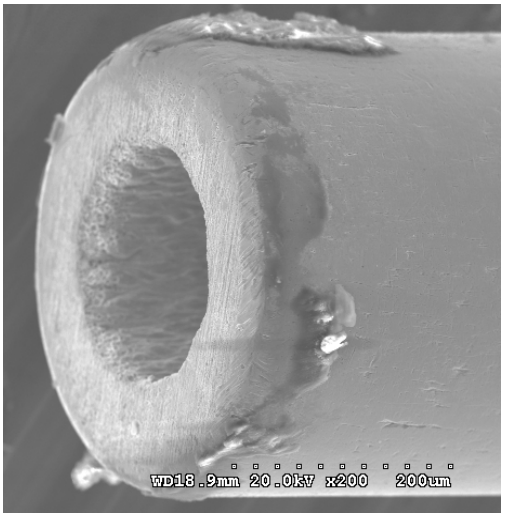

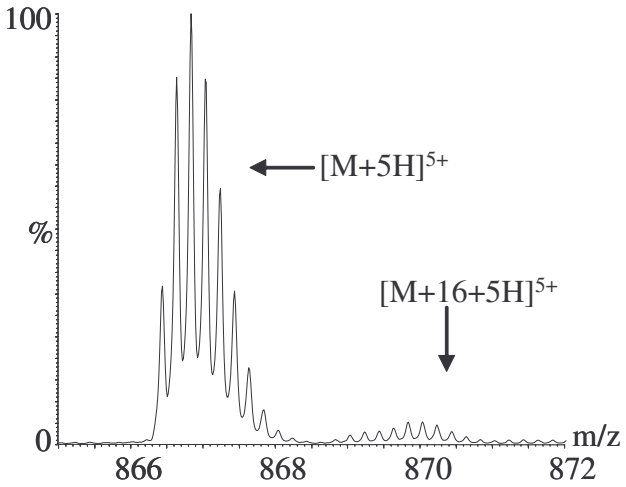

(b) 100 h in service

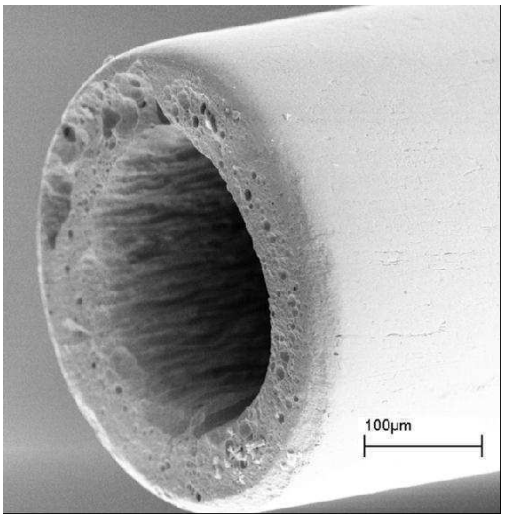

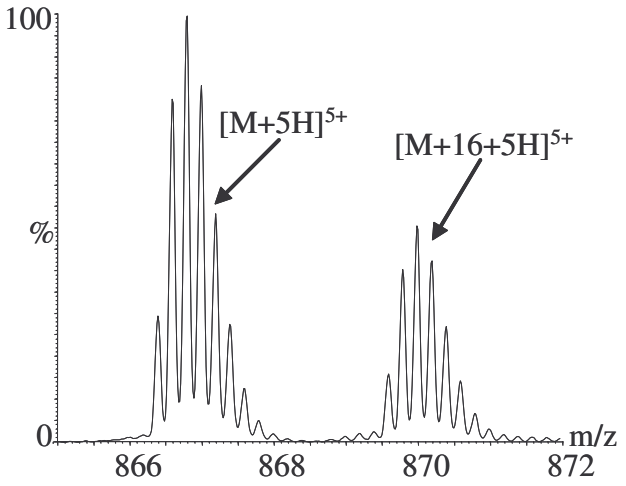

Figure 5.6. Electron micrographs and mass spectra acquired using emitter B in the triaxial mode on the Q-Star instrument (at 4.5kV): (a) < 1 h in service; (b) 100 h in service.

contaminate the ion source. Also, results show that the presence of 100 μM TCEP reduced the sensitivity to Aβ by ~ 13%. Furthermore, the redox buffer may react with Aβ to alter its structure and may affect the activity of pepsin during proteolysis. Thus, the best way to counteract discharge is to eliminate it, not to find substitutes for water and/or analyte oxidation.

Control of currents

The occurrence of discharge lowers the resistance of the gap between the emitter and the counter electrode [141]. Thus, adding a high resistance (typically 10 GΩ, comparable to the gap resistance) in series with the emitter can inhibit the occurrence of discharge [187]. Placing a 0.5 GΩ resistor in series with the power supply decreased the ES current from a maximum value of ~ 12.6 μA (for emitter A after 200 h in use) to 0.8 μA (stable). However, no MS signal could be detected under these conditions, so adding a larger resistor was not attempted. Further studies are needed to explain the observation.

Reduction of electric field

Electrical discharge is prevented to a large extent by reduction of the electric field, which is related to the curvature of the tip of the electrode. The higher the curvature, the higher the potential gradient around the tip, the more serious the discharge. Apparently, the rather rough tip surface (such as that shown in Figure 5.5a) favors the occurrence of discharge. On the other hand, smoothing the rough tip surface reduces the electric field gradient and reduces discharge. Oxidation was essentially eliminated after polishing the tip of emitter A, as shown in Figure 5.5b; the current dropped to ~ 0.2 μA and the oxidized peak intensity fell to ~ 5.2 % ± 0.1% of the $[M+5H]^{5+}$ base peak. Similarly, polishing the emitter B (Figure 5.6b) after ~ 150 h use also reduced the oxidized peak to ~ 5.0% ± 0.2% of the unoxidized peak from ~ 256% ± 3%, and reduced the current to ~ 0.2 μA.

In the course of these studies, it was also noted that the lifetime of emitters depended somewhat on the shape of the emitter tip. After polishing emitter A, the

oxidation remained under control (~ 5.4 ± 0.3% relative abundance for the oxidized species) after an additional ~ 165 h of use (Figure 5.7a), and the emitter current had increased only to ~ 0.4 μA (from 0.2 μA). Similarly, emitter C showed only ~ 5.0% ± 0.2% relative abundance for the oxidized species after < 1 h in service (current ~ 0.2 μA) (Figure 5.7b), increasing to only ~ 8% ± 1% after ~ 140 h of usage (current ~ 2.6 μA). However, the relatively square-cut emitter B started to show ~ 11% ± 1% relative abundance for the oxidized species after being used for only ~ 50 h, increasing to ~ 51 % ± 4% after ~ 100 h of usage (Figure 5.6b) and to ~ 256% ± 3% after ~ 150 h of usage. Rounded emitters appear to have a higher resistance to corrosion, perhaps because the curvature reduces the electrical field, and therefore the discharge.

The pits on the corroded surfaces evident in the micrographs may suggest that segregation or depletion of metal elements takes place as corrosion proceeds. However, X-ray fluorescence maps of emitter B showed that the distribution of major elements (such as Fe, Ni, Cr, Mo) was uniform (Figure 5.8). Therefore, pits may just result from the random attack of the tip surface by the reactive plasma.

5.5 Conclusions

The electrochemical properties of electrospray mass spectrometry must be considered when using the technique. In this study, oxidation of a methionine residue was promoted by an electrical discharge resulting from an eroded emitter. One straightforward consequence is loss of sensitivity due to dilution of the signal over more than one species. In HDX studies, further complications can result from the mass increase unrelated to deuterium.

All the tested stainless steel tubes were vulnerable to discharge which resulted in corrosion. Since the magnitude of oxidation increases as the emitter ages, the addition of a reducing agent is not an ideal way to control oxidation. Polishing the tube helps prevent discharge and reduces its effects. Monitoring current provides a convenient way

(a) polished emitter A (in service for ~ 165 h after polishing)

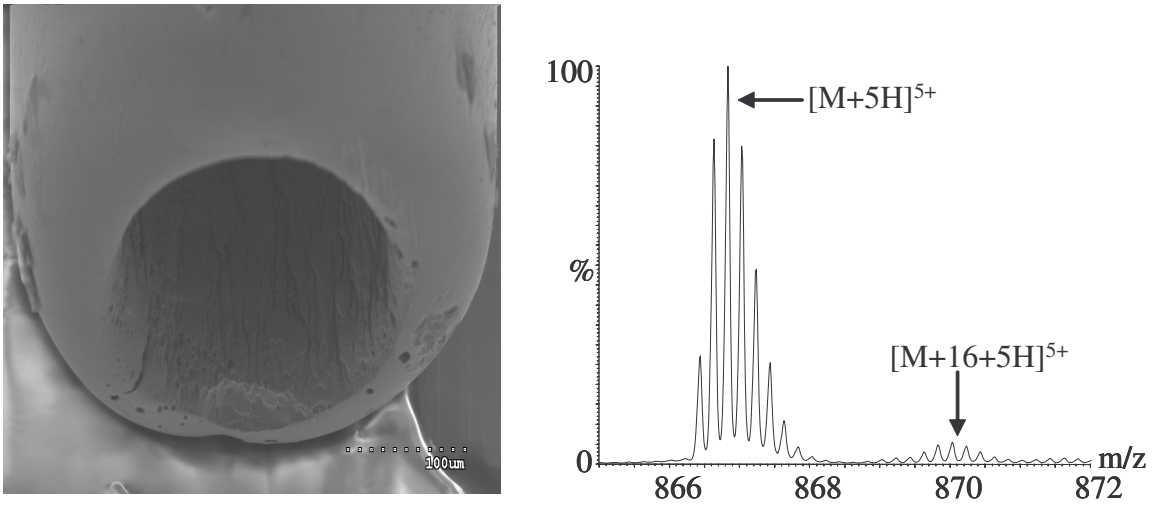

(b) emitter C (in service for < 1 h)

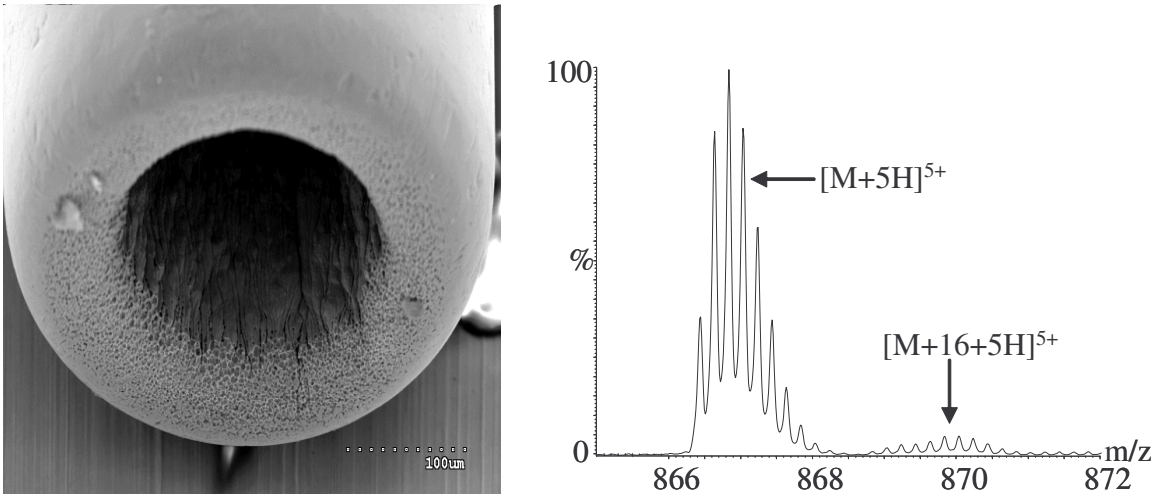

Figure 5.7. Electron micrographs and mass spectra acquired using the emitters in the triaxial mode on the Q-Star instrument (at 4.5 kV): (a) polished emitter A (in service for ~ 165 h after polishing); (b) emitter C (in service for < 1 h).

(1)

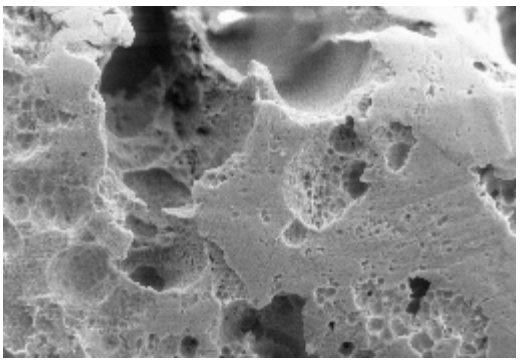

(2)

(a) Fe

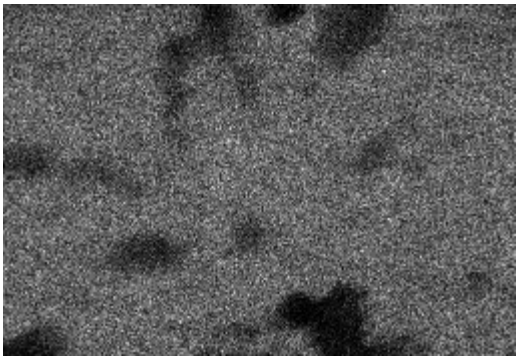

(b) Cr

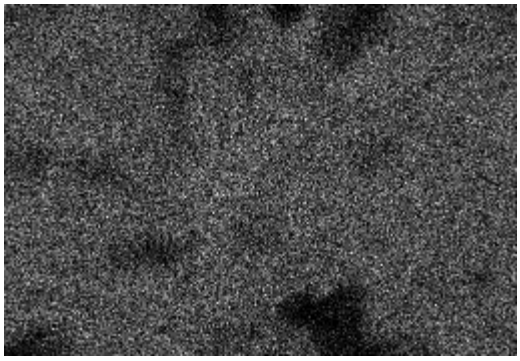

(c)Ni

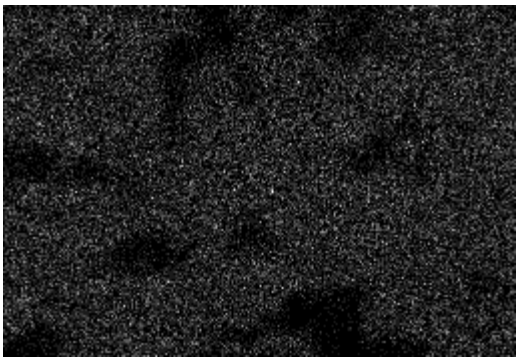

(d) Mo

Figure 5.8. (1) Electron micrograph of a certain area of the tip of emitter B (after ~ 100 h use); (2) X-ray maps of elements (a) Fe, (b) Cr, (c) Ni and (d) Mo in the area shown in (1).

to diagnose the presence of discharge (current typically > 1 μA) and the need for tube polishing or replacement.

CHAPTER 6

CONCLUSIONS AND SUGGESTIONS FOR FUTURE WORK

Triaxial Probe

The novel triaxial probe front end to the MS described in this dissertation has demonstrated ability to facilitate on-line digestion of Aβ amyloid fibrils coupled with HDX-MS, thus enabling examination of the regional distribution of deuteriums exchanged into Aβ fibrils. This works by first exposing fibrils to a dissolving solvent consisting of aqueous acid plus pepsin, after which the digest gets mixed with acetonitrile before going into the MS. The delayed introduction of co-solvent (acetonitrile) helps reduce any possible adverse effects induced by the addition of the organic solvent. The triaxial probe may prove very important in other aspects of HDX experiments on fibrils, including looking at other amyloids that don't dissolve well in the coaxial quenching/dissolution/analysis buffer. Another possible application is to use the triaxial probe to obtain structural information on fibrils by the comparative proteolysis of the Aβ(1-40) monomer and Aβ(1-40) fibrils without resorting to HDX. Proteolytic enzymes act on a particular sequence element within a fibril-incorporated peptide based on the accessibility of the cleavage sites. Within the same time frame, sites cleaved in the monomer but not in fibrils can be assumed to be involved in hydrogen bonding (β-sheet), or positioned within or near the fibril core. Experimentally, different digestion times can be controlled by varying the length (volume) of Tube 1 (see Figure 2.1 or Figure 2.2) in the triaxial probe or the flow rates of the sample and/or enzyme solution, and the digestion products can be monitored by MS. By comparing the intensity-time profiles of the digestion products from monomer and fibrils samples, information regarding which residues in fibrils are inaccessible to the enzyme may be obtained. The intensity-time profiles of the intact monomer sample and its digestion products can also be used to

derive enzymatic kinetics of pepsin or pepsin-like enzymes [404].

HDX at single-residue resolution

The goal of this research was to establish the positions of each amino acid residue of the primary sequence within the three-dimensional structure of the protofilament and fibril. HDX-MS coupled with on-line proteolysis has enabled localization of deuterium distribution to 4 peptides derived from Aβ(1-40) (discussed in Chapter 4). The next step lies in obtaining HDX data at single residue resolution. Direct MS-MS of intact peptides is questionable because of issues related to scrambling of amide hydrogen atoms in the gas phase [235, 304-309]. A more promising approach would involve the use of the triaxial probe, which can facilitate MS/MS studies by converting the released monomers into a reasonably simple mixture of more easily characterized hydrolysis products (using pepsin or pepsin-like enzymes). In addition to the improved sensitivity and more straightforward interpretation afforded by MS/MS of smaller peptides, there is some evidence in the literature suggesting that such an approach reduces the potential for deuterium scrambling upon MS/MS of the intact peptide [235, 247]. Proteolysis using pepsin-like enzymes either individually or in combination has potential to provide HDX data of Aβ fibrils at single-residue resolution without the use of MS/MS (discussed in section 4.2). Such single-residue information can be used to corroborate that obtained using the approach combining proteolysis and HDX-MS/MS. One drawback of any method involving proteolysis is that deuteration information at the cleavage sites will be lost.

HDX of conformational variants of Aβ(1-40)

Recent studies have indicated that there are at least two conformational variants of Aβ(1-40) amyloid fibrils, produced by growth in low salt either with ("agitated") or without ("quiescent") shaking or stirring [37]. There is little information on the nature of the structural differences between these reported conformations. One difference may be in the nature of the H-bonding network that defines the β-sheets within the amyloid fibril. It would be desirable to use HDX-MS and HDX-MS/MS to study these different

conformers grown under different conditions to find out what structural differences are. In another aspect, it would be interesting to study how temperature, pH, ionic strength and other solution conditions influence the H/D exchange profile of Aβ fibrils. As fibrils are exposed to extreme conditions, identifiable elements of structure may melt out; as fibrils are exposed to stabilizing conditions such as low temperature, additional structural features may become stabilized and provide additional protection against HDX. For example, it might be possible to observe melting out or consolidation of the terminal H-bonds in the amyloid β-sheets by studying temperature dependence.

HDX of Aβ fragments

It may also be important to analyze the structures of amyloid fibrils derived from smaller Aβ fragments such as Aβ(25-35) (the shortest sequence having been reported to form fibrils [35]), to test the hypothesis intrinsic to many previous fragment studies that the core element of the fibril of the Aβ(1-40) molecule is retained in the fibrils of the fragments [76, 79-80]. If the HDX results show that one, two, or three sequence elements of the Aβ(1-40) molecule exist as protected chain elements in β-sheet in the fibril, will these same exact sequences in an Aβ fragment - to the extent that they are presented in the fragment - be involved in fibril structure? The results obtained in these fibril studies will not only address the reasonableness of using fragments of a protein to model the amyloid fibrils of the full-length protein, but will also go to the heart of the question of the sequence requirements for amyloid formation.

HDX of other Aβ forms and aggregation intermediates

Our current HDX studies are mainly focused on chemically synthesized Aβ(1-40). The same methodologies can be applied to other forms of Aβ. Protofibrils and other aggregation intermediates can also be similarly determined using the HDX-MS and HDX-MS/MS methodology. Comparing the HDX-MS and HDX-MS/MS data to that for the Aβ(1-40) fibril, structural differences between these various forms or states can be elucidated. This knowledge would allow us to dissect fibril assembly and disease pathways. Great advance has been made in characterizing protofibrils (discussed in

section 4.1) and Aβ(1-42) fibrils (Dave Kaleta *et. al.*, unpublished results) using HDX-MS in our group. However, structural information of protofibrils and Aβ(1-42) fibrils at single-residue resolution using HDX-MS is yet to be obtained. HDX-MS and HDX-MS/MS methodology is also promising to give insights into the structural plasticity (i.e. the ability to accommodate destabilizing mutations through packing adjustments within the three-dimensional structure) observed in amyloid fibrils [63] by comparing the protection patterns of mutants (such as proline and alanine mutants) to those of wild-type fibrils up to single-residue resolution.

HDX of Aβ grown *in vivo*

The ultimate goal of this project is to carry out HDX experiments on enriched preparations of amyloid plaque cores from AD brains. Once the HDX-MS and HDX-MS/MS methodologies have been successful in identifying the Aβ chain folding characteristics within synthetic Aβ fibrils, it is feasible to apply the same methodology to determining the exchangeable and protected portions of the Aβ sequence within the AD plaque core fibril. Since neuritic plaques from AD brains are complex structures (containing fragments of dystrophic neuritis, amyloid fibrils, other proteins, and lipids), it is expected to see more challenges than those encountered with the HDX studies of synthetic fibrils and protofibrils (in simple matrixes). The MS spectra will be complicated by the presence of multiple molecular species of Aβ, but at the same time these should be recognizable and quantifiable since MS is well suited to analysis of mixtures with high sensitivity. Although fibrils isolated from plaque cores fulfill all of the (low resolution) structural criteria for amyloid fibrils and resemble fibrils generated from synthetic Aβ (addressed in section 1.1), it is reasonable to ask whether this structural similarity extends to the details of the molecular structure of the fibril. Does the presence of lipid, the heterogeneity of the Aβ molecules in the fibril, or the presence of other proteins, alter fundamental aspects of the *in vivo* fibril's structure? How good a model for biologically relevant amyloid, as isolated from human tissue, are the fibrils we can construct in vitro from synthetic peptides? Even if high resolution structural information of synthetic fibrils becomes available some time in the future, it is not clear

that it will be possible to adapt the same techniques onto biological amyloid, given its intrinsic heterogeneity. However, the methods outlined in this dissertation may in fact be capable of a comparative analysis of synthetic and naturally derived amyloid fibrils at the resolution offered by HDX.

Other interesting and important studies

Determination of Cr for Aβ(1-40) in 2mM tris buffer. It has been shown that the residual peptide monomer remaining when an Aβ(1-40) fibril assembly reaction reaches a plateau is a true critical concentration (C_r) value reflecting a point of dynamic equilibrium in fibril assembly [38-41]. It is known that monomer at concentrations below the critical concentration (*Cr*) in a given solvent will not grow into fibrils [41]. In our studies, PBS buffer (20.4 mM Na_2HPO_4, 3.6 mM KH_2PO_4, 274 mM NaCl, 5.4 mM KCl) was used to grow fibrils, while 2 mM deuterated or protonated tris was the buffer used to prepare fibrils for HDX studies (discussed in section 2.2). The *Cr* value for Aβ(1-40) in PBS buffer has been determined to be ~ 0.8 μM over a 24 h period [40-41]. It would also be desirable to know the *Cr* for fibrils in 2 mM Tris.HCl (pH 7.5). This knowledge would contribute to our better understanding of fibril solubility in 2 mM tris buffer (so that fibrils of adequate concentration would be used for HDX studies) and of the presence of the fully exchanged peak B (discussed in section 4.1.3). It is likely that the *Cr* value for fibrils in 2 mM Tris buffer would be higher than that in PBS buffer, and that the fibril formation would take a longer time because of the lower salt concentration in the buffer; higher salt concentrations tend to enhance hydrophobic interactions [405], which are known to play a significant role in the stability of the Aβ(1-40) fibril [63].

Study of the interaction between Thioflavin T and fibril. Thioflavin T (ThT) is a reagent known to become strongly fluorescent upon binding to amyloid fibrils. ThT assay has been a standard method to distinguish amyloid fibrils from non-fibrillar material. Studies have shown that there are at least three kinds of binding sites on Aβ(1-40) fibrils [41, 406-407]. However, none of the sites has been localized within the fibril structure [41, 406-407]. HDX-MS has been used as a powerful tool to study the interaction between

ligands and proteins [246]. Ligand binding is predicted to mask specific regions from deuterium exchange by steric hindrance at the binding site, and/or by changes in structure that limit solvent exposure. As a result, the sites which are engaged in the interaction will not exchange. It should be feasible to apply HDX-MS to characterize the interaction between ThT and Aβ fibrils, and find out which residues in Aβ are engaged in the binding and what effects ThT binding has on the structure of Aβ during the interaction. Using HDX-MS and HDX-MS/MS coupled with proteolysis, binding sites could be localized, on the condition that residue-specific HDX data is available for the particular fibrils. Once the binding patterns of the complexes formed between fibrils and ThT are available, insights could be obtained into the mechanism of ThT binding selectivity and into structural differences between fibrils and protofibirls (low response to ThT [40, 94]) could be obtained. Knowledge of the ThT-fibril binding mechanism, along with knowing the existence of multiple binding sites on fibrils, may be useful to the design of ligands selective to particular forms of fibrils that are connected with the pathogenesis of AD and potentially other protein misfolding diseases.

LIST OF REFERENCES

REFERENCES

1. Price, D. L. and Sisodia, S. S. *Annu. Rev. Neurosci.* **1998**, *21*, 479–505.
2. Nussbaum, R. L. and Ellis, C. E. *N. Engl. J. Med.* **2003**, *348*, 1356–1364.
3. Buck, K.; Amaducci, L.; Pepeu, G., Ed. *The Early Story of Alzheimer's Disease*. **1987**; Rana Press: New York; pp 1-3.
4. Grandy, S. and Greengnard, P. *Trends in Pharmacol. Science*, **1992**, *13*, 108-113.
5. Sipe, J. D. *Annu. Rev. Biochem.* **1992,** *61*: 947-975.
6. Selkoe, D. J. *JAMA*, **2000**, *283*, 1615-1617.
7. Selkoe, D. J. *Scientific American*, **1991**, *265*, 68-71.
8. Sipe, J. D., and Cohen, A. S. *J. Struct. Biol.* **2000**, *130*, 88-98.
9. O'Nuallain, B., and Wetzel, R. *Proc. Natl. Acad. Sci. U.S.A.* **2002**, *99*, 1485-1490.
10. Glenner, G. G. *N. Engl. J. Med.* **1980**, *302*, 1283-1292.
11. Yankner, B. A. *Neuron* **1996**, *16*: 921-932.
12. Selkoe, D. *Nature*, **1999**, *399*, A23-A31.
13. Daly, J., Girish, J. *The Immunologist*, **1997**, 157-165.
14. Seubert, P.; Oltersdorf, T.; Lee, M. G.; Barbour, R.; Blomquist, C.; Davis, D. L.; Bryant, K.; Fritz, L. C.; Galasko, D. *Nature* (London, United Kingdom) **1993**, *361*(6409), 260-263.
15. Selkoe, D. *J. Biol. Chem.*, **1996***, 271*, 18295-18298.
16. Robert, V.; Bennett, B. D.; Babu-Khan, S.; Kahn, S.; Mendiaz, E. A.; Denis, P.; Teplow, D. B.; Ross, S.; Amarante, P.; Loeloff, R.; Luo, Y.; Fisher, S.; Fuller, J.; Edenson, S.; Lile, J.; Jarosinski, M. A.; Biere, A. L.; Curran, E.; Burgess, T.; Louis, J.; Collins, F.; Treanor, J.; Rogers, G.; Citron, M. *Science* (Washington, D. C.) **1999**, *286*(5440), 735-741.
17. Hardy, J. and Selkoe, D.J. *Science* **2002**, *297*, 353–356.
18. Selkoe, D. *Science*, **1997**, *275*, 630-631.
19. Masters, C. L.; Simms, G.; Weinman, N. A.; Multhaup, G.; McDonald, B. L.;

Beyreuther, K. *Proc. Natl. Acad. Sci. U.S.A.* **1985**, *82*(12), 4245-4249.

20. Hsiao, K., Chapman, P., Nilsen, S., Eckman, C., Haigaya, Y., Younkin, S., Yang, F., Cole, G. *Science*, **1996**, *274*, 99-102.
21. Games, D.; Adams, D.; Alessandrin, R.; Barbour, R.; Berthelette, P.; Schenk, D.; Seubert, P.; Snyder, B.; Soriano, F.; Tan, H.; Vitale, J.; Wadsworth, S.; Wolozin, B.; Zha, J. *Nature*, **1995**, *373*, 523-527.
22. Stenh, C.; Lannfelt, L.; Nilsberth, C.; Inst, K.; Sweden, H. *Effects of Intra-A Beat Mutations on A Beta Secretion From Transiently Transfected Cells.* In World Alzheimer Congress 2000. **2000**. Washington, D. C., USA: Elsevier.
23. Martin, J. B. *N. Engl. J. Med.* **1999**, *340*, 1970-1980 [erratum: (1999) *N. Engl. J. Med. 341*, 1407].
24. Aleshkov, S.; Abraham, C. R.; Zannis, V. I. *Biochem.* **1997**, *36*(34), 10571-10580.
25. Wolfe, M. S.; Xia, W.; Ostaszewski, B. L.; Diehl, T. S.; Kimberly, W. T.; Selkoe, D. J. *Nature* (London) **1999**, *398*(6727), 513-517.
26. Kowalska, A. *Folia Neuropathologica* **2004**, *42*(4), 235-237.
27. Naslund, J.; Haroutunian, V.; Mohs, R.; Davis, K. L.; Davies, P.; Greengard, P.; Buxbaum, J. D. *JAMA, the Journal of the American Medical Association* **2000**, *283*(12), 1571-1577.
28. Katzman, R. *Curr. Opin. Neurobiol.* **1994**, *4*(5), 703-707.
29. Roses, A. *Scientific American*, Science and Medicine, **1995**, *269*, 16-25.
30. Lambert, M. P.; Barlow, A. K.; Chromy, B. A.; Edwards, C.; Freed, R.; Liosatos, M.; Morgan, T. E.; Rozovsky, I.; Trommer, B.; Viola, K. L.; Wals, P.; Zhang, C.; Finch, C. E.; Krafft, G. A.; Klein, W.L. *Proc. Natl. Acad. Sci. U.S.A.* **1998**, *95*, 6448–6453.
31. Walsh, D.M.; Hartley, D.M.; Kusumoto, Y.; Fezoui, Y.; Condron, M.M.; Lomakin, A.; Benedek, G.B.; Selkoe, D.J.; Teplow, D.B. *J. Biol. Chem.* **1999**, *274*, 25945–25952.
32. Hoshi, M.; Sato, M.; Matsumoto, S.; Noguchi, A.; Yasutake, K.; Yoshida, N.; Sato, K. *Proc. Natl. Acad. Sci. U.S.A.* **2003**, *100*, 6370–6375.

33. Walsh, D. M.; Klyubin, I.; Fadeeva, J. V.; Cullen, W. K.; Anwyl, R.; Wolfe, M. S.; Rowan, M. J.; Selkoe, D. J. *Nature* **2002**, *416*, 535–539.
34. Kirkitadze, M. D.; Bitan, G.; Teplow, D. B. *J. Neurosci. Research* **2002**, *69*(5), 567-577.
35. Caughey, B.; Lansbury, P. T., Jr. *Annual Rev. Neurosci.* **2003**, *26*, 267-298.
36. Kirkitadze, M. D.; Kowalska, A. *Acta Biochimica Polonica* **2005**, *52*(2), 417-423.
37. Petkova, A. T.; Leapman, R. D.; Guo, Z.; Yau, W.; Mattson, M. P.; Tycko, R. *Science* **2005**, *307*(5707), 262-265.
38. Hasegawa, K.; Ono, K.; Yamada, M. and Naiki, H. *Biochem.* **2002**, *41*, 13489-13498.
39. Cannon, M. J.; Williams, A.; Wetzel, R. and Myszka, D. G. *Anal. Biochem.* **2004**, *328*, 67-75.
40. Williams, A.; Portelius, E.; Kheterpal, I.; Guo, J-T, Cook, K., Xu, Y.; Wetzel, R. *J. Mol. Biol.* **2004**, *335*, 833-842.
41. O'Nuallain, B.; Shivaprasad, S.; Kheterpal, I. and Wetzel, R. *Biochem.* **2005**, *44,* 12709-12718.
42. Harper, J. D. and Lansbury, P. T. *Annu. Rev. Biochem.* **1997**, *66*, 385-407.
43. Nybo, M.; Svehag, S. E.; Holm, N. *Scandinavian J. Immun.* **1999**, *49*(3), 219-23.
44. Harper, J. D.; Wong, S.S.; Lieber, C. M. and Lansbury Jr., P. T. *Biochem.* **1999**, *38*, 8972–8980.
45. Walsh, D. M.; Lomakin, A.; Benedek, G. B.; Condron, M. M; Teplow, D. B. *J. Biol. Chem.* **1997**, *272*(35), 22364-72.
46. Lansbury, P. T. *Curr. Opin. Chem. Biol.* **1997**, *1*, 260-267.
47. Harper, J. D.; Wong, S.S.; Lieber, C. M. and Lansbury, P. T. *Chem. Biol.* **1999**, **4**, 119–125.
48. Yong, W.; Lomakin A.; Kirkitadze M. D.; Teplow D. B.; Chen S. H.;Benedek G. B. *Proc. Natl. Acad. Sci. USA* **2002***, 99***,** 150-154.
49. Bitan, G.; Kirkitadze, M. D.; Lomakin, A.; Vollers, S. S.; Benedek, G. B.; Teplow, D. B. *Proc. Natl. Acad. Sci. U.S.A.* **2003**, *100*(1), 330-335.
50. LeVine, H. *Methods Enzymol.* **1999**, *309*, 274-284.

51. Naiki, H.; Gejyo, F. In *Methods in Enzymology Amyloid, Prions, and other Protein Aggregates* Wetzel, R. ed.; Acdemic Press: SanDiego, **1999**; pp 305-318.
52. Serpell, L. C.; Smith, J. M. *J. Mol. Biol.*, **2000**, *299*, 225-231.
53. Tomski, S. J; Murphy, R. M. *Archives Biochem. Biophys.* **1992**, *294*(2), 630-638.
54. Fraser, P. E.; Duffy, L. K.; OMalley, M. B.; Nguyen, J.; Inouye, H. & Kirschner, D. A. *Neurosci. Res.* **1991**, *28*, 474-485.
55. Blake, C.; Serpell, L. C. *Structure*, **1996**, *4*, 989-998.
56. Wood, S.; Maleef, B.; Hart, T.; Wetzel, R. *J. Mol. Biol.* **1996**, *256*, 870-877.
57. Kirschner, D. I.; Duffy, L.; Sinclair, A.; Lind, M.; Selkoe, D. *Proc. Natl. Acad. Sci.* **1987**, *84*, 6953-6957.
58. Kheterpal, I., Zhou, S., Cook, K. D., and Wetzel, R. B. *Proc. Natl. Acad. Sci. U.S.A.*, **2000**, 13597-13601.
59. Kheterpal, I.; Wetzel R.; Cook K. D. *Protein Sci.* **2003**, *12*, 635-643.
60. Kheterpal, I.; Williams, A.; Murphy, C.; Bledsoe, B.; and Wetzel, R. *Biochem.* **2001**, *40*, 11757-11767.
61. Whittemore, N. A.; Mishra, R.; Kheterpal, I.; Williams, A. D.; Wetzel, R.; Serpersu, E. H. *Biochem.* **2005**, *44*(11), 4434-4441.
62. Shivaprasad, S. and Wetzel, R. *J. Biol. Chem.* **2006**, *281*, 993–1000.
63. Williams, A. D.; Shivaprasad, S.; Wetzel, R. *J. Mol. Biol* **2006**, *357*(4), 1283-1294.
64. Petkova, A. T.; Ishii, Y.; Balbach, J. J.; Antzutkin, O. N.; Leapman, R. D.; Delaglio, F. & Tycko, R. *Proc. Natl. Acad. Sci. USA*, **2002**, *99*, 16742–16747.
65. Torok, M.; Milton, S.; Kayed, R.; Wu, P.; McIntire, T.; Glabe, C. G.; Langen, R. *J. Biol. Chem.* **2002**, *277*, 40810-40815.
66. Iwata, K.; Eyles, S. J.; and Lee, J. P. *J. Am. Chem. Soc.* **2001**,*123*, 6728-6729.
67. Wang, S. S. S.; Tobler, S. A.; Good, T. A. and Fernandez, E. J. *Biochem.* **2003**, *42*, 9507-9514.
68. Talafous, J.; Marcinowski, K. J.; Klopman, G. and Zagorski, M. G. *Biochem.* **1994**, *33*, 7788-7796.
69. Roher, A. E.; Baudry, J.; Chaney, M. O.; Kuo, Y. M.; Stine, W. B. and

Emmerling, M. R. *Biochim. Biophys. Acta* **2000**, *1502*, 31-43.

70. Kohno, T.; Kobayashi, K.; Maeda, T.; Sato, K. and Takashima, A. *Biochem.* **1996**, *35*, 16094-16104.
71. Garzon-Rodriguez, W.; Vega, A.; Sepulveda-Becerra, M.; Milton, S.; Johnson, D. A.; Yatsimirsky, A. K. and Glabe, C. G. *J. Biol. Chem.* **2000**, *275*, 22645-22649.
72. Lakdawala, A. S.; Morgan, D. M.; Liotta, D. C.; Lynn, D. G. & Snyder, J. P. *J. Am. Chem. Soc.* **2002**, *124*, 150–151.
73. Sikorski, P.; Atkins, E. D. & Serpell, L. C. *Structure (Camb)*, **2003**, 11, 915–926.
74. Guo, J.-T., Wetzel, R., and Xu, Y. *Proteins* **2004**, *57*, 357-364.
75. Li. L.; Darden. T. A.; Bartolotti, L.; Kominos, D.; Pedersen, L. G. *Biophys J.* **1999**, *76*, 2871-2878.
76. Tjernberg, L. O.; Callaway, D. J.; Tjernberg, A.; Hahne, S.; Lilliehook, C.; Terenius, L.; Thyberg, J.; Nordstedt, C. *J. Biol. Chem.* **1999**, *274*, 12619-12625.
77. Chaney, M.O.; Webster, S. D.; Kuo, Y. M.; Roher, A. E. *Protein Eng.* **1998**, *11*, 761-767.
78. George, A. R. & Howlett, D. R. *Biopolymers* **1999**, *50*, 733-741.
79. Lansbury, P. T. Jr.; Costa, P. R.; Griffiths, J. M.; Simon, E. J., Auger, M.; Halverson, K. J.; Kocisko, D. A.; Hendsch, Z. S.; Ashburn, T.T.; Spencer, R. G, *et al*. *Nat. Struct. Biol.* **1995**, *2*, 990-998.
80. Serpell, L. C.; Blake, C. C.; Fraser, P. E. *Biochem.* **2000**, 39, 13269-13275.
81. Burkoth, T. S.; Benzinger, L. S.; Urban, V.; Morgan, D. M.; Gregory, D. M.; Thiyagarajan, P.; Botto, R. E. *J. Am. Chem. Soc.* **2000**, *122*, 7883-7889.
82. Benzinger, T. L. S.; Gregory, D. M.; Burkoth, T. S.; Miller-Auer, H.; Lynn, D. G.; Botto, R. E. & Meredith, S. C. *Biochem.* **2000**, *39*, 3491-3499.
83. Benzinger, T. L. S.; Gregory, D. M.; Burkoth, T. S.; Miller-Auer, H.; Lynn, D. G.; Botto, R. E. & Meredith, S. C. *Proc. Natl. Acad. Sci. USA* **1998**, 95, 13407-13412.
84. Ma, B.; Nussinov, R. *Proc. Natl. Acad. Sci. USA* **2002**, *99*, 14126-14131.
85. Hilbich, C.; Kisters-Woike, B.; Reed, J.; Masters, C. L. and Beyreuther, K. *J. Mol. Biol.* **1991**, *218*, 149-163.

86. Lazo, N. D. & Downing, D. T. *Biochem.*, **1998**, *37*, 1731–1735.

87. Petkova, A. T.; Yau, W-M. & Tycko, R. *Biochem.* **2006**, *45*, 498-512.

88. Antzutkin, O. N.; Balbach, J. J.; Leapman, R. D.; Rizzo, N. W.; Reed, J. & Tycko, R. *Proc. Natl. Acad. Sci. USA* **2000**, *97*, 13045-13050.

89. Balbach, J. J.; Petkova, A. T.; Oyler, N. A.; Antzutkin, O. N.; Gordon, D. G.; Meredith, S. C. & Tycko, R. *Biophys. J.* **2002**, *83*, 1205-1216.

90. Antzutkin, O. N.; Leapman, R. D.; Balbach, J. J. & Tycko, R. *Biochem.* **2002**, *41*, 15436-15450.

91. Morimoto, A. I. K, Murakami, K.; Ohigashi, H.; Shindo, M.; Nagao, M.; Shimizu, T.; Shirasawa, T. *Biochem. Biophys. Res. Commun.* **2002**, *295*, 306-311.

92. Shivaprasad, S. and Wetzel, R. *Biochem.* **2004**, *43*, 15310-15317.

93. Kheterpal, I.; Lashuel, H. A.; Hartley, D. M.; Walz, T.; Lansbury, P. T., Jr.; Wetzel, R. *Biochem.* **2003**, *42*(48), 14092-14098.

94. Williams, A. D.; Sega, M.; Chen, M.; Kheterpal, I.; Geva, M.; Berthelier, V.; Kaleta, D. T.; Cook, K. D.; Wetzel, R. *Proc. Natl. Acad. Sci. U.S.A.* **2005**, *102*(20), 7115-7120.

95. Soreghan, B.; Joseph K.; Glabe, C. *J. Biol. Chem.* **1994**, 269 (46), 28551-28554.

96. Kirkitadze, M. D.; Condron, M. M.; Teplow, D. B. *J. Mol. Biol.* **2001**, *312*(5), 1103-1119.

97. Hardy, J; Selkoe, D. J. *Science* **2005**, *297*, 353-362.

98. Marchesi, V. T. *Proc. Natl. Acad. Sci. USA* **2005**, *102*(26), 9093-9098.

99. Sommer, Bernd. *Curr. Opin. Pharmac.* **2002**, *2*(1), 87-92.

100. Talaga, P. *Drug Discovery Today: Therapeutic Strategies* **2004**, *1*(1), 7-12.

101. Dominguez, D. I. and Strooper, B. D. *Trends in Pharmacological Sciences*, **2002**, *23(7)*, 324-330.

102. Luo, Y.; Bolon, B.; Kahn, S.; Bennett, B.D.; Babu-Khan, S.; Denis, P.; Fan, W.; Kha, H.; Zhang, J.; Gong, Y.; Martin, L.; Louis, J.-C.; Yan, Q.; Richards, W. G.; Citron, M.; Vassar, R. *Nat. Neurosci.* **2001**, *4*, 231–232.

103. Roberds, S. L.; Anderson, J.; Basi ,G.; Bienkowski, M. J.; Branstetter, D. G.; Chen, K. S.; Freedman, S. B.; Frigon, N. L.; Games, D.; Hu, K.; Johnson-Wood,

K.; Kappenman, K. E.; Kawabe, T. T.; Kola, I.; Kuehn, R.; Lee M.; Liu W.; Motter, R.; Nichols, N. F.; Power, M.; Robertson, D.W.; Schenk, D.; Schoor, M.; Shopp, G. M.; Shuck M.E.; Sinha S.; Svensson K.A.; Tatsuno G.; Tintrup H.; Wijsman J.; Wright S.; McConlogue L. *Hum. Mol. Genet.* **2001**, *10*, 1317–1324.

104. Dovey, H. F.; John, V.; Anderson, J. P.; Chen, L. Z.; De Saint, Andrieu, P.; Fang, L. Y.; Freedman. S.B.; Folmer. B.; Goldbach. E.; Holsztynska. E. J.; Hu. K. L.; Johnson-Wood. K. L.; Kennedy. S. L.; Kholodenko. D.; Knops. J. E.; Latimer. L. H.; Lee. M.; Liao. Z.; Lieberburg. I. M.; Motter. R. N.; Mutter. L. C.; Nietz. J.; Quinn. K. P.; Sacchi. K. L.; Seubert. P. A.; Shopp. G. M.; Thorsett. E. D.; Tung. J. S.; Wu. J.; Yang. S.; Yin. C. T.; Schenk. D. B.; May. P. C.; Altstiel. L. D.; Bender. M. H.; Boggs. L. N.; Britton. T. C.; Clemens. J. C.; Czilli, D. L.; Dieckman-McGinty, D. K.; Droste, J. J.; Fuson, K. S.; Gitter, B. D.; Hyslop, P. A.; Johnstone, E. M.; Li, W.-Y.; Little, S.P.; Mabry, T. E.; Miller, F. D.; Ni, B.; Nissen, J. S.; Porter, W. J.; Potts, B. D.; Reel, J. K.; Stephenson, D.; Su, Y.; Shipley, L. A.; Whitesitt, C. A.; Yin, T.; Audia, J. E. *J. Neurochem.* **2001**, *76*, 173–181.

105. Schenk, D.; Barbour, R.; Dunn, W.; Gordon, G.; Grajeda, H.; Guido, T.; Hu, K.; Huang J.; Johnson-Wood K.; Khan K.; Kholodenko D.; Lee M.; Liao Z.; Lieberburg I.; Motter R.; Mutter L.; Soriano F.; Shopp G.; Vasquez N.; Vandevert C.; Walker S.; Wogulis M.; Yednock T.; Games D.; Seubert P. *Nature* **1999**, *400*, 173–177.

106. Bard, F.; Cannon, C.; Barbour, R.; Burke, R.-L.; Games, D.; Grajeda, H.; Guido, T.; Hu, K.; Huang, J.; Johnson-Wood,, K.; Khan, K.; Kholodenko, D.; Lee, M.; Lieberburg, I.; Motter, R.; Nguyen, M.; Soriano, F.; Vasquez, N.; Weiss, K.; Welch, B.; Seubert, P.; Schenk, D.; Yednock T. *Nat. Med.* **2000**, *6*, 916–919.

107. DeMattos, R. B.; Bales, K. R.; Cummins, D. J.; Dodart, J.-C.; Paul, S. M.; Holtzman, D. M. *Proc. Natl. Acad. Sci. U.S.A.* **2001**, *98*, 8850–8855.

108. Rich, J. B.; Rasmusson, D. X.; Folstein, M. F.; Carson, K. A.; Kawas, C.; Brandt, J. *Neurol.* **1995**, *45*, 51–55.

109. In't Veld, B. A.; Ruitenberg, A.; Hofman, A.t; Launer, L. J.; van Duijn, C. M.;

Stijnen, T.; Bretteler, M. M. B.; Stricker, B. H. C. *New Engl. J. Med.* **2001**, *345*, 1515–1521.

110. Weggen, S.; Eriksent, J. L.; Dast, P.; Sagi, S. A.; Wang, R.; Pietrzik, C. U.; Findlay, K. A.; Smith, T. E.; Murphy, M. P.; Bulter, T.; Kang, D. E.; Marquez-Sterling, N.; Golde, T. E.; Koo, E. H. *Nature* **2001**, *414*, 212–216.
111. Permanne, B.; Adessi, C.; Saborio, G. P; Fraga, S.; Frossard, Marie-José; V. D., Jo; Dewachter, I.; Banks, W.A; Van Leuven, F.; Soto, C. *FASEB J.* **2002**, *16*, 860–862.
112. Findeis, M. *Curr. Topic Med. Chem.* **2002**, *2*, 417–423.
113. Geerts, H. *Curr. Opin. Invest. Drugs* **2004**, *5*, 95–100.
114. Ritchie, C. W.; Bush, A. I.; Mackinnon, A.; Macfarlane, S.; Mastwyk, M.; MacGregor, L.; Kiers, L.; Cherny, R.; Li Q.-X.; Tammer, A.; Carrington, D.; Mavros, C.; Volitakis, I.; Xilinas, M.; Ames, D.; Davis, S.; Beyreuther, K.; Tanzi, R.E.; Masters, C.L. *Arch. Neurol.* **2003**, *60*. 1685–1691.
115. Chang, L.; Bakhos, L.; Wang, Z.; Venton, D. L.; Klein, W. L. *J. Mol. Neurosci.* **2003**, *20*, 305–313.
116. Racchi, M.; Baetta, R.; Salvietti, N.; Ianna, P.; Franceschini, G.; Paoletti, R.; Fumagalli, R.; Govoni, S.; Trabucchi, M.; Soma, M. *Biochem. J.* Part 3 **1997**, *322*, 893–898.
117. Kojro, E.; Gimpl, G.; Lammich, S.; März, W.; Fahrenholz, F. *Proc. Natl. Acad. Sci. U.S.A.* **2001**, *98*, 5815–5820.
118. Bodovitz, S.; Klein, W.L. *J. Biol. Chem.* **1996**, *271*, 4436–4440.
119. Ledesma, M. D.; Da Silva, J. S; Crassaerts, K.; Delacourte, A.; De Strooper, B.; Dotti, C. G. *EMBO Rep.* **2000**, *1*, 530–535.
120. Hu, J.; Igarashi, A.; Kamata, M.; Nakagawa, H. *J. Biol. Chem.* **2001**, *276,* 47863–47868.
121. Eckman, E. A.; Reed, D. Kim; Eckman, C. B. *J. Biol. Chem.* **2001**, *276*, 24540–24548.
122. Cherny, R. A.; Legg, J. T.; McLean, C.A.; Fairlie, D.P.; Huang, X.; Atwood, C.S.; Beyreuther, K.; Tanzi, R.E.; Masters, C.L.; Bush, A.I. *J. Biol. Chem.* **1999**, *274*,

23223–23228.

123. Grutzendler, J.; Morris, J. C. *Neuron* **2001**, *30*, 665–676.

124. Janus, C.; Pearson, J.; McLaurln, J.; Mathews, P. M.; Jiang, Y.; Schmidt, S. D,.; Chishti, M. A.; Horne, P.; Heslin, D.a; French, J.; Mount, H. T. J.; Nixon, R. A.; Mercken, A.; Bergeron, C.; Fraser, P. E.; St George-Hyslop, P.; Westaway, D. *Nature* (London) **2000**, *408*(6815), 979-982.

125. Plant, L. D. *et al. J. Neurosci.* **2003**, *23*, 5531–5535.

126. Bishop, G. M.; Robinson, S. R. *Drugs & Aging* **2004**, *21*(10), 621-630.

127. Rayleigh, Lord. *Philos. Mag.* **1882**, *14*, 184.

128. Zeleny, J. *Phy. Rev.* **1914**, *2*, 69-91.

129. Taylor, G. I. *Proc. R. Soc. Lond A* **1964**, *280*, 383–397.

130. Pfeifer, R. J.; Hendricks, C. D. *AIAA J.* **1968**, *6*, 496-502.

131. Smith, D. P. H. **1986**, *IA-22*, 527-5XX.

132. Bailey, A. G. *Electrostatic Spraying of Liquids*; John Wiley & Sons: New York, **1988**; pp 30-48.

133. Taflin, D. C.; Ward, T. L.; Davis, E. J. *Langmuir*, **1989**, *5*, 376-384.

134. Gomez, A.; Tang, K. *Phys. Fluids* **1994**, *6*, 404-412.

135. Dole, M.; Mack, L. L.; Hines, R. L.; Mobley, R. C.; Ferguson, L. D.; Alice, M. B. *J. Chem. Phys.* **1968**, *49*, 2240-2249.

136. Mack, L. L.; Kralik, P.; Rheude, A.; Dole, M. *J. Chem. Phys.* **1970**, *52*, 4977-4986.

137. Evans, C. A., Jr.; Hendricks, C. D. *Rev. Sci. Instrum.* **1972**, *43*, 1527-1530.

138. Cook, K. D. *Mass Spectrom. Rev.* **1986**, 5, 467-519.

139. Yamashita, M. and Fenn, J. B. *J. Phys. Chem.* **1984**, *88*, 4451–4459.

140. Yamashita, M. and Fenn, J. B. *J. Phys. Chem.* **1984**, *88*, 4671–4675.

141. Fenn, J. B., Mann, M., Meng, C. K., Wong, S. F. and Whitehouse, C. M. *Science* **1989**, *246*, 64-71.

142. Alexandrov, M. L.; Gall L. N.; Krasnov, N. V.; Nikolaev, V. I.; Pavlenko V. A.; Shkurov, V. A. *Bioorg. Khim.* **1984**, *10*, 710–712.

143. Kebarle, P.; Tang, L. *Anal. Chem.*, **1993**, *65*, 972A-986A.

144. Iribarne, J. V.; Thomson, B. A. *J. Chem. Phys.*, **1976**, *64*, 2287-2294.

145. Constantopoulos, T. L.; Jackson, G. S.; Enke, C. G. *Anal. Chim. Acta* **2000**, *406*, 37–52.

146. Labowsky, M.; Fenn, J. B.; De la Mora, J. F. *Anal. Chim. Acta* **2000**, *406*, 105–118.

147. Kebarle, P. *J. Mass Spectrom.* **2000**, *35*, 804-817.

148. Brown, R. S.; Lennon, J. J. *Anal. Chem.* **1995**, *67*, 1998-2003.

149. Hillenkamp, F. In *Biological Mass Spectrometry: Present and Future*; Mastsua T.; Caprioli, R. M.; Gross, M. L.; Seyama, Y. Ed.; John Wiley: New York, **1994**; pp. 101-118.

150. Severs, J. C.; Smith, R. D. In *Electrospray Ionization Mass Spectrometry*; Cole, R. C., Ed.; John Wiley & Son: New York, **1997**; pp 343-382.

151. Voksner, R. In *Electrospray Ionization Mass Spectrometry*; Cole, R. C., Ed.; John Wiley & Son: New York, **1997**; pp. 323-342.

152. Mclafferty, F. W. *Science*, **1981**, *214*, 280-287.

153. Mann, M.; Meng, C. K.; Fenn, J. B. *Anal. Chem.* **1989**, *61*, 1702-1708.

154. Rockwood, A. L.; Busmann, M.; Smith, R. D. *Int. J. Mass Spectrom. Ion Processes* **1991**, *111*, 103-126.

155. Loo, J. A.; Edmonds, C. G.; Smith, R. D. *Anal. Chem.* **1993**, *65*, 425-438.

156. Schaaff, T. G.; Cargile, B. J.; Stephenson, J.L. Jr. Mcluckey, S. A. *Anal. Chem.* **2000**, *72*(5), 899-907.

157. Zubarev, R. A.; Kelleher, N. L. and McLafferty, F. W. *J. Am. Chem. Soc.* **1998**, *120*, 3265-3266.

158. Zubarev, R. A.; Haselmann, K. F.; Budnik, B. A.; Kjeldsen, F. and Jensen, F. *Eur. J. Mass Spectrom.* **2002**, *8*, 337–349.

159. Syka John E P; Coon Joshua J; Schroeder Melanie J; Shabanowitz Jeffrey; Hunt Donald, F. *Proc. Natl. Acad. Sci. USA* **2004**, *101*(26), 9528-33.

160. Roepstorff, P.; Fohlman J. *Biol. Mass Spectrom.* **1984**, *11*, 601-609.

161. Banks, F.; Whitehouse, C. M. *Methods Enzymol.* **1996**, *270*, 486-519.

162. Bier, M. E.; Schwartz, J. C. In: *Electrospray Ionization Mass Spectrometry*, Cole,

R. B., Ed.; John Wiley & Sons: New York, **1997**; pp 235-289.

163. Chernushevich, I. V.; Ens, W.; Standing, K. G. in: *Electrospray Ionization Mass Spectrometry*, Cole, R. B., Ed.; John Wiley & Sons: New York, **1997**; pp 203-234.

164. Laude, D.A.; Stevenson, E.; Robinson, J.M. In: *Electrospray Ionization Mass Spectrometry*, Cole, R.B., Ed.; John Wiley & Sons: New York, **1997**; pp 291-319.

165. Morris H. R.; Paxton T.; Dell A.; Langhorn B.; Berg M.; Bordoli R. S. *et al. Rapid Commun. Mass Spectrom.* **1996**, *10*, 889–896.

166. Whitehouse, C. M.; Dreyer, R. N.; Yamashita. M.; Fenn, J. B. *Anal. Chem.* **1985**, *57,* 675-679.

167. Fenn, J. B.; Mann. M.; Meng, C. K.; Wong, S. F. *Mass Spectrom. Rev.* **1990***, 9,* 37-70.

168. Smith, R. D.; Loo, J. A.; Edmonds. C. G.; Barlnaga, C. J.; Udseth, H. R. *Anal. Chem.* **1990**, *62,* 882.

169. Chowdhury, S. K.; Katta, V.; Chait, B. T. *Rapid Commun. Mass Spectrom.* **1990**, *4*, 81-87.

170. Chowdhury, S. K. and Chait, B. T. *Anal.* Chem. **1991**, *63*, 1660-1664.

171. Ikonomou, M. G.; Blades, A. T.; Kebarle, P. *Anal. Chem.* **1991**, *63*(18), 1989-98.

172. Zhou, S.; Hamburger, M. *Rapid Comm. Mass Spectrom.* **1995**, *9*, 1516-1521.

173. Drozin, V. G. *J Colloid Sci* **1955**, *7*, 616-614.

174. Wilm, M. S.; Mann, M. *Int. J. Mass Spectrom. Ion Processes* **1994,** *136*, 167-180.

175. Juraschek, R.; Dulcks, T.; Karas, M. *J. Am. Soc. Mass Spectrom.* **1999,** *10*, 300-308.

176. Gangle, E. T.; Annan, A.; Spooner, N.; Vouros, P. *Anal. Chem.* **2001,** *73*, 5635-5644.

177. Valaskovic, G. A.; Kelleher, N. L.; McLafferty, F. W. *Science* **1996**, *273* (5279), 1199–1202.

178. Van Berkel, G. J.; Zhou, F. *Anal. Chem.* **1995**, *67*, 2916-2923.

179. Tang, L.; Kebarle, P. *Anal. Chem.* **1991**, *63*, 2709-2715.

180. Hayati, I.; Bailey, A. I. and Tadros, T. F. *J. Colloid Interface Sci.*, **1987**, *117*, 222-230.

181. Juhasz, P.; Ikonomou, M. G.; Blades, A. T. and Kebarle, P. In *Methods and Mechanisms for Producing Ions from Large Molecules*, W. Ens, Ed.; Plenum Press: New York, **1991**.

182. De la Mora, J. F. and Loscertales, I. G. *J. Fluid Mech.*, **1994**, *260*, 155-165.

183. Loeb, L. B.; Kip, A. F.; Hudson, G.G.; Bennett, W. H. *Phys. Rev.* **1941**, *60*, 714-725.

184. Kebarle, P.; Ho, Y. In *Electrospray Ionization Mass Spectrometry: Fundamentals, Instrumentation and Applications*, Cole, R. B. Ed.; John Wiley & Sons: New York, **1997**; pp 3-63.

185. De la Mora, J. F. *J. Fluid Mech.*, **1992**, *243*, 561-569.

186. Cole, R. B. *Electrospray Ionization Mass Spectrometry: Fundamentals, Instrumentation, & Applications*, John Wiley & Sons: New York, **1997**.

187. Jackson, G. S.; Enke, C. G. *Anal. Chem.* **1999**, *71*, 3777-3784.

188. Blades, A. T.; Ikonomou, M. G. and Kebarle, P. *Anal. Chem.*, 1991, **63**, 2109-14.

189. Dean, J. A. Langes's Handbook of Chemistry, 15th ed.; McGraw-Hill: New York, **1997**.

190. Van Berkel, G. J.; McLuckey, S. A. and Glish, G. L. *Anal. Chem.*, **1991**, **63**, 1098-1109.

191. Van Berkel, G. J. and Zhou, F. *J. Am. Soc. Mass Spectrom.* **1996**, *7*, 157-162.

192. Van Berkel, G. J.; Quirke, J. M.; Tigani, E. R. A.; Dilley, A. S. and Covey, T. R. *Anal. Chem.* **1998**, *70*, 1544-1554.

193. Van Berkel, G. J. *J. Am. Soc. Mass Spectrom.* ***2000***, *11*, 951-960.

194. Van Berkel, G. J.; Zhou, F. *Anal. Chem.* **1995**, *67*, 3958-3964.

195. Bateman, K. P. *J. Am. Soc. Mass Spectrom.* **1999**, *10*, 309-317.

196. Van Berkel, G. J.; McLuckey, S. A. and Glish, G. L. *Anal. Chem.*, **1992**, *64*, 1586-1593.

197. Van Berkel, G. J.; Zhou, F.; Aronson, J. T. *Int. J. Mass Spectrom. Ion Processes*

1997, *162*, 55-62.

198. Karancsi, T.; Slegel, P.; Novak, L.; Pirok, G.; Kovacs, P.; Vekey, K. *Rapid Commun. Mass Spectrom.* **1997**, *11*, 81-84.
199. Van Berkel, G. J. *J. Mass Spectrom.* **2000**, *35*, 773-783.
200. Van Berkel, G. J. In The Electrolytic Nature of Electrospray. In *Electrospray Ionization Mass Spectrometry: Fundamentals, Instrumentation and Applications*; Cole, R., Ed.; John Wiley: New York, **1997**; pp 65-105.
201. Van Berkel, G. J.; McLuckey, S. A.; Glish, G. L. *Anal. Chem.* **1992**, *64*, 1586-1593.
202. Van Berkel, G. J.; Giles, G. E.; Bullock, J. S., IV; Gray, L. J. *Anal. Chem.* **1999**, *71*, 5288-5296.
203. Van Berkel, G. J. *J. Am. Soc. Mass Spectrom.* **2000**, *11*, 951-960.
204. De la Mora, J. F.; Van Berkel, G. J.; Enke, C. G.; Cole, R. B.; Martinez-Sanchez, M.; Fenn, J. B. *J. Mass Spectrom.* **2000**, *35*, 939-952.
205. Michelson, D. *Electrostatic Atomization.* **1990**, 164 pp.
206. Bruins, A. P.; Covey, T. R. and Henion, J. D. *Anal. Chem.* **1987**, *59***,** 2642–2646.
207. Wampler, F. M. III; Blades, A. T.; Kebarle, P. *J. Am. Soc. Mass spectrom.* **1993**, *4*(4), 289-295.
208. Cole, R. B.; Harrata, A. K. *Rapid Commun. Mass Spectrom.* **1992**, *6*, 536-539.
209. Karas, M. and Hillenkamp, F. (**1988**) *Ultraviolet laser desorption of ions above 10 kDa.* In: Abstracts, 11th Int. Mass Spectrom. Conf., Bordeaux, 29 August – 2 September.
210. Karas, M. and Hillenkamp, F. *Anal. Chem.* **1988**, *60*, 1299–2301.
211. Tanaka, K.; Waki, Ido, H.; Akita, Y., S.; Yoshida, Y. and Yoshida, T. *Rapid Commun. Mass Spectrom.* **1988**, *2*, 151-153.
212. Cotter, R. J. *Time-of-Flight Mass Spectrometry: Instrumentation and Applications in Biological Research* Am. Chemical Society, Washington, D.C., **1997**; pp 131–134.
213. Roepstorff, P. *MALDI-TOF mass spectrometry in protein chemistry. In: Proteomics in Functional Genomics: Protein Structure Analysis* Jollès P. and

Jörnvall H. Eds.; Birkhäuser: Basel, **2000**; pp 81–97.

214. Vorm, O. and Mann, M. *J. Am. Soc. Mass Spectrom.* **1994**, *5*, 955–958.

215. Gobom, J.; Nordhoff, E.; Mirgorodskaya, E.;Ekman, R. and Roepstorff, P. *J. Mass Spectrom.* **1999**, *34*, 105–116.

216. Bonk, T. & Humeny, A. *Neuroscientist* **2001**, *7*, 6-12.

217. Colby, S. M.; King, T. B. and Reilly J. P. *Rapid Commun. Mass Spectrom.* **1994**, *8*, 865–868.

218. Vestal, M. L.; Juhasz P. and Martin S. A. *Rapid Commun. Mass Spectrom.* **1995**, *9*, 1044–1050.

219. Brown, R. S. and Lennon, J. J. *Anal. Chem.* **1995**, *67*, 1998–2003.

220. Mamyrin, B. A.; Karataev, V. I.; Shmikk D. V. and Zagualin V. A. *Sov. Phys. JETP*. **1973**, *37*, 45–48.

221. Shevchenko, A.; Jensen, O. N.; Podtelejnikov, A. V. ; Sagliocco, F.; Wilm, M.; Ole Vorm, Mortensen, P.; Shevchenko, A.; Boucherie, H. and Mann, M. *Proc. Natl. Acad. Sci. U S A.* **1996**, *93*(25): 14440**–**14445.

222. Hillenkamp, F.; Karas, M.; Beavis, R. C. and Chait, B. T. *Anal. Chem.* **1991,** *63*, 1193A–1203A.

223. Beavis, R. C. and Chait, B. T. *Proc. Natl. Acad. Sci. USA* **1990**, *87*, 6873–6877.

224. Stults, J. T. *Curr. Opin. Struct. Biol.* **1995**, *5*, 691–698.

225. Englander, S. W.; Mayne, L.; Bai, Y. and Sosnick, T. R. *Protein Sci.* **1997**, 5, 1101–1109.

226. Hvidt, A. and Linderstrom-Lang, K. *Biochim. Biophys. Acta* **1954**, *4*, 574–575.

227. Hvidt, A. and Linderstrom-Lang, K. *Biochim. Biophys. Acta* **1955**, *1*, 168–169.

228. Englander, J.; Rogero, J. R. and Englander, S. W. *Anal. Biochem.* **1985**, *1*, 234–244.

229. Rosa, J. J. and Richards, F. M. *J. Mol. Biol.* **1979**, *3*, 399–416.

230. Smith, D. L.; Deng, Y.; Zhang, Z. *J Mass Spectrom* **1997**, *32*, 135–146.

231. Engen, J. R.; Smith, D. L. *Anal. Chem*, **2001**, *73*, 256 A-265A.

232. Katta, V.; Chait, B. T. *J. Am. Chem. Soc.,* **1993,** *115*, 6317-6321.

233. Zhang, Z. and Smith, D. L. *Protein Sci.* **1993**, *4*, 522–531.

234. Johnson, R. S. and Walsh, K. A. *Protein Sci.* **1994**, *12*, 2411–2418.

235. Deng, Y.; Pan, H. and Smith, D. L. *J. Am. Chem. Soc.* **1999**, *121*, 1966–1967.

236. Wang, L.; Pan, H. and Smith, D. L. *Mol. Cell. Proteomics* **2002**, *2*, 132–138.

237. Cravello, L.; Lascoux, D. and Forest, E. *Rapid Commun. Mass Spectrom.* **2003**, *21***,** 2387–2393.

238. Mandell, J. G.; Falick, A. M.; Komives, E. A. *Proc. Natl. Acad. Sci. U S A* **1998**, *95*, 14705–14710.

239. Figueroa, I. D.; Russell, D. H. *J. Am. Soc. Mass spectrum.* **1999**, *10*, 719-731.

240. Powell, K. D.; Fitzgerald, M. C. *Anal. Chem.*, **2001**, *73*, 3300-3304.

241. Busenlehner, L. S.; Codreanu, S.G.; Holm, P.J.; Bhakat, P.; Hebert, H.; Morgenstern, R. and Armstrong, R.N. *Biochem.* **2004**, *43*, 1145–11152.

242. Busenlehner, L. S.; Armstrong, R. N. *Archives of Biochem. and Biophy.* **2005**, *433*(1), 34-46.

243. Hoofnagle, A. N.; Resing, K. A.; Ahn, N. G. *Annu. Rev. Biophys. Biomol. Struct.* **2003**, *32*, 1-25.

244. Lanman, J.; Prevelige, P. E. *Curr. Opin. Struct. Biol.* **2004**, *14*(2), 181-188.

245. Cai, X.; Dass, C. *Curr. Org. Chem.* **2003**, *7*(18), 1841-1854.

246. Garcia, R. A.; Pantazatos, D.; Villarreal, F. J. *Assay and Drug Develop. Technol.* **2004**, *2*(1), 81-91.

247. Kaltashov, I. A.; Eyles, S. J. *Mass Spectrom. Reviews* **2002**, *21*(1), 37-71.

248. Hasan, A.; Smith, D. L. and Smith, J. B. *Biochem.* **2002**, *41***,** 15876–15882.

249. Houliston, R. S.; Liu, C.; Singh, L. M. R.; Meiering, E. M. *Biochem.*, **2002**, *41*, 1182-1194.

250. Li, R.; Woodward, C. *Protein Sci.* **1999,** *8*, 1571-1590.

251. Bai, Y.; Englander, S. W. *Proteins: Struct., Funct., Genet.*, **1996,** *26***,** 145-151.

252. Englander, S. W. *Annu. Rev. Biophys. Biomol. Struct.* **2000**, *29*, 213-238.

253. Dole Cotre, J.; Turk, E.; Kaback, H. R.; Wright, E. M. *Biochem.* **2002**, *41*, 8082.

254. Markely, J. L. and Urich E. L. *Ann. Rev. Biophys. Bioeng.* **1984**, *13*, 493-502.

255. Homans, S. W. *Angew Chem. Int. Ed.* **2004**, *43*, 290–300.

256. Thomas, G. J. Jr. *Annu. Rev. Biophys. Biomol Struct.* **1999**, *28*, 1–27.

257. Englander, S. W.; Sosnick, T. R.; Englander, J. J.; Mayne, L. *Curr. Opin. Struct. Biol.* **1996**, *6*, 18–23.

258. Voet, D.; Voet, J. G. *Protein folding, dynamics, and structural evolution.* In: *Biochemistry,* 2nd Ed.; John Wiley and Sons: Somerset, **1995**; pp 205–208.

259. Wintrode, P. L.; Friedrich, K. L.; Vierling, E.; Smith, J. B.; Smith, D. L. *Biochem.* **2003**, 42,10667–10673.

260. Bai, Y.; Milne, J. S.; Mayne, L.; Englander, S. W. *Proteins: Struct. Funct. Genet.* **1993**, *17*, 75-86.

261. Connelly, G. P., Bai, Y., Jeng, M. F., Englander, S. W. *Proteins: Struct. Funct. Genet.* **1993**, *17*, 87-92.

262. Scheiner, S., Cuma, M. *J. Am. Chem. Soc.* **1996**, *118*, 1511-1521.

263. Cioni, P.; Strambini, G. B. *Biophys. J.* **2002**, *82*, 3246-3253.

264. Englander, S. W. *Annu. Rev. Biophys. Biomol. Struct.* **2000**, *29*, 213–238.

265. Miranker, A.; Robinson, C. V.; Radford, S. E.; Aplin, R. T.; Dobson, C. M. *Science* **1993,** *262,* 896–900.

266. Yang, H.; Smith, D. L. *Biochem.* **1997,** *36,* 14992–14999.

267. Miranker, A.; Robinson, C.V.; Radford, S.E. and Dobson, C.M. *FASEB J.* **1996**, *10*, 93–101.

268. Deng, Y.; Smith D. L. *Biochem.* **1998**, *37*, 6256-6262.

269. Clarke, J.; Itzhaki, L. S. *Curr. Opin. Struct. Biol.* **1998**, *8*, 112–118.

270. Kim, K. S.; Fuchs, J. A.; Woodward, C. K. *Biochem.* **1993**, *32*, 9600-9608.

271. Bai, Y.; Sosnick, T. R.; Mayne, L.; Englander, S. W. *Science* **1995**, *269*, 192-197.

272. Engen, J. R.; Smithgall, T. E.; Gmeiner, W. H.; Smith, D. L. *Biochem.* **1997**, *36*, 14384-14391.

273. Xu, Y.; Mayne, L.; Englander, S. W. *Nat. Struct. Biol.* **1998**, *5*, 774-778.

274. Deng, Y.; Zhang, Z.; Smith, D. L. *J. Am. Soc. Mass Spectrom.* **1999**, *10*, 675-684.

275. Konermann, L.; Simmons, D. A. *Mass Spectrom. Rev.* **2003**, *22*(1), 1-26.

276. Robison, C. V. In *Protein and Peptide Analysis by Mass Spectrometry*, Chapman,

J. R. Ed.; Humana Press: Totowa, **1996;** pp 129-139.

277. Rist, W.; Jorgensen, T. J. D.; Roepstorff, P.; Bukau, B.; Mayer, M. P. *J. Biol. Chem.* **2003**, *278*(51), 51415-51421.

278. Lin, H.; Dass, C. *Rapid Commun. Mass Spectrom.* **2001**, *15*, 2341-2346.

279. (a) Simmons, D. A.; Dunn, S. D.; Konermann, L. *Biochem.* **2003**, *42*(19), 5896-5905; (b) Simmons, D. A.; Dunn, S. D.; Konermann, L. *Biochem.* **2003**, *42*(30), 9248.

280. Miranker, A.; Robinson, C. V.; Radford, S. E.; Aplin, R.; Dobson, C. M. *Science* **1993**, *262*, 896-900.

281. Heidary, D. K.; Gross, L. A.; Roy, M.; Jennings, P. A. *Nat. Struct. Biol.* **1997**, *4*, 725-731.

282. Udgaonkar, J. B.; Baldwin, R. L. *Nature* **1988**, *335*, 694-699.

283. Simmons, D. A.; Konermann, L. *Biochem.* **2002**, *41*, 1906-1914.

284. Kebarle, P.; Ho, Y. In *Electrospray Ionization Mass Spectrometry: Fundamentals, Instrumentation and Applications*, Cole, R. B. Ed.; John Wiley & Sons: New York, **1997**; pp 3-63.

285. Kaltashov, I. A. and Eyles, S. J. *J. Mass. Spectrom.* **2002**, *37*, 557-565.

286. Xu, N.; Lin, Y.; Hofstadler, S. A.; Matson, D.; Call, C. J.; Smith, R. D. *Anal. Chem.* **1998**, *70*, 3553-3556.

287. Raza, A. S.; Dharmasiri, K. and Smith, D. L. *J. Mass Spectrom.* **2000**, *35*, 612-617.

288. Zhang, Z.; Post, C. B.; Smith, D. L. *Biochem.* **1996**, *35*, 779-791.

289. Zhang, Z.; Smith, D. L. *Protein Sci.* **1996**, *5*, 1282-1289.

290. Liu, Y. and Smith, D. L. *J. Am. Soc. Mass spectrum.* **1994**, *5*, 19-28.

291. Dharmasiri, K. and Smith, D. L. *Anal. Chem.* **1996**, *68*, 2340-2344.

292. Yang, H.; Smith, D. L. *Biochem.* **1997**, *36*, 14992-14999.

293. Zhang, Z.; Li, W.; Li, M.; Logan, T. M.; Guan, S. and Marshall, A. G. *Tech. Rot. Chem. VIII*, **1997**, 703-713.

294. Wang, F.; Scapin, G.; Blanchard, J. S. and Angeletti, R. H. *Protein Sci.* **1998**, *7*, 293–299.

295. Anderson, M. D.; Shaffer, J.; Jennings, P.A.; and Adams, J.A. *J. Biol. Chem.* **2001**, *17***,** 14204–14211.

296. Tobler, S. A. and Fernandez, E.J. *Protein. Sci.* **2002**, *11***,** 1340–1352.

297. Nazabal, A.; Maddelein, M.; Bonneu, M.; Saupe, S. J.; Schmitter, J. *J. Biol. Chem.* **2005**, *280*(14), 13220-13228.

298. Englander, J. J.; Del Mar, C.; Li, W.; Englander, S. W.; Kim, J. S.; Stranz, D. D.; Hamuro, Y.; Woods, V. L., Jr. *Proc. Natl. Acad. Sci. USA* **2003**, *100*(12), 7057-7062.

299. Resing, K. A.; Hoofnagle, A. N.; Ahn, N. G. *J. Am. Soc. Mass Spectrom.* **1999**, *10*, 685**–**702.

300. Englander, S. W. & Kallenbach, N. R. *Q. Rev. Biophys.* **1984**, *16*, 521-655.

301. Zhang, Z.; Li, W.; Logan, T.M.; Li, M. and Marshall, A.G. *Protein Sci.* **1997**, *6*, 2203–2217.

302. Zhang, Z.; Guan, S. and Marshall, A. G. *J Am. Soc. Mass Spectrom.* **1997**, *8*, 659-670.

303. Palmblad, M.; Buijs, J.; Håkansson, P. *J. Am. Soc. Mass Spectrom.* **2001**, *12*, 1153-1162.

304. Kim, M. Y.; Maier, C. S.; Reed, D. J.; Deinzer, M. L. *J. Am. Chem. Soc.* **2001**, *123*, 9860-9866.

305. Eyles, S. J.; Dresch, T.; Gierasch, L. M.; Kaltashov, I. A. *J. Mass Spectrom.* **1999**, *34*, 1289-1295.

306. Eyles, S. J.; Speir, P.; Kruppa, G.; Gierasch, L. M.; Kaltashov, I. A. *J. Am. Chem. Soc.* **2000**, *122*, 495-500.

307. Akashi, S.; Naito Y.; Takio, K. *Anal. Chem*. **1999**, *71*, 4974-4980.

308. Akashi, S.; Takio, K. *Protein Sci.* **2000**, *9*, 2497-2505.

309. Kaltashov, I. A. and Eyles, S. J. *J. Mass. Spectrom.* **2002**, *37*, 557-565.

310. Demmers, J. A.A.; Rijkers, D. T. S.; Haverkamp, J.; Killian, J. A.; Heck, A. J. R. *J. Am. Chem. Soc.* **2002**, *124*, 11191-11198.

311. Hoerner, J. K., Xiao, H., Dobo, A., and Kaltashov, I. A. *J. Am. Chem. Soc.* **2004**, *126***,** 7709-7717.

312. Jorgensen, T. J., Gardsvoll, H., Ploug, M., and Roepstorff, P. *J. Am. Chem. Soc.* **2005**, *127*, 2785-93.

313. Kweon, H. K., and Hakansson, K. *Analyst (Cambridge, United Kingdom)* **2006**, *131*, 275-280.

314. Woods, V. L.; Hamuro, Y. *J. Cell. Biochem.* **2001**, *37*(Suppl.), 89-98.

315. Yan, X.; Zhang, H.; Watson, J.; Schimerlik, M. I. and Deinzer, M. L. *Protein Sci.* **2002**, *11*, 2113–2124.

316. Ghaemmaghami, S.; Fitzgerald, M. C.; Oas, T. G. *Proc. Natl. Acad. Sci. USA* **2000**, *97*, 8296–9301.

317. Ghaemmaghami, S.; Oas, T. G. *Nat. Struct. Biol.* **2001**, *8*, 879–82.

318. Powell, K. D.; Ghaemmaghami, S.; Wang, M. Z.; Ma, L.; Oas, T. G.; Fitzgerald, M. C. *J. Am. Chem. Soc.* **2002**, *124*(35), 10256-10257.

319. Nazabal, A.; Laguerre. M.; Schmitter. J.; Vaillier. J.; Chaignepain, S.; Velours, J. *J. Am. Soc. Mass spectrum.* **2003**, *14*(5), 471-481.

320. Reid, C. W.; Brewer, D.; Clarke, A. J. *Biochem.* **2004**, *43*(35), 11275-11282.

321. Dai, S. Y.; Gardner, M. W.; Fitzgerald, M. C. *Anal. Chem.* **2005**, *77*(2), 693-697.

322. Rosenbaum, D. M.; Roy, S.; Hecht, M. H. *J. Am. Chem. Soc.* **1999**, *121*, 9509–13.

323. Kipping, M.; Schierhorn, A. *J. Mass Spectrom.* **2003**, *38*(3), 271-276.

324. Buijs, J.; Vera, C. C.; Ayala, E.; Steensma, E.; Hakansson, P.; Oscarsson, S.; *Anal. Chem.* **1999**, *71*, 3219-3225.

325. Villanueva, J.; Canals, F.; Villegas, V.; Querol, E.; Aviles, F. X. *FEBS Letters* **2000**, *472*(1), 27-33.

326. Loboda, A. V.; Krutchinsky, A. N.; Bromirski, M.; Ens, W.; Standing, K. G. *Rapid Commun. Mass Spectrom.* **2000**, *14*, 1047-1057.

327. Medzihradszky, K. F.; Campbell, J. M.; Baldwin, M. A.; Falick, A. M.; Juhasz, P.; Vestal, M. L.; Burlingame, A. L. *Anal. Chem.* **2000**, *72*, 552-558.

328. Kraus, M.; Janek, K.; Bienert, M.; Krause, E. *Rapid Commun. Mass Spectrom.* **2000**, *14*, 1094-1104.

329. Kraus, M.; Bienert, M.; Krause, E. *Rapid Commun. Mass Spectrom.* **2003**, *17*(3),

222-228.

330. Englander, S. W.; Poulsen, A. *Biopolymers* **1969**, *7*, 379.

331. Barrett, A. J.; Rawlings, N. D. and Woessner, J. F. *Handbook of Proteolytic Enzymes*, edited by Academic Press, London, **1998**; pp 801-986.

332. Cooper, J. B. *Curr. Drug Targets* **2002**, *3*(2), 155-173.

333. Dunn, B. M. *Chem. Rev.* **2002**, *102*(12), 4431-4458.

334. Woods, V. L. PCT Int. Appl. **2003**, 134 pp.

335. Ehring, H. *Anal. Biochem.* **1999**, *267***,** 252–259.

336. Wu, Y.; Kaveti, S.; Engen, J. R. *Anal. Chem.* **2006**, *78*(5), 1719-1723.

337. Northrop, J. H. J. *Gen. Physiol.* **1930**, *13*, 739-748.

338. Lin, Y.; Fusek, M.; Lin, X.; Hartsuck, J. A.; Kezdy, F. J. and Tang, J. *J. Biol. Chem.* **1992**, *267*, 18413-18418.

339. Lin, X.; Wong, R. N. S. and Tang, J. *J. Biol. Chem.* **1989**, *264*, 4482-4489.

340. Tang, J. *Nature* **1963**, 1094-1095.

341. Fruton, J. S. *Adv. Enzymol.* **1976**, *44*, 1-36.

342. Yoshida, F. *Bull. Chem. Soc. Jpn.* **1956**, *20*, 252-256.

343. Lchishima, E. *Methods Enzymol.* **1970**, *19*, 397-406.

344. Tanak, N.; Takeuchi, M. and Ichishima, E. *Biochim. Biophys. Acta* **1977**, *485*, 406-416.

345. Shintani, T. and Ichishima, E. *Biochim. Biophys. Acta* **1994**, *1204*, 257-264.

346. Fukumo, J.; Tsuru, D. and Yamamoto, T. *Agri. Biol. Chem.* (Tokyo), **1967**, *31*, 710-717.

347. Delaney, R.; Wong, R. N.; Meng, g. Z.; Wu, N. H. & Tang, J. *J. Biol. Chem*, **1987**, *262*, 1461-1467.

348. Barkholt, V. *Eur. J. Biochem.* **1987**, *167*, 327-338.

349. Razanamparany, V.; Jara, P.; Legoux, R.; Delmas, P.; Msayeh, F.; Kaghad, M.; & Loison, G. *Curr. Genet.* **1992**, *21*, 455-461.

350. Choi, G. H.; Pawlyk, D. M.; Rae, B.; Shapira, R. & Nuss, D. L. *Gene* **1993**, *125*, 135-141.

351. Williams, D. C.; Whitaker J. R. & Caldwell, P. V. *Arch. Biochem. Biophys.* **1972**,

149, 52-61.

352. Drohse, H. B. & Foltmann, B. *Biochim. Biophys. Acta* **1989**, *995*, 221-224.

353. Dunn, B. M. & Kay, J. *Biochem Soc Trans* **1985**, *13*, 1041-1043.

354. Hofmann, T. & Hodges, R. S. *Biochem. J.* **1982**, *203*, 603-610.

355. Glasoe, P. K. and Long, F. A. *J. Phys. Chem.* **1960**, *64*, 188-193.

356. Zagorski, M. G., Yang, J., Shao, H., Ma, K., Zeng, H., and Hong, A. *Methods Enzymol.* **1999**, *309*, 189-204.

357. Naiki, H., and Gejyo, F. *Methods Enzymol.* **1999**, *309,* 305-318.

358. Xu, N.; Lin, Y.; Hofstadler, S. A.; Matson, D.; Call, C. J.; Smith, R. D. *Anal. Chem.* ***1*998**, *70*, 3553-3556.

359. Simon, L. M.; Laszlo, K.; Vertesi, A.; Bagi, K.; Szajani, B. *J. Mol. Catal. B: Enzym.* **1998**, *4*, 41-45.

360. Russell, W. K.; Park, Z. Y.; Russell, D. H. *Anal. Chem.* **2001**, *73*, 2682-2685.

361. Cech, N. B. & Enke, C. G. *Mass Spectrom. Rev.*, **2001**, *20*, 362-387.

362. Inouye, K.; Fruton J. S. *Biochem.* **1967**, *6*, 1765–1777.

363. Dunn, B. M. & Fink, A. L. *Biochem.* **1984**, *23*, 5241-5247.

364. Edelhoch, H. *J. Am. Chem. Soc.* **1958**, *80*, 6648-6655.

365. Klibanov A. M. *Trends Biotechnol.* **1997**, *15*, 97–101.

366. Powers, J. C.; Harley, A. D. & Myers, D. V. In *Acid Proteases, Structure, Function and Biology*, Tang, J. Ed.; Plenum Press: New York, **1977**; pp 141-157.

367. Kostiainen, R.; Bruins, A. P. *Rapid Commun. Mass Spectrom.* **1996**, *10(11)*, 1393-1399.

368. Konermann, L.; Silva, E. A. & Sogbein, O. F. *Anal. Chem.* **2001**, *73*, 4836-4844.

369. Zhou, S.; Edwards, A. G.; Cook, K. D; Van Berkel, G. J. *Anal. Chem.* **1999**, *71* (4), 769-776.

370. Zhou, S.; Prebyl B. S.; Cook, K. D. *Anal. Chem.* **2002**, *74* (19), 4885-4888.

371. Wang, G.; Cole, R. B. In *Electrospray Ionization Mass Spectrometry*; Cole, R. B., Ed.; John Wiley & Sons: New York, 1997; pp 137-174.

372. Busch, K. *Spectroscopy*, **2004**, *196*, 35-38.

373. Gale, D. C.; Smith, R. D. *Rapid Commun. Mass Spectrom.* **1993**, *7*(11), 1017-21.

374. Ikonomou, M. G.; Blades, A. T.; Kebarle, P. *Anal. Chem.* **1990**, *62*, 957-967.

375. Cole, R. B.; Harrata, A. K. *J. Am. Soc. Mass Spectrom.* **1993**, *4*(7), 546-556.

376. Harris, D. C. *Quantitative chemical analysis*, 5th ed.; W. H. Freeman: New York. **1998**.

377. Nelson, R.; Sawaya, M. R.; Balbirnie, M.; Madsen, A. O.; Riekel, C.; Grothe, R. & Eisenberg, D. *Nature* **2005**, *435*, 773-778.

378. Jarrett, J. T.; Costa, P. R.; Griffin, R. G. & Lansbury, P. T., Jr. *J. Am. Chem. Soc.* **1994**, *116*, 9741-9742.

379. Carulla, N.; Caddy, G. L.; Hall, D. R.; Zurdo, J.; Gairi, M.;Feliz, M.; Giralt, E.; Robinson, C. V. & Dobson, C. M. *Nature* **2005**, *436*, 554-558.

380. Serio, T. R.; Cashikar, A. G.; Kowal, A. S.; Sawicki, G. J.; Moslehi, J. J.; Serpell, L.; Arnsdorf, M. F. & Lindquist, S. L. *Science* **2000**, *289*, 1317-1321.

381. Esler, W. P.; Stimson, E. R.; Ghilardi, J. R.; Felix, A. M.; Lu, Y. A.; Vinters, H. V.; Mantyh, P. W. & Maggio, J. E. *.Nat Biotechnol.* **1997**, *15*, 258-263.

382. Tseng, B. P.; Esler, W. P.; Clish, C. B.;Stimson, E. R.; Ghilardi, J. R.; Vinters, H. V.; Mantyh, P. W.; Lee, J. P. & Maggio, J. E. *Biochem.* **1999**, *38*, 10424-10431.

383. Collins, S. R.; Douglass, A.; Vale, R. D. & Weissman, J. S. *PLoS* **2004**, *2*, 1582-1590.

384. Cech, N. B.; Enke, C. G. *Anal. Chem*. **2000**, *72*, 2717-2723.

385. Van Berkel, G. J. *J. Mass Spectrom.* **2000**, *35*, 773-783.

386. Morand K, Talbo G, Mann M. *Rapid Commun. Mass Spectrom.* **1993**, *7*, 738-743.

387. Chowdhury, S. K.; Eshraghi, J.; Wolfe, H.; Forde, D.; Hlavac, A. G.; Johnston, D. *Anal. Chem.* **1995**, *67*, 390-398.

388. Berlett, B. S.; Levine, R. L.; Stadtman, E. R. *J. Biol. Chem.* **1996**, *271*, 4177-4182.

389. Nightingale, Z. D.; Lancha, A. H. Jr.; Handelman, S. K.; Dolnikowski, G. G.; Busse, S. C.; Dratz, E. A.; Blumberg, J. B.; Handelman, G. J. *Free Radical Biol. Med.* **2000**, *29*, 425-433.

390. Kotiaho, T.; Eberlin, M. N.; Vainiotalo, P.; Kostiainen, R. *J. Am. Soc. Mass*

Spectrom. **2000**, *11*, 526-535.

391. Guan, Z.; Yates, N. A.; Bakhtiar, R. *J. Am. Chem. Soc.* **2003**, *14*(6), 605-13.

392. Lagerwerf, F. M.; van de Weert, M.; Heerma, W.; Haverkamp, J. *Rapid Commun. Mass Spectrom.* **1996,** *10*, 1905–1910.

393. Brot, N. and Weissbach, H. *BioFacfors* **1999,** *3*, 91-99.

394. Squier, T. C.; Bigelow, D. J. *Front. Biosci.* **2000**, *5*, 504–526.

395. Caldwell, P.; Luk, D. C.; Weissbach, H.; Brot, N. *Proc. Natl. Acad. Sci.* USA **1978**, *78*, 2155–2158.

396. Palmblad, M.; Westlind-Danielsson, A. and Bergquist, J. *J. Biol. Chem.* **2002**, *277*, 19506–19510.

397. Kuo, Y.-M.; Webster, S.; Emmerling, M.R.; De Lima, N. and Roher, A. E. *Biochim. Biophys. Acta* **1998**, *1406***,** 291–296.

398. Hong, J. and Schöneich, C. *Free Rad. Biol. Med.* **2001**, 31, 1432-1440.

399. Bateman K. P. *J. Am. Soc. Mass Spectrom.* **1999**, *10*, 309-317.

400. Kelly, J. F.; Ramaley, L.; Thibault, P. *Anal. Chem.* **1997**, *69*(1), 51-60.

401. Moini, M.; Cao, P. and Bard, A. J. *Anal. Chem.*, **1999**, *71*, 1658-1661.

402. Van Berkel, G. J. *J. Am. Chem. Soc.* **2000**, *11*, 951-960.

403. Lingane, J. J. *Electroanalytical Chemistry*, 2nd ed.; Interscience: New York, **1958**.

404. Liesener, A. and Karst, U. *Anal. Bioanal. Chem.* **2005**, *382*, 1451-1464.

405. Creighton, T. E. *Proteins: Structures and Molecular Properties*, W. H. Freeman: New York, **1984**.

406. LeVine, H., III . *Amyloid* **2005**, *12*, 5-11.

407. Lockhart, A.; Ye, L.; Judd, D. B.; Merritt, A. T.; Lowe, P. N.; Morgenstern, J. L.; Hong, G.; Gee, A. D.,; and Brown, J. *J. Biol. Chem.* **2005**, *280*, 7677-7684.

VITA

Maolian Chen was born in Hunan, China, like every person, at a very young age. Right after she completed her B.S. degree studies in Chemistry with honors from Hainan Normal University in June 1998, she entered Changchun Institute of Applied Chemistry, Chinese Academy of Sciences, where she got her M.S. degree in Physical Chemistry in June 2001. Then in the fall of 2001 she was admitted into the University of Tennessee at Knoxville. Maolian is currently a Ph.D. candidate in Analytical Chemistry under the direction of Dr. Kelsey D. Cook

Maolian married Thomas in December 2005. They live a happy life in Knoxville, TN.